



Durham E-Theses

Deposition, diagenesis, and reservoir development of the Cretaceous Lidam formation, SE Sirt Basin, Libya.

Abugares, Miloud M.

How to cite:

Abugares, Miloud M. (2007) *Deposition, diagenesis, and reservoir development of the Cretaceous Lidam formation, SE Sirt Basin, Libya.*, Durham theses, Durham University. Available at Durham E-Theses Online: <http://etheses.dur.ac.uk/2599/>

Use policy

The full-text may be used and/or reproduced, and given to third parties in any format or medium, without prior permission or charge, for personal research or study, educational, or not-for-profit purposes provided that:

- a full bibliographic reference is made to the original source
- a [link](#) is made to the metadata record in Durham E-Theses
- the full-text is not changed in any way

The full-text must not be sold in any format or medium without the formal permission of the copyright holders.

Please consult the [full Durham E-Theses policy](#) for further details.

**Deposition, Diagenesis, and Reservoir Development
of the Cretaceous Lidam Formation,
SE Sirt Basin, Libya.**

Miloud M. Abugares

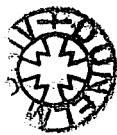
Supervisor: Dr. Moyra E. J. Wilson

The copyright of this thesis rests with the author or the university to which it was submitted. No quotation from it, or information derived from it may be published without the prior written consent of the author or university, and any information derived from it should be acknowledged.

**A thesis submitted to the University of Durham of degree of
Masters in carbonate sedimentology**

Department of Earth Science

January, 2007



Declaration

The content of this thesis are the original work of the author and has not previously been submitted for a degree at this or any other university. The work of other people is acknowledged by reference.

Miloud M. Abugares
Department of Earth science
University of Durham
January, 2007.

Depositional Environments, Diagenesis, and Sequence Development of the Lidam Formation, SE Sirt Basin, Libya.

ABSTRACT

This study concentrates on the deposition, diagenesis and reservoir characteristics of the Upper Cretaceous (Cenomanian) Lidam Formation. Core, petrography and geochemical data were studied from five wells (P3-97, N6-97, R1-97, 3V1-59E, and 3V3-59E) in the SE Sirt Basin, Libya. Although the Lidam Formation is one of the main producing subsurface carbonate reservoirs in the Sirt Basin, this work is one of the first detailed studies of the formation.

During this study, ten main facies and fourteen microfacies have been identified. These facies are; (1) anhydrite, (2) dolomite (3) sandstone (4) shale, (5) stromatolitic mudstone, (6) ostracod wackestone, (7) mollusc (8) bioclastic (9) peloidal, and (10) Algal facies. These deposits are inferred to have formed in supratidal sabkhas, intertidal, restricted marine shelf lagoon and higher energy shallow shoal environments. The overall depositional setting is interpreted as inner carbonate ramp deposits.

Facies variations appear to be related to depth and energy changes and proximity to areas of clastic deposition. The whole stacking pattern of these facies suggests that the Lidam Formation consists of two large-scale cycles. The first cycle began with the laminated stromatolite and anhydrite facies which overlie the Nubian Sandstone and pass upward into lagoonal ostracod facies, and then the peloidal shoal deposits and are indicative of a transgression. The second cycle occurred during a relative fall in sea level at the end of the Cenomanian with a return to evaporitic sabkha deposits. The small scale cycles trends formed under transgressive and regressive conditions. These changes may have been controlled by tectonic events and changes in the rate of basin subsidence as well as a eustatic sea level rise during Cenomanian times.

The carbonates of Cretaceous Lidam Formation have been altered by a variety of diagenetic processes inferred from petrography, Cathodoluminescence, SEM, and stable isotope analysis. Three major diagenetic environments have affected the Lidam Formation after deposition. These are: 1) early marine (micritization and isopachous cement), 2) meteoric & early burial (meniscus cement, neomorphism, dissolution, calcite cementation, early dolomitization, and anhydrite replacement). Finally, 3) Burial diagenesis resulted in compaction (Concavo-convex contacts, solution seams and stylolites), fracturing, equant calcite cement, and late dolomitization, replacement by pyrite and hydrocarbon emplacement. Good effective porosity is restricted to the ooidal peloidal packstone / grainstone facies and decreases in the bioclastic foraminifera, stromatolitic packstone, and anhydrite facies. Calcite cementation, late dolomitization, and compaction are the major factors controlling the reduction of the porosity in the Lidam Formation whilst dissolution and fracturing have increased porosity and permeability and enhanced the reservoir quality of the Lidam Formation.

ACKNOWLEDGMENTS

Firstly I must thank my father, my mother, brothers and sisters for their support. Special thanks also to my wife and my children. This thesis could have not been completed without their continuous encouragement and support.

I wish to express my sincere thanks to my supervisor; Dr. Moyra E. Wilson, for her continuous encouragement and giving guidance through all stages of this thesis. I greatly appreciated for her acceptance me to supervising my project in Durham University. I am grateful to the external examiner Dr Joanna Garland (Cambridge Carbonates) and the internal examiner Professor. M. E. Tucker for their excellent corrections in my thesis. I express my thanks to all members and technical staff in the Earth science department of the University of Durham for their help and assistance.

My special thanks to the all staff members in the Libyan Petroleum Institute (LPI) for their support in providing the funds for my study. Special thank must go to the General Manager: Dr. Bourima Belgasim for his ongoing support. Also, I would like to extend my thanks to my friends and colleagues in LPI, Tripoli particularly the exploration department for their support and in Durham University for their useful support.

Finally, I wish to extend special thanks to the exploration manage; Vallari Bosse, Wintershale Company Tripoli, Libya branch, and all staff members for their support and providing me to collect the samples from the company store.

Finally, I would like to thank Dr. Tarik Zambo for his great helpful to me and my family during our stay in Durham city.

TABLE OF CONTENTS

DECLARATION	ii
ABSTRACT	iii
ACKNOWLEDGEMENT	v
CHAPTER 1: INTRODUCTION.	2
1.1. Location of the Study Area.	2
1.2. Aims of The Study.	3
1.3. Methods of the Study.	3
1.4. Terminology.	4
1.5. Layout of Thesis.	4
CHAPTER 2: REGIONAL GEOLOGY AND TECTONIC SETTING OF THE SIRT BASIN.	
2.1. INTRODUCTION.	12
2.2. GEOLOGY AND HYDROCARBONS IN LIBYA.	12
2.3. MAJOR STRUCTURAL ELEMENTS AND LOCATION OF THE SIRT BASIN.	14
2.4. TECTONIC SETTING AND GEOLOGICAL HISTORY OF THE SIRT BASIN.	15
2.5. SIRT BASIN STRATIGRAPHY	20
2.5A. Basement.	20
2.5B. Cretaceous Stratigraphy.	20
2.5Bi. Pre-Upper Cretaceous (Lower part).	23
2.5Bii. Upper Cretaceous (Upper part).	23
2.5Biia. Lidam Formation (Cenomanian).	23
2.5Biib. Rakb Group:	23
2.5Biib1- Etel Formation (Turonian).	23
2.5Biib2- Rachmat Formation (Coniacian /Santonian).	24
2.5Biib3- Sirte Shale (Campanian).	24
2.5Biic. Kalash Limestone (Maastrichian).	25
2.5C. Palaeocene.	25

2.5Ci. Hagfa shale (Danian).	25
2.5Cii. Beda Formation (Selandian).	25
2.5Ciii. Dahra, Khalifa, Zeltan group and Khier (Selandian -Thanetian).	25
2.5D. Eocene.	26
2.5Di. Gir formation (Ypresian).	26
2.5Dii. Gialo Formation (Lutetian).	26
2.5Diii. Augila formation (Bartonian).	26
2.5E. Oligocene.	27
2.5Ei. Arida Formation.	27
2.5Eii. Diba Formation.	27
2.5F. Miocene (Marada Formation)	27
2.6. LIDAM FORMATION INTRODUCTION.	27
2.7. PREVIOUS WORKS ON THE LIDAM FORMATION.	29
2.8. CHAPTER SUMMARY.	30
CHAPTER 3: FACIES ANALYSIS OF THE LIDAM FORMATION	
3.1. INTRODUCTION.	32
3.2. FACIES ANALYSIS METHODOLOGY.	32
3.3. FACIES ANALYSIS OF LIDAM FORMATION.	37
3.3.1. Anhydrite Facies (AF).	37
3.3.2. Dolomite Facies (DF).	40
3.3.3. Sandy Facies (SF).	44
3.3.4. Shale Facies (SF).	47
3.3.5. Stromatolitic Facies (STF).	49
3.3.6. Ostracoda Facies (OSF).	51
3.3.7. Mollusc Facies (MF).	55
3.3.8. Bioclastic Facies (BF).	58
3.3.9. Peloidal Facies (PF).	63
3.3.10. Algal Facies (STPF).	68
3.4 DISCUSSION AND OVERALL DEPOSITIONAL INTERPRETATION	73
3.5 CHAPTER SUMMARY	77

CHAPTER 4: SEQUENCE DEVELOPMENT OF THE LIDAM FORMATION

4.1. INTRODUCTION	80
4.2. SEQUENCE STRATIGRAPHY OF THE LIDAM FORMATION.	80
4.2.1. INTRODUCTION TO SEQUENCE STRATIGRAPHY:	80
4.2.2. BOUNDARY SURFACES.	82
1-Sequence boundary (SB)	82
2- Maximum flooding Surface (MFS).	82
3- Transgressive surface (TS).	83
4.2.3. SYSTEM TRACT (ST):	84
1- Lowstand Systems Tract (LST).	85
2- Highstand systems tract (HST).	86
4.2.4. STACKING PATTERNS.	87
4.3. LITHOLOGICAL DESCRIPTION OF THE STUDIED WELLS.	88
4.3.1. R1-97 WELL	88
<i>i. Description</i>	88
<i>ii. Interpretation</i>	89
4.3.2. P3-97 Well	92
<i>i. Description</i>	92
<i>ii. Interpretation</i>	95
4.3.3. N6-97 Well	95
<i>i. Description</i>	95
<i>ii. Interpretation</i>	96
4.3.4. 3V1-95E Well	99
<i>i. Description</i>	99
<i>ii. Interpretation</i>	100
4.3.5. 3V3 - 59E Well	103
<i>i. Description</i>	103
<i>ii. Interpretation</i>	106

4.4. DISCUSSIONS ON SPATIAL VARIATION AND SEQUENCE DEVELOPMENT.	106
4.4.1 Small Scale Variations within the Wells.	107
a) intercalations of stromatolitic dolomudstone / anhydrite facies.	107
b) Shale based cycles	107
4.5. COMPARISON OF LARGE SCALE VERTICAL (TEMPORAL) AND LATERAL (SPATIAL) VARIATIONS.	109
4.5.1 Comparison between Wells in Platform.	109
4.5.2 Comparison in Trough.	110
4.6. SEQUENCE STRATIGRAPHY OF THE LIDAM FORMATION	
4.6.1. Sequence Stratigraphic Analysis of the Lidam Formation in the 3V1-59E, 3V3-59E, R1-97, P3-97, and N6-97.	114
4.7. SEQUENCE STRATIGRAPHIC INTERPRETATION AND CONTROLS ON LARGE SCALE VARIATIONS.	120
4.8. COMPARISON WITH OTHER CRETACEOUS SUCCESSIONS.	121
4.9. CHAPTER SUMMARY	124
CHAPTER 5: DIAGENESIS AND RESERVIOR QUALITY OF THE LIDAM FORMATION.	126
5.1 INTRODUCTION.	126
5.2. INTRODUCTION TO CARBONATE DIAGENESIS.	126
5.2.1 MARINE DIAGENESIS.	128
1. Marine Phreatic Zone.	128
5.2.2. METEORIC DIAGENESIS.	129
a. Phreatic Zone.	129
b. Vadose Zone.	130
c. Mixed Zone	130
5.2.3. BURIAL DIAGENESIS.	130
1. Burial Cementation.	132
5.3 DIAGENESIS OF THE LIDAM FORMATION.	133
5.3.1 INTRODUCTION.	133

5.3.2 METHODOLOGY.	133
5.3.3 EARLY MARINE DIAGENESIS.	134
a). Micritization.	134
b) Isopachous rim cement.	136
5.3.4. METEORIC AND EARLY BURIAL DIAGENESIS.	139
A) Meniscus Cement.	139
B. Dissolution.	140
C. Neomorphism.	143
D) Cementation (drusy and syntaxial overgrowth).	143
E) Early dolomitization (fine dolomite).	146
F). Anhydrite replacement.	149
5.3.5. LATE BURIAL DIAGENESIS.	152
1). Compaction (concave – convex contacts dissolution seams and stylolites)	152
2). Fracturing.	154
3). Cementation (equant calcite cement)	155
4). Late dolomitization (clear coarse dolomite cement).	157
5). Replacement by Pyrite.	160
5.4. CATHODOLUMINESCENCE (CL) ANALYSIS AND INTERPERTATION.	162
5.4.1. Introduction.	162
5.4.2. Cathodoluminescence (CL) Analysis of the Lidam Formation.	163
5.5. STABLE ISOTOP ANALYSIS AND INTERPRETATION.	177
5.5.1 Introduction.	177
5.5.2. Isotopes Analysis of the Lidam Formation.	178
a. Carbonate Skeletons and non-Skeletons.	181
b. Micrite matrix.	182
c. Carbonate Cement.	182
5.6 DISCUSSION OF RELATIVE TIMING AND PROCESSES OF DIAGENESIS.	185
5.7. RESREVOIR QUALITY OF THE LIDAM FORMATION.	189
5.7.1. Porosity and Permeability Variation and Relationship with Facies.	189
5.7.2. Hydrocarbons Emplacement.	190
5.8. COMPARISON OF DIAGENESIS AND RESERVIOIR QUALITY	

WITH OTHER CRETACEOUS FORMATIONS.	191
5.9. CHAPTER SUMMARY.	193
CHAPTER 6: Conclusions	

LIST OF FIGURES

CHAPTER 1:

Figure 1.1. Location map of the studied wells in the southeastern part of the Sirt Basin. Libya	6
--	---

CHAPTER 2:

Figure 2.1. Location of the study area in the Sirt Basin and adjacent basins.	12
Figure 2.2. Tectonic framework of the Sirt Basin (Modified after Mouzughi and Taleb, 1981).	13
Figure 2.3a. Precambrian (basement) in the area that will become the Sirt Basin,	16
Figure 2.3b. Tectonic evolution of the Sirt Basin during Cambro-Ordovician period.	16
Figure 2.3c. Tectonic evolution of the Sirt Basin during the Silurian period.	17
Figure 2.3d. Tectonic evolution of the Sirt Basin during the Devonian period.	17
Figure 2.3e. Tectonic evolution of the Sirt Basin during the Premo-carboniferous period.	18
Figure 2.3f. Tectonic evolution of the Sirt Basin during the Triassic and Jurassic period.	18
Figure 2.3g. Tectonic evolution of the Sirt Basin during the Early Cretaceous.	19
Figure 2.3h. Tectonic evolution of the Sirt Basin present day setting.	19
Figure 2.4. Generalized stratigraphic / lithologic chart of the Upper Cretaceous and Tertiary succession on the study area, (After Barr and Weegar, 1972	22
Figure 2.5. Type Section of the Lidam Formation in the Sirt Basin (After Barr and Weegar, 1972).	28

CHAPTER 3:

Figure 3.1. Core photographs of Anhydrite Facies showing chicken wire anhydrite structure (AF).	38
Figure 3.2. Photomicrograph showing excellent preservation of anhydrite needles oriented partially paralleling the lamination in the micritic sediment.	39
Figure 3.3. Photomicrograph shows nodules of aphanitic anhydrite, possibly partly	

retaining the shape of original gypsum crystals. Adjacent to micritic seams between clear, euhedral gypsum crystals have partially replaced the anhydrite	39
Figure 3.4. Photomicrograph shows well developed interlocking, rhomb shaped crystals of non ferroan dolomite and ferroan dolomite in a fine grained calcite matrix.	42
Figure 3.5. Photomicrograph shows fine dolomite rhombs in a matrix of pseudospar with patches of microspar and micrite. Mouldic porosity is filled by ferroan dolomite.	42
Figure 3.6. Photomicrograph showing well developed crystals of fine idiotopic dolomite texture.	43
Figure.3.7. Core photographs of Siliciclastic Facies showing the lamination of sand layers from different wells.	45
Figure 3.8. Photomicrograph showing bioclastic sandstone microfacies containing quartz grains with scattered small forams (rotaliids and miloild) and coralline algae.	45
Figure 3.9. Photomicrograph showing poorly sorted sandstone with scattered shell fragments .	46
Figure 3.10. Photomicrograph showing fine grained sand with a muddy matrix from the quartz sandstone microfacies.	46
Figure.3.11. Core photographs of Shale Facies showing lamination of fissile to sub-fissile layers of shale.	48
Figure 3.12 Photomicrograph showing stromatolitic laminations consist of alternating thin micritic layers and lighter-coloured layers containing a mixture of micrite and ferroan dolomite crystals.	49
Figure.3.13. Photomicrograph showing stromatolitic laminations consisting of alternating thin micritic layers and layers containing a mixture of micrite and spare calcite cement.	50
Figure 3.14. Core photographs of the ostracod facies showing the nodular bedding and lamination of layers from different wells.	52
Figure 3.15. Photomicrograph shows a group of ostracods concentrated as a burrow infill. Complete two valves shells are filled by sparry cement.	53

- Figure 3.16. Photomicrograph showing ostracods mudstone / wackestone completely filled by calcite cement with scattered miliolid and bioclastic debris in lime mud matrix. 53
- Figure 3.17. Photomicrograph shows abundant disarticulated ostracod valves (thin curved shell) associated with miliolid and foraminifera imbedded in micrite sediment 54
- Figure 3.18. Core photographs showing mollusc bioturbated packstone. 56
- Figure 3.19. Photomicrograph showing boring of a mollusc shell which has been filled by the host sediments. 56
- Figure 3.20. Photomicrograph shows two large mollusc fragments with extensive boring. The rest of the sediment comprises broken up bioclasts and ostracod shells. 57
- Figure 3.21. Photomicrograph showing mollusc shells affected by micritization and boring which is filled by bioclastic debris. 57
- Figure 3.22. Core photographs of showing lamination and bioturbation of the sediments in Bioclastic Facies. 59
- Figure 3.23. Photomicrograph showing bioclastic packstone with scattered ostracod, echinoderm and other bioclastic fragments. 60
- Figure 3.24. Photomicrograph shows echinoderm packstone containing echinoid spans with porous structure, bioclastic fragments and ostracod embedded in a lime mud matrix. 60
- Figure 3.25. Photomicrograph shows echinoderm packstone containing scattered echinoid fragments plates and bioclastic fragments with small forams embedded in a lime mud matrix. 61
- Figure 3.26. Photomicrograph shows syntaxial overgrowth around echinoderm fragments and other components are mollusc fragment and coralline algae cemented by ferroan calcite cement in bioclastic packstone / grainstone. 61
- Figure 3.27. Photomicrograph showing small miliolid foraminifera and ostracods with bioclasts debris in a foraminifera packstone. 62
- Figure.3.28. Core photographs showing peloidal facies with high amplitude Stylolites. 64
- Figure.3.29. Photomicrograph showing peloidal packstone / grainstone containing

- peloids and gastropods. Intragranular porosity filled by calcite cement. 64
- Figure 3.30. Photomicrograph showing ooids with well preservation of original concentric structure, intragranular and intragranular porosity is filled by bitumen and ferroan calcite cement. 65
- Figure 3.31. Photomicrograph showing peloidal packstone / grainstone with scattered small forams cemented by ferroan calcite cement. 65
- Figure 3.32. Photomicrograph showing ooids with some preservation of original concentric structure. Intragranular and intragranular porosity is well developed and partially filled by bitumen. 66
- Figure 3.33. Photomicrograph showing peloidal grainstone consisting of peloids, small forams and micritized bioclasts. Intragranular porosity is completely filled by ferroan calcite cement. 67
- Figure 3.34. Core photographs of showing nodular bedding of algal facies 68
- Figure 3.35. Photomicrograph showing laminar encrustation squamariacean (Polystrata) algae. Note calcite crystals along the filament walls 69
- Figure 3.36. Photomicrograph showing layered squamariacean algae crusts in domal and vertical filament walls and altered small foraminifera within dolomite rhombs. 70
- Figure 3.37. Photomicrograph shows large hypothallium cells and vertically arranged filaments. Note micritic microstructure of the cell walls with calcite crystals in the lower part of the cells. 70
- Figure 3.38. Facies Model of the Lidam Formation in the Studied Area, Southeast, Sirt Basin, Libya. 72
- Figure.3.39. Location of the studied and area studied by El Bakai (1992) with different depositional environment of the ramp setting during Upper Cretaceous (Cenomanian) time 75
- Figure 3.40. Thickness map of the Lidam Formation in Sirt Basin and study area. (Modified after Abadi, 2002). 76

CHAPTER 4:

Figure 4.1. different parasequence sets trends from lagoonal subtidal to supratidal environments in carbonate rocks (Moore,1999).	81
Figure 4.2. Sequence boundary formation (modified from, Van Wagoner.1990).	82
Figure 4.3. Ideal carbonates sequence with sequence boundary (SB) and maximum flooding Surface (MFS).	83
Figure 4.4. Transgression and regression of the sea results the retrogradational and progradation stacked patterns.	84
Figure 4.5. Diagram showing the Lowstand systems tract (LST).	85
Figure 4.6. Depositional model during Highstand systems tract (HST).	86
Figure 4.7. Stacked patterns of the different parasequences related to deposition and accommodation space generation.	87
Figure 4.8. Lithological Description of the Lidam Formation in well R1-97, Hamid Field, SE Sirt Basin, Libya.	90
Figure 4.9. Stratigraphic section of the Lidam Formation facies in well R1-97, Hamid oil field, SE Sirt Basin, Libya.	91
Figure 4.10 Lithological Description of the Lidam Formation in well P3-97, Al Nakhalah Field, SE Sirt Basin, Libya.	93
Figure 4.11. Stratigraphic section of the Lidam Formation facies in well P3-97, Al Nakhalah oil field, SE Sirt Basin, Libya.	94
Figure 4.12. Lithological description of the Lidam Formation in well N6-97, Al Nakhalah Field, SE Sirt Basin, Libya.	97
Figure 4.13. Stratigraphic section of the Lidam Formation facies in well N6-97, Al Nakhalah oil field, SE Sirt Basin, Libya.	98
Figure 4.14. Lithological Description of the Lidam Formation in well 3V1-59E, 3V area, SE Sirt Basin, Libya.	101
Figure 4.15. Stratigraphic section of the Lidam Formation facies in well 3V1-59E, 3V area, SE Sirt Basin, Libya.	102
Figure 4.16. Lithological Description of the Lidam Formation in well 3V3-59E, 3V area, SE Sirt Basin, Libya.	104
Figure 4.17. Stratigraphic section of the Lidam Formation facies in well 3V3-59E,	

3Varea, SE Sirt Basin, Libya.	105
Figure 4.18. Possible stratigraphic correlation between the studied well in the Gialo Platform and Hameimat trough, SE Sirt Basin, Libya.	111
Figure 4.19. Typical distribution stacking pattern of facies in the wells 3V3- 59E, 3V1-59, and R1-97 in Gialo Platform.	112
Figure 4.20. Typical distribution of stacking pattern of facies in the wells N6-97 and P3-97 in Hameimat Trough.	113
Figure 4.21. An example of the typical vertical distribution stacking patterns of facies retrogradational than progradational parasequence development (well: 3V1-59E).	116
Figure 4.22. Ideal depositional model sequence and system tract models of Lidam Formation carbonate-evaporite ramp associated with type 1 sequence boundaries of the Nubian sandstone.	117
Figure 4.23. Depositional sequence model of the Lidam Formation during transgression system tract.	118
Figure 4.24. Depositional sequence model of the Lidam / Etel Formation during falling stage of the lowstand system tract.	119
Figure 4.25. Paleogeography map illustrates Late Cenomanian facies belt on the North Africa and adjacent correlative areas. (Simplified after Philip <i>et al.</i> 2000 and Stampfli <i>et at.</i> 2001).	122
CHAPTER 5:	
Figure 5.1. Different diagenetic environments from near surface marine and meteoric environment, down into the deep burial environment.	127
Figure 5.2. Different types of marine carbonate cements.	128
Figure 5.3. Different meteoric cements morphologies.	129
Figure 5.4. Cementation stages of carbonate rocks during burial diagenesis.	131
Figure 5.5. Different types of cementation stages during burial diagenesis.	132
Figure 5.6. Photomicrograph showing mollusca shell affected by micritization.	135
Figure 5.7. Photomicrograph shows mollusca affected by micritization prior to later diagenesis of original shell.	135
Figure 5.8. Photomicrograph showing peloidal ooidal packstone facies with dark	

- aragonite isopachous cement coating around the peloids which is later affected by micritization. Porosity has been completely occluded by a later ferroan calcite cement. 137
- Figure 5.9. Photomicrograph showing peloidal ooidal packstone facies with well developed isopachous rim cement around the peloids and pore spaces filled by ferroan calcite cement. 137
- Figure 5.10. Photomicrograph showing bioclastic packstone facies with well developed isopachous rim cement around the mollusc shell fragment and pore spaces filled by ferroan calcite cement. 138
- Figure 5.11. Photomicrograph showing meniscus cement in grain to grain contact. 139
- Figure 5.12. Photomicrograph showing shape of foraminifera and bioclasts which have been totally affected by dissolution. 141
- Figure 5.13. Photomicrograph showing mollusc shell that has been dissolved and a micrite envelopes outline the shell shape. 141
- Figure 5.14. SEM image showing pore space of the dissolved bioclasts later filled by the growth of calcite crystals. 142
- Figure 5.15. Photomicrograph showing that the peloids has been complete affected by micritization and porosity occluded by drusy ferroan calcite cementation in peloidal ooidal packstone facies. 144
- Figure 5.16. Photomicrograph showing that the Echinoderm fragments, cements are difficult to recognize in the dense bioclastic muddy facies. 145
- Figure 5.17. Photomicrograph shows a foraminifera packstone facies containing very fine dolomite (type 1) selectively replacing the matrix. 146
- Figure 5.18. Photomicrograph showing mouldic porosity which has been infilled later with isolated dolomite rhombs. 147
- Figure 5.19. Photomicrograph showing very fine dolomite (Type 1) mosaic texture with anhedral and irregular crystal boundaries with bioclasts molds filled by ferroan dolomite cement and relicts of micrite lime mud. 147
- Figure 5.20. Photomicrograph showing dolomite mudstone facies with intensive dolomitization (Type 2) and well developed intercrystalline porosity. 148
- Figure 5.21. SEM image showing dolomite mudstone facies with intensive

dolomitization (dolomite rhombs seen) and well developed intercrystalline porosity.	148
Figure 5.22. Photomicrograph showing replacement by anhydrite cement partially occluded the intergranular porosity between peloid grains.	150
Figure 5.23. Photomicrograph showing the intergranular porosity occluded by ferroan calcite cement and anhydrite cement in the dolomite facies.	150
Figure 5.24. SEM photomicrograph showing the replacement of anhydrite cement partially occluded the intergranular porosity between the peloidal grains.	151
Figure 5.25. Photomicrograph showing stylolites and pressure solution seams with low amplitude in bioclastic foraminifera packstone.	152
Figure 5.26. Photomicrograph showing high concentration of pressure solution seams with low amplitude in bioclastic foraminifera packstone with scattered dolomite	153
Figure 5.27. Photomicrograph showing ferroan calcite cement reducing fracture porosity in a peloidal ooidal packstone/grainstone.	154
Figure 5.28. Photomicrograph showing later fracture has been completely occluded by ferroan calcite cement in the peloidal facies.	155
Figure 5.29. Photomicrograph showing well developed equant calcite cement occluding the most of the pore space.	156
Figure 5.30. Photomicrograph shows well developed equant mosaic calcite cementation occluding intragranular porosity of in ostracods.	156
Figure 5.31. Photomicrograph showing infill of dolomite cement in vuggy or mouldic porosity. Note also oil staining and intercrystalline porosity as shown by blue resin.	158
Figure 5.32. Photomicrograph shows filling of clear coarse dolomite cement in earlier vuggy or mouldic porosity.	158
Figure 5.33. SEM image shows filling of coarse dolomite cement in earlier vuggy or mouldic porosity.	159
Figure 5.34. Photomicrograph showing partial replacement of pyrite in a fracture zone.	160
Figure.5.35. Photomicrograph showing replacement of pyrite in a bioclastic facies.	161
Figure 5.36. Diagram showing Cathodoluminescence properties of zoned cements formed under different diagenetic conditions.	163

- Figure 5.37. Paired photomicrographs taken under normal light (PPL) (a) and CL (b), showing grainstone with coarse calcite cement. 166
- Figure 5.38. Photomicrographs under normal light (PPL) (a) and CL (b) (a) shows the grainstone texture with the cement fabric of meniscus cement grain to grain contact and coarse calcite cement filling porosity. 167
- Figure 5.39. Photomicrographs had taken under normal light (PPL) (a), showing grainstone texture with coarse calcite cement. 168
- Figure 5.40. Paired photomicrographs taken under normal light (PPL) (a) and CL (b), shows grainstone with pore space partially filled by a well developed dolomite rhombs crystal. 169
- Figure 5.41. Photomicrographs taken under normal light (PPL) (a) and CL (b), similar to the previous photomicrograph showing peloidal grainstone with pore space partially filled by dolomite rhombs crystal. 170
- Figure 5.42. Photomicrographs taken under normal light (PPL) (a) and CL (b) showing peloidal grainstone (PG) with bioclastic fragment filled by drusy calcite cement (DCC) and later by equant calcite cement. 171
- Figure 5.43. Paired photomicrographs taken under normal light (PLL) (a) and CL (b), showing equant calcite cement (ECC) filled the porosity. 172
- Figure 5.44. Photomicrographs under normal light (PPL) (a) showing peloidal grainstone (PG) filled by drusy and later by equant calcite cement. 173
- Figure 5.45. Paired photomicrographs taken under normal light (PPL) (a) showing similar peloidal grainstone (PG) pore filled with Equant coarse calcite cement 174
- Figure 5.46. Paired photomicrographs taken under normal light (PPL) (a) showing well developed cloudy fine to medium dolomite rhombs (FD) with a vuggy pores filled by later clear dolomite rhombs. 175
- Figure 5.47. Paired photomicrographs taken under normal light (PLL) (a) showing the intergranular porosity of peloidal packstone / grainstone filled by equant mosaic of calcite cement. 176
- Figure 5.48. Schematic C-O cross plot showing characteristic data fields for cements formed in different diagenetic environments. 178
- Figure 5.49. Cross plot of the $\delta^{13}\text{C}$ and $\delta^{18}\text{O}$ isotope results from the Lidam Formation. 181

Figure 5.50. Paragenetic diagram showing the relative timing of different diagenetic events and their diagenetic environments in the Lidam Formation in SE Sirt Basin, Libya.	184
Figure 5.51. Photomicrograph showing oil accumulation in intergranular and intragranular porosity.	191

LIST OF TABLES

CHAPTER 1:

Table 1.1. Summary of cored intervals from the studied wells.	7
Table 1.2. List of the core samples chosen from well: P3-97 Core # 1. Depth from: 11602 ft to 11681 ft. Core thickness: 79 ft.	8
Table 1.3. List of the core samples chosen from well: N6-97. Core # 1, Depth from: 11782 ft to 11871 ft. Core thickness: 89 feet.	8
Table 1.4. List of the core samples chosen from well: R1-97. Core# 1, Depth from: 10980 ft to 11074 ft, Core thickness: 94 ft.	8
Table 1.5. List of the core samples chosen for THIN SECTION, SEM, and XRD analysis from, Well 3V1-59E, Gialo oil field, Waha Oil Company.	9
Table 1.6. List of the core samples chosen for THIN SECTION, SEM and XRD analysis from Well 3V3-59E, Gailu oil field, Waha Oil Company.	10

CHAPTER 3:

Table 3.1. Facies and microfacies of the Lidam Formation in the studied wells, Southeastern part of the Sirt Basin, Libya.	33
Table 3.2. Whole rock X- ray diffraction (XRD) analysis in well: 3V1-59E.	35
Table 3.3. X-ray diffraction (XRD) analysis for < 2 micron clay in well: 3V1-59E .	35
Table 3.4. Whole rock X. ray diffraction (XRD) analysis in well: 3V3-59E.	36
Table 3.5. Differences between carbonate ramp and rimmed shelf depositional models.	74

CHAPTER 5:

Table 5.1. Results of oxygen and carbon isotope analyses of carbonate skeletons and cements of Lidam Formation.	180
---	-----

Table 5.2. Showing different dolomite types occurred during diagenetic process of Lidam Formation.	188
Table 5.3. Showing the average porosity and permeability in the studied wells.	189

CHAPTER ONE

THESIS INTRODUCTION

CHAPTER ONE

1. THESIS INTRODUCTION.

- 1.1. Location of the Study Area.
- 1.2. Aims of The Study.
- 1.3. Methods of the Study.
- 1.4. Terminology.
- 1.5. Layout of Thesis.



1- INTRODUCTION

The study concentrates on the sedimentology, diagenesis, depositional environment and reservoir characterization of the Lidam Formation. It includes facies analysis and interpretation of the data from three wells explored by Wintershale, Libya and two wells from Waha Oil Company (Table 1.1).

The Lidam Formation is located in the subsurface of the southeast Sirt Basin and is composed of a thick unit of carbonates and evaporites, which reaches approximately 200 feet in thickness. The formation unconformably onlaps different units including the Nubian and Bahi Formations as well as igneous basement and is usually overlain by the Upper Cretaceous Etel Formation. The Lidam Formation is considered as Cenomanian in age by Baar and Weegar (1972).

The Lidam Formation is an important hydrocarbon reservoir target in the Sirt Basin; it forms the reservoir rock in the Masrab Oil Field from the southeast Sirt Basin and Dor-Mansour Oil Field in the western Beda Platform from the central Sirt Basin.

1.1. Location of the Study Area

The study area is located in the southeastern part of the Sirt basin, Libya (Figure 1.1). This study is based on the study of subsurface well logs and cores which have been chosen from the Upper Cretaceous Lidam Formation (Table 1.1). Two wells operated by Waha Oil Company were chosen for detailed sedimentological study from the Gialo Platform (3V1-59E and 3V3-59E). An additional two wells (P3-97 and N6-97) from the Nakhalah Oil Field are located in the Hameimat trough. R1-97 was drilled in the Hamid Oil Field operated by Wintershale (Libya branch), which is located in the Gialo platform south east of the 3V area. The area is mainly desert covered by sand dunes with no surface geology; the climate is very hot in the summer due to the southern hot wind (locally known as Ghibli wind).

1.2. Aims of the Study

The principal aims of this study are:

1. To describe and identify the different lithofacies of the Lidam Formation cored in the studied wells (Figure. 1.1).
2. To identify and undertake a detailed petrographic and diagenetic analysis of the different lithofacies identified.
3. To evaluate the depositional environments of the Lidam Formation and investigate factors influencing deposition and diagenesis.
4. To study the reservoir properties of the formation and the relationship between primary depositional textures and diagenesis to porosity and permeability development.

1.3 Methods of the Study

The methodology used in this study is outlined below.

- 1- Cores were systematically described on standard log format at scale of 1: 50 (see Chapter 4).
- 2- Seventy (70) core samples were selected and cut into thin sections from the Lidam Formation. The prepared thin sections were impregnated with blue dye to highlight the porosity distribution. They were also stained with potassium ferricyanide and alizarin red-S solution to distinguish between dolomite, iron-rich dolomite non-ferroan and ferroan calcite. The method employed was similar to that described by Dickson (1986) and the preparation techniques are given in Adams et al. (1984).
- 3- Detailed petrography was through polarizing microscope analysis with thin section photomicrographs taken to illustrate key features. Full thin section descriptions were undertaken with an emphasis on factors affecting reservoir properties, such as porosity, textural parameters, sedimentary structures and mineralogical composition, as well as the post-depositional diagenetic features.
- 4- Six samples were selected for scanning electron microscope analysis in order to evaluate pore geometries and the morphology of cements or clay minerals.
- 5- Sixteen (16) stable isotope samples were collected from five wells to investigate likely diagenetic environments. These include; 4 samples of shell fragments, 4 samples of micrite matrix, 4 samples of different cements (fractured and coarse

equant and drusy cement), and 4 samples from different carbonate sediments (stromatolite, peloid / ooid, and dolomite).

- 6- Nineteen (19) samples from 3V3-59E and 3V1-59E were selected for X-Ray Diffraction (XRD) analysis to determine the component clays and mineralogy of the whole rock samples and six (6) samples from 3V1-59E for the <2-micron clay fraction.
- 7- Seven samples were chosen from different wells (3V1-59E, 3V3-59E, R1-97, P3-97, and N6-97) in the Lidam Formation from different depths for Cathodoluminescence (CL) microscopy analysis to determine the variation in fluid chemistry during precipitation cements.

1.4 Terminology

Terminologies used in this thesis are outlined below with illustrations and tables also given in the appendix at the end of this thesis:

1. Classification of carbonates is based on Dunham's (1962) textural scheme with reef-related textures added by Embry and Klovan (1971).
2. Terminologies used for microfacies analysis are according to Flugel (2004).
3. Dolomite crystal fabrics are described using the terminology of Friedman (1965), Warren (2002), and Machel (2005).
4. Terminology for carbonate crystal morphologies are after Flugel (2004).
5. Classification of porosity in carbonates is from Choquette and Pray (1970)

1.5 Thesis Layout:

This thesis is presented in six chapters. The **first chapter** introduces the reasons for the study, the location of the study area, together with the aims and methodology. The **second chapter** concentrates on the tectonic setting and geological history of the Sirt Basin. The focus is on the regional tectonics of the area of study in the Sirt basin. Also outlined is the tectonostratigraphic setting of the Lidam Formation and brief summaries of the pre-Upper Cretaceous Basement, as well as other Cretaceous and Tertiary formations in the study area. This chapter also describes the previous work undertaken on the Lidam Formation in the Sirt Basin. **Chapter 3** concentrates on the results and interpretation of microfacies analysis obtained through detailed petrographic analysis, lithological variation,

fossil content and the sedimentary structures from core description of the five studied wells (P3-97, N6-97, R1-97, 3V1-59E, and 3V3-59E). Identification and interpretation of different lithofacies and construction of an ideal model for the depositional environment of the Lidam Formation are the main targets of this chapter. The depositional model is based on the data collected and the interpretation is compared with previous facies models proposed for the Lidam Formation. **Chapter 4** describes the sedimentology of the Lidam Formation in detail, focusing on the main vertical and lateral variations in lithofacies analysis. Spatial and temporal variations in depositional environment are inferred and controls on deposition discussed. **Chapter 5** discusses the main diagenetic features and reservoir quality of the Lidam Formation. Diagenetic processes and environments are inferred from petrography, SEM, CL microscopy and stable isotopes. Controls on porosity and permeability characteristics are discussed. The relation between facies and reservoir development influenced by sedimentology and diagenesis is presented in this chapter. The final chapter (**Chapter 6**) is the conclusions and recommendations for future work. A list of references and appendixes are given at the end of the thesis.

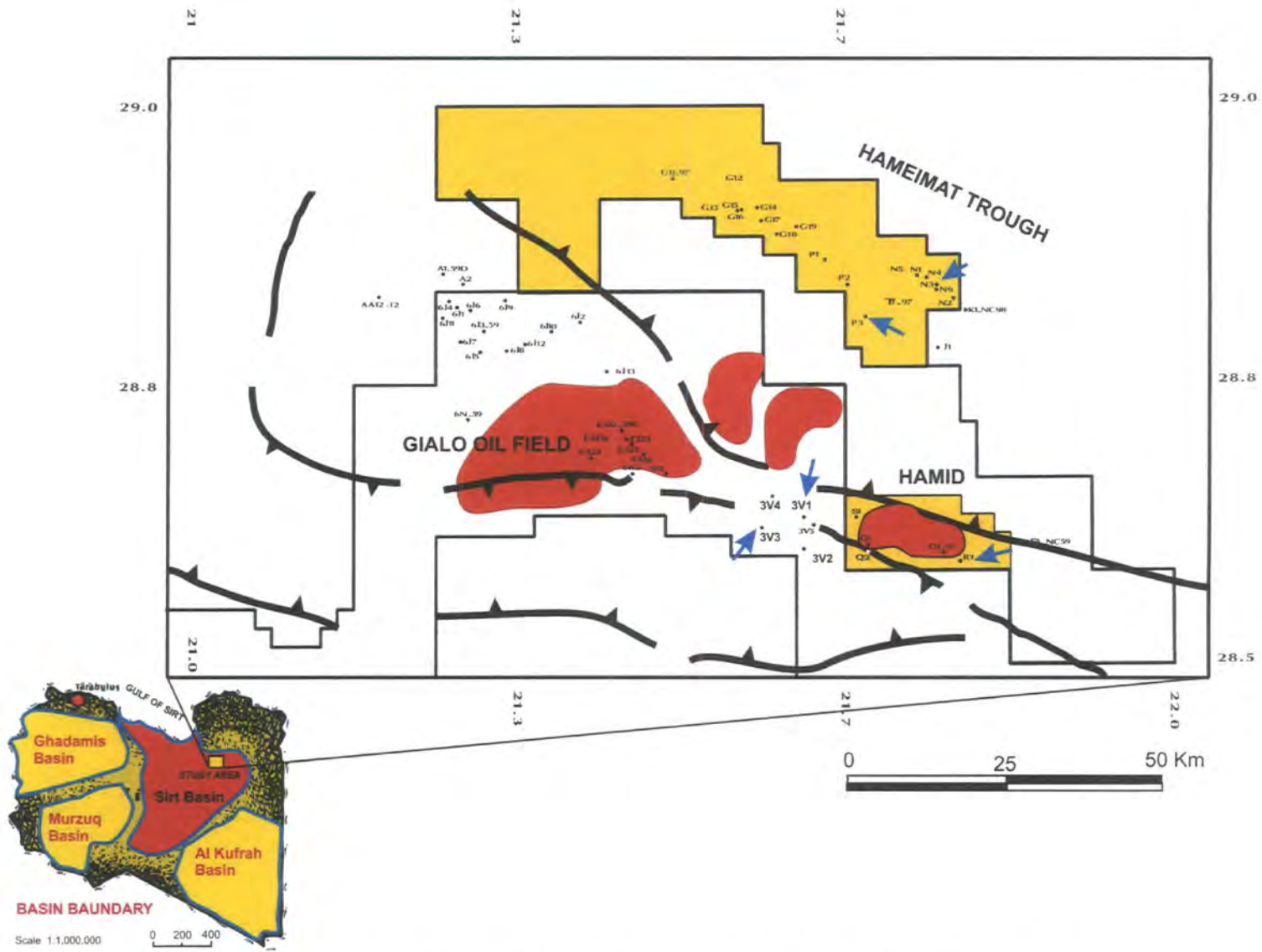


Figure 1.1. Location map of the studied wells in the southeastern part of the Sirt Basin, Libya.

Company	Formation	Well	Core No.	Core interval (ft)	Core thickness (ft)	Total cored thickness (ft)	Total thickness of Lidam Fm.	Thin sections	SEM	XRD	Notes
Waha	Lidam Fm.	3V1-59E	1 2 3 4	10441 <i>ft</i> to 10468 <i>ft</i> 10468 <i>ft</i> to 10486 <i>ft</i> 10486 <i>ft</i> to 10516 <i>ft</i> 10516 <i>ft</i> to 10546 <i>ft</i>	27 <i>ft</i> 18 <i>ft</i> 30 <i>ft</i> 30 <i>ft</i>	105 <i>ft</i>	105ft	20	10	11	No Gap
Waha	Lidam Fm.	3V3-95E	1 2 3 4	10198 <i>ft</i> to 10199 <i>ft</i> 10199 <i>ft</i> to 10228 <i>ft</i> 10228 <i>ft</i> to 10252 <i>ft</i> 10252 <i>ft</i> to 10280 <i>ft</i>	1 <i>ft</i> 29 <i>ft</i> 24 <i>ft</i> 28 <i>ft</i>	82 <i>ft</i>	82 ft	21	6	6	No Gap
Wintershale	Upper part of Lidam Fm.	R1-97	1	10980 <i>ft</i> to 11074 <i>ft</i>	94 <i>ft</i>	94 <i>ft</i>	205 ft	11			
Wintershale	Upper part of Lidam Fm.	P3-97	1	11602 <i>ft</i> to 11680 <i>ft</i>	78 <i>ft</i>	78 <i>ft</i>	260 ft	8			
Wintershale	Upper part of Lidam Fm.	N6-97	1	11782 <i>ft</i> to 11870 <i>ft</i>	88 <i>ft</i>	88 <i>ft</i>	360 ft	10			

Total 70

Table.1.1. Summary of cored intervals from the studied wells.

SAMPLE NO:	LAB NO:	FORMATION	DEPHT (FT)	CORE NO:	CL
1	1.	Lidam	11610	1	
2	2.	Lidam	11614	1	
3	3.	Lidam	11617	1	
4	4.	Lidam	11627	1	√
5	5.	Lidam	11632.5	1	
6	6.	Lidam	11639	1	
7	7.	Lidam	11651	1	
8	8.	Lidam	11674	1	

Table1.2 List of the core samples chosen for further thin section analysis from well **P3-97** Core # 1. Depth from: 11602 ft to 11681 ft. Core thickness: 79 ft

SAMPLE NO:	LAB NO:	FORMATION	DEPHT (FT)	CORE NO:	CL
1	1	Lidam	11788	1	
2	2	Lidam	11804	1	
3	3	Lidam	11806	1	
4	4	Lidam	11821	1	
5	5	Lidam	11831	1	
6	7	Lidam	11845	1	
7	8	Lidam	11846	1	
8	6	Lidam	11853	1	
9	9	Lidam	11862	1	
10	10	Lidam	11867	1	√

Table1.3. List of the core samples chosen for further thin section analysis from well **N6-97**. Core # 1, Depth from: 11782 ft to 11871 ft. Core thickness: 89 feet.

SAMPLE NO:	LAB NO:	FORMATION	DEPHT (FT)	CORE NO:	CL
1	10	Lidam	10984	1	√
2	11	Lidam	10991	1	
3	9	Lidam	10997.5	1	
4	1	Lidam	11004	1	
5	3	Lidam	11011	1	
6	2	Lidam	11017	1	
7	4	Lidam	11025.5	1	
8	5	Lidam	11041	1	
9	6	Lidam	11046	1	
10	7	Lidam	11052	1	
11	8	Lidam	11060.5	1	
11	11	Lidam	11060.5	1	

Table1.4. List of the core samples chosen for further thin section analysis from well **R1-97**. Core# 1, Depth from: 10980 ft to 11074 ft, Core thickness: 94 ft.

NO:	DEPHT (FT)	FORMATION	THIN SECTION	SEM	XRD	
					Whole-rock mineralogy	Clay mineralogy ($<2\mu\text{m}$)
1	10448	Lidam	√	√	√	√
2	10456.5	Lidam	√			
3	10458	Lidam	√			
4	10460	Lidam	X		√	√
5	10464	Lidam	√			
6	10468.5	Lidam	√	√	√	√
7	10472	Lidam	√			
8	10474.5	Lidam	√	√	√	√
9	10483	Lidam	√			
10	10484.5	Lidam	√	√	√	√
11	10489.5	Lidam	X		√	√
12	X	Lidam	X			
13	10495.5	Lidam	√			
14	X	Lidam	X			
15	10505	Lidam	√	√	√	√
16	10507.5	Lidam	√			
17	10511.5	Lidam	√	√	√	√
18	10518	Lidam	X			
19	10520	Lidam	√	√	√	√
20	10524	Lidam	√		√	√
21	10525	Lidam	√	√	√	√
22	19531	Lidam	√			
23	10539	Lidam	√	√	√	√
24	10542	Lidam	√	√	√	√

Table 1.5. List of the core samples chosen for THIN SECTION, SEM, and XRD analysis from, Well 3V1-59E, Gialo oil field, Waha Oil Company.

Sample No.	Core Depth (ft)	FORMATION	Thin Section Analysis	XRD Analysis (clay)	XRD Analysis (bulk)	SEM Analysis
1	10198	Lidam	✓	✓	✓	✓
2	10201	Lidam	✓			
3	10203	Lidam	✓			
4	10205	Lidam	✓			
5	10207	Lidam	✓	✓	✓	✓
6	10209	Lidam	✓			
7	10211	Lidam	✓			
8	10212	Lidam	✓	✓	✓	✓
9	10215	Lidam	✓			
10	10219	Lidam	✓			
11	10221	Lidam	✓	✓	✓	✓
12	10223	Lidam	✓			
13	10226	Lidam	✓			
14	10230	Lidam	✓	✓	✓	✓
15	10238	Lidam	✓			
16	10244	Lidam	✓			
17	10253	Lidam	✓	✓	✓	✓
18	10255	Lidam	✓			
19	10260	Lidam	✓			
20	10268	Lidam	✓			
21	10280	Lidam	✓			

Table1.6. List of the core samples chosen for THIN SECTION, SEM and XRD analysis from Well 3V3-59E, Gailu oil field, Waha Oil Company.

CHAPTER TWO

*REGIONAL GEOLOGY AND
TECTONIC SETTING OF THE
SIRT BASIN.*

CHAPTER TWO

2- REGIONAL GEOLOGY AND TECTONIC SETTING OF THE SIRT BASIN.

2.1. INTRODUCTION.

2.2. GEOLOGY AND HYDROCARBONS IN LIBYA.

2.3. MAJOR STRUCTURAL ELEMENTS AND LOCATION OF THE SIRT BASIN.

2.4. TECTONIC SETTING AND GEOLOGICAL HISTORY OF THE SIRT BASIN.

2.5. SIRT BASIN STRATIGRAPHY

2.5A. Basement.

2.5B. Cretaceous Stratigraphy:

2.5Bi. Pre-Upper Cretaceous (Lower part).

2.5Bii. Upper Cretaceous (Upper part).

2.5Bia. Lidam Formation (Cenomanian).

2.5Biib. Rakb Group:

2.5Biib1- Etel Formation (Turonian).

2.5Biib2- Rachmat Formation (Coniacian /Santonian).

2.5Biib3- Sirte Shale (Campanian).

2.5Biic. Kalash Limestone (Maastrichian).

2.5C. Palaeocene:

2.5Ci. Hagfa shale (Danian).

2.5Cii. Beda Formation (Selandian).

2.5Ciii. Dahra, Khalifa, Zeltan group and Khier (Selandian - Thanetian).

2.5D. Eocene:

2.5Di. Gir formation (Ypresian).

2.5Dii. Gialo Formation (Lutetian).

2.5Diii. Augila formation (Bartonian).

2.5E. Oligocene:

2.5Ei. Arida Formation.

2.5Eii. Diba Formation.

2.5F. Miocene (Marada Formation)

2.6. LIDAM FORMATION INTRODUCTION.

2.7. PREVIOUS WORKS ON THE LIDAM FORMATION.

2.8. CHAPTER SUMMARY.

2. REGIONAL GEOLOGY AND TECTONIC SETTING OF THE SIRT BASIN

2.1. INTRODUCTION

This chapter will focus on the geological history and major structural elements of the Sirt Basin and adjacent areas in Libya. The aim is to outline the geological context of the Lidam Formation (the subject of the research), to outline the regional stratigraphic succession of the sediments in the Sirt Basin during the Late Cretaceous and Tertiary Period, and to detail previous research on the Lidam Formation.

2.2. GEOLOGY AND HYDROCARBONS IN LIBYA

Libya is situated on the Mediterranean foreland of the Africa Shield, and includes a number of Palaeozoic to Mesozoic sedimentary basins (Figure 2.1).

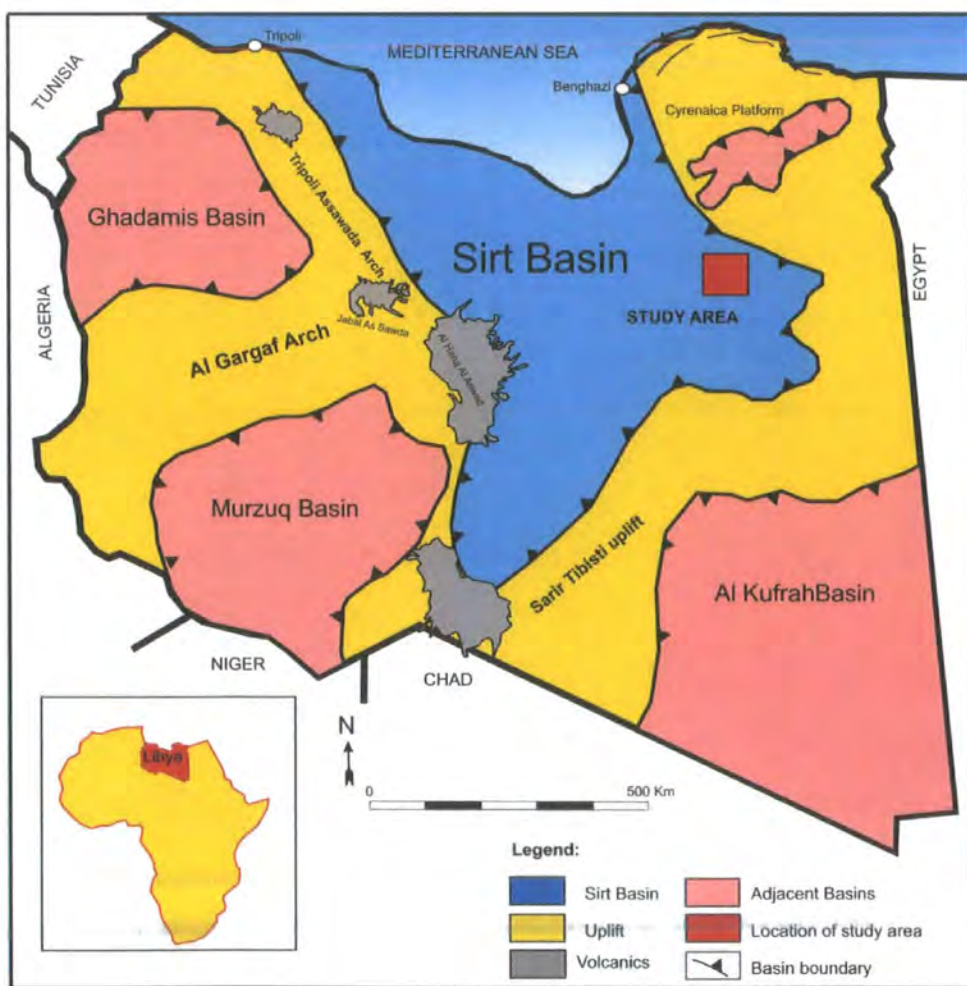


Figure 2.1. Location of the study area in the Sirt Basin and adjacent basins.

North Africa (including Libya) underwent tectonic subsidence during the Late Cretaceous as a result of reversed dextral shear along the trans-tensional plate boundary of the European and African plates. This resulted in formation of a series of basins, including; the Sirt, Ghadamis, Murzuq, and Al Kufra Basins as well as the Cyrenaica Platform (Gumati, et al., 1991) (Figure 2.1).

Major hydrocarbon discoveries have been made in the Mesozoic and Cenozoic succession in the Sirt Basin. The Sirt Basin province is highly prolific ranking 13th among the world's petroleum provinces with 500 million barrels of oil equivalent (MMBOE). Recent studies estimated that more than 50 billion barrels of oil remain in the Sirt Basin, and 10.6 billion barrels remain in the Ghadamis Basin (Thomas, 2001). Exploration in Sirt Basin began in the 1950s, with major onshore discoveries in Libya. The late 1950s saw a string of large finds in the Libyan Sirt Basin, including the Gialo (at 5 billion barrels), Sarir (at 4.5 billion barrels) and Amal (4.25 billion barrels) Fields (Ahlbrandt, 2001).

Petroleum geochemistry data confirm the dominance of the Upper Cretaceous Sirte Shale (equivalent to upper part of Rakb Group, see Figure 2.4) as the source rock of the hydrocarbons in the Sirt basin (El-Alami, 1996). The reservoirs in the Sirt basin vary in rock type and age. Reservoirs include fractured Precambrian basement and clastics of the Cambro-Ordovician Gargaf Sandstone. The Lower Cretaceous Nubian Sandstone (or Sarir Sandstone) forms the main reservoir for major giant oil fields (Abu-Attifel, Sarir and Messlah). The Sarir field is the reservoir of one of the largest oil fields in Libya with 6.5 billion barrels of recoverable oil (Clifford, 1986). It is a prolific producer in the southeastern part of the Sirt Basin. Some of the oil shale horizons of Lower Cretaceous age (the middle member of Nubian Shale or Sarir Sandstone) and some shales interbedded with halite in the Etel Formation, are possible source rocks. It is observed that these shales are confined to the southern part of the Sirt Basin, and hence their potential capacity is geographically limited in contrast to the widespread occurrence of the Sirte Shale (El-Alami, 1996).

The Lidam Formation of Upper Cretaceous (Cenomanian) age is an important carbonate reservoir rock in the southeastern part of the Sirt Basin and in the area of study. Oil fields producing from the Lidam Formation include the Masrab oil field of the southeast Sirt Basin and the Dur Mansur oil field in the western Al Bayda Platform of the central Sirt Basin (Figure 2.2). In the Sirt Basin some oil fields also produce from carbonates of the Paleocene Zeltan Formation and Eocene carbonates.

The major exploration in the Sirt basin has focused on the structural highs, principally the horst blocks, which are dominated by carbonates and Tertiary bioherms (Figure 2.2).

2.3. MAJOR STRUCTURAL ELEMENTS AND LOCATION OF THE SIRT BASIN.

The Sirt Basin (Figure 2.2) in north central Libya is one of the youngest sedimentary basins of the African craton. It was formed by large-scale subsidence and block faulting during late Jurassic /early Cretaceous rifting. In turn, the structural fabric subsequently controlled the pattern of sedimentary deposition during the late Cretaceous and early Tertiary (Gumati, 1985). The Sirt Basin covers an area of approximately 375,000 km². It is bounded to the south by the Tibesti Massif and to the west by Al Gargaf uplift separating it from the Ghadamis and Murzuq Basins. To the east, it is bounded by the Cyrenaica Platform and Al Bottnan Basin and to the north by the Gulf of Sirt (Figure 2.1).

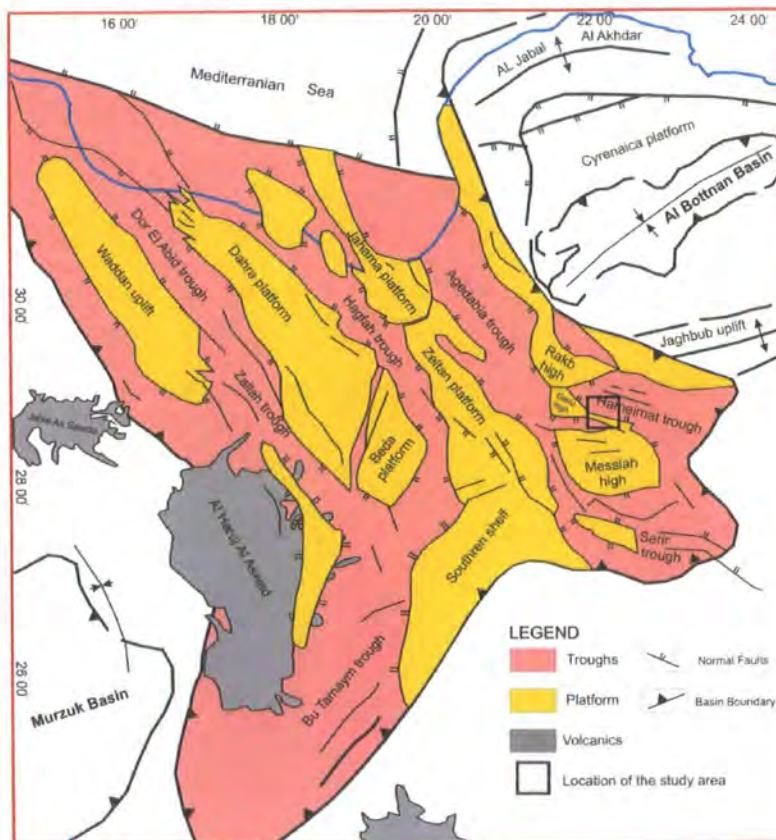


Figure 2.2. Tectonic framework of the Sirt Basin.
(Modified after Mouzoughi and Taleb, 1981).

The Sirt Basin is one of the important structural features of north Libya and to date is unsurpassed in its petroleum potential by other Libyan onshore or offshore locations, for example, the Ghadamis or Pelagian Basins. It contains more than one hundred oil and gas fields, including several giant oil fields. The Sirt Basin is heavily fractured with major faults resulting in a number of major NW-SE trending grabens (Figure 2.2). These are from NW to SE; the Hun Graben, Dor El Abid, Zallah, Bu Tamaym, Hagfa, Agedabia, Hameimat, and Sarir Troughs. The platforms on intervening horst blocks are from the west to the east; the Waddan Uplift, Dahra, Beda, Zelten, Jahamah Platforms and Rakb High (Abadi, 2002).

The major hydrocarbon pools are related to the platforms and palaeohighs. Overall the basin slopes considerably tilted in an ENE direction towards the Mediterranean Sea. The area of study is located on the Gailu Platform (wells 3V1-59E, 3V3-59E, and R1-97) and the Hameimat trough (wells P3-97 and N6-97).

2.4. TECTONIC SETTING AND GEOLOGICAL HISTORY OF THE SIRT BASIN.

The North African region was subjected to diachronous rifting with subsequent post-Mesozoic continental collision, leading to the development of basins with complex histories. A number of different tectonic domains existed, with each basin having a unique tectonic history (Carr, 2003). The Sirt Basin is a major intracratonic rift system on the north central African plate and comprises a complex of horst and grabens that began to develop during the Latest Jurassic / Early Cretaceous. The tectonic evolution of the Sirt Basin involved thermal arching and repeated phases of rifting that culminated in the Late Cretaceous and Paleocene to Early Eocene, which were followed by thermal subsidence from Late Eocene onwards (Abadi, 2002). The sedimentary succession of the Sirt Basin reflects its tectonic and structural evolution, which is closely related to the opening of the Atlantic Ocean and the convergence of the Tethys in Mesozoic and Tertiary times (Gras and Thusu, 1998).

The geologic history and the major structural elements of the region were first clearly elucidated by Klitzsch, (1970). Early in the geologic history, a long period of erosion prevailed throughout North Africa, and by the beginning of the Paleozoic Era a great part of Libya had been peneplained (Goudarzi, 1980). According to El Alami (1996), the geological history of the Sirt Basin during the Upper Cretaceous period demonstrated that there has been gradual onlapping over the fault-block topography

by marine sediments and it was the very end of the late Cretaceous that almost all the topographic eminences were buried. According to Massa and Delorite (1984) the structural development of the Sirt basin region from Lower Palaeozoic to the present (Figures 2.3a, b, c, d, e, f, g, and h) are outlined below:

1- At the beginning of the Palaeozoic Era a great part of Libya had been eroded through various surface processes. Precambrian crystalline rocks were exposed after a long period of erosion prevailed throughout North Africa. Small exposures of the basement occur in the south central part of the Sirt basin, also in the Tibisti area, in the SE part near the border with Sudan and Egypt, Jabal Al Hasawinah and north of Waw an Namus.

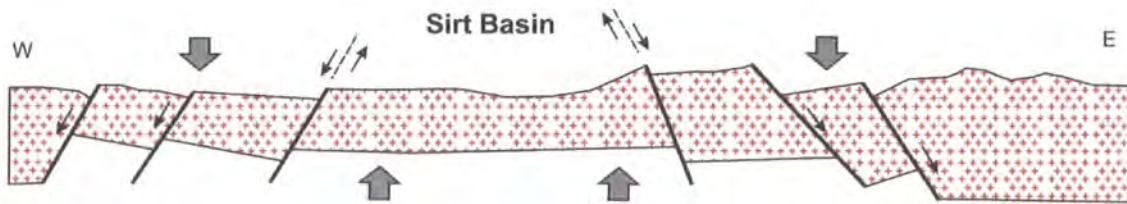


Figure 2.3a. Precambrian (basement) in the area that will become the Sirt Basin, (Key on Figure 2.3h).

2- During the Cambro-Ordovician quartzitic sandstone were deposited up to 1000m thick, overlying the Precambrian basement throughout the northern part of the Sirt basin (Anketell, 1996).

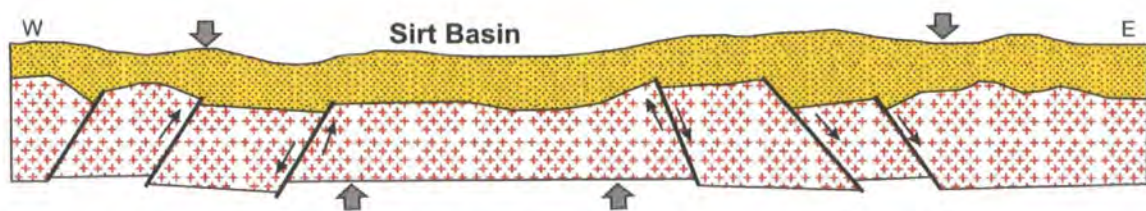


Figure 2.3b. Tectonic evolution of the Sirt Basin during Cambro-Ordovician period (Key on Figure 2.3h).

3- The Silurian deposits thin across the area that will become the Sirt Basin. Alkaline magmatism is associated with the uplift of the Tibisti-Sirt arch during the Hercynian Orogeny (Klitzch, 1970).

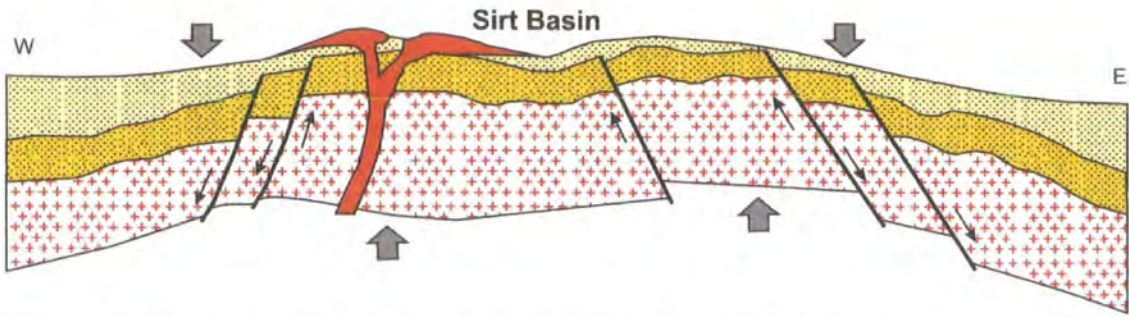


Figure 2.3c. Tectonic evolution of the Sirt Basin during the Silurian period.

(Key on Figure 2.3h).

4- During the Devonian sedimentation continued in the adjacent areas to the east and west while inversion of the region, together with increased igneous activity, continued in the region that will become the Sirt Basin.

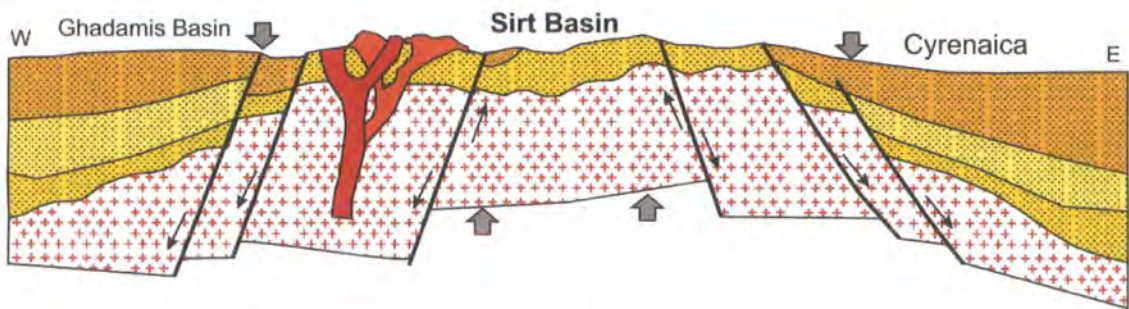


Figure 2.3d. Tectonic evolution of the Sirt Basin during the Devonian period.

(Key on Figure 2.3h).

5- The sedimentation continued during the Permo-Carboniferous both to the west and east of the palaeohighs of the Sirt arch, where there was active subsidence. Volcanic activity continued from the Devonian and reached a maximum during the Permo-Carboniferous period.

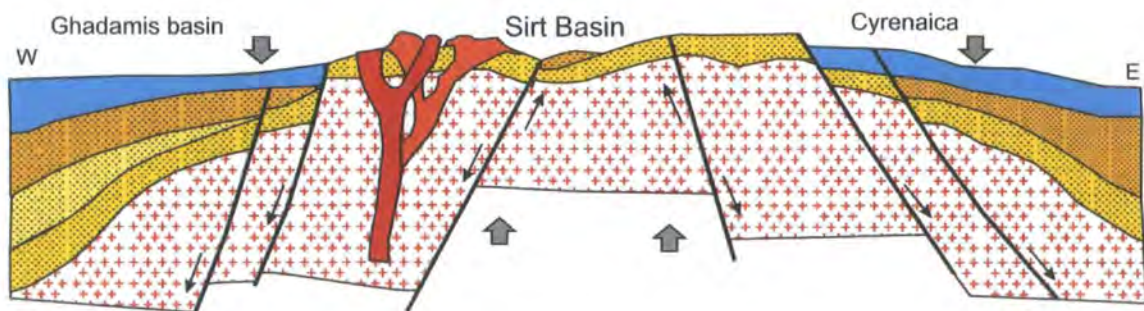


Figure 2.3e. Tectonic evolution of the Sirt Basin during the Permo-Carboniferous period.

(Key on Figure 2.3h).

6- Post-Hercynian movement affects the area that will become the Sirt Basin during the Triassic to Jurassic. Movement is accompanied by eruption of basic magma. The deposition of sediment during the Triassic- Jurassic continued on the eastern and western sides of the Sirt Arch.

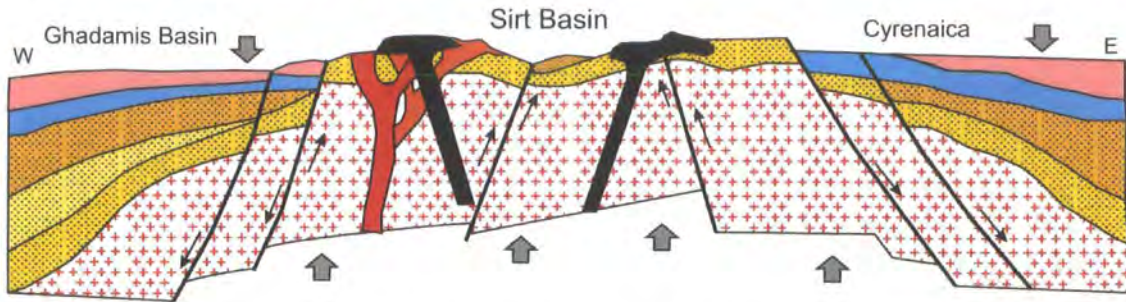


Figure.2.3f. Tectonic evolution of the Sirt Basin during the Triassic and Jurassic period.

(Key on Figure 2.3h).

7- The area that will become the Sirt Basin remained a positive feature until the Latest Jurassic when the Sirt Basin area gradually subsided, probably for the first time since the Early Paleozoic. Subsidence resulted from extension that led to the collapse of the pre-existing Sirt arch (Klitzch, 1970). The Sirt Basin area experienced stretching and down faulting during the Cretaceous. Large scale subsidence and block faulting began in the Latest Jurassic / Early Cretaceous.

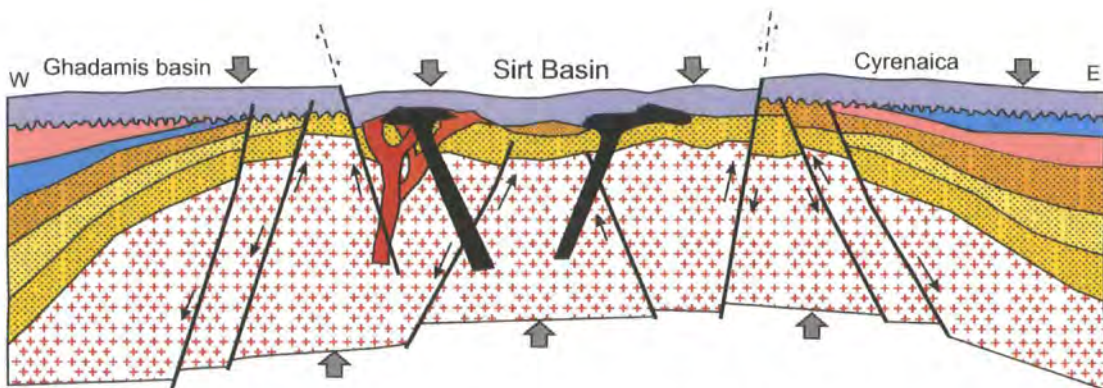


Figure.2.3g. Tectonic evolution of the Sirt Basin during the Early Cretaceous.

(Key on Figure 2.3h).

8- The faults in the Sirt Basin reactivated during the Late Cretaceous with reactivation continuing into the Early Palaeocene and Late Eocene. Volcanic activity resumed again in post-Eocene times and is believed to have been concurrent with movement along major basement fault zones situated outside the Cretaceous rift on

the western side of the Sirt Basin. According to Gumati and Kanes (1985) subsidence of the Sirt basin reached a maximum during Paleocene/ Eocene time.

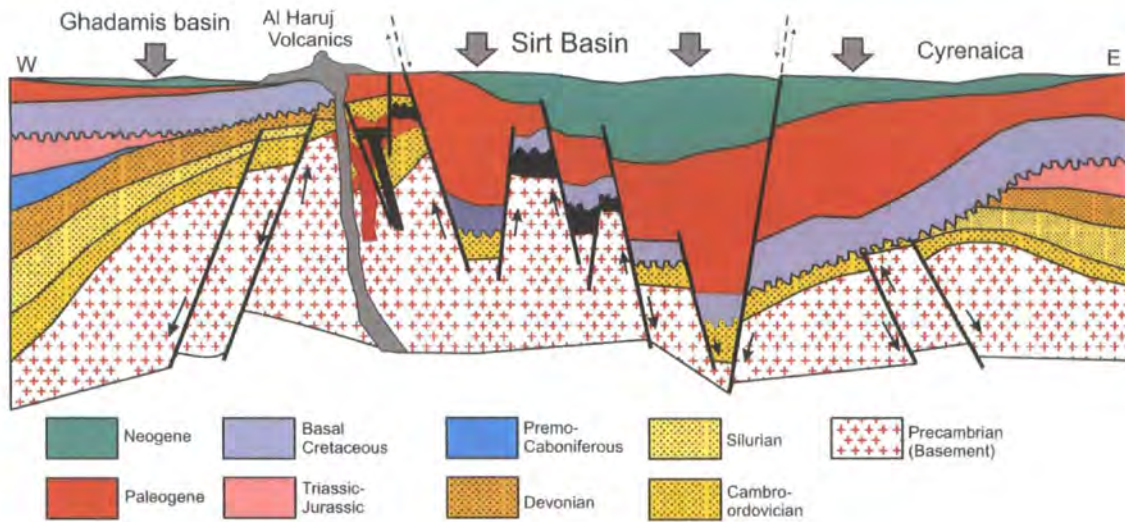


Figure.2.3h. Tectonic evolution of the Sirt Basin: present day setting.

2.5. SIRT BASIN STRATIGRAPHY

This section outlines the stratigraphic succession of the Sirt Basin including the Upper Cretaceous Lidam Formation, the topic of this research (Figure 2.4). Deposition in the Sirt Basin was accompanied by intensive basement block-faulting, which dominated depositional trends. Regional subsidence occurred in the Late Cretaceous with progressive marine onlap onto highs (Belazi, 1989). Marked variation in the stratigraphic thickness of offshore marine mudstone is recognized, with thick mudstone deposited in troughs thinning onto highs on which shallow-marine sandstone was coevally deposited (Belazi, 1989). Marine deposition took place within the Sirt Basin grabens which had a sandy paralic to non-marine fringe (Van Houten, 1980; Wenneker et al. 1996; El-bakai, 1996).

These clastic units pass transgressively up into Late Cretaceous shallow water limestone and sandstone, which pass laterally, basinward into interbedded open-marine limestones and shales (Belazi, 1989). The limestones pass gradually into shales with thin interbeds of limestone and sandstone. In the latest Cretaceous, the Sirt Basin was an open marine domain (Belazi, 1989 and Wenneker et al. 1996). The transgression had reached the Murzuq Basin by the late Cenomanian, and continued to spread southwards from the Sirt Basin (Van Houten, 1980).

2.5A. BASEMENT

The Palaeozoic succession in the Sirt Basin is poorly developed due to non-deposition in the late Palaeozoic, and to Hercynian uplift and resultant early Mesozoic erosion. Cambro-Ordovician or Precambrian rocks immediately underlie Cretaceous strata. The basement, cored in wells in the subsurface of southeastern part of the basin, is mainly metamorphic rocks (chlorite schist and phyllites) and crystalline granites (Figure 2.3a).

2.5B. CRETACEOUS STRATIGRAPHY

The Cretaceous rocks in the Sirt Basin can be divided into two parts;

2.5Bi. Pre-Upper Cretaceous: (Lower Part)

The term "Nubian Sandstone" is used in North Africa for a thick package of clastic dominated sediments spanning an interval from the Palaeozoic in Egypt to Early Cretaceous in Libya. In Libya, some of the oil companies prefer to use the term 'Sarir Sandstone'. This formation is a significant reservoir target with major fields such as the Sarir (5 billion barrels recoverable oil / hydrocarbons) and Messla Fields (3 billion barrels recoverable oil / hydrocarbons).

The Nubian Sandstone is a well-defined and widespread stratigraphic unit, which can only be recognized from subsurface wells in the Sirt Basin. The Nubian Sandstone consists of three members; Upper sandstone, Middle shale and Lower sandstone. The Nubian sediments are overlain by younger Upper Cretaceous sediments in the eastern part of the Sirt Basin. Thicknesses in excess of 15,000ft of Nubian sediments are thought to be present in the Agedabia, Sarir and Hameimat Trough. (Figure 2.4)

The Hercynian unconformity separates the Nubian Sandstone from the underlying granite, metamorphic and Camro-Ordovician basement. The upper contact of the sandstone is also unconformable, where it is overlain by the early Late Cretaceous Lidam Formation throughout the basin. The Nubian Sandstone of the Sirt Basin, according to Barr and Weegar (1972), is composed of a variety of interbedded non-marine lithofacies including sandstones, siltstones, shales and conglomerates. The sandstones are very fine to coarse grained quartzite, tan to grey in colour and poorly to moderately sorted, with a clay matrix and very porous.

This formation is very important in the Sirt Basin, where it forms the principal petroleum reservoir in the giant oil fields of the Southeastern part of the Sirt Basin.

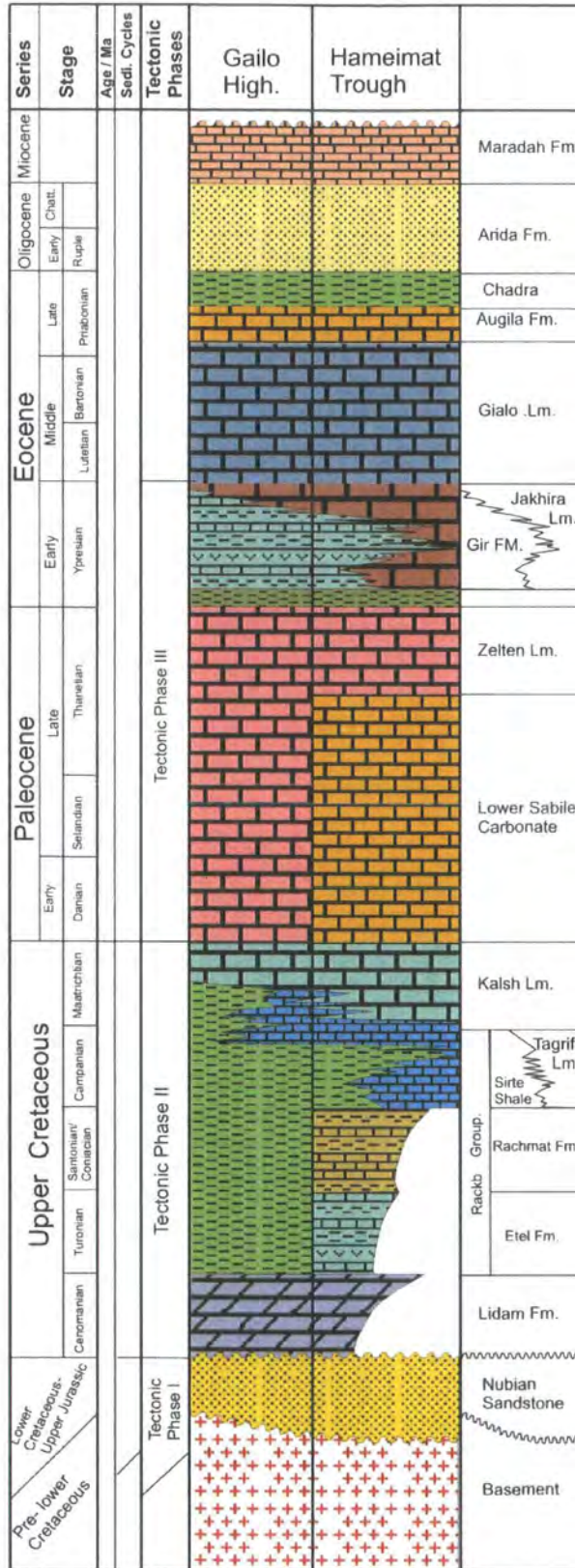


Figure 2.4. Generalized stratigraphic / lithologic chart of the Upper Cretaceous and Tertiary succession on the study area, (After Barr and Weegar, 1972).

2.5Bii- Upper Cretaceous: (Upper Part)

In the study areas the Upper Cretaceous strata consists of four formations which are described below in order of younging:

2.5Biia- Lidam Formation (Cenomanian)

This formation is the focus of this study. Previous published data on the formation is described in section 2.7 and new data collected during this study is discussed in more detail throughout the rest of the thesis. The name (Lidam) was proposed for the formation by Barr and Weegar (1972), and was first applied to subsurface units in various parts of the Sirt Basin. The name is derived from the Mobil Lidam well (B1-57). The Lidam Formation is considered as Cenomanian in age (Figure 2.4). It consists of light brown - grey coloured dolomite, the lower part some times sandy indicating a local mixing with the underlying sandstone. Ooid rich intervals are present in the upper part of the Lidam Formation (Barr and Weegar, 1972). The Lidam Formation is considered the first marine transgressive unit in the Sirt Basin. It unconformably overlies the Bahi and Nubian Sandstone (Sarir Sandstone), Palaeozoic strata (Hofra and Amal formations) or igneous and metamorphic basement, (Barr and Weegar, 1972).

2.5Biib. Rakb Group:

The Rakb Group is divided into three formations (Etel, Rachmat and Sirt shale) and is unconformably overlain by the Maastrichian Kalash Limestone, and underlain by the Lidam Formation, (Figure.2.4).

These sediments thicken to the troughs and thin to the platforms. This group was deposited during a marine transgression and is subdivided into the following formations:

2.5Biib1- Etel Formation (Turonian)

The Etel Formation is widespread across the central and southern part of the Sirt Basin but is absent on regional highs. The formation consists of thin-bedded carbonates, shale, anhydrite, siltstone and sandstone. Formation thickness ranges from 660 m in the Hagfa Trough to over 700 m in the Hameimat Trough. The Etel Formation usually conformably overlies the Lidam Formation and underlies the Rachmat Formation in the study area (Figure.2.4). The Aragub carbonate is regarded as a basinward equivalent of the Etel Formation (Barr and Weegar, 1972). The shale intervals within the Etel formation are considered to be the principal source rock in the Hameimat Trough (El Alami, 1996).

2.5Biiib2- Rachmat Formation. (Coniacian /Santonian)

The Rachmat Formation consists of shales interbedded with minor limestones, sandstones and dolomites. The shales are dominantly grey, fissile to slightly blocky, slightly to non-calcareous, and glauconitic and pyritic in many locations, (Barr and Weegar 1972). The dolomites are common in the basal part and characterized by tan to brown, microcrystalline dolomite (Duronio and Colombi, 1983). The microfossil assemblage indicates that this formation is Santonian to Coniacian in age. This formation is present in the study area and it is absent on the platform highs in the Sirt Basin, but has a maximum thickness of up to 600 m in the Agedabia Trough. It unconformably overlies the Aragub carbonate, Etel Formation, the Bahi or Maragh Sandstone or rests unconformably on the Amal Formation or granite basement. The Rachmat Formation is mostly conformably overlain by the Sirte Shale, depending on its position in the Sirt Basin (Figure.2.4). This formation was deposited in a shallow open-marine to slightly protected setting (Barr and Weegar, 1972).

The Rachmat Formation is a significant petroleum source rock for the oil fields located along the crest axis of the basement highs of the Sirt Basin. The Rachmat shale also provides an excellent seal over the Etel Formation (El Alami, 1996).

2.5Biiib3- Sirte shale (Campanian)

The Sirte Shale is considered the main source rock in the Sirt Basin and it is widely distributed throughout the grabens of the Sirt Basin. It consists of a dark-grey to brown shale succession with minor limestone interbeds. Occasionally, the shale is calcareous, silty, sandy and glauconitic or pyritic with small phosphatic nodules in the lower part. The Sirte Shale is conformably overlain by the Maastrichtian Kalash Limestone and underlain by the Rachmat Formation (Figure 2.4). This formation was initially deposited in a shallow restricted marine environment, rapidly subjected to deepening (Duronio and Colombi, 1983). The formation attains an average thickness of about 270 ft increasing towards the troughs in the Sirt Basin and thinning towards palaeohighs of the Sirt Basin. This formation ranges in age from lower Maastrichtian to lowermost Campanian according to Barr and Weegar (1972).

2.5Biic. Kalash limestone (Maastrichian)

The Kalash Limestone is widely distributed in most of the Sirt Basin with a near uniform thickness reaching 600 m in the northern part of Agedabia and Hameimat Troughs (study area). The limestone is conformably overlain in many places by the Paleogene Hagfa Shale or Lower Sabil Carbonate, (Figure 2.4). The Kalash Limestone consists of white, tan or grey to dirty white argillaceous calcilutite intercalated with thin beds of dark grey shale. Both benthic and planktonic foraminifera are abundant (*Globotruncana*, *Rugoglobigerina*), which indicates that this formation was deposited under open-marine, probably neritic conditions during the Maastrichtian time (Barr and Weegar, 1972).

2.5C. PALAEOCENE SEDIMENTS

2.5Ci- Hagfa shale (Danian)

The Hagfa Shale is located throughout the central and western Sirt Basin. It formed in an open sea environment during the Danian. The Hagfa shale is conformably overlain by the Beda Formation, and conformably overlies the Kalash Limestone (Figure 2.4). It consists of shale with thin limestone interbeds that are more common in the upper part. The depositional environment of the Hagfa shale in the central and western part of the Sirt Basin was deep marine, probably outer to neritic upper bathyal (Barr and Weegar, 1972).

2.5Cii. Beda Formation (Selandian)

The Beda Formation is Selandian deposits consisting mainly of various interbedded limestone lithofacies with subordinate dolomite and calcareous shale in the southwestern Sirt Basin (Figure 2.4). In the northwestern part of the basin the formation becomes more shaly. This formation was deposited in a shallow-marine environment (Barr and Weegar, 1972).

2.5Ciii. Dahra, Khalifa, Zelten Group and Khier (Thanetian)

The Dahra Formation are Thanetian deposits which consist mainly of white to light grey chalky, calcarenite, calcilutite and subordinate tan to brown microcrystalline dolomite and thin interbeds of dark shale with minor anhydrite in the upper part of the formation (Barr and Weegar, 1972). In the southwestern part of the basin, the lower part of the formation becomes more shale. This formation is the lateral equivalent of the lower shale units of the Khalifa Formation. The Khalifa Formation is located in the subsurface of the western and central basin, and consists mainly of

argillaceous limestones which were deposited in a shallow-marine environment, (Barr and Weegar, 1972). The Jabal Zelten Group is subdivided into two formations; the Zelten and Harash Formations (Figure 2.4). The Zelten Formation consists mainly of limestone with shale. The Harash Formation consists mainly of white to brown, argillaceous calcilutite and muddy calcarenite with thin interbeds of calcareous, fissile shale (Barr and Weegar, 1972). The Khier Formation formed under open marine environments and consists mainly of shale with some clay, marl and limestone.

2.5D. EOCENE

2.5Di. Gir Formation, Early Eocene (Ypresian)

The Gir Formation is subdivided into three members; the Facha, Hun Evaporite and Mesdar Members (Figure 2.4). The Gir Formation consists of a massive succession of interbedded anhydrite, dolomite and limestone with thin beds of shale in the central and eastern part of the basin. It is thought to have formed in an open-marine environment (Barr and Weegar, 1972).

2.5Dii. Gialo Formation, Middle Eocene (Lutetian & Bartonian)

The Gialo Formation is widespread in most of the basin. It consists of a thick sequence of shallow marine limestones including muddy Nummulitic calcilutite and calcarenite. The depositional environment was shallow, open marine conditions (Barr and Weegar, 1972).

2.5Diii. Augila Formation, Late Eocene (Priabonian)

The Augila Formation is subdivided into three members; the lower member is soft shale interbedded with thin argillaceous limestone or dolomite, the middle member is porous, glauconitic quartz sandstone, and the upper member is a sandy, slightly glauconitic limestone. The lower member is characterized by open marine environments and the upper by shallow marine environments. The upper part of the formation is unconformably overlain by the sandstone of the Arida Formation (Barr and Weegar, 1972).

2.5E. OLIGOCENE

The **Najah Group** is located in the eastern and central part of the basin; with the Arida as the lower formation and the Diba as the upper formation of the Najah Group, (Figure 2.4).

2.5Ei. The **Arida Formation** is located in the south-central part of the basin. It is subdivided into a lower unit that consists mainly of sandstone and an upper unit consisting of shale. The formation was deposited under laterally variable conditions, as represented by a rapid change in the environment from continental sandstones in the southeast to carbonates in the north.

2.5Eii. The **Diba Formation** is located in the south-central part of the basin and consists of an alternating sequence of thick, fine to coarse sandstone units and thin, soft shale (Barr and Weegar, 1972).

2.5F. MIOCENE

The **Marada Formation** is Miocene deposits within the basin, consisting of interbedded shales, sandstone, sandy limestone and calcarenite. The formation includes a number of rapidly changing facies, which accumulated as interfingering of various continental, littoral, and shallow-marine deposits (Barr and Weegar, 1972).

2.6. LIDAM FORMATION INTRODUCTION

The Lidam Formation is the target of this study, and it is a widespread unit extending over much of the Sirt Basin. In the type section (Figure 2.5) it consists of well cemented packstone/ grainstone containing skeletal grains, peloids in the upper part and very fine to coarsely grained crystalline dolomite in the lower part, (Barr and Weegar, 1972).

The Lidam Formation in the study area, of the southeast Sirt Basin is composed of a thick unit of carbonates, evaporites and sand layers. At the base, it consists of light grey stromatolitic dolomite interbedded with anhydrite and sand layers, the middle part are packstone / grainstone grading into grainstone.

The upper part is light brown bioturbated limestone, slightly argillaceous, and mottled with intercalation of shale. The upper part is mainly peloidal wackestone / packstone, light to dark grey, dolomitized lime mudstone interbedded with nodular anhydrite and shale. The Lidam Formation is the main reservoir unit in the south-east and central part of the Sirt Basin.

The Lidam Formation unconformably overlies various units including the Nubian Sandstone, Bahi Formation and igneous-metamorphic basement. It is usually overlain by the Etel Formation (Figure 2.4). It is considered as Cenomanian in age by Barr and Weegar (1972).

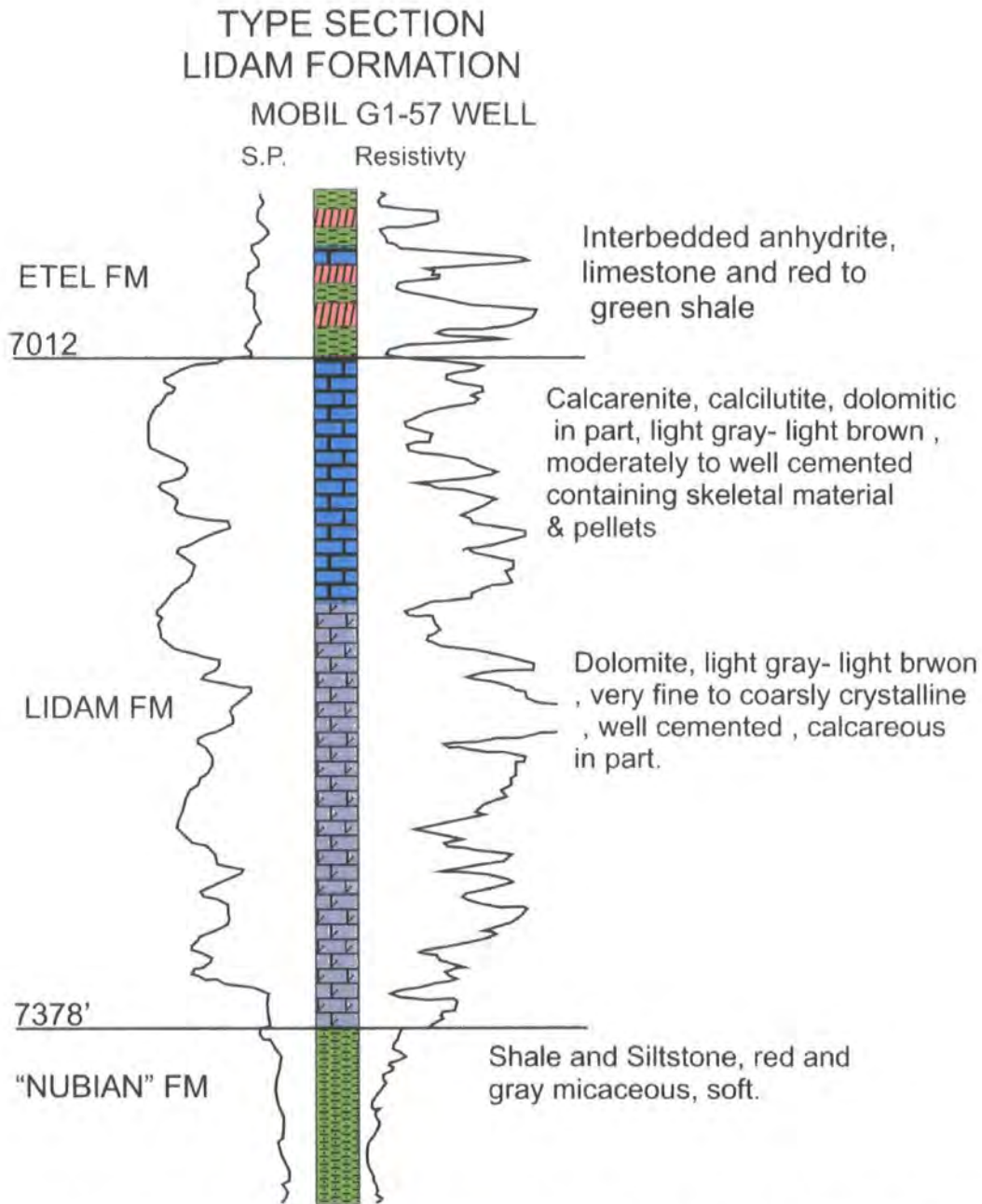


Figure 2.5. Type Section of the Lidam Formation in the Sirt Basin (After Barr and Weegar, 1972).

2.7. PREVIOUS WORKS ON THE LIDAM FORMATION.

Little detailed work has previously been published on the sedimentology of the Lidam Formation. The formation was first mentioned by Barr and Weegar (1972) in the Stratigraphic Nomenclature of the Sirt Basin, Libya. Some unpublished reports on this stratum have been generated by oil companies, and most of the data remains in closed company files.

Recently hydrocarbon exploration has targeted the Lidam Formation because of its potential as an oil producing zone in the Sirt Basin and several detailed papers and reports on these strata have recently been published in the petroleum research journal (Libya). Bakai (1991) undertook a petrographic and diagenetic study of the Lidam Formation (Carbonate units) from four cored wells; D1, A1, A4, and A6 concession 32, (Bahi field) located on the Dahra Platform, central Sirt Basin. Bakai, (1991) divided the Lidam Formation into two units; a limestone unit and a dolomite unit. These units were interpreted as accumulating in tidalflat settings of supratidal, intertidal and subtidal environments.

Bakai (1992) discussed the environment of deposition of the Lidam Formation in the NW of Sirt Basin. Three lithofacies were recognized in the Lidam Formation; the lower lithofacies were deposited in an open marine (outer ramp), the middle lithofacies represent sedimentation in an inner ramp setting, and the upper lithofacies represents sedimentation in a restricted marine or inner-ramp setting.

Bakai (1992) studied the diagenesis and diagenetic history of the Lidam Formation in the NW Sirt Basin. It was recognized that the Lidam Formation in this area is mainly mudstone / wackestone and oolitic grainstone. Diagenetic changes recognized included boring, burrowing, compaction, dolomitization and cementation, and five diagenetic types of dolomite were recognized in the Lidam Formation.

Bakai (1993) studied microprobe analysis of glauconitic pellets from the Lidam Formation in the NW Sirt Basin, Libya. The glauconitic pellets have been classified into three types. These are; grass-green pellets, light-green pellets, and brownish-yellow pellets. These glauconitic pellets are a valuable marine indicator, they occur mainly in relatively shallow water, at depths between 60- 500 m. They are particularly characteristic of the inner part of the continental shelf.

2.8. CHAPTER SUMMARY

The Sirt Basin formed as a result of reversed shear along the trans-tensional plate boundary of Europe and Africa. The tectonic subsidence of the basin was continuous throughout Late Cretaceous and Tertiary times, reaching a maximum during the Paleocene and Eocene, when a major reactivation of faults occurred controlling the pattern of sedimentary deposition of the Sirt Basin. The facies variation and thickness in the Sirt Basin are controlled by pre-existing topographic highs, whether structural or geomorphic.

The stratigraphic succession of the Sirt Basin area during the pre-Upper Cretaceous is dominated by deposition of non marine clastic sediments including; sandstone, siltstone, shales, and conglomerates. During late Cretaceous from Cenomanian to Maastrichian time several hundred feet of carbonate and shale were deposited, reaching a maximum thickness in low areas, these sediments were deposited in open marine environments. From the Paleocene to late Eocene the Sirt Basin was dominated by shallow marine facies of limestone, dolomite and evaporite. These facies grade upwards into continental to shallow-marine sediments, which formed under arid conditions during the Oligocene and Miocene.

CHAPTER THREE

*FACEIS ANALYSIS OF THE LIDAM
FORMATION*

CHAPTER THREE

FACEIS ANALYSIS OF THE LIDAM FORMATION

3.1. INTRODUCTION.

3.2. FACIES ANALYSIS METHODOLOGY.

3.3. FACIES ANALYSIS OF LIDAM FORMATION.

3.3.1. Anhydrite Facies (AF).

3.3.2. Dolomite Facies (DF).

3.3.3. Sandy Facies (SF).

3.3.4. Shale Facies (SF).

3.3.5. Stromatolitic Facies (STF).

3.3.6. Ostracoda Facies (OSF).

3.3.7. Mollusc Facies (MF).

3.3.8. Bioclastic Facies (BF).

3.3.9. Peloidal Facies (PF).

3.3.10. Stromatoporoid Facies (STPF).

3.4 DISCUSSION AND OVERALL DEPOSITIONAL INTERPRETATION

3.5 CHAPTER SUMMARY

3. FACEIS ANALYSIS OF THE LIDAM FORMATION

3.1. INTRODUCTION.

This chapter concentrates on defining and interpreting the depositional environment of facies of the Lidam Formation from the five studied wells (P3-97, N6-97, R1-97, 3V1-59E, and 3V3-59E). Facies were defined on the basis of detailed petrographic study and core description, including fossil content, sedimentary structures, and lithological description. The main objectives of this chapter are:

1. To detail petrographic and core analysis and to infer the depositional setting of the different lithofacies identified from the Lidam Formation in the studied wells.
2. To investigate an overall model for the depositional environment of the Lidam Formation.

3.2. FACIES ANALYSIS METHODOLOGY

Core descriptions were combined with petrographic analysis performed on 70 thin sections. The classification of the microfacies of the Lidam Formation is based on the standard microfacies (SMF) types of Wilson (1975), the main criteria used in differentiating SMFs comprise: grain types, matrix types, and depositional textures. These petrographic features are combined with additional information from core descriptions, such as fossil content, and the depositional texture types defined by Dunham in his classification (1962). Vertical variations in the lithology were also noted from core including sedimentary structures, vertical facies relationship, and evidence for biogenic activity. Microfacies names used here combine the textural classification of Dunham (1962) with the components of the lithology.

Facies names are simplified and based on the main component, for example the bioturbated mollusc packstone and partially dolomitized mollusc packstone microfacies together make up the Mollusc Facies. The facies and microfacies identified are summarized on Table 3.1.

No:	FACIES	MICROFACIES	GRAIN TYPES	DEPOSITIONAL ENVIRONMENT
1	Anhydrite	1.Chicken wire anhydrite	Light grey anhydrite interbedded with dolomitic layers. Nodular chicken wire fabric common.	Sabkhas and tidal flats.
2	Replacive dolomite	1.Fine dolomite	Light to dark grey, rhombic fine crystalline dolomite (idiotopic texture) and mosaic dolomite. Dolomite facies contains scattered bioclastic debris and may show remnant mudstone / wackestone.	Diagenetic overprint probably originally restricted, shallow water lagoon and/ or peritidal deposits.
3	Siliciclastic	1. Lithic sandstone 2. Bioclastic sandstone	Fine grained and fine clay matrix with thin iron oxide rims. Carbonate grains are lithoclasts, mixture of small forams and bioclastic debris scattered through the bioclastic sandstone facies.	Near coastal plain sandstones, with reworking of shallow marine material.
4	Shale	Shale	Dominantly intercalated with dolomite and limestone, these shales are medium dark grey to black grey. Silt- and clay-sized particles dominate and the rock is laminated and fissile.	Protected, or perhaps restricted, lagoonal area with terrestrial clay input.
5	Stromatolitic	1. Stromatolitic mudstone	Light grey, wavy to crinkly stromatolitic laminae.	Mainly formed by the growth of microbial mats, near the margins of the shallow coastal lagoons and intertidal area.
6	Ostracod	1.Ostracod bioturbated wackestone	Light - medium brown, fine to very fine grained bioclasts, slightly argillaceous and highly bioturbated. Dominant depositional fabric is mudstone / wackestone grading into packstone. The skeletal grains are ostracods associated with small forams (rotaliids and miloilids), echinoderm, bryozoans, dasycladcean algae and mollusc fragments.	Shallow-water intertidal to subtidal environments. These sediments are deposited under low wave energy with restricted circulation and possibly hypersaline conditions.

Table 3.1. Facies and microfacies of the Lidam Formation in the studied wells, Southeastern part of the Sirt Basin, Libya.

No:	FACIES	MICROFACIES	GRAIN TYPES	DEPOSITIONAL ENVIRONMENT
7	Mollusc	1. Mollusc bioturbated packstone. 2. Partially dolomitized Mollusc Packstone.	Wackestone / Packstone, light grey, fine to coarse, highly bioturbated, contains mollusc fragments (bivalves and oysters), echinoderm, and other bioclastic grains of small foraminifera (rotaliids) and ostracods.	Low energy environment below wave base, shallow marine conditions, inner platform setting.
8	Bioclastic	1. Foraminifera packstone / grainstone. 2. Echinoderm packstone.	Wackestone / packstone into grainstone. Medium grey, fine-very fine grained, slightly argillaceous, highly bioturbated with intercalations of shale, and irregularly laminated. Skeletal grains are mollusc and echinoderm fragments and miliolids, calcareous algae, and bioclastic debris. Non skeletal grains are mainly peloids.	Shallow shoal to back shoal intertidal to subtidal environments in shallow-water with wave influence.
9	Peloidal	1. Peloidal grainstone. 2. Peloidal ooidal grainstone.	Light grey to dark grey, slightly argillaceous, laminated oolitic grainstone, slightly bioturbated, medium-grained, moderately sorted. Non-skeletal allochems are peloids, ooids and intraclasts associated with skeletal grains of miliolids, mollusc fragments, bryozoans, and other bioclastic debris.	Oolitic shoal to back shoal, high energy subtidal environment.
10	Algal	1. Squamariacean / coralline algae bindstone.	Light grey to medium grey, slightly nodular in structure with pressure solution seams. The facies has a packstone depositional texture. Two types of algae are found coralline algae and squamariacean (Polystrata) crusts algae that occur at this interval together with encrusting foraminifers. The matrix is replaced by dolomite crystals.	Probably deposited as a localized patch reefs.

Table 3.1 (continued). Facies and microfacies of the Lidam Formation in the studied wells, southeastern part of the Sirt Basin, Libya.

Facies	Depth (feet)	Illite/Smect.	Illite + mica	Kaolinite	Chlorite	Quartz	K Feldspar	Plagio-clase	Calcite	Dolomite	Barite	Anhydrite	Pyrite	Total
Stromatolitic	10448	0.0	0.0	0.0	0.0	1.1	0.0	0.0	0.0	5.5	0.0	93.5	0.0	100
Stromatolitic	10460	0.0	0.0	0.0	0.0	6.4	0.0	0.0	1.4	89.7	0.0	2.4	0.0	100
Ooidal peloidal	10468.5	0.0	0.0	0.0	0.0	3.0	0.0	0.0	94.1	2.2	0.0	0.6	0.0	100
Foraminifera bioclastic	10474.5	6.1	6.9	0.0	0.0	11.6	0.0	0.0	5.4	66.2	0.0	1.1	2.7	100
Ostracod	10484.5	0.0	0.0	0.0	0.0	3.5	0.0	0.0	95.1	0.7	0.0	0.6	0.0	100
Ostracod	10489.5	0.0	0.0	0.0	0.0	3.5	0.0	0.0	95.8	0.7	0.0	0.0	0.0	100
Anhydrite	10505	0.0	0.0	0.0	0.0	2.2	0.0	0.0	4.0	28.2	0.0	65.6	0.0	100
Ostracod	10511.5	3.7	2.9	0.0	0.0	11.6	0.0	0.0	77.6	1.5	0.0	1.8	1.0	100
Anhydrite	10520	0.0	0.0	0.0	0.0	0.8	0.0	0.0	4.1	0.0	0.0	94.3	0.8	100
Anhydrite	10524	0.0	0.0	0.0	0.0	0.5	0.0	0.0	1.2	1.1	0.0	97.2	0.0	100
Bioclastic sandstone	10525	0.0	0.0	4.7	0.8	88.8	0.0	0.0	0.4	0.0	0.0	3.1	0.0	100
Anhydrite	10539	0.0	0.0			3.2	0.0	0.0	6.1	0.0	0.0	90.7	0.0	100
Sandstone	10542	0.0	3.2	1.0	1.5	69.3	1.7	3.2	4.6	0.0	0.6	14.9	0.0	100

Table.3.3. Whole rock X-ray diffraction (XRD) analysis in well: 3V1-59E

Facies	Depth (feet)	Illite/Smectite	Illit	Kaolinite	Chlorite	Quartz	Calcite	Dolomite
Foraminifera bioclastic	10474.5	41.4	47.0	0.0	0.0	7.5	0.0	4.2
Ostracod	10511.5	37.4	3.0	32.5	0.0	1.9	28.2	0.0
Bioclastic sandstone	10525	0.0	Tr	70.1	17.4	12.5	0.0	0.0
Sandstone	10542	0.0	62.0	9.1	22.5	6.4	0.0	0.0

Table.3.4 X-ray diffraction (XRD) analysis for < 2 micron clay in well: 3V1-59E

Facies	Depth (feet)	Illite/Smect.	Illite + mica	Kaolinite	Chlorite	Quartz	K Feldspar	Plagioclase	Calcite	Dolomite	Barite	Anhydrite	Pyrite	Total
Ooidal peloidal	10198	0.0	0.0	0.0	0.0	8.0	0.0	0.0	61.5	30.5	0.0	0.0	0.0	100
Ooidal peloidal	10207	0.0	0.0	0.0	0.0	6.8	0.0	0.0	2.9	90.3	0.0	0.0	0.0	100
Ooidal peloidal	10212	0.0	0.0	0.0	0.0	3.3	0.0	0.0	92.3	2.8	0.0	1.7	0.0	100
Ostracod	10221	0.0	0.0	0.0	0.0	5.2	0.0	0.0	93.4	0.9	0.0	0.5	0.0	100
Bioclastic	10230	0.0	0.0	0.0	0.0	4.2	0.0	0.0	93.3	2.5	0.0		0.0	100
Dolomitic mudstone	10253	0.0	0.0	0.0	0.0	7.9	0.0	0.9	7.0	64.4	0.0	12.7	0.0	100

Table.3.5 Whole rock X-ray diffraction (XRD) analysis in well: 3V3-59E

3.3. FACIES ANALYSIS OF LIDAM FORMATION

Ten main facies and fourteen microfacies have been identified within the Lidam Formation during this study. These are summarized on Table 3.1 and are listed in approximate order of appearance from the base of the formation upwards. A detailed description and interpretation of each facies follows. The description of these facies was then used to evaluate lithological variation, reservoir potential of the carbonates, evaporites and clastics and this is presented in more detail in subsequent chapters.

3.3.1. ANHYDRITE FACIES (AF):

Includes: Microfacies: A: Chicken-wire Anhydrite (CWA)

i. Facies description:

This facies occurs predominantly at the base and the top of the Lidam Formation. Based on the observations of cores and geophysical logs, this facies forms a thick zone at the bottom of the Lidam Formation, 30 feet in well 3V3 from a depth of 11080 feet up to 11055 feet. Also present in the basal parts of the cores are 26 feet in 3V1-59E from a depth of 10546 feet up to 10520 feet, and in well R1-97 approximately 17 feet from a depth of 11074 up to 11058 feet.

This facies is present as three units in the lower part of well 3V3-59E. The anhydrite facies also caps the Lidam Formation in well 3V1-59E where it is interbedded with laminated stromatolitic facies. Each anhydrite unit has a thickness ranging from 4 up to 10 feet (see chapter 4).

The anhydrite facies is dominated by white to light grey anhydrite interbedded with dolomitic layers, including stromatolitic facies mudstones and dark grey shales (Figure 3.1). The few relict grains are replaced by anhydrite or dolomite. Crystal size of lath-shaped anhydrite ranges from <100 μm to laths several millimeters long and commonly contain fluid inclusions parallel to the crystal faces (Figure 3.2) Bedding is massive and commonly has a nodular texture with chicken wire fabric or is finely laminated with fine dolomite crystals. Laminated nodular-banded and chicken wire structures are distinguished in the chicken-wire anhydrite (CWA) microfacies. Thin cloudy beds up to 5cm thick form the nodular bedding anhydrite.



Figure 3.1. Core photographs of Anhydrite Facies showing chicken wire anhydrite structure. **A**, depth: 10966 ft, R1-97, **B**; depth: 10605 ft, P3-97.

The anhydrite is present in the Lidam Formation as pore-filling cement and as a replacement phase. Three different types of crystals are present: fibrous, bladed, and equant anhydrite (Figure 3.2 and Figure 3.3). Fibrous anhydrite is fan-shaped clusters of needle-like crystals and is present throughout the Lidam Formation and occurs in small pores and along micro fractures. Bladed or lath-shaped anhydrites are elongated crystals, typically 100 to 500 μ m in the long dimension, and fill pore spaces and replace various grains. Equant anhydrite crystals have a blocky appearance, and are present as pore filling phases and replacement features of the surrounding matrix and or grains. XRD analysis was undertaken on three samples from the anhydrite facies in the lower part of the Lidam Formation at depths of 10520 feet, 10524 feet, and 10539 feet in 3V1-59E and upper part at a depth of 10448 feet. These lower samples are composed of anhydrite (94.1% on average) with minor quartz (3.2%), dolomite (1.1%) and calcite (6.1%), traces of dolomite (1.1%) and no clay content. In contrast a sample from the upper part contains 93.5% anhydrite with minor dolomite (5.5%), quartz (1.1%) and no clay (Table 3.2).

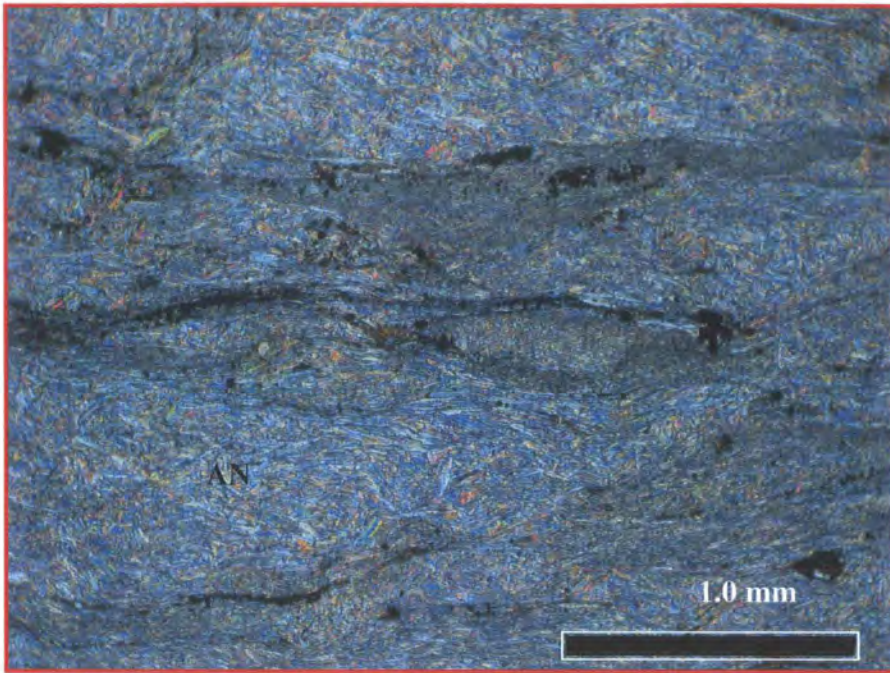


Figure.3.2. Photomicrograph showing excellent preservation of anhydrite needles (AN) oriented partially paralleling the lamination in the micritic sediment. (XPL, stained section), 10255ft, 3V3-95E.

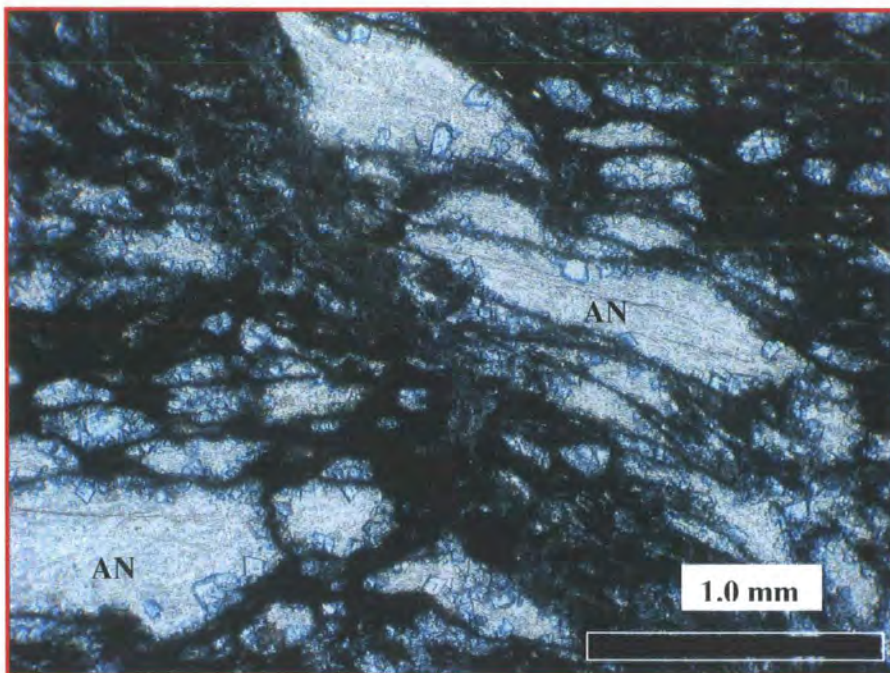


Figure.3.3. Photomicrograph shows nodules of aphanitic anhydrite (AN) possibly partly retaining the shape of original gypsum crystals. Adjacent to micritic seams between clear, euhedral gypsum crystals have partially replaced the anhydrite. 10280 ft, 3V3-95E, PPL.

ii. Environmental Interpretation:

The lack of fossils in this facies may indicate that the environment was hypersaline restricted marine or non-marine. This conclusion is supported by the presence of anhydrite (either primary, or pseudomorphous after precursor gypsum). This facies is interpreted as a low energy, lower supratidal environment. The formation of anhydrite requires an arid climate with mean annual temperature above 22° C and seasonal temperatures in excess of 35° C (Tucker, 2001). Where the climate is less arid, then primary nodules of gypsum may develop within the sediment, as has happened in sabkhas bordering the Mediterranean and Arabian Gulf (Tucker, 2001).

Displacive precipitation of anhydrite within sediments results in closely packed nodules with host sediments restricted to thin stringers, this structure produced is referred to as chicken-wire anhydrite (Schreiber. *et, al* 2000). Chicken wire or nodular anhydrite forms in peritidal depositional environments, such as sabkhas or tidal flats, as evaporitic growth within sediments. According to Tucker (2001) key features for the identification of sabkha evaporite are the shallow-water and intertidal sedimentary structures contained within the associated carbonates. Here, the anhydrite facies is interbedded with stromatolitic facies of inferred intertidal origin (section 3.3.5). Lamination is characterized by laterally continuous mm-scale laminae, indicating accumulation in low energy. Comparatively simple depositional models of extensive, prograding supratidal sabkhas have been applied to facies associations of stromatolite and bedded anhydrite (Kirkham, 2004).

3.3.2. DOLOMITE FACIES (DF):

Includes: Microfacies: A. Fine Replacive Dolomite Microfacies (FRD)

i. Facies description:

This fine replacive dolomite microfacies occurs in the lower part of the Lidam Formation in well 3V3-59E. Layers may exceed 8 feet in thickness at different depths in the lower part of the core, but generally range from 3 feet to 5 feet. It is interbedded with the chicken-wire anhydrite (CWA) microfacies. This microfacies is mainly composed of light grey, rhombic fine crystalline dolomite with a tightly packed idiopic texture. Dolomite is typically very finely crystalline (~0.1) but locally exceeds 0.2 mm. Crystals are

typically subhedral to euhedral. Some of the crystals are zoned with a clear to turbid (locally calcite) centre and a clear dolomite rim (Figure 3.4).

The dolomite facies (DF) contains small forams of rotaliids and miliolids with scattered undifferentiated bioclastic fragments in a mudstone / wackestone texture (Figure 3.5). The finely crystalline dolomite may contain intercalated micrite or traces of micrite within dolomite crystals. Aragonitic bioclastic grains (identified from their original shell shape) have been dissolved out with molds filled by ferroan dolomite cement (Figure 3.6).

Dolomitized lime-mudstones are locally interbedded with peloidal wackestone / packstone which may be completely dolomitized and contain dascycladacean green algae with a few relict grains partly replaced by anhydrite /or fine dolomite crystals (Figure 3.6). Locally some dolomites are cut by stylolites and some dissolution seams contain rhombohedral replacive dolomite. Original sedimentary structures are difficult to identify due to complete dolomitization. Moldic and intercrystalline porosity are evident and some voids result from leaching of grains. Based on the shape of vugs, original grains were probably peloids or mollusc shells.

XRD analysis was undertaken on two samples from this facies in the upper part of the Lidam Formation in 3V1-59E. At a depth of 10460 feet a dolomitic mudstone is mainly composed of dolomite (89.7%) with minor quartz (6.4%), anhydrite (2.4%), calcite (1.4%) and no clay. The second sample is from 3V3-59E from a depth of 10207 feet, contains dolomite (90.3%) and quartz (6.8%) with a minor amount of calcite (2.9%) and no clay (table.3.2).

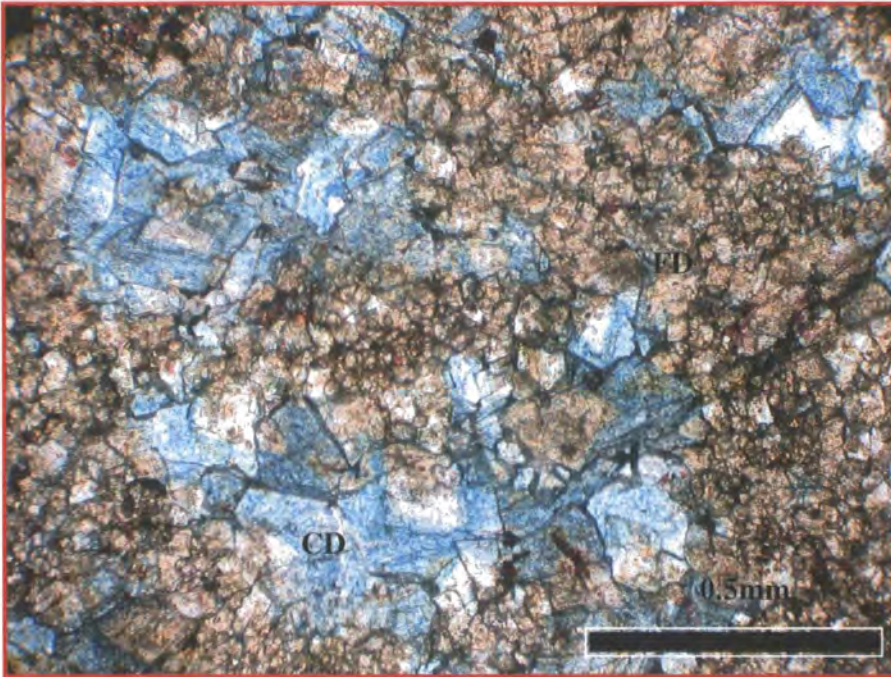


Figure 3.4 Photomicrograph shows well developed interlocking, rhomb shaped crystals of non ferroan dolomite (FD) and ferroan coarse dolomite (CD) in a fine grained calcite matrix. 10269 ft, 3V3-95E, PPL.

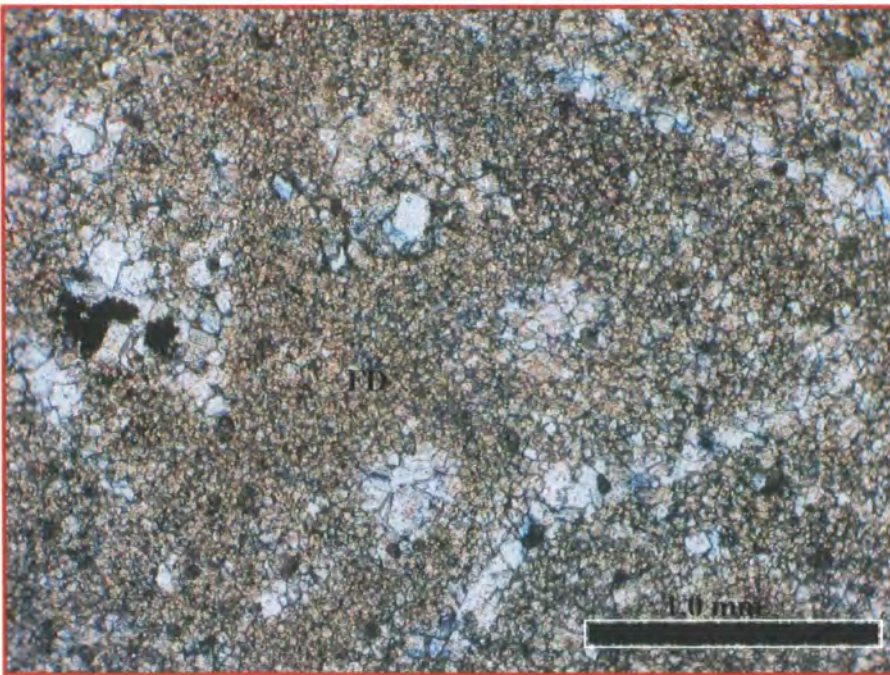


Figure 3.5 Photomicrograph shows fine dolomite rhombs (FD) in a matrix of pseudospar with patches of microspar and micrite. Mouldic porosity is filled by ferroan dolomite. 10253 ft, 3V3-95E, PPL.

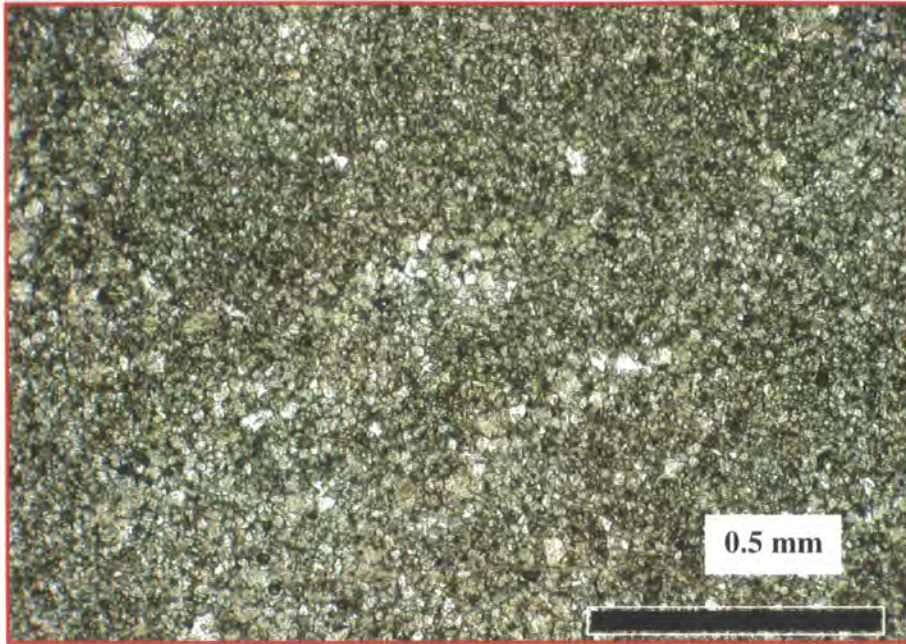


Figure 3.6 Photomicrograph showing well developed crystals of fine idiopathic dolomite texture. 11853 ft, N6-97, PPL.

ii. Environmental interpretation:

The bioclasts within this facies (molluscs, miliolids, and rotaliids) are often replaced, but are indicative of normal marine to perhaps restricted condition. The dolomitized mudstone / wackestone texture of this facies suggest deposition was under low energy conditions. It is suggested that deposition probably occurred in a restricted, evaporative ramp, lagoon or supratidal environment (cf. Tucker, 2001).

The mudstone / wackestone texture and macro-shell bearing wackestone mud-supported texture may reflect a back shelf lagoon in which relatively low energy conditions prevailed (Flügel, 1982). Very fine to fine crystalline dolomite often formed in intertidal, tidal flat, and sabkha settings.

Dolomite can form in a variety of settings and is discussed in more detail in the chapter on diagenesis (Chapter 5). Here a few possible origins are inferred but the reader is referred to Chapter 5. The dolomite formed from evaporated sea water in near surface environments with the evidence suggesting that dolomite formed in hyper-saline conditions (Qilong, 2006). Dolomite units associated with evaporites are commonly interpreted as resulting from reflux of hypersaline brine (Morrow, 1990 and Whittakar,

1996). This facies is interpreted as SMF22 according to the standard microfacies types of Wilson (1975).

3.3.3. SANDSTONE FACIES (SF):

Includes: Microfacies: A: Quartz Sandstone (QS)
B: Bioclastic Sandstone (BS)

i. Facies description:

This facies is observed in the lower part of wells 3V1-59E, N6-97 and P3-97. These units range in thickness from 2 to 3 feet. In most of the cored sections this facies is intercalated with the anhydrite and stromatolitic facies. The sandstone facies consists of two main microfacies; quartz sandstone and bioclastic sandstone. The quartz sandstone microfacies occurs in the lower part of the Lidam Formation intercalated with anhydrite facies. It contains well-sorted to poorly sorted, fine to medium grained sandstones with a clay matrix and thin iron oxide rims to grains (Figure.3.7). The bioclastic sandstone microfacies occurs in the middle part of the formation where beds are \approx 2 feet thick at a depth of 10492 to 10494 feet in well 3V1-59E. The same microfacies occurs between depths of 11805.5 to 11807.5 feet in well N6-97 and between 11619 to 11620 feet in well P3-97. Fine-grained sandstones sharply overlie, and are sharply overlain by laminated mudstones facies. This facies consists of tan grey to green-grey, fine to medium grained sandstone. Grains are sub rounded to sub angular and poorly sorted. Detrital quartz grains (60%) dominate and the facies contains \approx 10% clay matrix (Figure 3.8 and Figure 3.10). Carbonate grains (30%) are bioclastic debris including stick-shaped coralline algae. Other components such as echinoderm fragments and small forams (rotaliids) are scattered through the sandstone facies. The bioclastic fragments show poor sorting (Figure.3.9).

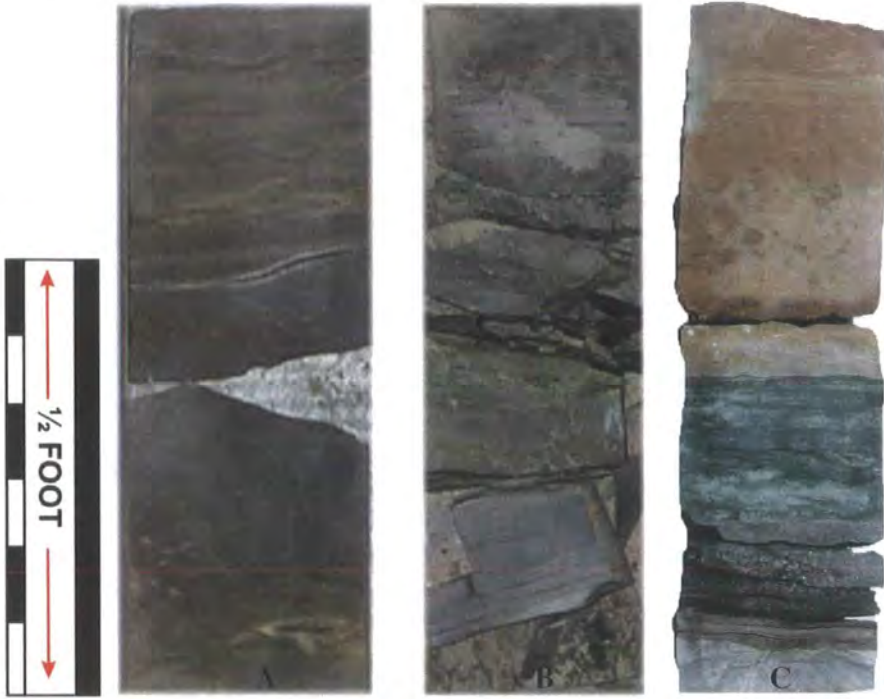


Figure.3.7. Core photographs of Siliciclastic Facies (SF) showing the lamination of sand layers from different wells: A; depth from 10542 ft, B from depth: 10526 ft well 3V1-59E, and C; from depth: 11619, P3-97.

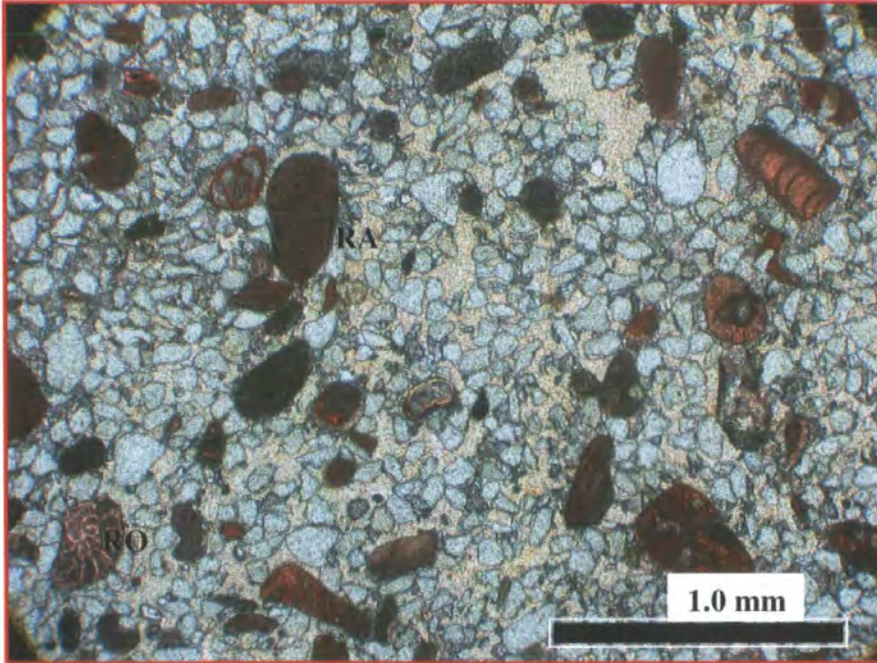


Figure.3.8. Photomicrograph showing bioclastic sandstone microfacies containing quartz grains with scattered small forams (rotaliids and miloilid) (RO) and coralline algae (RA). 10493 ft, 3V1-59E, PPL.

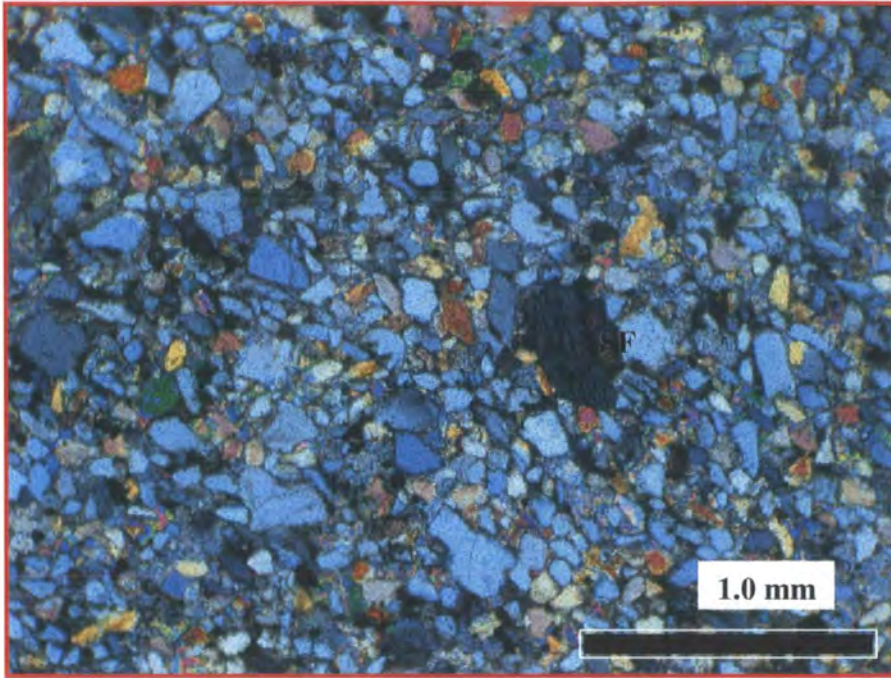


Figure 3.9 Photomicrograph showing poorly sorted sandstone with scattered shell fragments (SF). 11806 feet, N6-97, XPL.

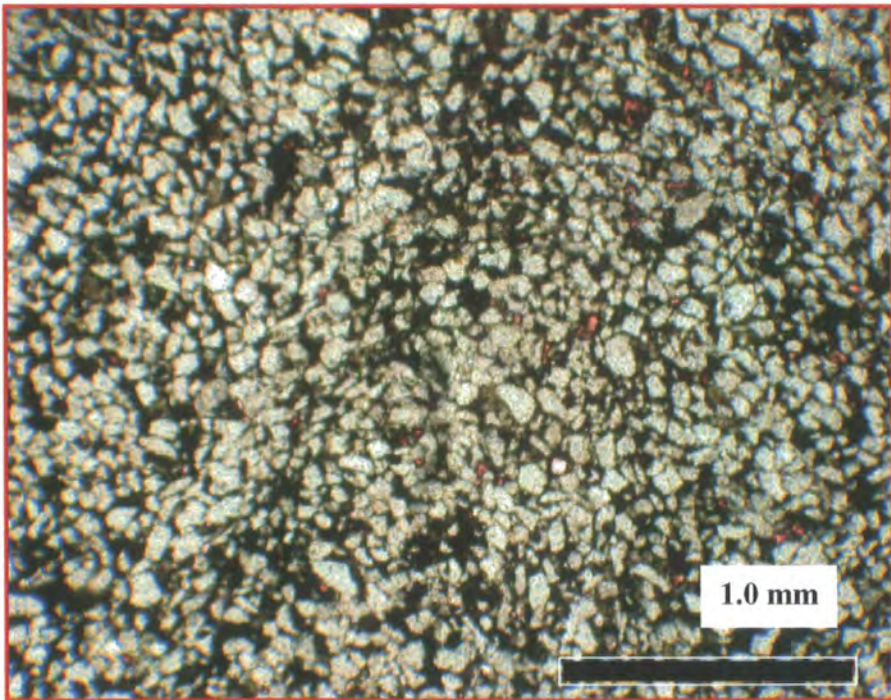


Figure 3.10 Photomicrograph showing fine grained sand with a muddy matrix from the quartz sandstone microfacies. 10525 feet, 3V1-59E, PPL.

ii. Environmental interpretation:

The sandy facies with poorly to moderately sorted quartz grains mixed with scattered bioclastic fragments is interpreted as being deposited in a shallow near-shore environment. For the quartz sandstone microfacies the fine grain size and low abundance of marine fauna suggests deposition under low to moderate energy conditions and a continental shoreface environment setting. However, medium grain size and abundant, abraded shallow-marine bioclastic debris, of the bioclastic sandstone facies is suggestive of a slightly higher-energy, possibly shallower depositional environment for this microfacies compared with the quartz sandstone microfacies (Wilson 1975). Shallow-marine reworking of sand derived from the underlying formation is proposed for the bioclastic sandstone microfacies based on the abundance of shallow marine fauna such as small foraminifera (rotaliids) and coralline algae and bioclastic debris. The bioclastic fragments were probably reworked and deposited within the sand facies (Figures 3.8, 3.9 and 3.10).

3.3.4. SHALE FACIES (SF):

i. Facies description:

Shale intervals are common throughout the Lidam Formation from bottom to top and are generally intercalated with dolomite and limestone. These shales are medium dark grey to black. Silt- and clay-sized particles dominate and there is a notable presence of thin layers or laminae along which the rock easily splits (fissile to sub-fissile) with laminae 0.1 to 0.5 cm in thickness. Units range in thickness from 2 feet in the upper part of the formation to 4 feet in the lower part (Figure 3.11). The Shale facies intervals are particularly common in wells P3-97, N6-97, and R1-97 and are intercalated with ostracod facies (Section 4).



Figure.3.11. Core photographs of Shale Facies (SF) showing lamination of fissile to sub-fissile layers of shale from well: 3V3-59E, A; depth from 10261 ft, B from depth: 10273 ft.

ii. Environmental interpretation:

The grain size and sedimentary structures indicate that this facies originated under low energy conditions where mud deposition and preservation was possible. The depositional environment of this facies is interpreted to have been in a protected or probably restricted lagoonal area, because most of the shale interval is interbedded with the shallow water intertidal-restricted lagoonal facies. Jones (1992) stated that the calcareous mud in a warm water settings comes from the break down of green calcareous algae, inorganic precipitation from sea water, and/or from the disintegration of large skeletal particles into their smallest crystallographic unit. These muds accumulated in quiet water areas that were not affected by tidal and/or strong oceanic currents. In this facies, some of the clay-size fraction are likely to be clays (due to the grey colour) and may have been washed in from nearby land areas.

3.3.5. STROMATOLITIC FACIES (STF):

Includes: Microfacies: Stromatolitic Mudstone (STM)

i. Facies description:

This microfacies occurs in the middle part of the Lidam Formation in well 3V1 and 3V3-59E. It lies between dolomite facies and ostracod facies. The thickness of this microfacies is 3 feet between depths of 10235 to 10248 feet in well 3V1-59E and between depths of 10495 to 10498 feet in well 3V3-59E. This microfacies is composed of light grey to yellowish grey, medium hard, wavy to crinkly stromatolitic laminae interbedded with layers of light grey dolomite, and dolomitic limestone (Figures 3.12 and 3.13). The laminated structures are usually characterized by thin, alternating light and dark layers that may be flat, crinkly, hummocky, or dome-shaped (Figures 3.12 and 3.13). Observed primary porosity (10%) is filled by anhydrite. Internal sediment in some fenestral cavities or a long laminae consists of alternating thin micritic layers and layers containing a mixture of micrite and ferroan dolomite crystals (Figure 3.12).

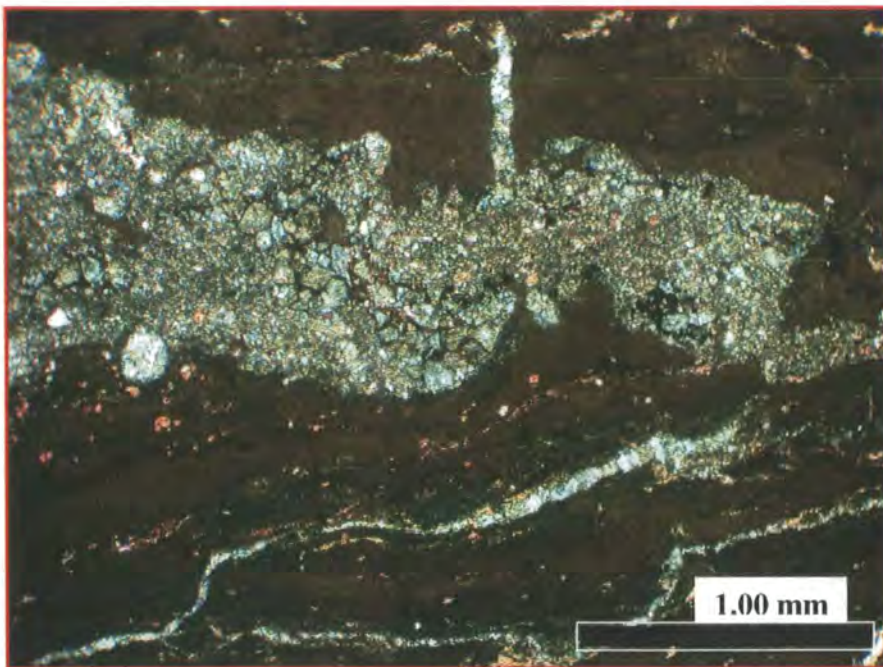


Figure 3.12 Photomicrograph showing stromatolitic lamination consist of alternating thin micritic layers and lighter-coloured layers containing a mixture of micrite and ferroan dolomite crystals. 10238 ft, 3V3-59E, PPL.



Figure.3.13 Photomicrograph showing stromatolitic lamination consisting of alternating thin micritic layers and layers containing a mixture of micrite and sparse calcite cement. 10495.5 ft, 3VI-59E, PPL.

ii. Environmental interpretation:

Highly irregular laminae, together with alternating lighter and darker micritic laminae are characteristic features of stromatolites formed by microbial associated biotic assemblages as well as sedimentary structures indicate that these stromatolites originated in a shallow- restricted marine environment. They most likely formed in the upper subtidal – peritidal zone and are associated with anhydrites of supratidal origin.

Brain (1992) stated that microbial mats form thick, leathery carpets that can be locally shrunken and folded and exhibit various surfaces such as pustules, and small domal stromatolites. These irregularities relate to variations in surface growth, and some layers may be partly diagenetically deformed through growth of evaporite minerals. Changes of stromatolite structures are also due to changes in current velocities and sediment movement during growth of stromatolitic communities (Piatkowski, 1975).

Jones (1992) reported that laminated fine/ grained sediments with occasional coarser intercalations reflect deposition by storms and in some regions by winds blowing off the neighboring land surface. (see Section 3.3.1). Stromatolites often form in intertidal areas with raised salinities where grazing organisms are restricted (Tucker, 2001). According to the standard microfacies types of Wilson (1975), this facies is interpreted as SMF25 formed in the upper intertidal flats to supratidal environment setting.

3.3.6. OSTRACOD FACIES (OSF)

Includes: Microfacies: A: Ostracod Bioturbated Wackestone (OBW)

i. Facies description:

The thicknesses of successions including this microfacies are around 16 feet in most of the studied wells. This facies lies between the lower stromatolite unit and the upper peloidal packstone / grainstone in well 3V1-59E between depths of 10456 ft to 10492 ft, well 3V3-59E between depths of 10218 ft to 10233 ft, well R1-97 between depths of 11030 ft to 11052 ft, well P3-97 between depths of 11665 ft to 11681 ft, and between depths of 11814 ft to 11833 ft in well N6-97. The ostracod facies consists of massive limestone; light brown to light olive grey and locally interbedded with fissile dark-grey shale. Irregular lamination and nodular bedding structures are observed in core. Locally, sub horizontal burrows and scattered shell fragments are well developed and observed in most of this facies (Figure 3.14).

This facies contains fine to very fine grained bioclastic fragments and benthic foraminifera (miloilid and rotaliid), is slightly argillaceous, and highly bioturbated (Figure 3.15). The matrix is composed of micrite and small fragmented bioclasts.

The dominant depositional fabric is mudstone / wackestone grading into packstone. The skeletal grains are dominated by ostracods (40%) associated with other bioclastic debris. The ostracods have complete thin valves with finely prismatic or granular microstructures and may be filled by ferroan calcite cement and embedded in micrite lime mud (25%) (Figure.3.16). Other bioclasts (30%) are fragments of small benthic foraminifera (rotaliids and miloilids), echinoderm fragments, bryozoans, dascycladacean algae, and mollusc fragments. Calcispheres are also present and are up to 0.5 mm in diameter and composed of calcite (usually sparry calcite) (Figure. 3.17).



Figure 3.14 Core photographs of the ostracod facies (OSF) showing the nodular bedding and lamination of layers from different wells: **A**; depth 11050 ft R1-97, **B**; depth: 11840, N6-97 and **C**; from depth: 11675, P3-97.

XRD analysis reveals that two samples from the upper part at depths of 10484.5 and 10489.5 ft in 3V1-59E contain similar amount of calcite (95.8%) with minor quartz (3.5%), traces of dolomite (0.7), anhydrite (0.6%) and no clay content. A lower sample from 10511.5 feet in 3V1-59E is mainly composed of calcite (77.6%) with minor quartz (11.6%), clays (6.6%), traces of anhydrite (1.8%) and pyrite (1.0%). XRD clay fraction analysis from this second sample shows approximately equal amounts of illite-smectite (37.4%), kaolinite (32.5%), calcite (28.2%) and minor quartz (1.9%). A sample from 3V3-59E from a depth of 10221 feet is massive limestone mainly composed of calcite (93.4%) with minor amounts of dolomite (0.9%), quartz (5.2%), anhydrite(0.5%), and no clay (Tables. 3.2, 3.3, and 3.4).

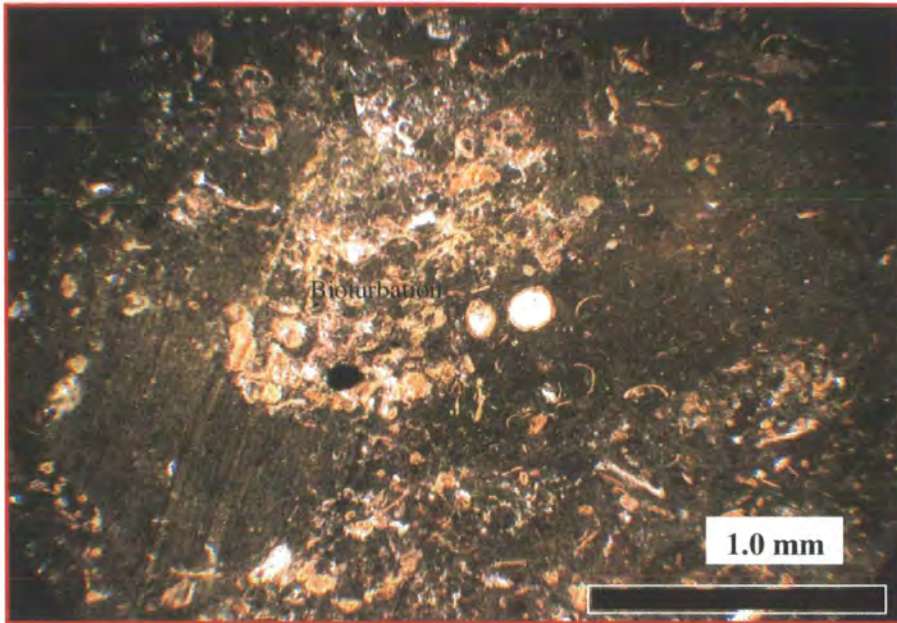


Figure 3.15 Photomicrograph shows a group of ostracods concentrated as a burrow infill. Complete two valved shells are filled by sparry cement. 11041 feet, R1-97, PPL.

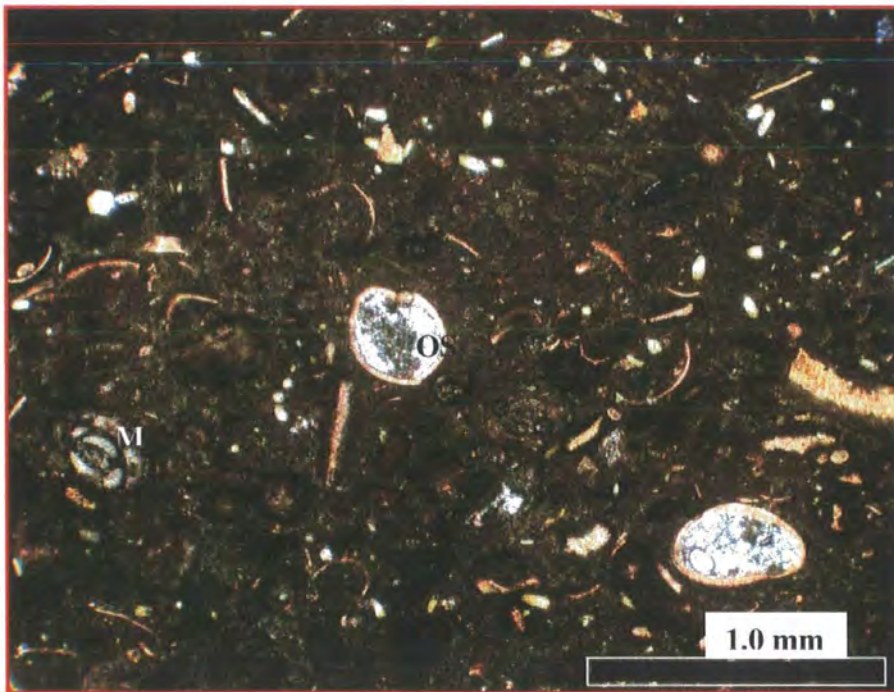


Figure.3.16 Photomicrograph showing ostracod (OS) mudstone / wackestone with ostracods completely filled by calcite cement, with scattered miloilid (M) and bioclastic debris in lime mud matrix, 10483 ft, 3V1-59E, PPL.

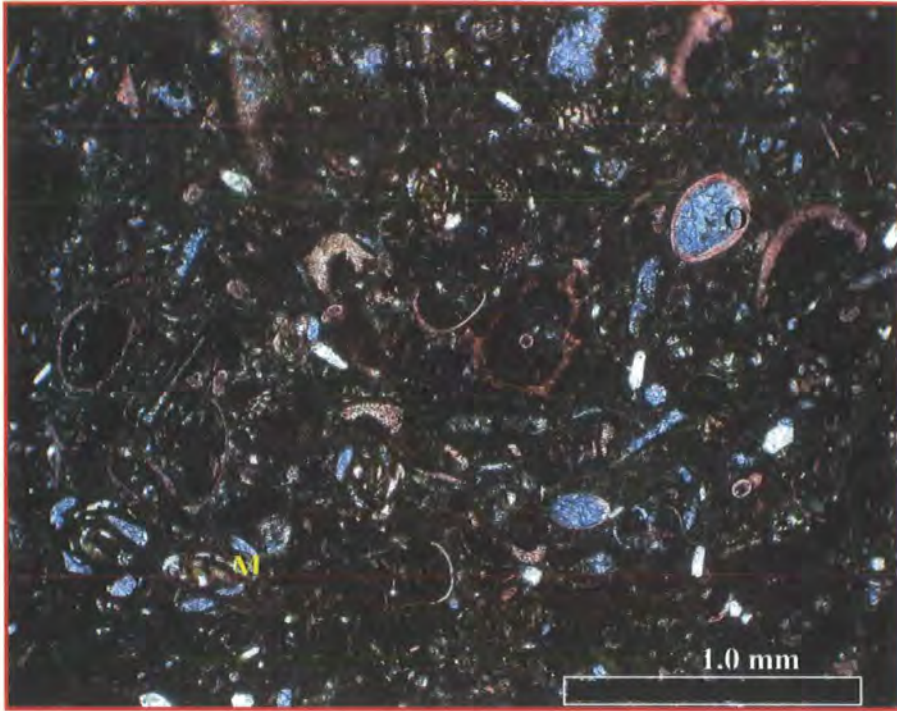


Figure 3.17 Photomicrograph shows abundant disarticulated ostracod (OS) valves (thin curved shell) associated with miliolid foraminifera (M) embedded in micrite sediment, 10221 ft 3V3-59E, PPL.

ii. Environmental interpretation:

The ostracods and foraminifera may form under normal marine conditions. However both ostracods and miliolids can tolerate raised or lowered salinity. Tucker (2001) describes ostracods living at shallow depths in marine, brackish or freshwater, and having a small (around 1mm in length) thin valved shell, which may be smooth or ornamented and are composed of calcite with radial-fibrous structure. Wackestone textures are transitional between low-energy mudstones and moderate-energy packstones. Jones and Desrochers (1992) stated that the chlorozoan assemblage, foraminifera and ostracod components occur in warm water areas where water temperature is above 18°C and developed in places where salinities range between 32 and 40‰. This facies is inferred to have formed under low energy conditions, perhaps in a protected lagoon with normal marine to raised salinity. This facies is interpreted as SMF18 according to the standard microfacies types of Wilson (1975), where the main feature of this SMF type is the abundance of arthropoda (ostracod) and calcareous green algae. The calcispheres are

probably of algal origin, (Flügel, 2001) and are often associated with foraminifera, particularly in fine grained micrite of lagoonal origin (Tucker, 2001).

3.3.7. MOLLUSC FACIES (MF):

Includes: Microfacies: A: Mollusc Bioturbated Packstone (MBP).
B: Partial Dolomitized Mollusc Packstone (PDMP).

i. Facies description:

This facies is observed in the lower and middle part of well R1-97. It lies between the lower stromatolitic and anhydrite facies and upper ostracod facies in the lower part of the Lidam Formation. The thickness of this microfacies is approximately 7 feet and it occurs between depths of 11058 to 11065 feet, and 11022 to 11030 feet (Figure 3.18).

The mollusc facies is composed mainly of light grey to medium grey, fine to coarse grained skeletal bioturbated wackestone / packstone. Dominant bioclasts are mollusc fragments (40%) including; bivalves and oysters, as well as echinoderm fragments. Other bioclastic grains (25%) are small foraminifera (rotaliids) together with ostracods (Figure 3.19 and 3.20).

The matrix sediment contains a mixture of bioclastic debris (30%). Some of the mollusc shells have been partially or completely affected by micritization with thin micritic rims around the margins of the shells (Figure.3.19). The cement now infilling the bivalve is fine drusy sparry calcite cements becoming coarser toward the centre of the pore space. Boring of mollusc shells is common, with borings filled by bioclasts and background sediment (Figure 3.20 and 3.21)..

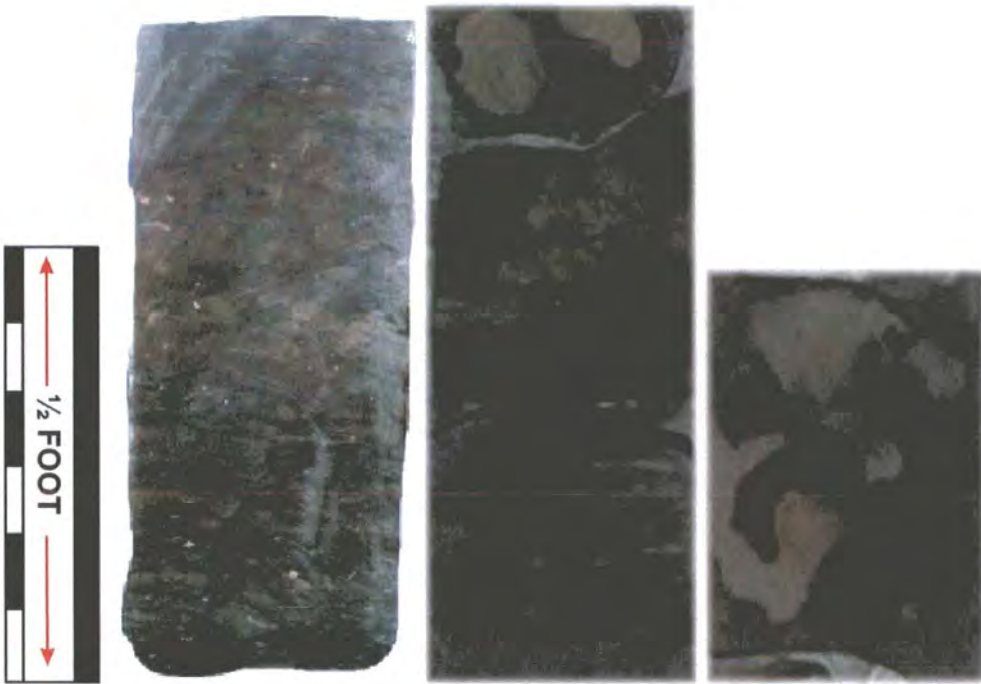


Figure.3.18 Core photographs showing Mollusc Bioturbated Packstone (MBP): A; depth 11060 ft R1-97, B; depth: 10475 3V1-59E and C; from depth: 10482 ft, 3V1-59E.

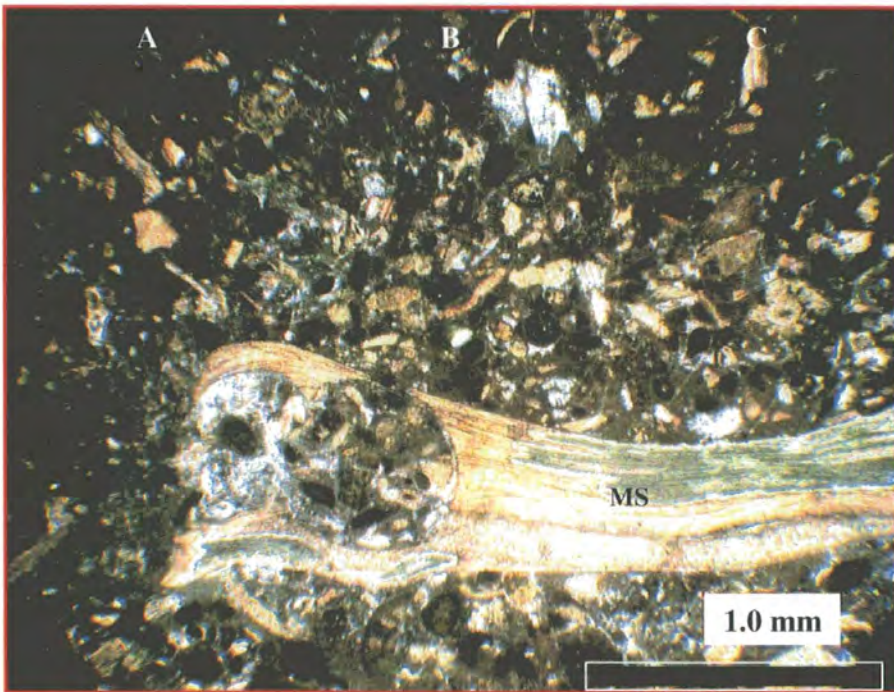


Figure.3.19 Photomicrograph shows boring of mollusc shell (MS) which has been filled by the host sediments. 11025.5 ft, R1-97, PPL.

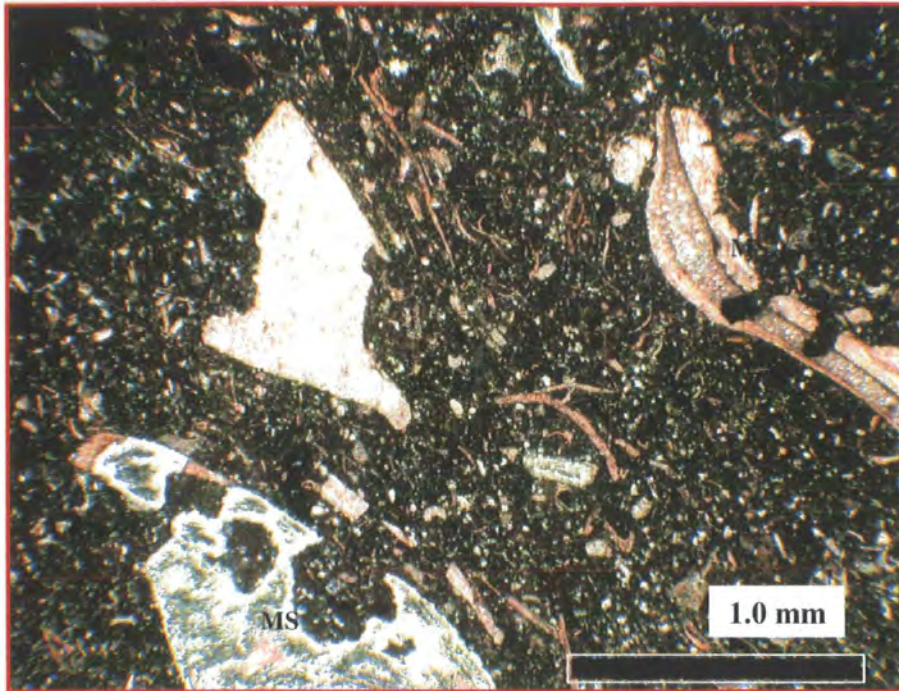


Figure.3.20 Photomicrograph shows two large mollusc fragments (MS) with extensive boring. The rest of the sediment comprises broken up bioclasts and ostracod shells. 10060.5 ft, R1-97, PPL.

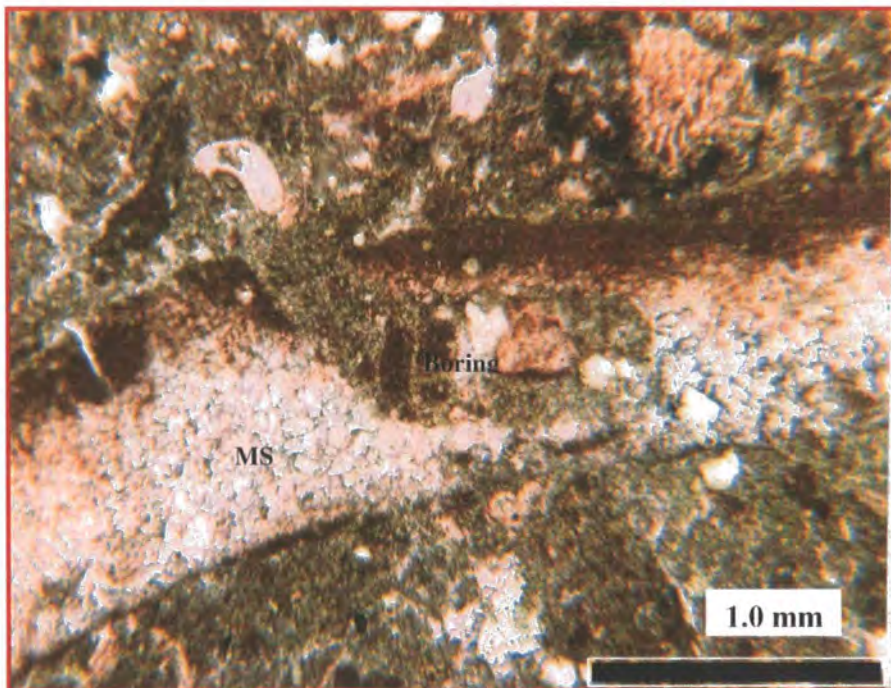


Figure.3.21 Photomicrograph showing mollusc shells (MS) affected by micritization and boring which is filled by bioclastic debris, 10226 ft, 3v3-95E, PPL.

ii. Environmental interpretation:

The molluscs are often found in normal marine conditions. However, the limited variety of abundant oysters and other bivalves suggests conditions may have become restricted at times. The nature and size of the mollusc fragments are all indicative of moderate to low energy conditions. Oysters are usually found in normal marine salinity and developed in places where salinities of less than 40‰ occur, and cannot be found in places of increased salinities such as transitional restricted marine or hypersaline environments (Jones, 1992). With many broken bioclasts it is suggested that at times higher energy resulted in reworking.

The likely water depth of the mollusc facies is ~6 to 10m (Tucker, 2001). Deposition in a protected lagoonal area is the inferred environment of these mollusc facies sediments. The abundant micrite is indicative of deposition in lower energy conditions. This facies is interpreted as SMF8 according to the standard microfacies types of Wilson (1975).

3.3.8. BIOCLASTIC FACIES (BF):

Includes: Microfacies: A: Foraminifera Packstone / Grainstone (FPG)
B: Echinoderm Packstone (EP)

i. Facies description:

This facies is observed in the upper part of the Lidam Formation in most of the studied wells. It occurs at depths between 10222 to 10231 feet in well 3V3-59E, 10469 to 10476 feet in well 3V1-59E, in well R1-97 it occurs between 11007 to 11019 feet, 11058 to 11065 feet, and between 11022 to 11030 feet. Generally; the bioclastic facies is overlain by ooidal peloidal grainstone facies and overlies the ostracod facies (Figure 3.22). The thickness of this microfacies ranges between 7 to 10 feet.

This facies is composed of limestone and dolomitic limestone in most of the studied wells. The bioclastic facies is dominated by wackestone / packstone grading into grainstone textures. It is medium grey to light olive grey, fine to very fine grained, slightly argillaceous, fossiliferous, and highly bioturbated with intercalations of shale (Figure 3.23). Locally, there are sub horizontal burrows and scattered shell fragments. Microstylolites and pressure solution seams are common (Figure 3.22).

The facies is composed of a mixture of micrite with scattered skeletal debris contributing to a fine bioclastic matrix. In the foraminifera microfacies the main skeletal

grains (60%) are abundant small miliolid foraminifera, mollusc fragments, and echinoderm fragments together with coralline algae and bioclastic debris. Rare ostracods and coralline algae are locally present. Non skeletal grains are mainly peloids (10%). The depositional texture of this facies is a foraminifera packstone / grainstone.

The echinoderm microfacies is observed between depths of 10228.6 to 10230 feet in well 3V1-59E. Units range in thickness from 2.5 to 3 feet (Figure 3.23 and 3.25). The microfacies is poorly sorted and consists of light grey, fine wackestone / packstone. This facies contains common echinoderm fragments (mainly echinoids) (40%). Other components include scattered bioclastic fragments and small miliolids (25%). Most of the sediment in this facies is surrounded by micrite lime mud (15%) and there is some micritization of bioclasts. In grainstone units drusy calcite cement fills the pore spaces between the skeletal grains (10%). Some of the echinoderm fragments are rimmed by syntaxial overgrowth cement (Figure 3.24).



Figure.3.22 Core photographs showing lamination and bioturbation of the sediments in the bioclastic facies (BF): **A**: depth 11655 ft P3-97, **B**: depth: 11016, R1-97 and **C**: from depth: 11057ft R1-97.

XRD analysis reveals that one sample taken from the echinoderm facies at a depth of 10474.5 feet in 3V1-59E contains dolomite (66.2%) with minor quartz (11.6%), calcite (5.4%), traces of pyrite (2.7%) and anhydrite (1.1%). XRD clay fraction analysis contains

about equal amounts of illite (47%) and illite-smectite (41.4%) with minor quantities of quartz (7.5%) and dolomite (4.2%) (Tables 3.2 and 3.3).

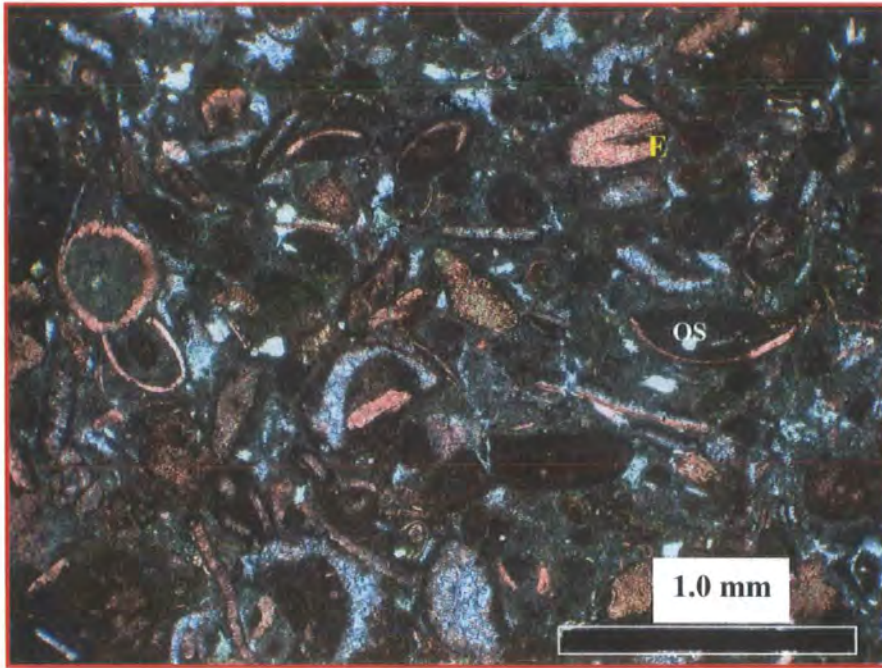


Figure 3.23 Photomicrograph showing bioclastic packstone with scattered ostracod (OS), echinoderm (E) and other bioclastic fragments, 10230 ft, 3V3-59E PPL.

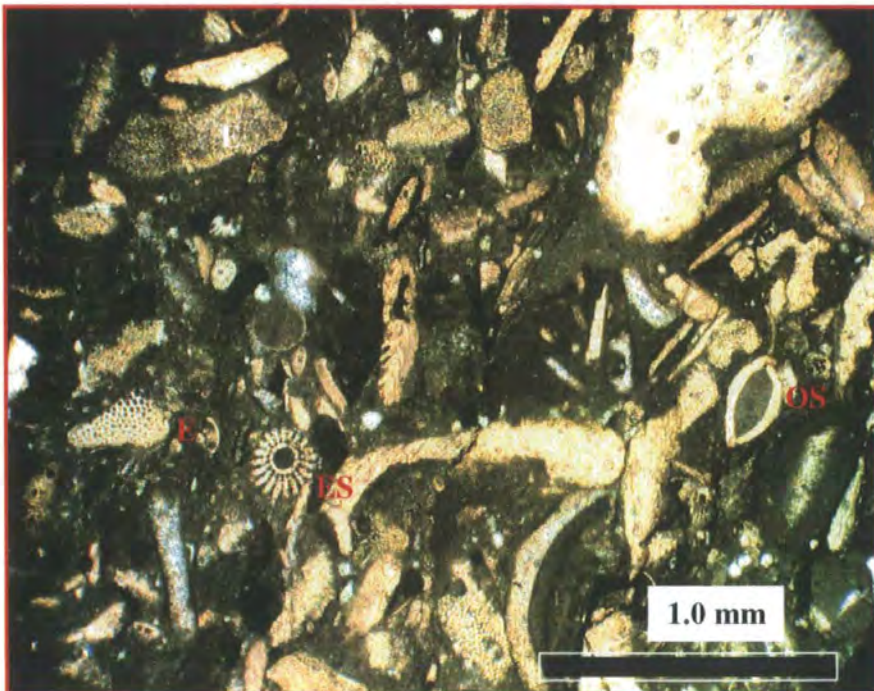


Figure 3.24 Photomicrograph shows echinoderm packstone containing echinoid plates (E) and echinoid spines (ES) with porous structure, bioclastic fragments and ostracod (OS) embedded in a lime mud matrix, 11017 ft , R1-97 , PPL.

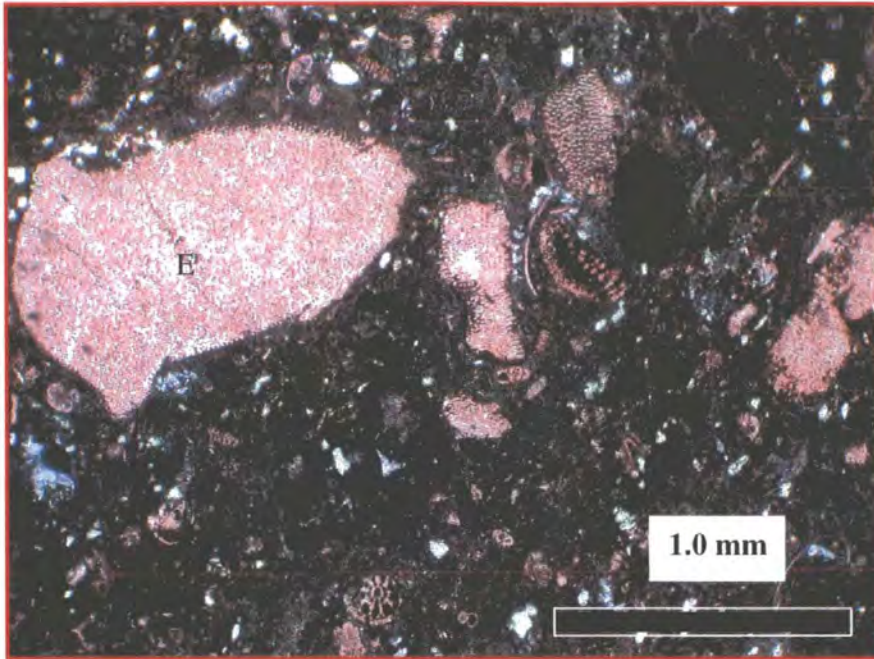


Figure 3.25 Photomicrograph shows echinoderm packstone containing scattered echinoid fragments plates (E) and bioclastic fragments with small forams embedded in a lime mud matrix, 10230 ft, 3V3-59E, PPL.

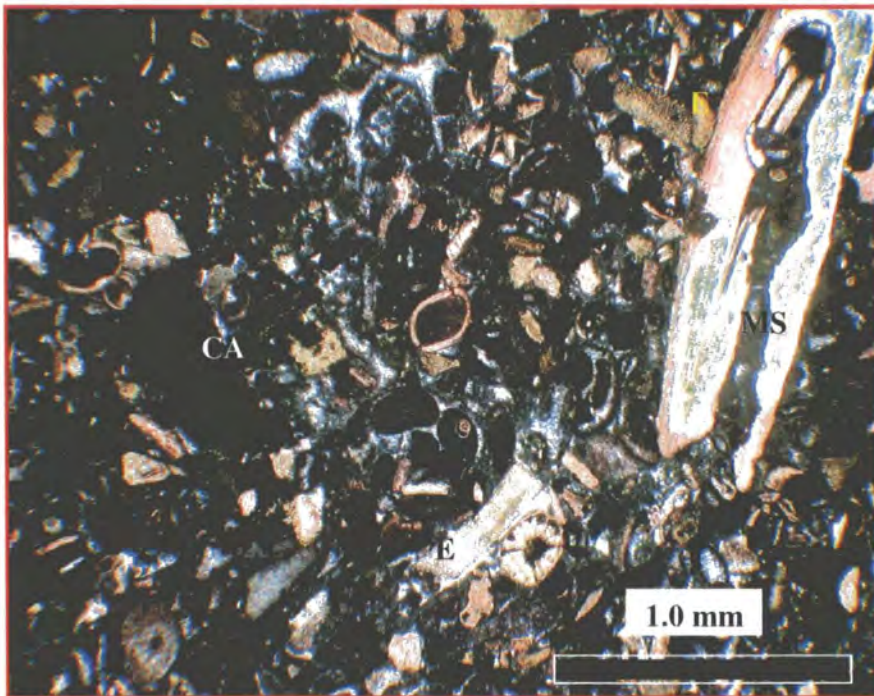


Figure 3.26 Photomicrograph shows syntaxial overgrowth around echinoderm fragments (E) and other components are mollusc fragment (MS) and coralline algae (CA) cemented by ferroan calcite cement in bioclastic packstone / grainstone. 11052 ft, R1-59E PPL.

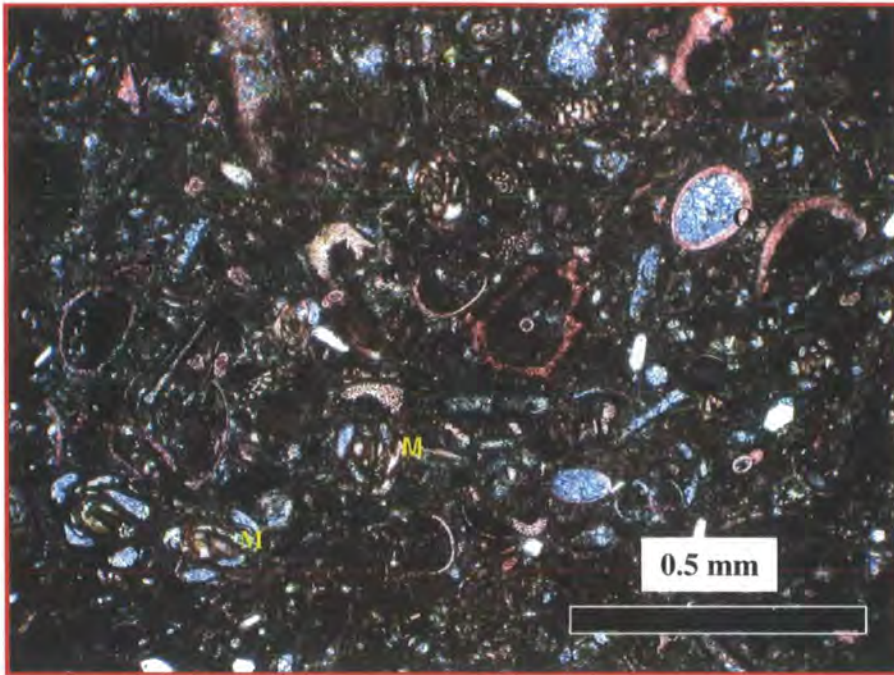


Figure 3.27 Photomicrograph showing small miliolid foraminifera (M) and ostracods (OS) with bioclasts debris in a foraminifera packstone. 10221 ft, 3V3-59E, PPL.

ii. Environmental interpretation:

The wackestone / packstone texture indicates deposition in low to moderate energy conditions. The abundance of foraminifera (rotaliids and miliolids), ostracods, echinoderm, and bioclasts fragments and associated other bioclastic debris (bryozoans, coralline algae, mollusc fragments) indicate normal marine conditions. The muddy fabric indicates low energy conditions and the foraminiferal assemblage reflects protected inner-shelf affinities. The occurrence of small forams suggests occasional connections with open marine environments and the abundance of miliolids is additionally indicative of a protected inner-shelf environment (Hallock & Glenn, 1986 and Nebelsick, 2000).

Rott (2005) stated that the crinoidal mudstone / wackestone facies is thought to be representative of low- to moderate-energy back shoal sediments deposited around the shelf edge of a rimmed carbonate shelf, and low-energy sediments deposited on the inner shelf, protected by an oolitic shoal. The echinoderm packstone microfacies with an abundance of skeletal components such as echinoderm fragments, small foraminifera (miliolids and rotaliids), coralline algae and bioclastic debris again indicate deposition under normal marine, shallow water conditions. The dominance of well preserved coralline algal growth forms in the foraminifera packstone facies indicates a relatively quiet-water environment

with stable substrate and low sedimentation rates (Nebelsick, 2000). According to the standard microfacies types (SMF) by Wilson (1975), this facies is interpreted as SMF 26.

3.3.9. PELOIDAL FACIES (PF):

Includes: Microfacies: A: Peloidal Grainstone (PG).
B: Peloidal Ooidal Packstone / Grainstone (POPG).

i. Facies description:

Units of this facies are between 10 to 20 feet thick and are present in most of the studied wells. This facies was observed between depths of: 10198 to 10218 feet in well 3V3-59E, 10462 to 10476 feet in well 3V1-59E, 10997 to 11007 feet in well R1-97, 11857 to 11870 feet in well N6-97, and 11626 to 11644 feet in well P3-97. This facies is overlain by bioclastic facies and overlies the interbedded stromatolitic and anhydrite facies.

This facies is composed mainly of limestone, which is light to dark grey, slightly argillaceous, and may be laminated. Bioturbation is slight and vugs are filled by ferroan calcite cement. Stylolites and fractures are common (Figure 3.27).

This facies consists of two microfacies; a peloidal ooidal packstone / grainstone and a peloidal grainstone. It is formed principally of fine to medium grained, moderately sorted non-skeletal grains (60%) including peloids, ooids and intraclasts associated with skeletal grains (15%) of miliolids, mollusc fragments, bryozoans, and other bioclastic debris (Figure.3.28).

Most of the ooids are uniform in shape, are well sorted and have been strongly micritized with some showing original internal structure. Other micritic grains lacking internal structure are peloids. The size of ooids and peloids ranges between 0.2 mm to 0.5 mm in diameter (Figures 3.29 and 3.30). Stylolites and pressure solution seams are common in this facies (Figure 3.27). The pore spaces (15%) between the grains are filled with calcite rim cement and some micritic matrix (5%) may be present. Intergranular pores are occluded by ferroan calcite, ferroan and non-ferroan dolomite cement (Figure 3.29). Micritization, partial dissolution, later calcite cementation, and dolomite are the most significant diagenetic processes affecting this facies.



Figure.3.28 Core photographs showing peloidal facies (PF) with high amplitude stylolites A; depth: 11005ft R1-97. B; depth: 11862ft, N6-97. C: from depth: P3 11632 ft.

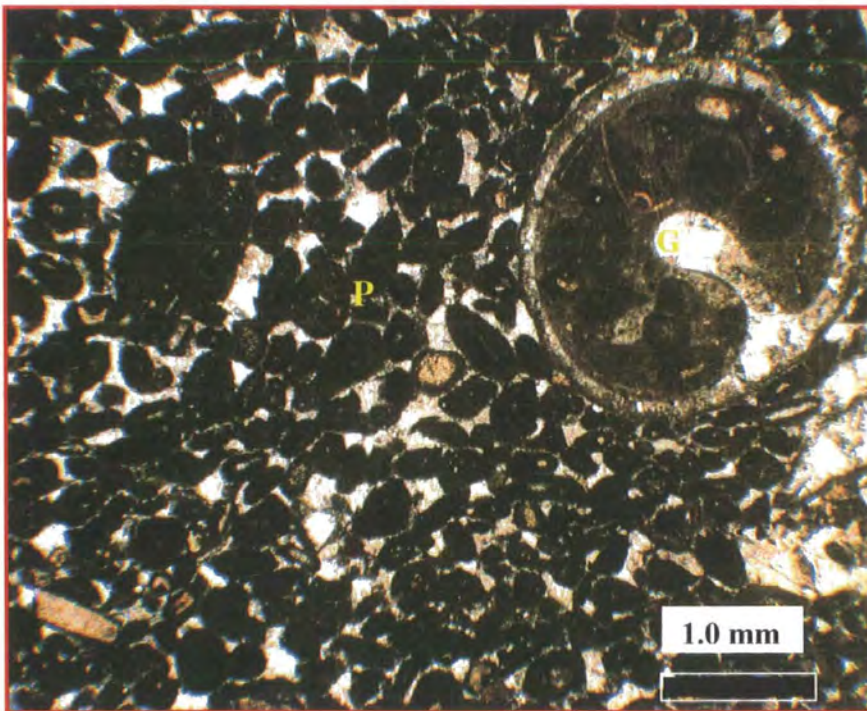


Figure.3.29 Photomicrograph showing peloidal packstone / grainstone containing peloids (P) and gastropods (G). Intragranular porosity filled by calcite cement. 11867 ft, N6-97, PPL.

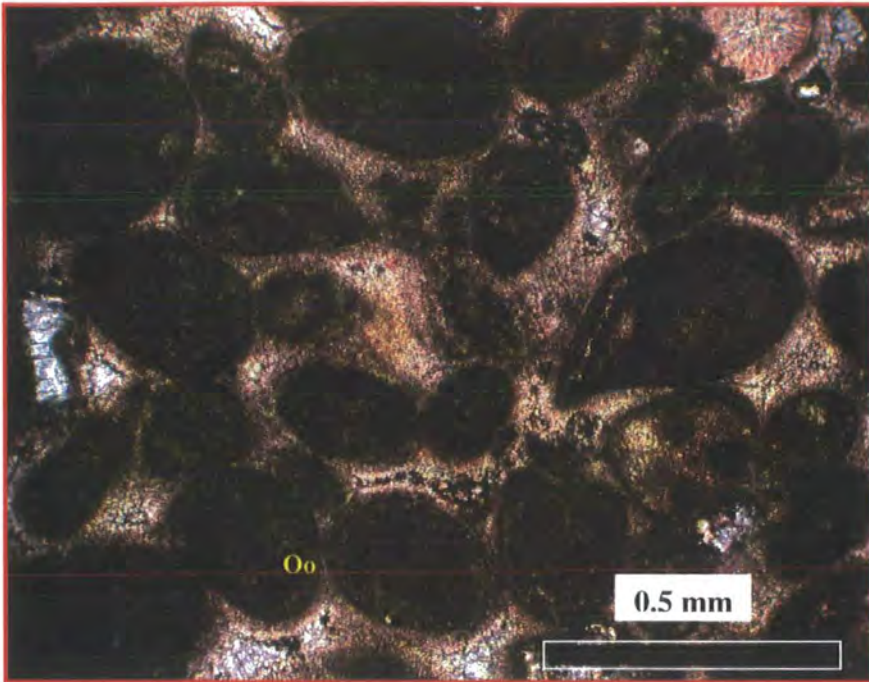


Figure 3.30 Photomicrograph showing ooids (Oo) with faint preservation of original concentric structure. Intragranular porosity is filled by bitumen and ferroan calcite cement. 10211 ft 3V3-59E, XPL.

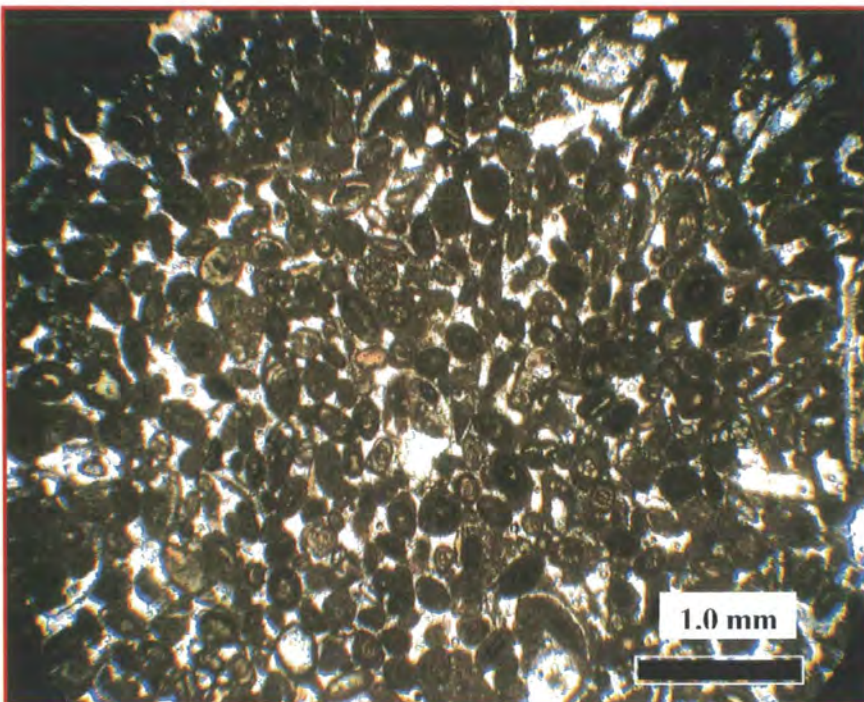


Figure.3.31 Photomicrograph showing peloidal packstone / grainstone with scattered small forams cemented by ferroan calcite cement. 11004 ft, R1-97, PPL.

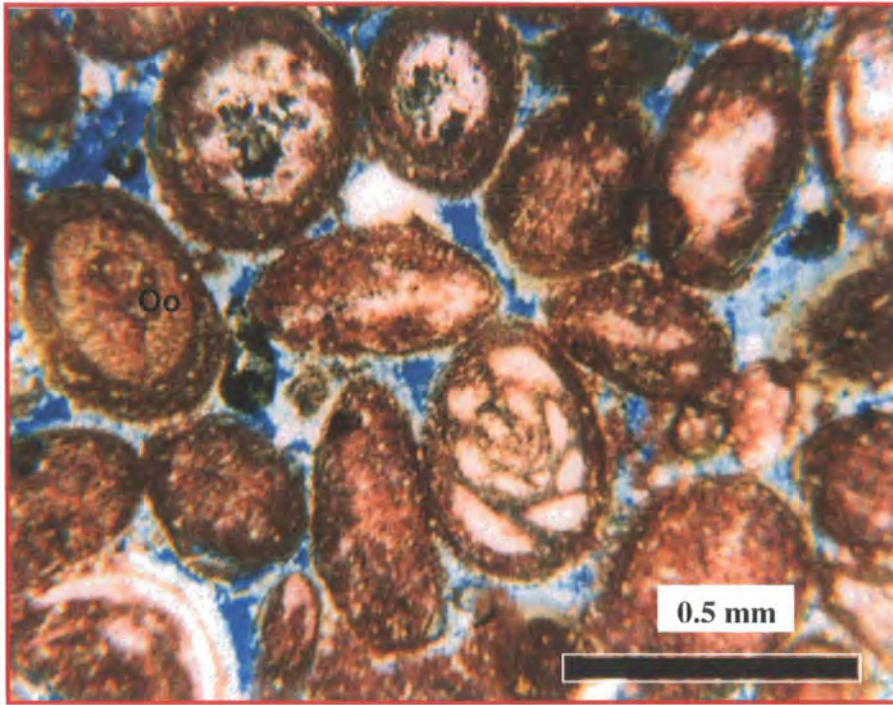


Figure 3.32 Photomicrograph showing ooids (Oo) with some preservation of original concentric structure. Intergranular and intragranular porosity is well developed and partially filled by bitumen. 10211 ft 3V3-59E, PPL.

Porosity is fair to good (4.23 to 16.50%) and represented mainly by mouldic and intergranular types. XRD analysis reveals that one sample from a depth of 10468.5 feet in 3V1-59E is limestone composed of calcite (94.1%), with minor quartz (3%), dolomite (2.2%), traces of anhydrite and no clay. Two samples from 3V3-59E reveal that one sample from a depth of 10198 feet is well cemented and massive dolomitic limestone with calcite (61.5%), dolomite (30.5%) and minor quartz (8.0%). The second sample from a depth of 10207 feet has been dolomitized containing dolomite (90.3%) and quartz (6.8%), with minor amount of calcite (2.9%) and no clay.



Figure 3.33 Photomicrograph showing peloidal grainstone consisting of peloids, small forams and micritized bioclasts. Intragranular porosity is completely filled by ferroan calcite cement. 10468.5 ft, 3V1-59E, PPL.

ii. Environmental interpretation:

The skeletal grains of small miliolid forams, mollusc fragments, bryozoans, and other bioclasts debris indicate that this sediment formed in areas with normal marine salinity to perhaps slightly raised salinity. Grainstone textures are indicative of moderate to high energy, as is the rounding and abrasion of many grains. Tucker (2001) discussed that peloids often form through coating due to micritization by microborers. Peloids occur preferentially in very shallow environments and are common in shallow – marine tidal and subtidal shelf carbonates and in reef and mud mounds but are also be present in deep water carbonates.

Flügel (2001) describes peloids as grains composed of micro- and cryptocrystalline carbonate and are commonly devoid of internal structures but may contain fine grained skeletal debris and other grains. Common non-skeletal grains such as peloids and ooids suggests deposition in a high energy subtidal environment of an oolitic shoal to back shoal setting (Figure 3.36). According to the standard microfacies types (SMF) by Wilson (1975), this facies is interpreted as SMF 11.

3.3.10. ALGAL FACIES (AF):

Includes: Microfacies A: Squamariacean / coralline algae bindstone.

i. Facies description:

This facies is observed in the upper part of the Lidam Formation. It occurs between a depth of 10980 to 10986 feet in well R1-97. This facies has a range in thickness of approximately 6 feet (Figure 3.31).

This facies is light grey to medium grey, slightly nodular in structure with pressure solution seams. The facies has a packstone depositional texture (Figure 3.32). Two types of alga are found; coralline and squamariacean (Polystrata) algae, both as encrusting forms. The squamariacean is a family of red algae that resemble coralline algae in its thallus structure, but has an aragonitic rather than calcite composition. The microstructures of squamariacean (Polystrata) walls are often highly altered (after aragonite), and have laminar domed and tabular growth forms. Each layer of squamariacean alga is about 0.1 mm in width to several centimeters length and these have grown as tightly laminar encrusting forms.



Figure 3.34 Core photographs showing nodular bedding of Algal Facies (STPF). A; depth: 10982ft R1-97.

Under the microscope the squamariacean (Polystrata) crusts show the typical central mesothalium with its horizontally arranged cells (Buchbinder, 1985). The crusts show the transparent golden tint typical of fossil squamariaceans and the pore spaces between the walls have been replaced by dolomite crystals. Filament walls consist of flat calcite crystals up to $2.5\ \mu\text{m}$ in size and less than $0.5\ \mu\text{m}$ in thickness. These cells are filled with either randomly oriented, micritic crystals or with microspar calcite oriented parallel to filament walls. Under XP, the calcite crystals along the filament walls show a uniform parallel extinction and under PPL, the same crystals appear darker when filament walls are vertical. However, the coralline algae have a uniform dark appearance and under XP do not show any preferred extinction pattern.

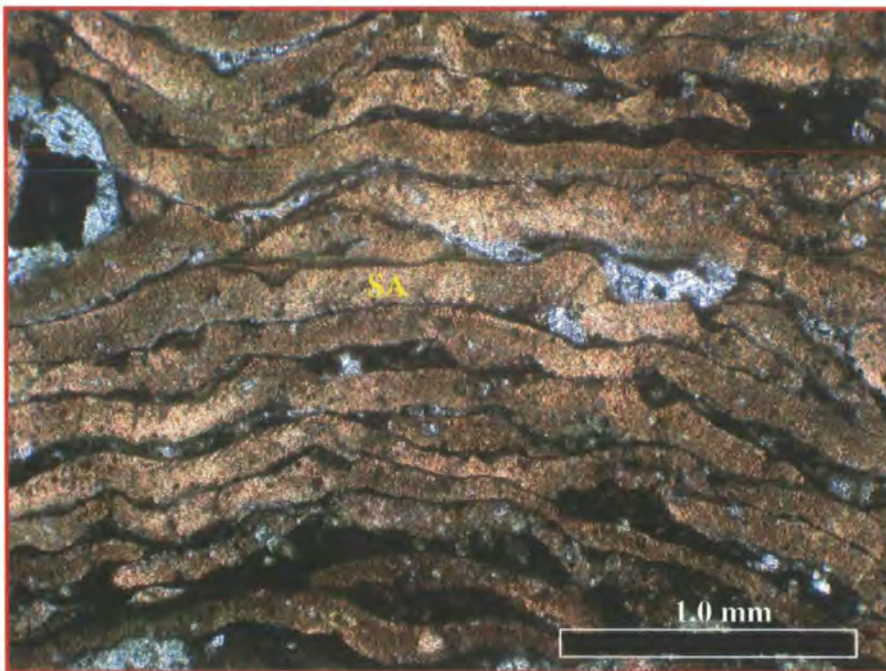


Figure 3.35 Photomicrograph showing laminar encrustation squamariacean (Polystrata) algae (SA). Note calcite crystals along the filament walls. 10984 ft, R1-97, PPL.



Figure 3.36 Photomicrograph showing layered squamariacean algae (SA) crusts in domal and vertical filament walls and altered small foraminifera (F) within dolomite rhombs. 10984 ft, R1-97, PPL.

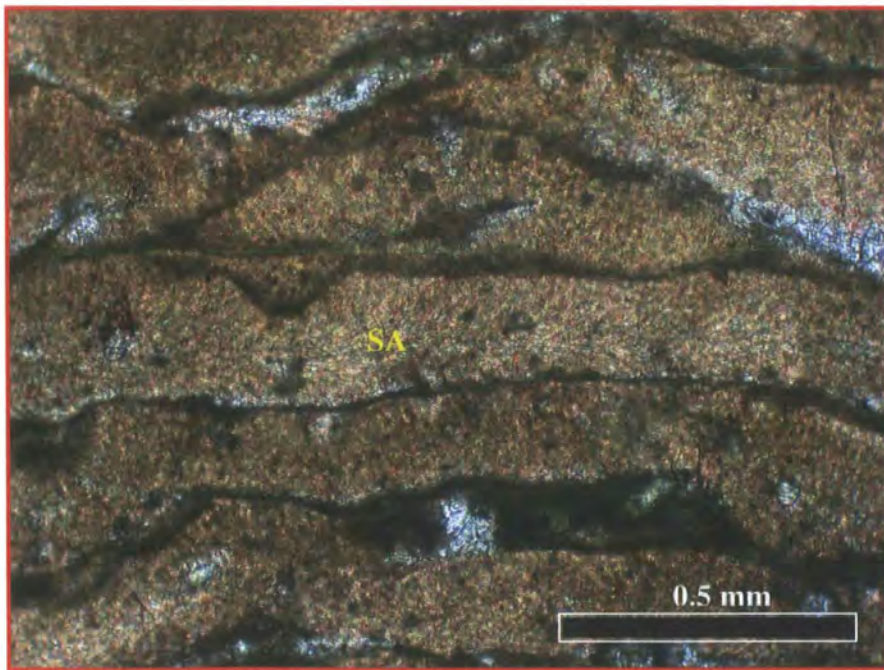


Figure.3.37 Photomicrograph shows large hypothallium cells and vertically arranged filaments. Note micritic microstructure of the cell walls with calcite crystals in the lower part of the cells. 10984 ft, R1-97, PPL.

ii. Environmental interpretation:

These algae probably formed localized developments, perhaps like small scale patch reefs since they have limited thickness and were only seen in one well. The shapes of the algae suggest they probably formed as domal patch reefs, and or tightly ingrown rhodoliths (algal balls). squamariacean (Polystrata) crusts and coralline algae have a widespread distribution in modern tropical-to subtropical shallow marine environments and many Cenozoic limestones (Wray, 1977). Squamariacean and coralline algae grew simultaneously, intermixed on a relatively shallow and sometimes partially exposed platform. The alteration of wall structure of the algae is likely due to replacement of the original aragonite by calcite.

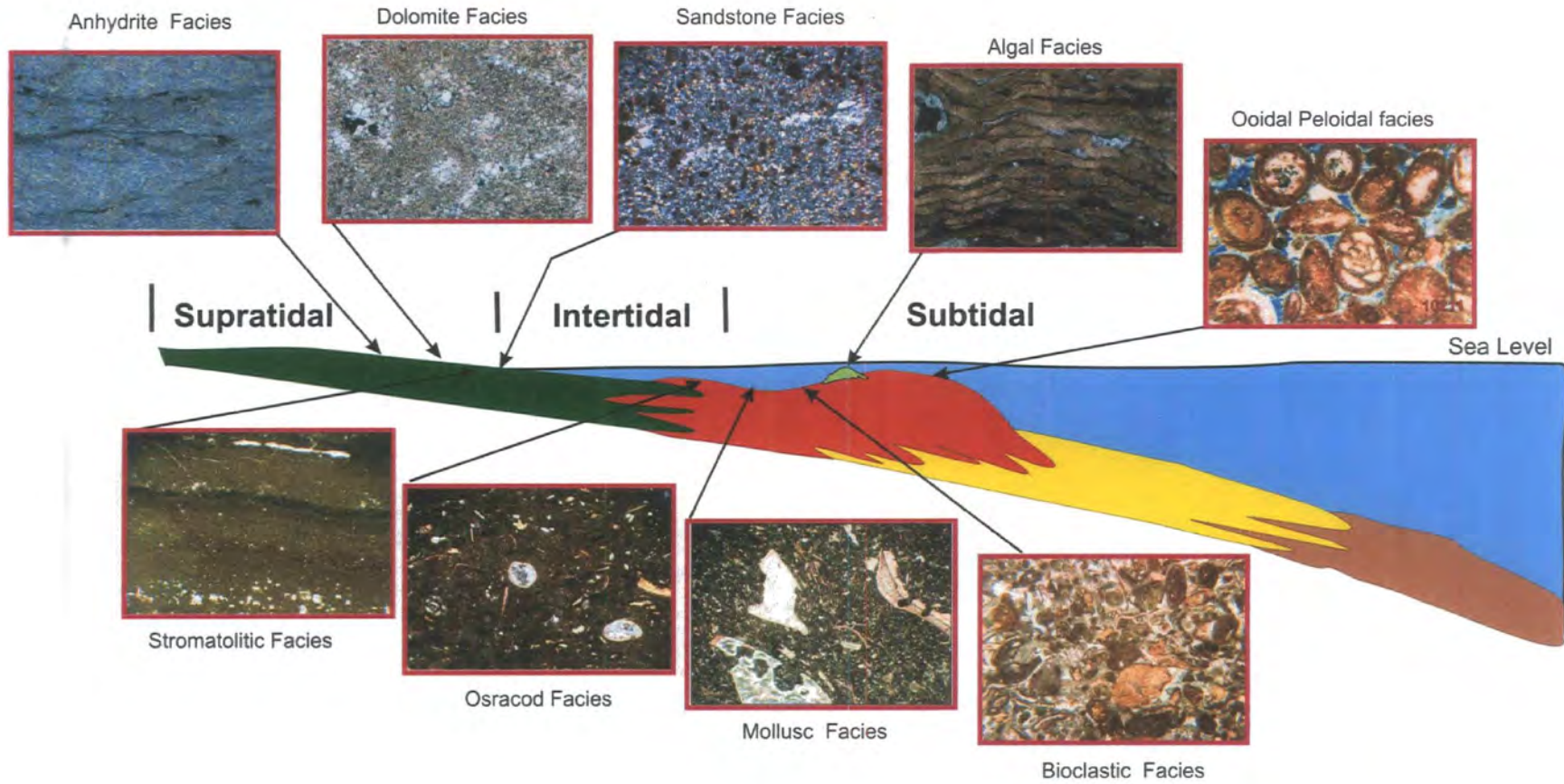


Figure.3.38. Facies model of the Lidam Formation in the studied area, SE, Sirt Basin, Libya.

3.4 DISCUSSION AND OVERALL DEPOSITIONAL INTERPRETATION

On the basis of petrographic analysis and the lithological description ten facies and fourteen microfacies have been identified and their inferred depositional environment has been discussed. These facies and microfacies can be interpreted as having been deposited in supratidal sabkhas, intertidal and sub tidal environments. These are all coastal or shallow-water near-coastal deposits from the inner part of a carbonate platform. However interpretation of the overall platform is hindered because no outer platform deposits were encountered in the study wells. Current models of rimmed shelves and warm-water carbonate ramps could both have very similar inner platform facies.

Many ramps, particularly those from temperate climates have high energy coastal deposits because there is no shelf margin rim to protect inner platform areas from wave and storm energy.

In the tropics, inner platform areas on ramps can have low energy areas, because high productivity and accumulation can result in shallow protective shoals. This is particularly the case in arid settings, where raised salinities can promote development of shallow oolitic shoals, but hinder the development of extensive reef rimmed margins. Therefore, the inner platform deposits of a ramp with shoals could have very similar facies to a rimmed shelf, which typically also has a protected inner platform area. Example of modern platforms with low energy interior includes the ramp of the Trucial Coast and rimmed shelf of Andros Island, Bahamas (Jones, 1992). A ramp versus rimmed shelf setting might be difficult to distinguish based on available data from just the studied well. A comparison and the difference between the two models are illustrated in Table 3.2. The preferred depositional setting of the Lidam Formation (see discussion below) is an inner ramp. This is consistent with the ramp model as proposed by Ahr (1973), Read (1982 and 1985), Wilson (1974), Wright (1986), Mullins et al (1988), Buxton and Pedley (1989) and El Bakai, (1989), with the last author inferring a ramp model for the Lidam Formation. However, as more data becomes available on the Lidam Formation it should be possible in the future to better define the overall depositional setting

	Carbonate ramp	Carbonate rimmed shelf
	<p>Models of carbonate ramp and rimmed shelf (after Tucker and Wright, 1990)</p>	
Energy	Ramps are commonly swept by onshore waves because they lack a barrier along their seaward margin.	Characterized by the development of reefs and carbonate sand bodies along the shelf margin.
Morphology	Ramps have gentle slopes and relatively uniform (a few meters/Km or <math><1^\circ</math>) on which shallow wave-agitated facies of the nearshore zone (oid-peloid shoals or skeletal banks) pass downslope into low energy, deep ramp muds.	Rimmed shelves are shallow reef-rimmed, flat-topped platforms whose outer wave-agitated rim slopes steeply into the basin. Slopes commonly are few degrees to 60. they have semicontinuous to continuous reefal rim or barrier along the shelf edge, backed by skeletal or oolitic sands
Area of high energy	High energy carbonate sands in the wave-and /or tide-agitated, inner shelf (above fair-weather wave base).	Shelf margin is a turbulent, high energy zone, storm waves impinge on the sea floor, organic productivity is higher under this condition
Presence of shoals	Shoals of skeletal debris (grainstones) and coarser debris (rudstones) can be formed through reworking by storm waves + waves + tides	CaCO_3 occur in the form of ooids and cements along shelf margins.
Inner platform	A back ramp is dominated by low energy protected coastal lagoons, although one without shoal development typically has a high energy interior. Water depth approximately 20 to 30m during the high tide	Behind the rim there is usually a shelf lagoon.(very quiet environment with poor circulation and perhaps hypersalinity during the dry season) This is usually protected by a barrier (reefs and sand shoals) from the marginal turbulent zone. Deep water shelves have lagoons up to 30m deep
Reef development	Major reef development is rare since there is no major break of slope in shallow water for colonizing by reef organisms. Pinnacle reefs may develop in deeper water setting. Small patch reef occurring in the back barrier lagoon. Often the local conditions are not suitable for reef development (too cool, or too saline)	Usually reefs developed a long the marginal slope in the turbulent zone.
Modern examples	Trucial Coast of Arabian Gulf and Shark Bay in western Australia are modern examples of carbonate ramps	Belize shelf Gulf of Mexico and Florida Shelf South of Miami are examples of rimmed shelves.

Table 3.5. Differences between carbonate ramp and rimmed shelf depositional models.

The following lines of evidence are consistent with an inner ramp interpretation for the study area:

- 1- The interpretation of the overall platform facies is hindered because no outer platform deposits were encountered in the study wells.
- 2- No evidence has been seen in the studied wells, or unpublished well reports for shallow rimmed shelf deposits, resedimented slope and deeper water basinal facies containing reworked shallow water debris. These reworked debris such as slumps, breccias, lower slope muds, turbidities and down slope bioherms, are not seen in the studied wells which would be typical of slope deposits from a rimmed shelf (Figure 3.39).
- 3- The gradual thickness changes increasing gradually into a northwesterly and southeasterly direction (i.e. from land to sea) in the Lidam Formation suggest that the morphological profile upon which the carbonate facies was deposited was gently sloping. El Bakai (1992) concluded that the homoclinal ramp model is the most acceptable model for the lithofacies depositional environment developed in the Lidam formation (Figure 3.40), but he did not expand on this statement.

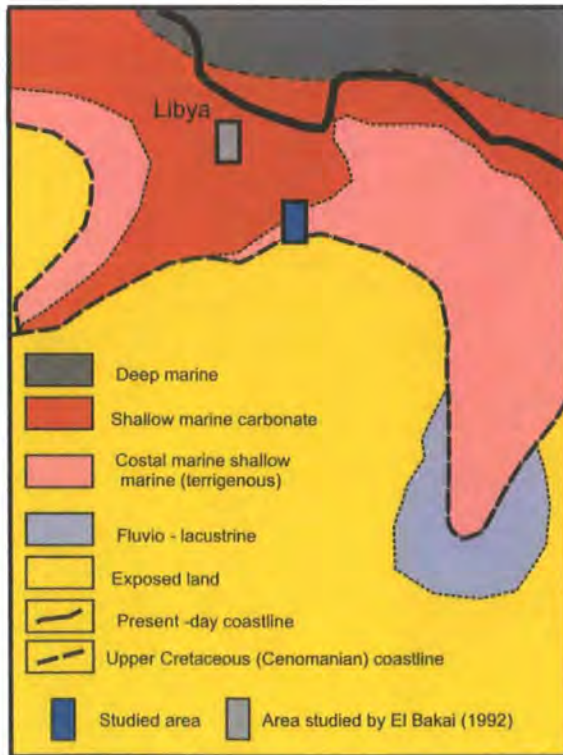


Figure.3.39. Location of the studied area and area studied by El Bakai (1992) with different depositional environment of the ramp setting during Upper Cretaceous (Cenomanian) time.

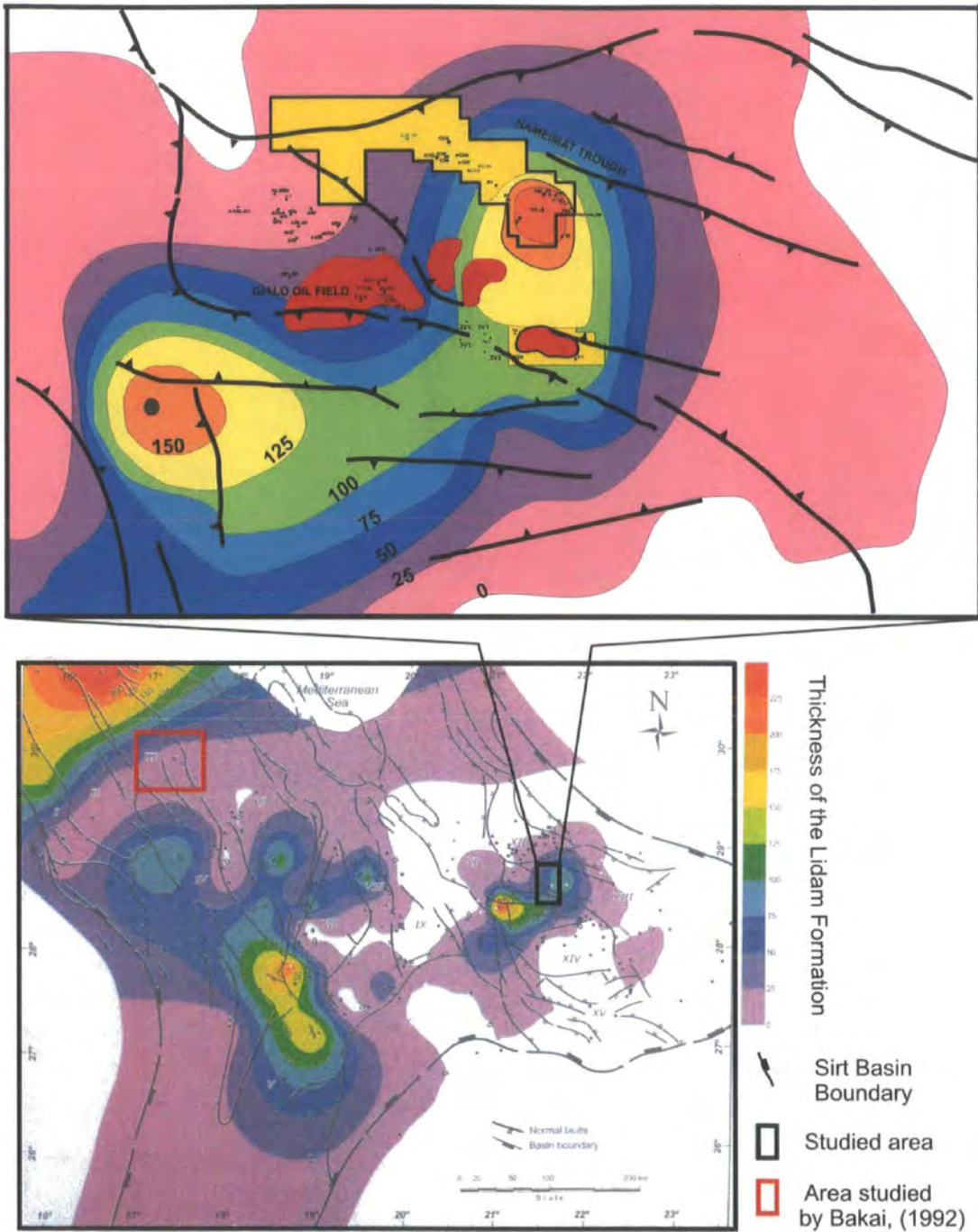


Figure 3.40. Thickness map of the Lidam Formation in Sirt Basin and study area. (Modified after Abadi, 2002).

4- In the studied wells there is almost no evidence for major reef builders being present in the Lidam Formation. The algal lithofacies was much localized and may have formed minor constructional highs in the platform interior. The lack of major reefal builders,

such as corals, in the inner platform cannot be taken as a clear indicator that these elements did not form a seaward barrier. However, on many rimmed platforms, such as Florida, where reefs are present at the margins of the shelf, coral patch reefs are commonly present in the platform interior.

- 5- El- Bakai, (1993) reported that glauconitic-rich sediments are common in the Lidam Formation to the north of the study area. Glauconite typically forms in marine settings down to water depths of 60-500 m where sedimentation rates are low. No reef related components were found in these northern deposits. It is inferred that the Lidam Formation was most likely to have sloped gently down from shallow water in the study area to depths of around 60m in the area to the north, without reefs forming a pronounced break in slope.
- 6- There may have been spatial variations in the depositional setting of the Lidam Formation, although further research is required to verify this. The structural topography and sedimentary patterns during the Cenomanian time suggests an asymmetry in depositional facies (see section 4.6). The Lidam Formation may have developed as a partially rimmed system in a northeasterly direction but as a ramp in a south-easterly direction in the Sirt Basin (Figure 3.39 and 3.40). El-Bakai (1987) concluded that farther to the south and southeast in the Sirt Basin the Lidam sediments are represented by intertidal-supratidal environments. The Lidam Formation generally was deposited in a vary shallow marine environment over the whole Sirt Basin (Barr and Weegar, 1972). Variations in platform style are seen on modern platforms such as offshore Florida, where both rimmed and ramp margins are seen.

3.5 CHAPTER SUMMARY:

The major objective of this chapter focused on facies description and microfacies analysis based on core description and petrographic analysis of the Lidam Formation. The interpretations of depositional environment were inferred through detailed petrographic examination of approximately 70 thin sections. This allowed ten facies and fourteen microfacies to be identified and their different depositional environment to be inferred. The ten facies recognized in the Lidam Formation are: anhydrite facies, replacive dolomite facies, sandy facies, shale facies, stromatolitic facies, ostracod facies, mollusc facies, bioclastic facies, peloidal facies, and algal facies (Table 4.1).

These sediments are interpreted to have been deposited in supratidal, tidal flats, intertidal, and shallow low energy and agitated subtidal environments. The anhydrite, sandy bioclastic and stromatolitic facies dominate in the lower and uppermost part of the Lidam Formation (see chapter 4) and represent the nearshore or part of the inner platform with features indicative of tidal flats.

The mixing of sandstone and bioclastic fragments resulted from nearshore reworking of the sediments probably by wave action. The middle parts (see chapter 4) of the Lidam Formation represent sedimentation of low-energy lagoonal lime-mud in an inner platform environment. These deposits are characterized by the presence of ostracod, small forams (miliolids, and rotaliids), bioturbation, and lamination, mudstone / wackestone texture dominate.

The deposition of the ooidal peloidal packstone and ooidal grainstone facies was in moderate to high energy conditions with sedimentation in a shallow shoal. This is indicated by a well sorted and washed coarse oolitic grainstone and peloidal packstone, including small foraminifera (miliolids). The position of the different facies upon a depositional model has been inferred on the basis of the main components.

The various facies from tidal flat to subtidal shallow water zone deposits in the five wells are more compatible with a ramp depositional model than a rimmed shelf model. This interpretation is on the basis of combining the data from the study wells with evidence of gradual thickness changes, absence of slope slumps or breccias containing reworked shallow water material, and the paucity of reefal framework builders and the lack of evidence for reef development. However, an extensive restricted lagoonal facies could form in the inner part of a ramp protected by oolitic shoals, or on a rimmed shelf landward of the main barrier. Further work on the Lidam Formation is likely to be helpful in differentiating the overall platform development.

CHAPTER FOUR

*SEQUENCE DEVELOPMENT OF THE
LIDAM FORMATION*

CHAPTER FOUR

4. SEQUENCE DEVELOPMENT OF THE LIDAM FORMATION

4.1. INTRODUCTION

4.2. SEQUENCE STRATIGRAPHY OF THE LIDAM FORMATION.

4.2.1. INTRODUCTION TO SEQUENCE STRATIGRAPHY:

4.2.2. BOUNDARY SURFACES.

- 1-Sequence boundary (SB)
- 2- Maximum flooding Surface (MFS).
- 3- Transgressive surface (TS).

4.2.3. SYSTEM TRACT (ST):

- 1- Lowstand Systems Tract (LST).
- 2- Highstand system tract (HST).

4.2.4. STACKING PATTERNS.

4.3. LITHOLOGICAL DESCRIPTION OF THE STUDIED WELLS.

4.3.1. R1-97 WELL

- i. Description*
- ii. Interpretation.*

4.3.2. P3-97 Well

- i. Description*
- ii. Interpretation.*

4.3.3. N6-97 Well

- i. Description*
- ii. Interpretation*

4.3.4. 3V1-95E Well

- i. Description.*
- ii. Interpretation*

4.3.5. 3V3 - 59E Well

- i. Description.*
- ii. Interpretation.*

4.4. DISCUSSIONS ON SPATIAL VARIATION AND SEQUENCE DEVELOPMENT.

4.4.1 Small Scale Variations within the Wells.

- a) intercalations of stromatolitic dolomudstone / anhydrite facies.
- b) Shale based cycles.

4.5. COMPARISON OF LARGE SCALE VERTICAL (TEMPORAL) AND LATERAL (SPATIAL) VARIATIONS.

4.5.1 Comparison between Wells in Platform.

4.5.2 Comparison in Trough.

4.6. SEQUENCE STRATIGRAPHY OF THE LIDAM FORMATION

4.6.1. Sequence Stratigraphic Analysis of the Lidam Formation in the 3V1-59E, 3V3-59E, R1-97, P3-97, and N6-97.

4.7. SEQUENCE STRATIGRAPHIC INTERPRETATION AND CONTROLS ON LARGE SCALE VARIATIONS.

4.8. COMPARISON WITH OTHER CRETACEOUS SUCCESSIONS.

4.9. CHAPTER SUMMARY.

4. SEQUENCE DEVELOPMENT OF THE LIDAM FORMATION

4.1. INTRODUCTION

The aim of this chapter is to describe spatial and temporal variation of the Lidam Formation by focusing on the main lithofacies variations in each of the studied wells. In addition, to interpreting variations in the depositional environment, sequence stratigraphic controls on deposition are discussed and a sequence stratigraphic analysis attempted. The first part of the chapter summarizes sequence stratigraphic concepts (4.2). Lithological descriptions and interpretations of individual wells (4.3) are followed by discussions on the temporal and spatial variations (4.4) and an interpretation of sequence development (4.5). A comparison with other Cretaceous successions is made in section 4.6.

4.2. SEQUENCE STRATIGRAPHY OF THE LIDAM FORMATION

4.2.1. INTRODUCTION TO SEQUENCE STRATIGRAPHY:

Sequence stratigraphic frameworks are defined on the basis of surfaces of erosion and non-deposition, sequence boundaries (SB), and flooding transgressive surfaces and/or maximum flooding surfaces (MFS) that can be recognized in 2-D and 3-D seismic, well log data and outcrops. These surfaces are assumed to have time significance and hence provide a relative time framework for the sedimentary succession. This technique for subdividing sedimentary successions is used as an aid to understand better the inter-relationship of the depositional settings and their lateral correlation and relates development of sedimentary packages to relative sea-level changes (Posamentier et al, 1988 and Van Wagoner et al., 1988).

The sequence stratigraphic terminology presented here is based on the classical concepts introduced by Posamentier et al. (1988), Posamentier and Vail (1988), and particularly by Van Wagoner et al. (1990). Recent reviews and criticisms of these concepts have been presented in the literature (Emery and Myers, 1996; Miall, 1977; Posamentier and Allen 1999). The basic principal of sequence stratigraphy is that deposition of sediments and their spatial and temporal distribution in the basin are controlled by the interplay between sediment supply, basin floor physiography and changes in the relative sea level. The latter refers to changes in the elevation of sea

level by a combination of eustatic fluctuation and basin-floor subsidence or uplift. Sequence stratigraphic analysis aims to divide the stratigraphic record into depositional sequences, in which the sequence boundaries are subaerial erosion surfaces (unconformities) or their correlative conformities. Sequence boundaries are formed by an abrupt fall in relative sea level, i.e., type one sequence boundary (Van Wagoner et al., 1990) (Figure 4.1)

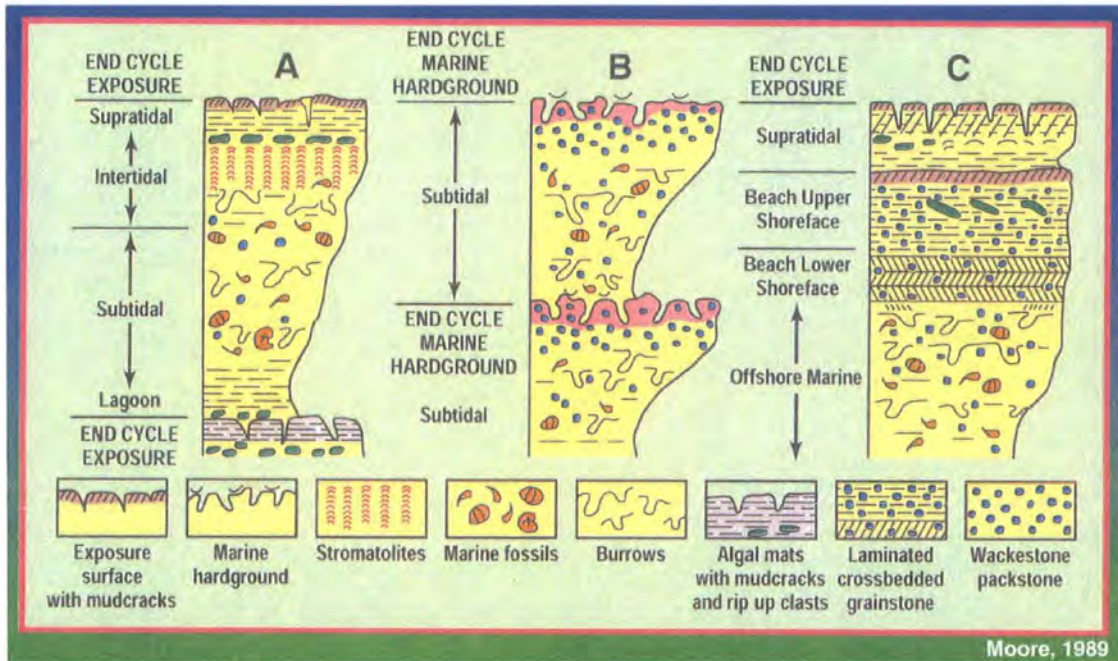


Figure 4.1 different parasequence sets trends from lagoonal subtidal to supratidal environments in carbonate rocks (Moore,1989).

Sequence: a relative conformable succession of genetically related strata bounded by unconformities or their correlative conformities (Mitchum, 1977). A sequence corresponds to a full cycle of base-level change and depositional trends that emerge from the interplay of accommodation space available for sediments to fill and sedimentation. The definition of a sequence is independent of temporal and spatial scales.

Sequences are comprised of *parasequences*, which are defined as a relatively conformable succession of genetically related beds or bed sets bounded by marine flooding surfaces and their correlative surfaces. In addition to these defining characteristics, most parasequences are asymmetrical shallowing-upward sedimentary cycles (Van Wagoner et al., 1990). Each parasequence commonly shows a shallowing upward trend, i.e. regressive deposition of intertidal/supratidal strata on top of shallow water subtidal (Figure 4.1). Parasequences are grouped into parasequence sets

according to their stacking pattern, which is controlled by the rate of deposition compared with the rate of accommodation generation (Van Wagoner et al., 1990).

Systems tracts (ST) are based on the stacking patterns, position within the sequence, and types of bounding surfaces. The definition of systems tract was gradually defined from the earlier work of Exxon scientists (Vail, 1987, Posamentier et al, 1988, and Van Wagoner et al. 1988, 1990). Four systems tracts have been defined; the lowstand, transgressive, highstand, and shelf margin system tracts. The basics and fundamental units of the stratigraphic sequence are discussed below:

4.2.2. BOUNDARY SURFACES.

1- Sequence boundary (SB):

Sequences are enveloped by sequence boundaries (SB) that are identified as significant erosional unconformities and their correlative unconformities. Sequences are controlled by changes in relative sea level, and as they are bounded top and bottom by unconformities, they necessarily begin with a lowstand of sea level. The lowstand exposes the continental shelf, or in an epeiric sea, the shallower portions of the sea floor, to subaerial exposure and erosion (Figure 4.2). These boundaries are diachronous, capping the previous highstand systems tract (HST) and during which there is erosion of the surface of the down stepping sediments deposited during the sea level fall (Catuneanu, 2002).



Figure 4.2 Sequence boundary formation (modified from Van Wagoner 1990).

2- Maximum flooding Surface (MFS):

A surface of deposition at the time the shoreline is at its maximum landward position (i.e. the time of maximum transgression) (Posamentier & Allen, 1999). The surface marks the time of maximum flooding or transgression of the shelf and it separates the transgressive and highstand systems tract (HST). Seismically, it is often

expressed as a downlap surface. Marine shelf and basinal sediments associated with this surface are the result of slow rates of deposition by pelagic-hemipelagic sediments and they are usually thin and fine grained. An MFS is often characterized by the presence of radioactive and often organic rich shales, glauconite, and hardgrounds (Mitchum, 1977).

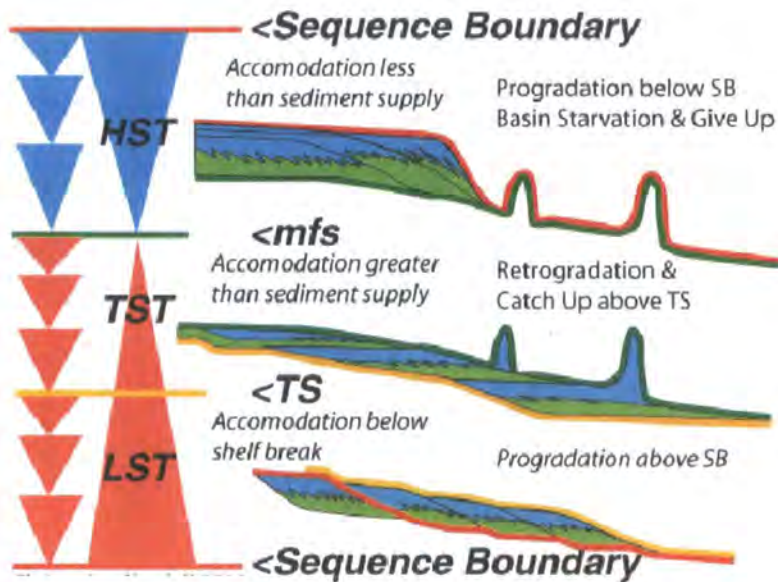


Figure.4.3. Ideal carbonates sequence with sequence boundary (SB) and maximum flooding surface (MFS).

The maximum flooding surface (MFS) is commonly associated with widespread thin bedded concentrations of fauna with high abundance and diversity. An MFS can often be the only portion of a sedimentary cycle which is rich in fauna. Often in a landward direction the maximum flooding surface may coincide with the underlying transgressive surface formed during or just after the initial transgressive phase that, immediately followed a sea level lowstand (Figure 4.3). The MFS is not commonly burrowed or bored. Any burrowing or boring are likely connected to the preceding transgressive surface before the water deepens and conditions become inimicable for colonization but favour preservation. The MFS often marks the bounding surface between coarsening and/or fining upward cycles and is used to relate these cycles to deepening and shallowing in the geological section (Helland-Hansen and Martinsen, 1996)

3- Transgressive surface (TS).

This is a marine-flooding surface that forms the first significant flooding surface in a sequence. The transgressive surface (TS) in most siliciclastic and some carbonate

successions marks the onset of the period when the rate of creation of accommodation space is greater than the rate of sediment supply. It forms the base of the retrogradational parasequence stacking patterns of the Transgressive Systems Tract. In areas of high sediment supply, e.g. on rimmed carbonate platforms, the rate of sediment supply may keep pace with the rate of relative sea-level rise and thus the TS will mark a change from a progradational to an aggradational parasequence stacking patterns (Catuneanu, 2006).

The transgressive surface (TS) is often characterized by the presence of a surface marked by consolidated muds of firm grounds or hardgrounds that are cemented by carbonates. Both surfaces are often penetrated by either burrowing or boring organisms. For instance burrows are found penetrating the firm grounds and are often filled by an overlying widespread winnowed, sorted and often conglomeratic sediment, or lag. If the rate of sediment supply is low over the transgressive surface this may merge landward with the maximum flooding surface (Figure 4.4) (Catuneanu, 2006).

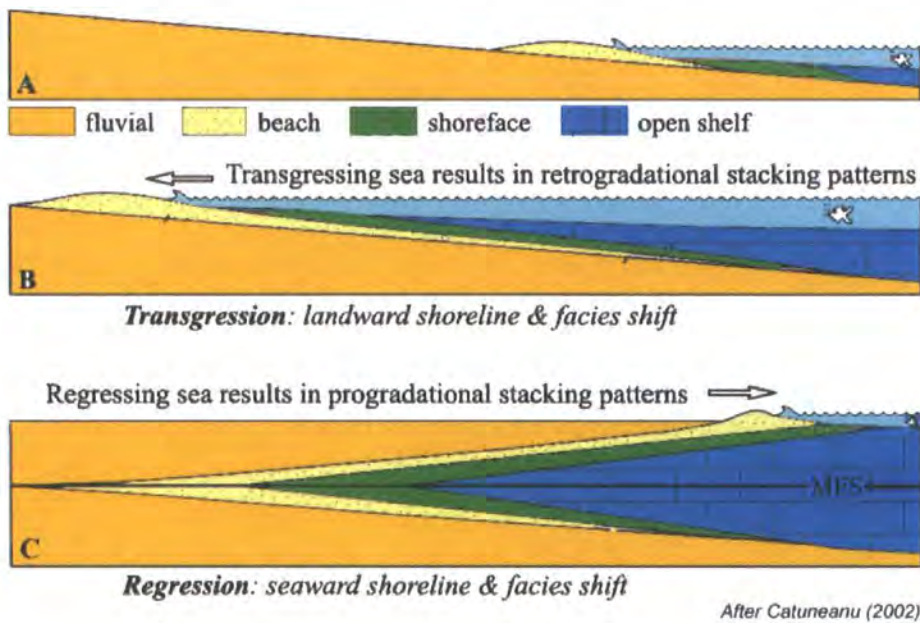


Figure 4.4. Transgression and regression of the sea results in retrogradational and progradational stacking patterns. MFS = max flooding surface.

4.2.3. SYSTEMS TRACT (ST):

Three main systems tracts are defined; the lowstand systems tract (LST), the transgressive systems tract (TST), and the highstand systems tract (HST).

1-Lowstand Systems Tract (LST).

The lowstand systems tract is bounded by the highstand systems tract (HST) below and the transgressive systems tract (TST) above. This system tract is represented by the sedimentary accumulation that straddles the lowest position of the relative sea-level curve. It often forms a prograding wedge at the base of a shelf margin with its lower boundary onlapping onto the progradational clinoforms and/or downlapping onto a downslope fan (Plint and Nummedal, 2000 and Coe et al, 2002).

The depositional setting of the lowstand systems tract (LST) occurs below the shelf margin break; the depth of water in the adjacent basin determines whether the sediments are subaerial, and/or submarine. This subaerial onlap might be equated by some with the Transgressive Systems Tract (Mitchum,1977).

The upper boundary of the lowstand systems tract (LST) is marked by the development of the Transgressive Surface that steps up onto the shelf margin (Figure 4.5). The characterization of the boundary between falling stage systems tract (FSST), or the early lowstand systems tract and the overlying sediments becomes subaerial if the onlapping wedge of the lowstand systems tract (LST) fills incised valleys (Posamentier & Allen, 1999 and Plint & Nummedal, 2000).

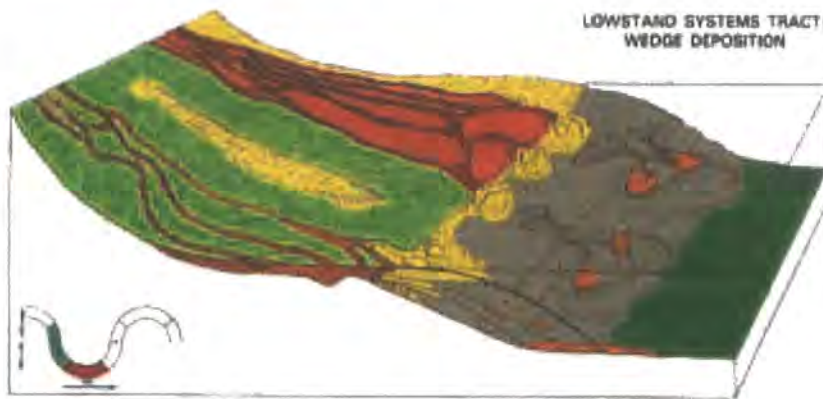


Figure 4.5. Diagram showing the Lowstand systems tract (LST).

Posamentier and Allen (1999) refer to the falling stage systems tract (FSST) as the early lowstand systems tract (LST). Traditionally the sediments of the lowstand systems tract, as defined by Posamentier and Allen (1999), included the deposits that accumulated after the onset of relative sea-level fall directly on the sequence boundary over the highstand systems tract (LST) as a basin-floor fan, slope fan, and Lowstand wedge.

The lowstand systems tract (LST) is divided into the falling stage systems tract (FSST) and lowstand wedges (LSW). These latter often filling incised valleys that cut

down into highstand systems tract (HST). This systems tract is equated with development of limited accommodation associated with a small rise in relative sea level during an essentially lowstand of the sea. Earlier papers that defined systems tracts including Vail (1987) and Posamentier and Vail (1988), placed part of the falling stage systems tract (FSST) within the lowstand systems tract (LST).

The falling stage systems tract (FSST) includes all regressive deposits that accumulated after the onset of a relative sea-level fall and before the start of the next relative sea-level rise. The FSST lies directly on the sequence boundary and is capped by the overlying lowstand systems tract sediments. A variety of parasequence stacking patterns can be produced including: downward stepping prograding clinoforms, stranded parasequences, and mass flow deposits in distal areas. Each of these parasequence stacking patterns depends on the depositional profile, the rate of sediment supply, and the rate of relative sea-level fall. The FSST was first defined by Plint and Nummedal (2000). This systems tract has also been termed the early lowstand systems tract (ELST) (Posamentier and Allen, 1999).

2- Highstand system tract (HST).

The highstand system tracts (HST) are regressive deposits that form when sediment accumulation rates exceed the rate of relative sea-level rise, and increases in accommodation. This constitutes the upper systems tract in a sequence (Figure 4.6).



Figure 4.6. Depositional model during Highstand systems tract (HST).

The base of this systems tract is formed by the maximum flooding surface (MFS) over which the highstand systems tract (HST) sediments prograde and aggrade. The top of this systems tract is formed by the eroded unconformity surface that develops

when a sea-level fall initiates erosion of the subaerial highstand systems sediment surface (i.e. a sequence boundary). The HST may be characterized by one or more aggradational to progradational parasequence sets with prograding carbonate sediments.

4.2.4. STACKING PATTERNS:

Parasequences are grouped into parasequence sets according to their stacking pattern, which, in turn, are controlled by the ratio of depositional rate and accommodation rate (Van Wagoner et al., 1990).

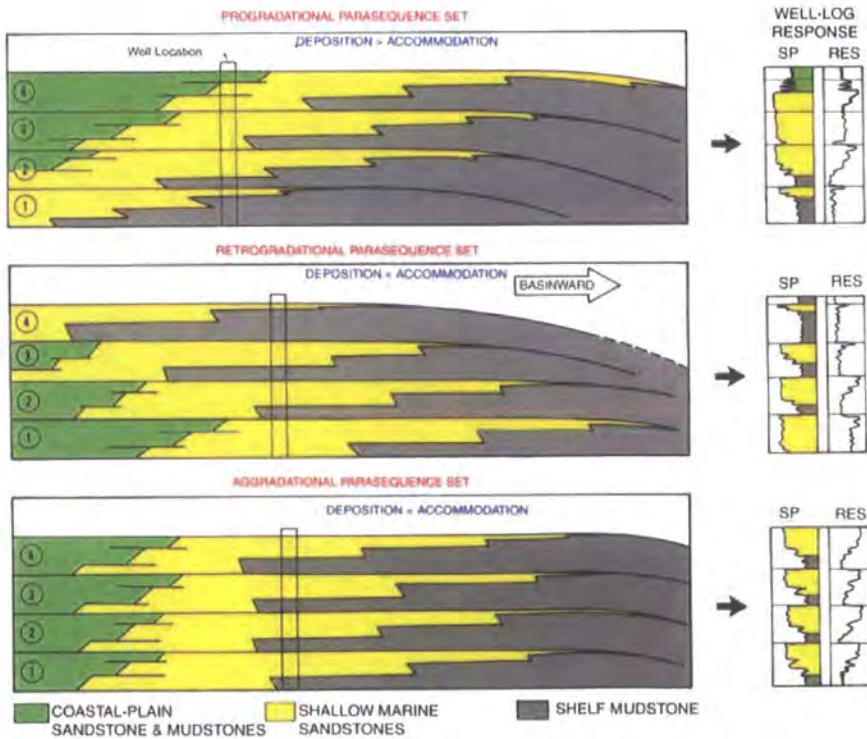


Figure 4.7. Stacked patterns of the different parasequences related to deposition and accommodation space generation.

Three main depositional parasequence sets are defined:

- **Progradational:** A parasequence set in which successively younger parasequences are deposited farther basinward; overall the rate of deposition is greater than the rate of accommodation (Figure 4.7).
- **Retrogradational:** A parasequence set in which successively younger parasequences are deposited farther landward in a backstepping pattern. Overall, the rate of deposition is less than the rate of accommodation (Figure 4.7).

- **Aggradational:** Vertical upward building of a sedimentary succession. This usually occurs when there is a relative rise in sea level produced by subsidence and/or eustatic sea-level rise, and the rate of sediment influx is sufficient to maintain the depositional surface at or near sea level (i.e. carbonate sedimentation with relative sea level). The results are aggradational stacking patterns in parasequences when the patterns of facies at the top of each parasequence are essentially the same (Posamentier, 1999; Wilgus et al.; 1988, Emery, 1996) (Figure 4.7).

4.3. LITHOLOGICAL DESCRIPTION OF THE STUDIED WELLS:

The general lithological description and the thickness of the Lidam Formation in the study area has been described from combined analysis of electric logs, core description, and core samples (including petrography) taken from each well (Table 1.1).

A wide range of features were described in the cores and microfacies samples. These included; lithology, texture, composition, rock colour, fossils, sedimentary structures, and diagenetic features as well as petrophysical criteria (e.g. porosity and permeability). For each of the measured sections through cored intervals features are expressed by symbols with standard abbreviations and codes given in appendix (1). The lithological descriptions of the Lidam Formation for each of the studied wells are outlined below:

4.3.1. R1-97 WELL:

i. Description:

This well is located in concession 97, Hamid oil field, Gialo Platform in the southeastern part of the Sirt Basin (Figure 1.1). The coordinates of this well are Latitude: 28° 35' 31.71" N and Longitude: 21° 46' 58.32" E. The total depth reached is 11714 feet and the total thickness of the Lidam Formation is approximately 205 feet. Only the upper 94 ft of the Lidam subsurface succession has been cored between depths of 10980 ft to 11074 ft (Figure 4.8).

- The lower 21 feet from the bottom of the cored interval from a depth of 11074 feet to 11053 feet is dominated by anhydrite facies with chicken wire structure intercalated with stromatolitic facies. These are overlain by 7 feet of dolomitised mollusc facies and then 2 feet of laminated shale facies.
- The cored ostracod wackestone/ packstone facies totals about 37 feet and occurs at two different depths between 11053 to 11028 feet and at the top of the cored

interval between 10996 to 10984 feet (Figure 4.8). The depositional texture of this interval ranges from mudstone / wackestone to packstone with dark grey shale interbeds. Bioturbation is common, as are ostracods, together with bioclastic debris including molluscs, small foraminifera and echinoderms.

- The middle part is the main reservoir unit, about 29 feet from a depth of 11027 to 10998 feet and is characterized by medium to light grey, highly bioturbated wackestone / packstone interbedded with thin laminated layers of dark grey shale. This interval contains three different facies, these are mollusc, foraminifera bioclastic wackestone / packstone and ooidal peloidal grainstone facies. These deposits consist of packstone / grainstone containing ooids, peloids, small forams (miliolids), echinoderms, and mollusc fragments. Bioturbation is abundant. Stylolites and pressure solution seams are common, as are vertical fractures.
- As mentioned the upper 18 feet from a depth of 10998 to 10980 feet is dominated by dolomitic limestone wackestone / packstone of the ostracod facies intercalated with shale. Pressure solution seams and vertical fractures are common. Toward the top of this interval there is a decimetre thick bed of the Algal (squamariacean / coralline algae bindstone) facies.

ii. Interpretation:

The cored interval of this well begins with the anhydrite facies (including nodular chicken-wire structure) interpreted as forming in a supratidal sabkha environment. Intercalated shale and stromatolitic intervals probably formed in intertidal lows and protected areas with clay influx. There is an upward change to subtidal deposits with ostracod facies interbedded with shales probably deposited in a protected low energy, restricted lagoonal environment with some clay influx. The bioclastic wackestone / packstone accumulated in shallow, more wave-influenced water. These sediments grade up into intertidal to subtidal environments.

The facies change into oolitic shoal to back shoal deposits, formed in high energy subtidal environments. The upper most intervals are bioturbated wackestone with reefal patches of Algal (squamariacean / coralline algae bindstone) facies. These sediments were deposited under low wave energy conditions, probably in a lagoonal area (Figure 4.9).

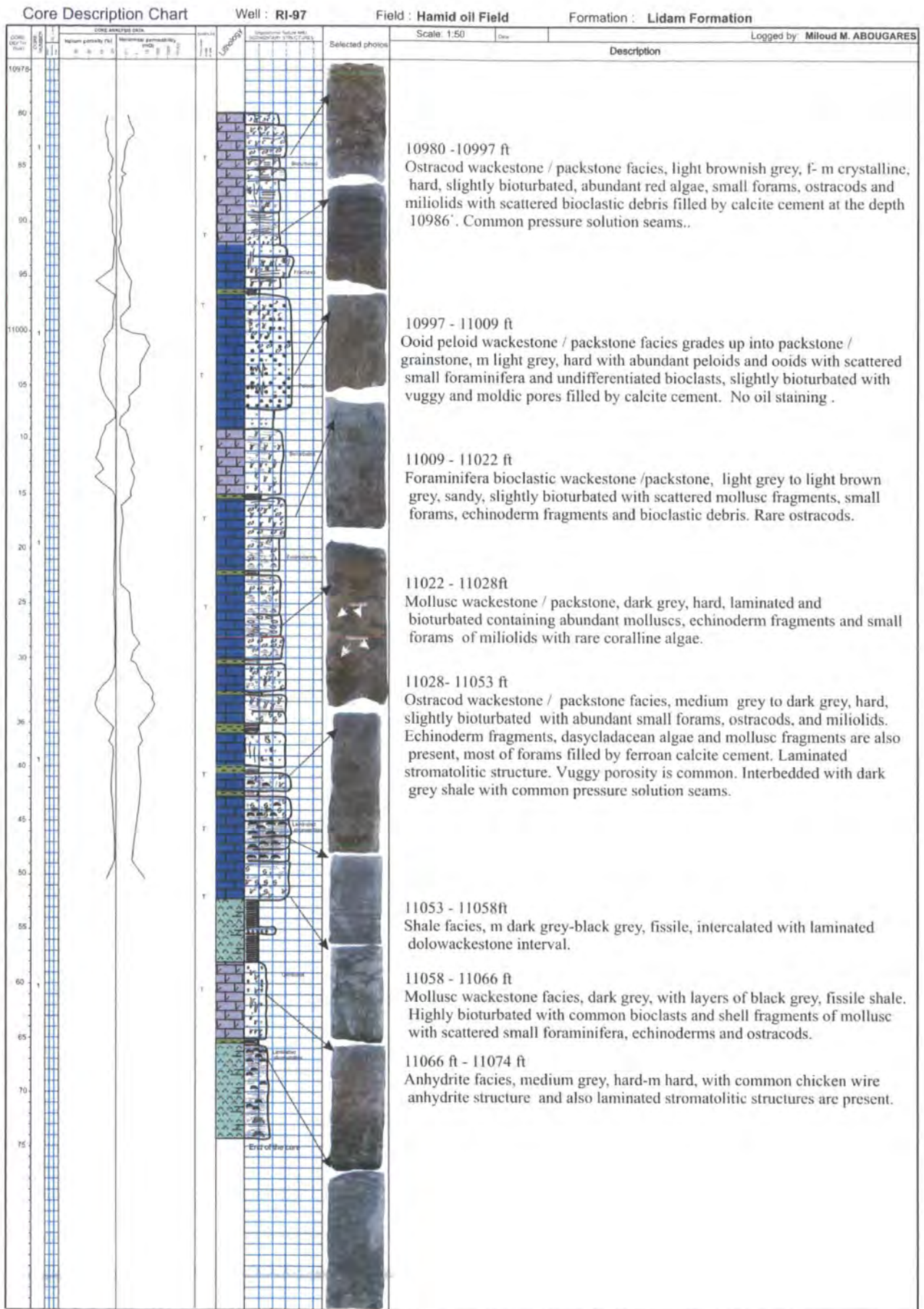


Figure 4.8. Lithological Description of the Lidam Formation in well R1-97, Hamid Field, SE Sirt Basin, Libya.

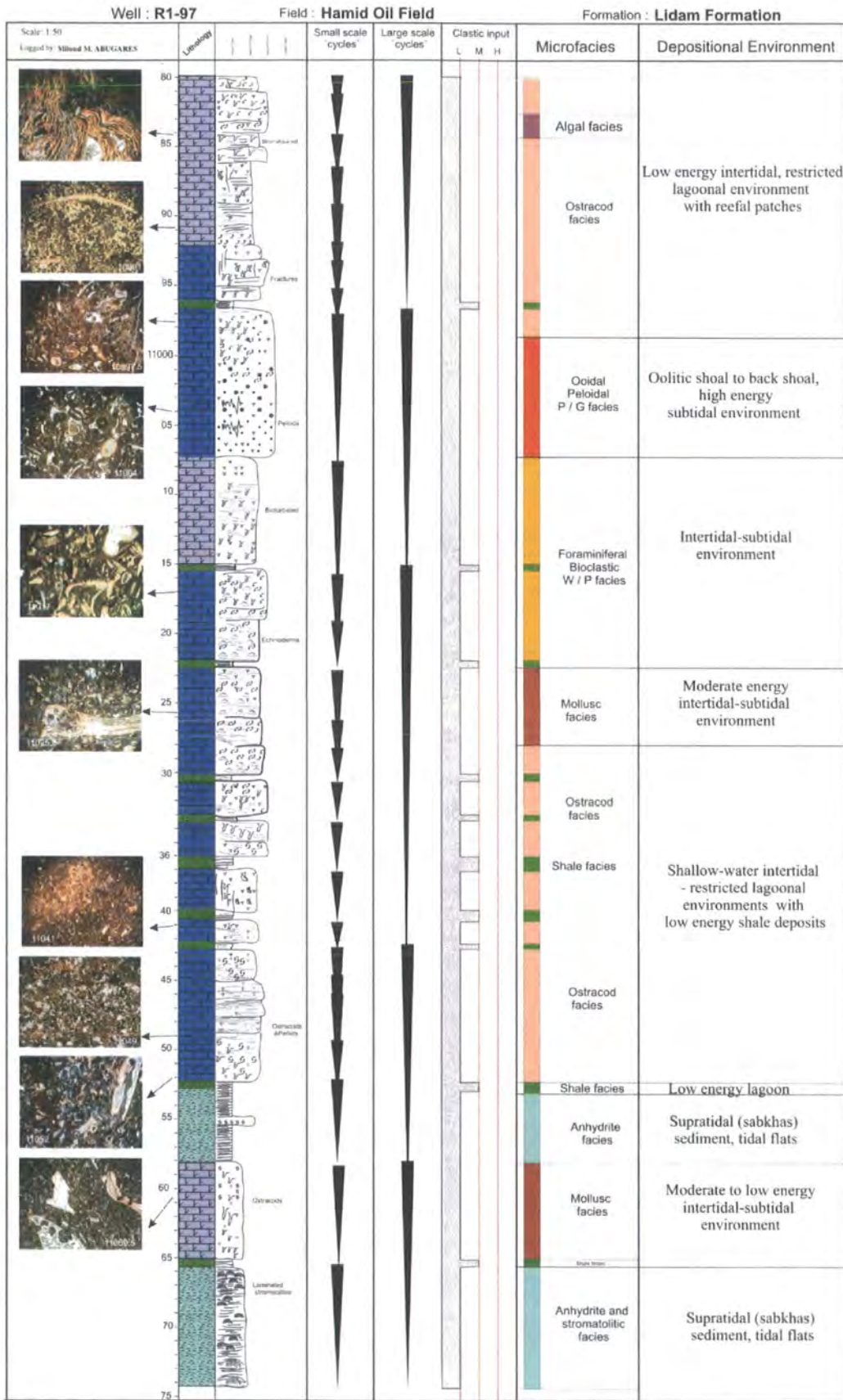


Figure 4.9. Stratigraphic section of the Lidam Formation facies in well R1-97, Hamid oil field, SE Sirt Basin, Libya. Vertical triangles show shallowing upwards.

4.3.2. P3-97 Well:

i. Description:

This well is located in Concession 97 in the Al Nakhalah Field (P. discovery), Longitude: 21 41' 16.70"N and Latitude: 28 48 31.60 E, SE in the Sirt Basin, Libya (Figure.1.1). The total thickness of the Lidam Formation in this well, based on well logs, is about 260 feet from a depth of 11600 to 11860 feet. Only the upper 78 feet of the formation has been cored between depths of 11602 to 11680 feet (Figure 4.10).

- The lower cored 40 feet from a depth of 11681 to 11640 feet is dominated by dolomitic limestone and dolomite wackestone / packstone interbedded with dark grey shale. The shales are often highly bioturbated and may contain ripup clasts and laminated stromatolitic structures. These sediments contain abundant ostracods, small forams (miliolids), and echinoderm fragments with scattered bioclastic debris, and are mainly from the ostracod facies with intercalated shale facies.
- The middle 29 feet of the cored interval (11626 to 11640 feet) is an important reservoir in this well. As well as including the upper undolomitized part of the ostracod- rich unit argillaceous, fossiliferous, dolomite and dolomitic limestone with packstone / grainstone to grainstone texture dominate. The upper part of the interval consists of foraminifera wackestone / packstone and ooidal peloidal packstone/ grainstone facies. These deposits contain abundant peloids, ooids, small forams (miliolids) and dascycladacean green algae. High amplitude stylolites and ripup clasts are present in the lower part. Intercrystalline and vuggy porosity is common, and may be partially filled by calcite cement.
- The 8 foot interval between 11626 to 11618 feet is characterized by siliciclastic facies intercalated with anhydrite facies and intervals of dark shale. The uppermost part of the cored interval 11618 feet to 11602 feet is dolomitized ostracod facies interbedded with mudstone / wackestone textures. This interval is light brownish grey, hard, bioturbated with abundant scattered bivalves. Mouldic porosity is filled by non-ferroan and ferroan calcite cement and anhydrite crystals. Most of the interval is poorly oil stained (Figure 4.10).

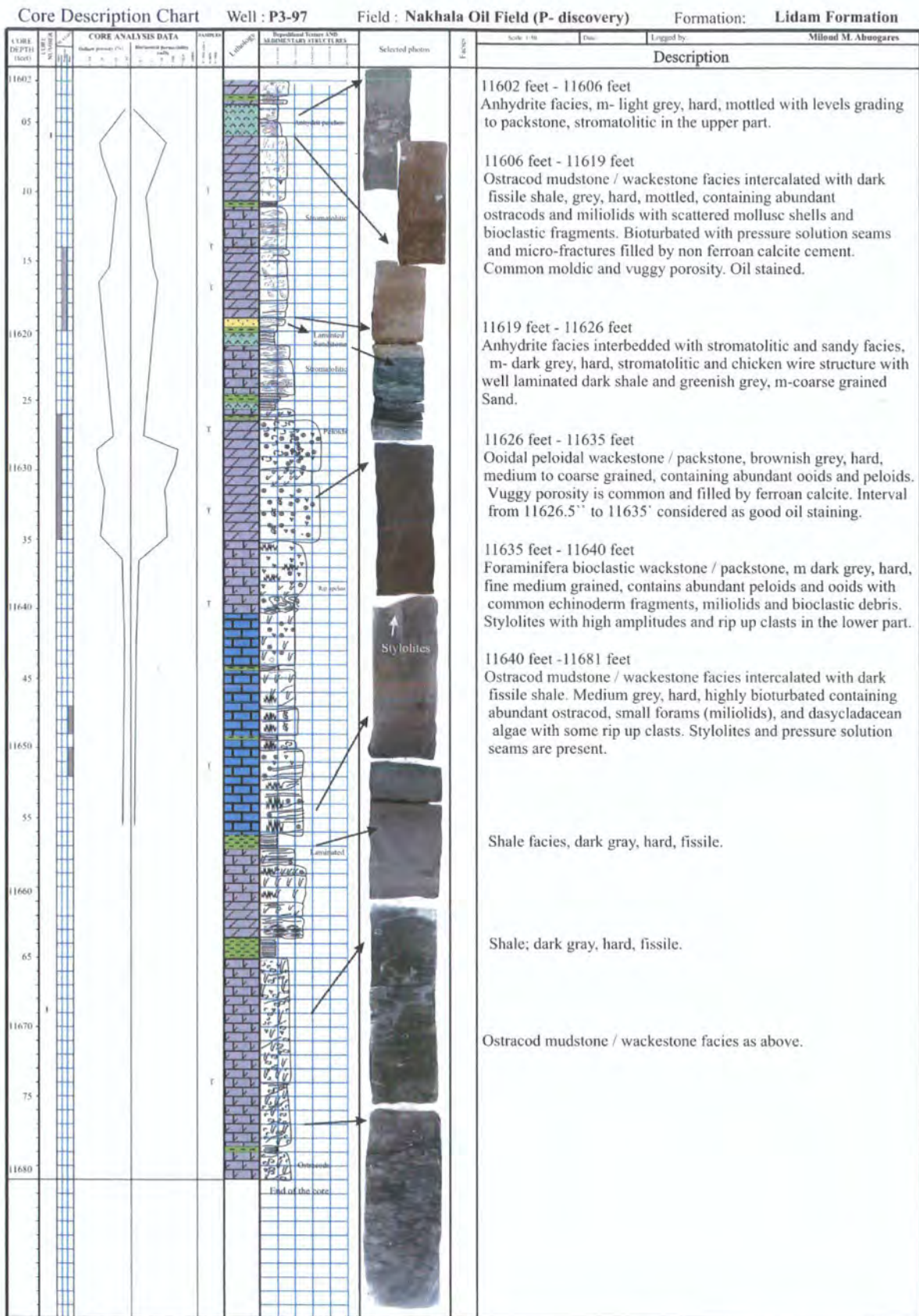


Figure.4.10. Lithological Description of the Lidam Formation in well P3-97, Al Nakhalah Field, SE Sirt Basin, Libya.

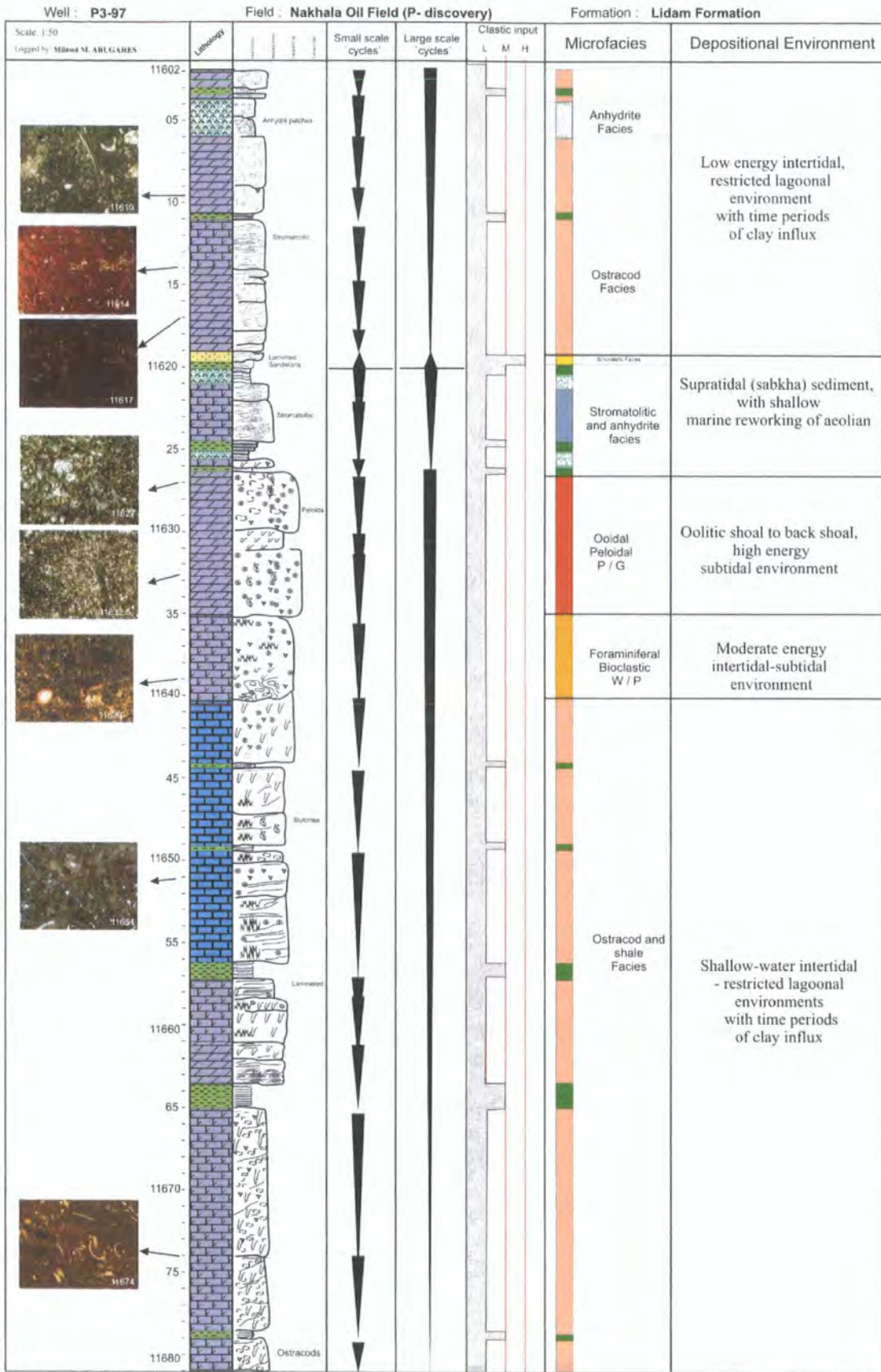


Figure 4.11. Stratigraphic section of the Lidam Formation facies in well P3-97, Al Nakhalah oil field, SE Sirt Basin, Libya. Vertical triangles show shallowing upwards

ii. Interpretation:

The cored interval of the Lidam Formation in this well begins with ostracod wackestone / packstone intercalated with dark grey shale deposited in a shallow-water restricted lagoonal (intertidal to subtidal) environment. These sediments shallow up into back-shoal to shoal facies from foraminifera wackestone / packstone into ooidal peloidal grainstone facies (Figure 4.11). The later sediments are deposited in shallow high wave energy or less protected settings than the ostracod facies.

Above this the facies continue to shallow upwards into supratidal to intertidal deposits of the anhydrite facies and stromatolitic facies intercalated with siliciclastic facies. The siliciclastic facies may have accumulated through reworking of terrestrially derived clastics into shallow marine nearshore sediments. The upper part of the cored section is predominantly ostracod packstone facies, which were deposited in an intertidal to restricted lagoonal environment. Intercalated nodular bedded anhydrite facies with dark grey shale were deposited mainly under supratidal, to perhaps intertidal conditions. Generally, the cored section in this well is interpreted as forming in a restricted lagoonal setting, passing into shallow shoal / backshoal (Transgressive Systems Tract) and then back into restricted lagoonal and supratidal deposits (Highstand Systems Tract)(Figure 4.11).

4.3.3. N6-97 Well:

i. Description:

This well is located in Concession- 97, Al Nakhalah field (N. discovery), Longitude: 28° 50` 1.974`` N and Latitude: 21° 46` 1.787``E, in the Hameimat Trough, SE Sirt Basin (Figure.1.1). The total thickness of the Lidam Formation on the basis of well logs is about 360 feet from a depth of 11770 to 12130 feet. Only the upper part of the formation has been cored (88 feet) between depths of 11782 to 11870 feet (Figure 4.12).

- The lower cored 14 feet (11857 to 11871 feet) are dominated by peloidal ooidal packstone / grainstone facies, which are mottled, slightly bioturbated and contain abundant ooids and peloids. Small forams (miliolids) and mollusc shells (gastropods and bivalves) are common. Intergranular and intragranular pores are completely filled by ferroan and non ferroan calcite cement. Stylolites and vertical fractures are also present.

- The middle 46 feet from a depth of 11811 to 11857 feet is dolomitic limestone interbedded with laminated, black grey, fissile shale. This carbonate interval is dominated by ostracod facies with mudstones grading up into wackestone / packstone, which are brownish grey in colour, hard, and slightly bioturbated. The ostracod facies contains abundant ostracods and small forams, with other common bioclasts including echinoderms and mollusc fragments. Mouldic and vuggy porosity is filled by calcite cement. Pressure solution seams and stylolites are common.
- The upper 29 feet is dominated by dolomitic limestone, the lower 10 feet of this interval contains mudstones and wackestone from the anhydrite and stromatolitic facies. These are laminated and interbedded with dark grey shale and a laminated dark greenish grey, fine to medium grained sandstone layer. The uppermost part of this interval (9 feet) is foraminifera bioclastic wackestone, containing abundant small foraminifera (miliolids and rotaliids) and common bioclastic debris. No oil staining or porosity was visible.

ii. Interpretation:

The sediments in the lower part of the cored interval in well N6-97 start with fine to medium-grained, moderately sorted ooidal peloidal packstone / grainstone interpreted as moderate to high energy oolitic shoal facies (Figure 4.13). This facies grades upwards into the ostracod facies, which were deposited in a shallow water intertidal or subtidal-restricted lagoonal environment. Intercalated shales result from clay input in a protected, or probably restricted lagoonal area. The succession moves up into the supratidal (sabkha deposit), tidal flat deposits with possible shallow marine reworked of sandstone deposits. These facies are dominated by anhydrite chicken wire structures and well laminated layers of shale associated with a layer of fine to medium grained sandstone. These facies are indicative of a regressive succession ending with accumulation of anhydrite and shale and reworking of terrestrial sand at the end of the cycle. Above this package, the facies show an increase in water depth. These overlying facies are foraminifera bioclastic facies dominated by abundant small foraminifera of miliolids with common mollusc, echinoderm fragments, and desycladacean algae. These facies have been deposited in low to moderate energy intertidal to shallow-subtidal settings. Intercalated shale accumulated in low energy protected areas. These

packages are transgressive deposits from supratidal (sabkhas) into low to moderate energy intertidal to subtidal conditions (Figure 4.13).

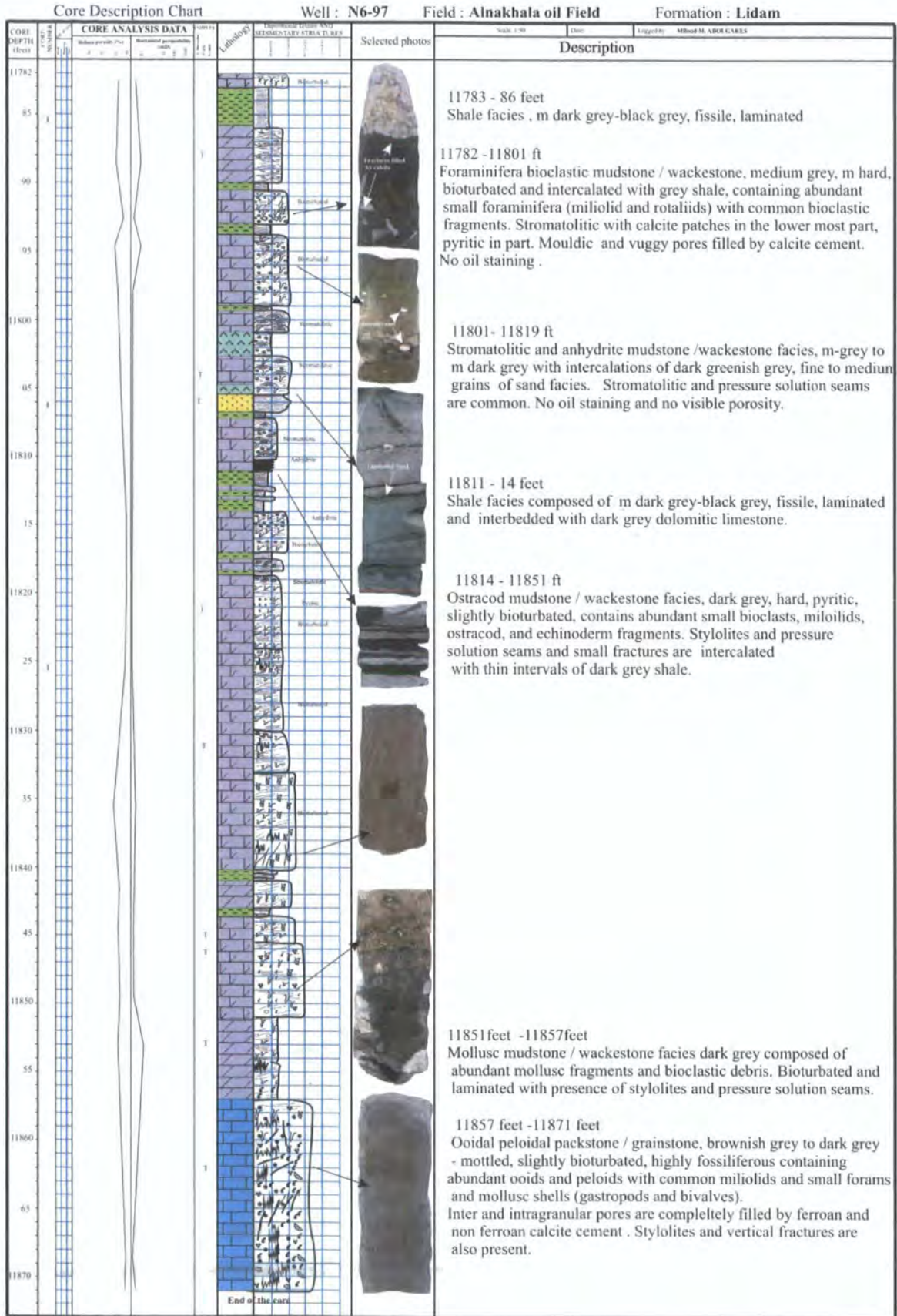


Figure 4.12. Lithological description of the Lidam Formation in well N6-97, Al Nakhalah Field, SE Sirt Basin, Libya.

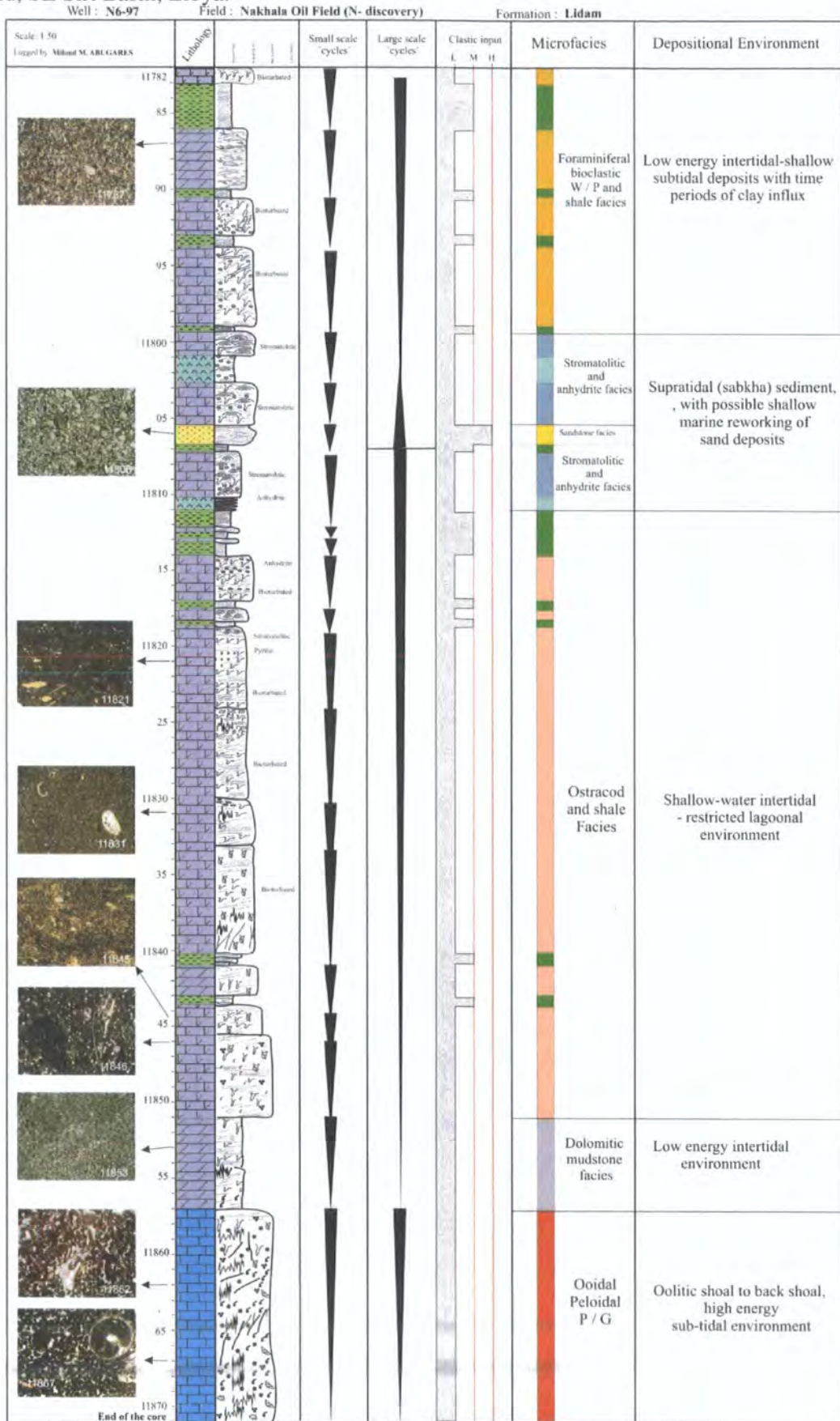


Figure 4.13. Stratigraphic section of the Lidam Formation facies in well N6-97, Al Nakhalah oil field, SE Sirt Basin, Libya. Vertical triangles show shallowing upwards

4.3.4. 3V1-95E Well:

i. Description:

This well lies at Longitude: 28° 36' 45" N and Latitude: 21° 38' 46" E, in concession 59E, the 3V area, drilled in the Gialo platform from the SE Sirt Basin. (Figure 1.1). The thickness of the Lidam Formation in this well is 105 feet, which has been totally cored between depths of 10441 to 10546 feet (Figure 4.14).

- The lower 28 feet of Lidam Formation in core # 4 measured between the depth of 10518 and 10546 feet, overlies the Nubian Sandstone. This interval is characterized by the occurrences of laminated stromatolitic and anhydrite facies interbedded with lithic sand, bioclastic sand, and shale. Sandy units contain well-rounded quartz grains of fine sand / silt grain size. This interval is light to medium dark grey, argillaceous with a depositional texture of dolomitized mudstone / wackestone with nodular anhydrite. Nodular bedding of anhydrite which forms cloudy chicken-wire structure is common. Pyrite nodules are observed within this interval.
- The middle part of the Lidam Formation is represented by about 58 feet between depths of 10462 to 10518 feet. This consists of two of different intervals; the first is dominated by massive limestone, which is light to medium brown, slightly argillaceous, highly bioturbated with stromatolitic structures and intercalations of laminated anhydrite and shale. This interval is characterized by ostracods, anhydrite, peloidal packstone, and stromatolitic facies. The second interval is dominated by a depositional fabric of packstone / grainstone grading into grainstone. This succession has foraminifera bioclastic packstone which pass upwards into ooidal peloidal packstone / grainstone facies. This interval is the important reservoir unit in this well. The bioclasts are fragmented and include small benthic foraminifera (miliolids), ostracods, together with bioclastic debris of echinoderms, bryozoans, dasycladecean algae, and molluscs (including, gastropods).
- The upper 20 feet of the cored interval of the Lidam Formation between depths of 10442 to 10462 feet is characterized by the occurrence of laminated stromatolitic and anhydrite facies. This interval is mainly composed of tan to light grey, slightly argillaceous, microcrystalline to fine crystalline dolomite interbedded

with reddish to medium dark grey shale and a 3 foot thick bed of nodular anhydrite facies. The nodular anhydrite facies was partly enclosed by dark brown mudstone, forming the familiar “chicken-wire” structure and is slightly bioturbated, containing pellets with small bioclasts. It contains lamination and is locally fractured. No oil staining has been observed in this interval. This interval is capped by an irregularly bedded, reddish brown mudstone of the Etel Formation.

ii. Interpretation:

The lower part of the Lidam Formation in this well starts with stromatolitic and anhydrite facies interbedded with bioclastic sandstone facies and is interpreted as a transgressive succession over the Nubian sandstone. The Nubian sandstone sequence consists of three members- a lower sandstone, middle shale, and upper sandstone. The upper and lower sandstone members in the Sirt Basin represent fluvial (braided and meandering stream facies) sedimentation that has taken place under regressive conditions. The middle shale member represents lacustrine and marginal marine conditions. The transgression initiated with the deposition of supratidal sabkha sedimentation. However the sandstone beds indicate there was still influx of terrestrial clastic, perhaps reworked from the Nubian Sandstone. Moving upwards the depositional texture changes progressively to packstone / grainstone dominated by ostracod facies interbedded with anhydrite and stromatolitic facies. This sediment was mostly deposited in a shallow-water restricted lagoon, with intertidal and supratidal setting. Again there was reworking and influx of sandy deposits into the environment.

Up section the low energy deposits change to less restricted subtidal deposits of foraminifera bioclastic wackestone / packstone. The succession ended with high energy, oolitic shoal sediments of ooidal peloidal packstone / grainstone facies.

The upper part of the cored interval is characterized by the presence of anhydrite and stromatolitic facies deposits deposited in supratidal (sabkha) to shallow hypersaline lagoons. A shallowing or regression is inferred for the top of the succession. The whole stacked pattern of lithofacies in this well (from bottom to top) indicates initial transgression then regression (Figure 4.15).

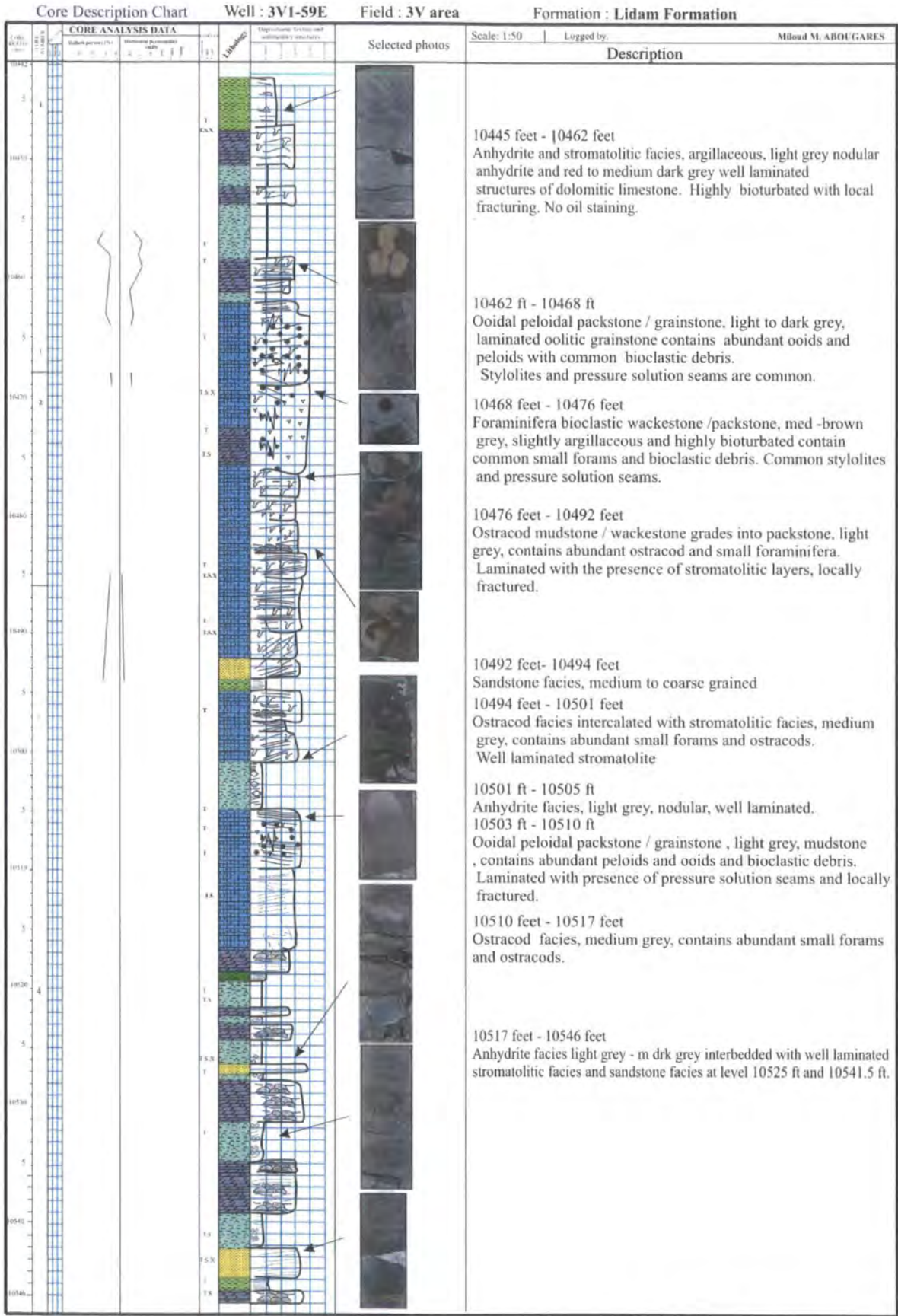


Figure.4.14. Lithological Description of the Lidam Formation in well 3V1-59E, 3V area, SE Sirt Basin, Libya.



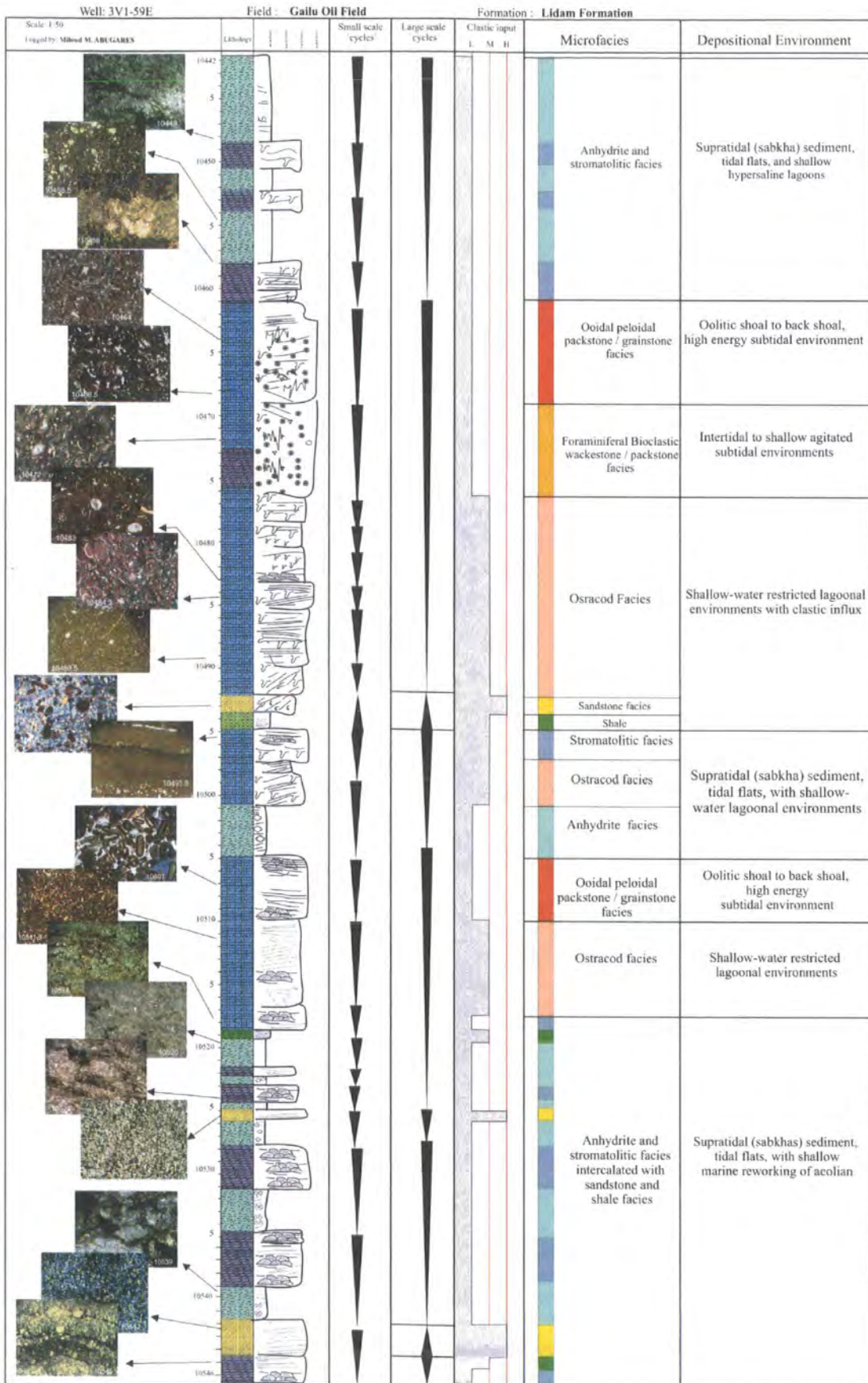


Figure 4.15. Stratigraphic section of the Lidam Formation facies in well 3V1-59E, 3V area, SE Sirt Basin, Libya. Vertical triangles show shallowing upwards

4.3.5. 3V3 - 59E Well:

i. Description:

This well is located southeast of well 3V1-59E along the Gialo platform in concession 59E, at Longitude: 28° 31' 23.4" N and Latitude: 21° 30' 20" E, in the SE Sirt Basin, (Figure 1.1). The total thickness of the Lidam Formation in this well is about 82 feet which has been totally cored between depths of 10198 to 10280 feet (Figure 4.16). Three main different intervals are recognized.

- The lower part of Lidam Formation is dominated by anhydrite, dolomitic mudstone and stromatolitic facies (core # 4) between depths of 10254 to 10280 feet. This interval overlies the Nubian Sandstone and begins with nodular anhydrite facies interbedded with homogeneous and laminated stromatolitic and dolomudstone facies.
- This succession grades up into the middle part which is dominated by the presence of bioturbated foraminifera bioclastic wackestone / packstone facies and ostracod facies. The total thickness of these facies is 35 feet, between depths of 10219 to 10254 feet. The limestones are argillaceous, highly bioturbated, contain well developed stromatolitic structures and are interbedded with thin intervals of dark grey shale. Small foraminifera, mollusc fragments and bioclastic debris are abundant.

Above this package, the succession changes to moderately to well sorted peloidal ooidal packstone / grainstone facies. This interval has deposits with abundant non skeletal grains of peloid and ooids intercalated with foraminifera bioclastic wackestone/ packstone facies, and its thickness about 21 feet between depths of 10198 to 10219 feet. Small forams, mollusc fragments, bryozoans, and other bioclastic debris are also present. Porosity is good and represented mainly by mouldic and intragranular type. These facies are the main reservoir unit in this well (Figure 4.16).

- The uppermost beds of the Lidam Formation in this well are characterized by the occurrence of laminated stromatolitic and anhydrite facies changing to dark grey, fissile shale, which may belongs to the Etel Formation and are considered the main cap rock of the Lidam carbonate reservoir in the Sirt Basin.

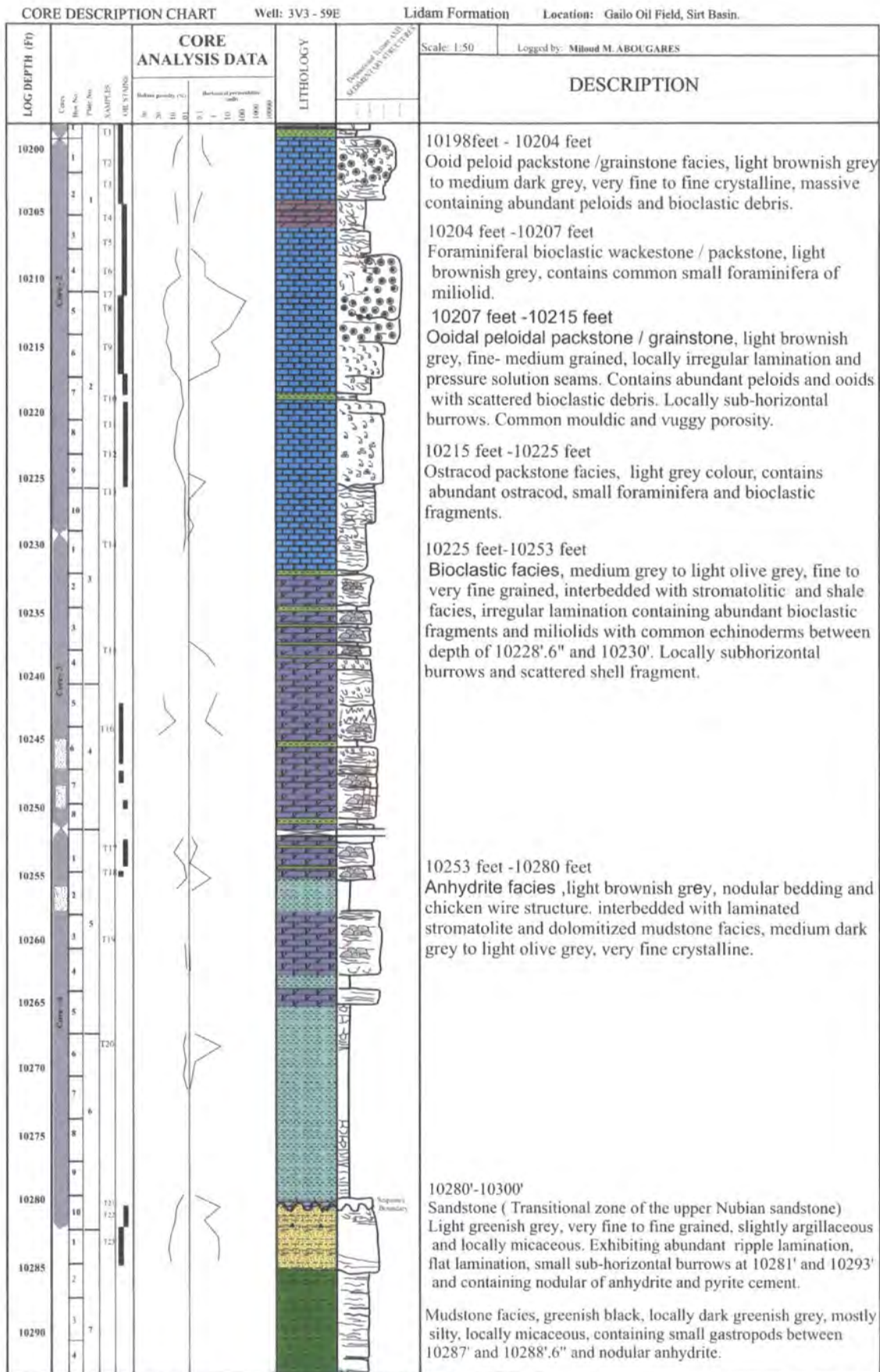


Figure 4.16. Lithological Description of the Lidam Formation in well 3V3-59E, 3V area, SE Sirt Basin, Libya.

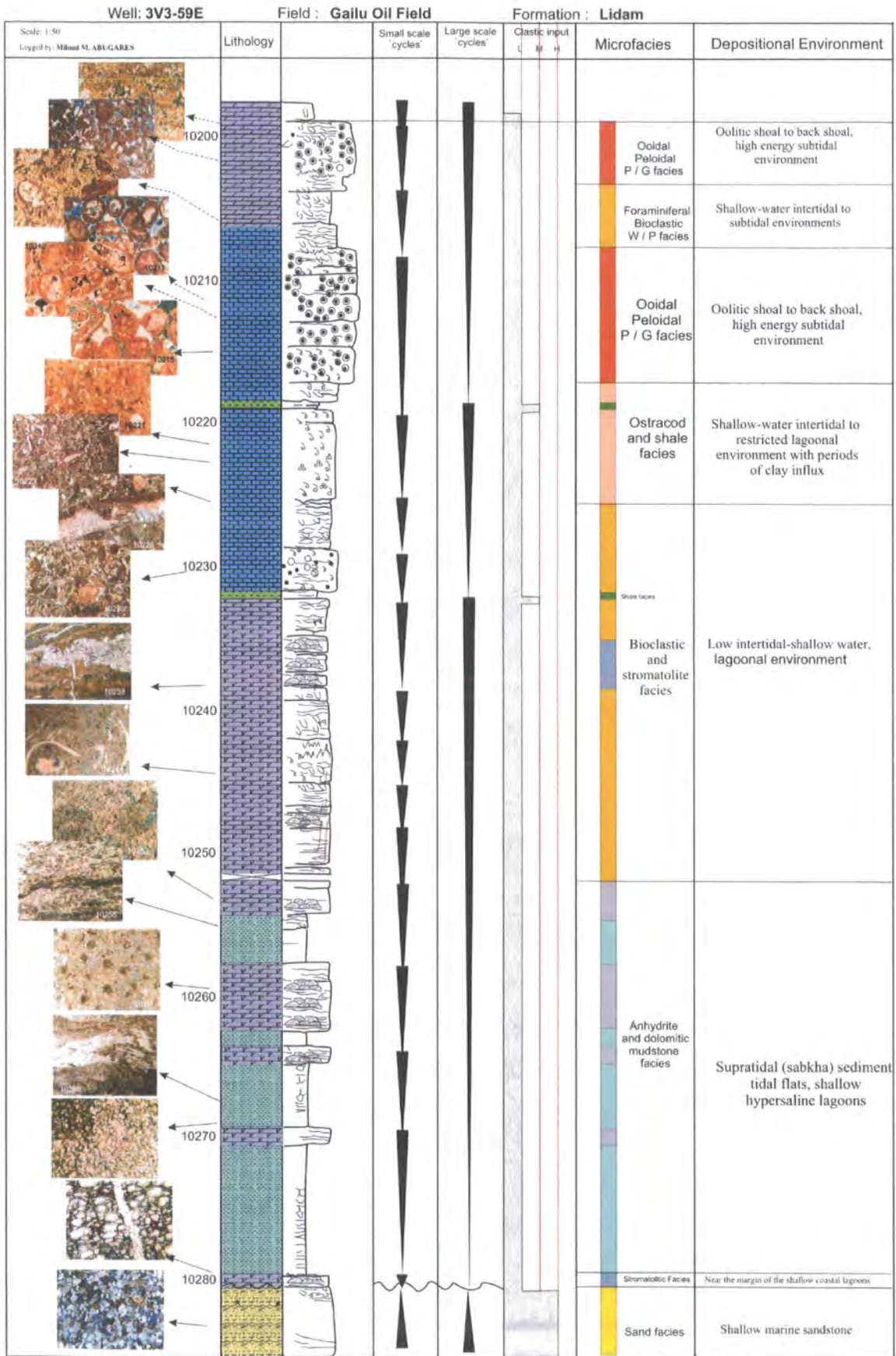


Figure 4.17. Stratigraphic section of the Lidam Formation facies in well 3V3-59E, 3Varea, SE Sirt Basin, Libya. Vertical triangles show shallowing upwards

ii. Interpretation:

Deposition of the lower part of the Lidam Formation initiated with coastal and shallow water sediments overlying the Nubian Sandstone. The Nubian Sandstone sequence comprises of lower and upper sandstone members representing braided and meandering fluvial system and middle shale member representing lacustrine and marginal marine conditions (seen in this well). The succession of the Lidam Formation began with the deposition of anhydrite and stromatolite facies which formed in a supratidal to intertidal setting with the input of terrestrial sand. Deposition occurred during relative sea level rise and the transgression of the sea over much of the Sirt Basin. These sediments were dominantly deposited in a shallow hypersaline subaqueous environment, and with sabkha conditions.

Upwards the succession passes into bioclastic wackestone / packstone and ostracod packstone facies. The components and textures of these facies suggest deposition in a lagoonal environment under low energy conditions and a relative rise in sea level is inferred. Above this high energy conditions resulted in deposition of oolitic packstone / grainstone facies accumulated under shallow subtidal to lower intertidal conditions.

Generally, the depositional sequence of this well formed during transgression resulting in the build up of all the facies (supratidal, tidal flat, lagoonal to shoal) deposited (Figure 4.17)

4.4. DISCUSSIONS ON SPATIAL VARIATION AND SEQUENCE DEVELOPMENT.

The Cretaceous Lidam Formation seen in the studied wells is most likely to have been deposited in shallow carbonate ramp environments (see section 4.3). The Cretaceous Lidam Formation in the Sirt Basin is likely to have evolved as a consequence of the interplay between global eustatic and regional tectonics. These have led to establishment of stratigraphic subdivision of Lidam Formation sequence in most of the Sirt Basin. Here, spatial and temporal variations in the thickness of unit are discussed. The frequency of the sedimentation units, sedimentology, facies geometries and cycle stacking patterns are also evaluated. These changes are interpreted in terms of fluctuations in relative sea-level and variations in accommodation space and other controlling factors are considered.

4.4.1 Small Scale Variations within the Wells.

The cycle sets are defined by variation in facies, lithology, porosity and thickness of the component cycle. The cycle sets in the lower part are different from the middle and upper part of the Lidam Formation (see section 4.3). Two basic small scale cycles are recognized in the Lidam Formation; intercalations of stromatolitic dolomudstone / anhydrite facies and shale based cycles.

c) intercalations of stromatolitic dolomudstone / anhydrite facies

The small scale cycles of intercalated stromatolitic dolomudstone and anhydrite facies are mostly seen at the lower part of the Lidam Formation. These cycles are also present in the upper part. The lower part of the Lidam Formation shows one general shallowing-up sequence consisting of up to ten small scale shallowing-up cycles of stromatolitic and anhydrite intercalations.

Only seven cycles have been identified in the lower part and three in the upper part of the Lidam Formation in well 3V1-59E (Figure 4.15). Five cycles are also seen in the lower part of well 3V3-59E and one small cycle at the base of well R1-97. Two small cycles of the stromatolitic and anhydrite intercalations occurred in the upper part of the Lidam Formation in well P3-97. N6-97 also exhibits shallowing-up attributes similar to the lower part in the 3V1 and 3V3-59E wells.

The general thickness variations of the cycles in most of the wells are up to 7 feet. The cycle begins with a stromatolitic packstone and laminated microbial stromatolite and grades upwards into nodular and laminated anhydrite facies. The cyclicity exhibited by these stromatolitic and anhydrite deposits consists of a series of smaller cycles that display a general increase in thickness and frequency of the anhydrite unit towards the top of this unit. Each cycle may change laterally in thickness and perhaps time duration. These small scale cycles formed in supratidal (sabkha deposits) to intertidal environments and reflect deposition during shallowing upwards (regression) and emergence. These cycles are possibly controlled by eustatic sea level fluctuations, subsidence and the infill of the sediment, or shifting sedimentation patterns. Small scale shallowing upwards cycles or parasequences may relate to 4th or 5th order eustatic fluctuations (Heckel, 1985; Koershner and Read, 1989; Goldhammer et al., 1990).

d) Shale based cycles

Cycle sets in the middle part of the Lidam Formation typically begin with a cycle dominated by siltstone or lime mudstone at the base, followed by a relatively thick

succession (about 5 to 15 feet in thickness) of subtidal carbonate wackestone or packstone grading up into grainstone cycles. The upper contact is commonly sharp and is frequently overlain by siltstone or lime mudstone at the base of the subsequent cycle set.

Most of the shale based cycles occurred in the trough areas in the middle part of the Lidam Formation and thicknesses range between 5 to 20 feet. Shale based cycles are present in most of the wells, particularly in the ostracod and bioclastic facies. Most cycles occurred in well N6-97 (12 cycles) and 7 cycles in well P3-97, both from trough areas. Eight cycles were present in R1-97 from a platform area (Figures 4.11, 4.13 and 4.18). Fewer cycles (3-5) are generally seen in platform area wells 3V1 and 3V3-59E (Figures 4.15 and 4.17). A sharp basal contact overlain by packstone / grainstone facies is the main characteristic of the shale-based units. The cycles have a symmetric facies stacking pattern, which shows an upward increase in carbonate content.

The upper part of the shale based cycle is interpreted as forming in intertidal to subtidal lagoonal setting (see section 4.3). One interpretation is that the shale deposits are part of the cycle accumulated below fair weather wave base and possibly below storm wave base. The upward increase and thickening of the carbonate deposits together with the increase in skeletal grain size in the upper part of the cycle may indicate increased energy as a result of progressive shallowing. However, another interpretation is that the shales formed during periods of influx of fine clastics into low-energy lagoonal areas. Given their intercalation with very shallow to supratidal deposits the second interpretation is perhaps the more likely. The consistency between some wells of the shale-based cycles and the upward increase in carbonate components suggests an allocyclic mechanism for the middle part of the Lidam Formation. This may be related to a short-term fluctuation in eustatic sea level and an overall relative eustatic fall in scenario one. However, for scenario two (preferred herein) climatic changes with slight increases in runoff, or changes to storminess may influence the clay deposition. Variations in numbers of cycles between wells are probably due to local variation in shifting environments (autocyclic) and accommodation space, with less accommodation space on platform areas.

4.5. COMPARISON OF LARGE SCALE VERTICAL (TEMPORAL) AND LATERAL (SPATIAL) VARIATIONS.

The distribution of the facies described in the previous section is shown as a log correlation panel in Figure 4.17. The correlation presented here is based mainly on information from core. A number of problems are associated with the correlation of the individual facies in the Lidam Formation. These include: 1) no complete cores are available for the Lidam Formation in wells R1, P3, and N6-97. Just the upper part of the formation was cored in these wells. 2) Rapid lateral facies change that cannot always be correlated between the wells. 3) Different formation nomenclature used by the two main operating companies Waha Oil Company and Wintershall, Libya.

A local development of the ooidal peloidal packstone / grainstone facies is a diagnostic facies and found in all wells but in various thicknesses from south to north (Figure 4.18). Many companies operating in Libya correlate on this oolitic / peloidal facies due to its widespread development, although in modern environments many oolitic shoals have a localized development. The extent of the ostracod facies is unknown due to lack of core information at well P3-97 and N6-97 in the lower part of Lidam Formation and therefore does not make good units for correlation between the five wells. The total thickness of the Lidam Formation in the Hameimat trough based on the well logs is about 260 feet in well P3-97 and 360 feet in well N6-97 (and much of the cored section belongs to Etel Formation using the definition of Wintershall Company. Lower thicknesses are present on the platform; 82 feet in well 3V3-59E, 3V1-59E about 105 feet, and 205 feet in R1-97. These variations in thickness and vertical facies distribution of the Lidam Formation must have been controlled by the palaeogeography and differential tectonic subsidence in the Sirt Basin during the Upper Cretaceous period.

4.5.1 Comparison between Wells in Platform:

The three wells 3V1-59E, 3V3-59E, and R1-97 located along the Gialo Platform have similar thicknesses variations in deposits (Figure 4.18). The cored section of the Lidam Formation in these wells are composed of five main facies; anhydrite, stromatolitic, ostracod packstone, foraminifera wackestone, and ooidal peloidal packstone /grainstone. These facies overall show a deepening upward cycle interpreted as having been deposited and accumulated in supratidal sabkha deposit, shallow subtidal-intertidal restricted lagoonal and oolitic shoal setting, respectively. Wells 3V1-59E and R1-59 also include anhydrite / stromatolitic facies and ostracod / algal facies

respectively in their uppermost part deposited during a relative fall in sea level, which may belong to the Etel Formation. The main factors controlling the depositional environment, style and temporal and spatial thickness variations in facies are probably the result of paleogeography, global eustatic sea-level changes (rising and falling), and tectonic subsidence during the deposition of the Lidam Formation (Figure 4.19).

4.5.2. Comparison in Trough:

Two wells (P3-97 and N6-97) were drilled by Wintershall Company, Libya in the Hameimat Trough. Most of the cored interval in well N6-97 may have been drilled in the Etel Formation (uppermost anhydrite, stromatolite and ostracod facies) and it may be that just the lower 15 feet is from the Lidam Formation. A variation in the shallow lagoonal facies means that these deposits are unsuitable for correlation (Figure 4.20). The two wells have again been correlated on the ooidal peloidal packstone facies in the upper part of the Lidam Formation, which have similar thicknesses. The packstone intercalated with shale and ostracod and foraminifera wackestone / packstone is the dominant facies in these wells. The ostracod facies occurred in the lower part of the cored interval in well P3-97 overlaid by ooidal peloidal facies, but in well N6-97 the ostracod facies dominate and occur above the ooidal peloidal facies.

Cross-correlation is difficult between these two wells because they have been drilled through non-equivalent intervals. More data are required, but it seems that the facies in the trough may show a similar trend to those on the platform of deepening and then shallowing. Facies are interpreted as having formed in shallow-water intertidal to lagoonal environment under arid conditions interrupted in the middle part by an oolitic, high-energy shoal in well P7-97. These differences and variations in the depositional environments are probably due to global sea-level change, climatic changes, and rate of the tectonic subsidence which are the most important factors controlling the deposition of the Lidam Formation in the Sirt Basin during Cenomanian time (see below).

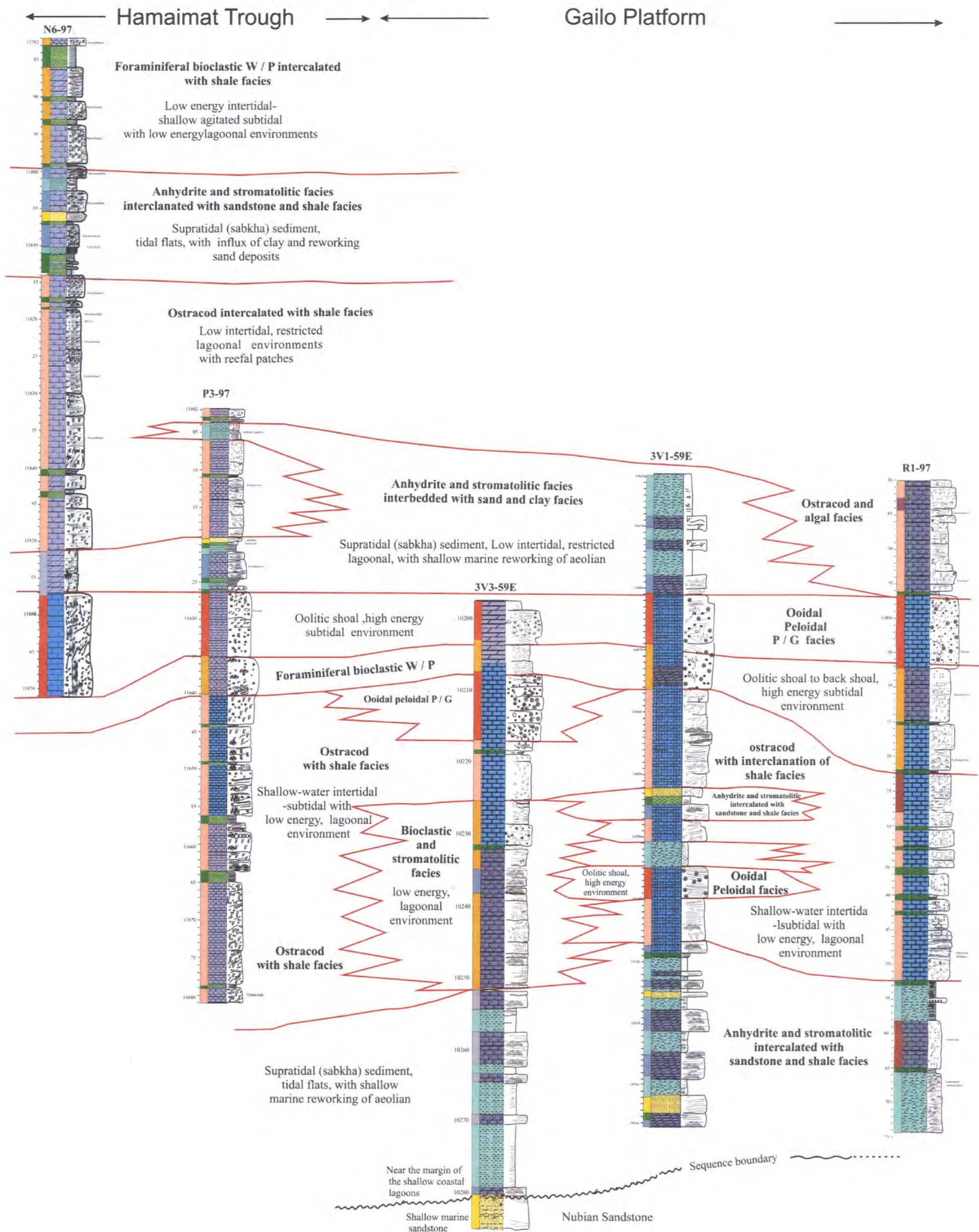


Figure 4.18. Possible stratigraphic correlation between the studied well in the Gailo Platform and Hameimat trough, SE Sirt Basin, Libya.

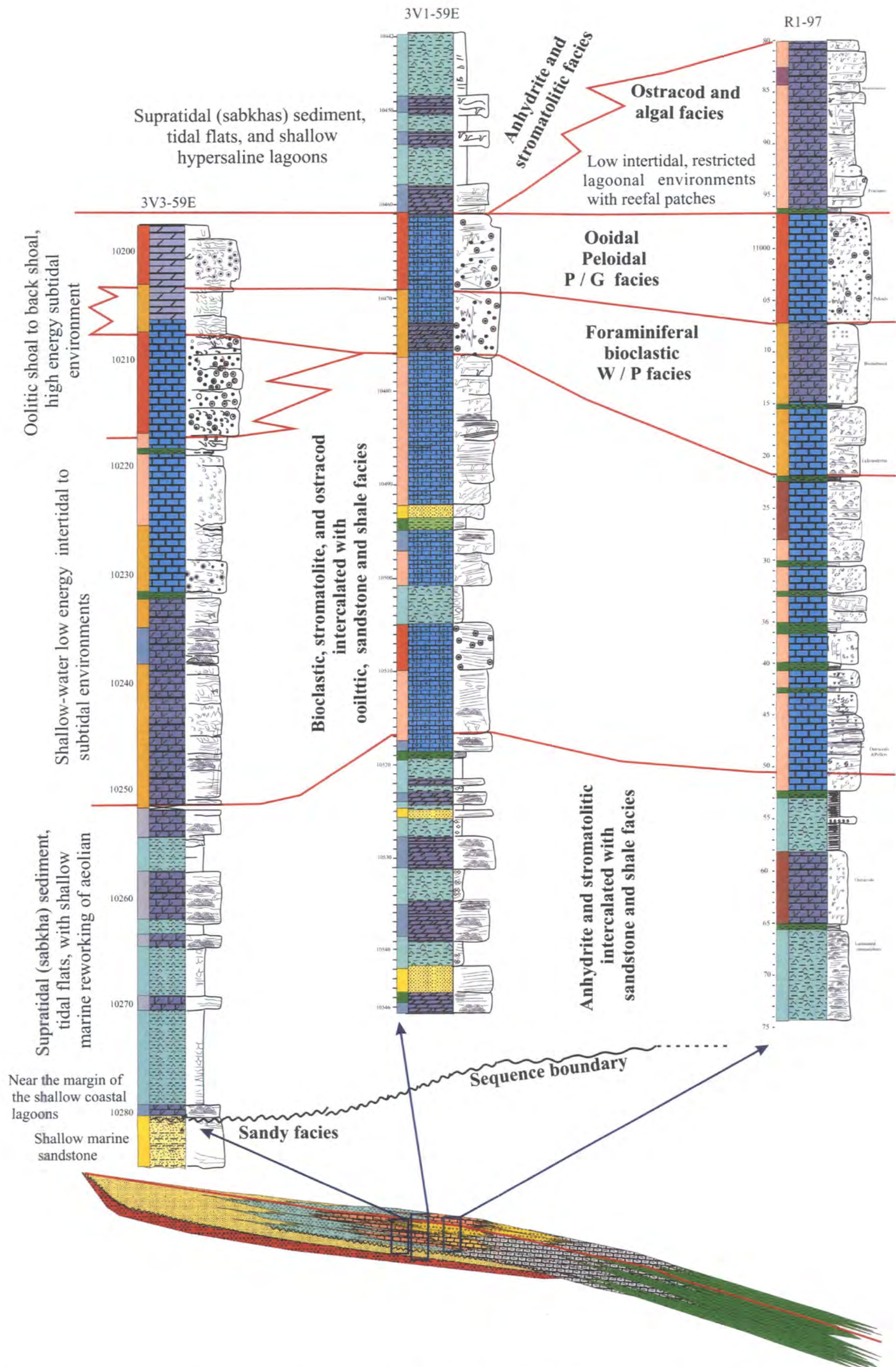


Figure 4.19. Typical distribution of stacking patterns of facies in wells 3V3- 59E, 3V1-59, and R1-97 on the Gialo Platform.

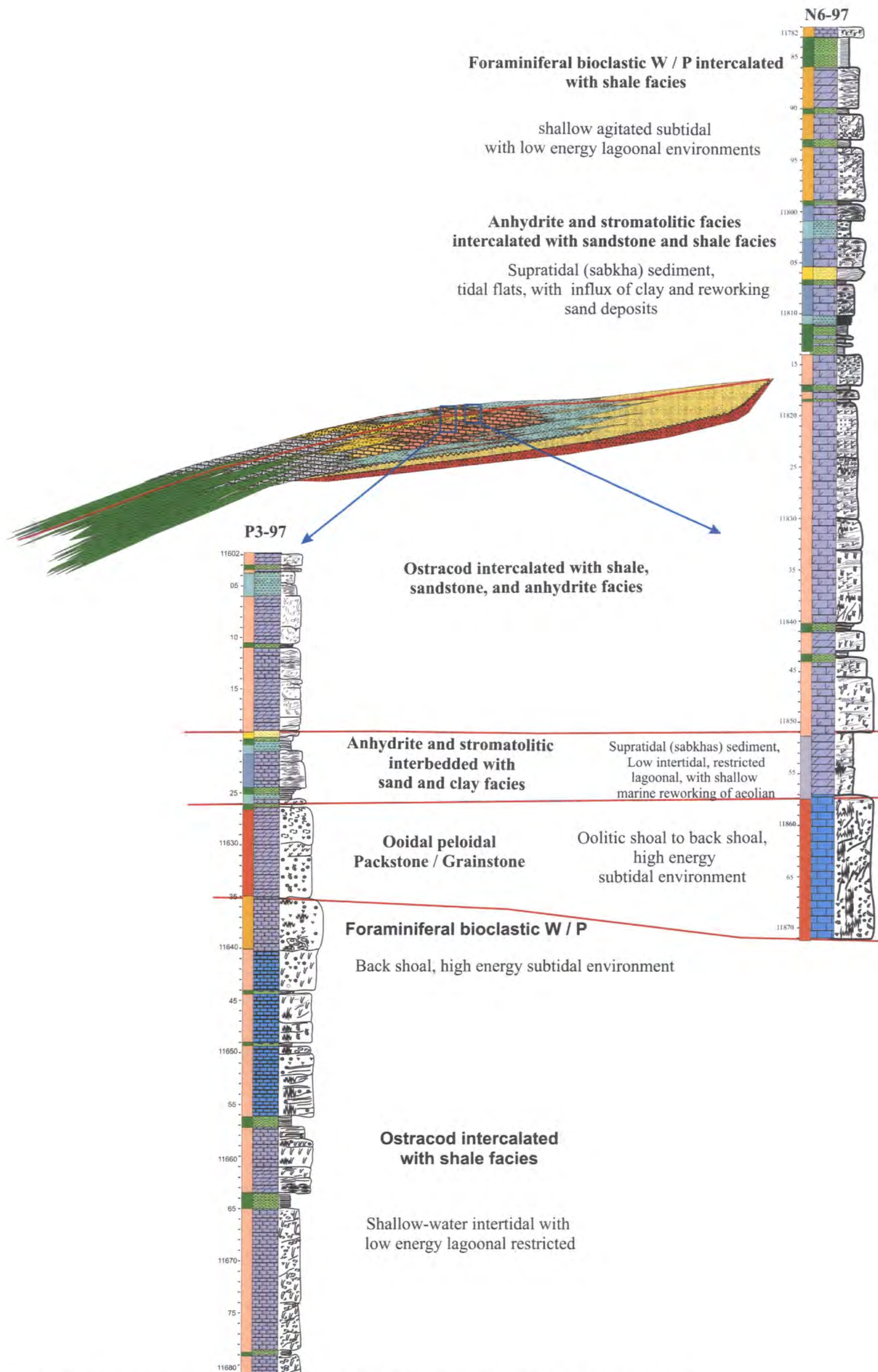


Figure 4.20. Typical distribution of stacking pattern of facies in the wells N6-97 and P3-97 in Hameimat Trough.

4.6. SEQUENCE STRATIGRAPHY OF THE LIDAM FORMATION

4.6.1. Sequence Stratigraphic Analysis of the Lidam Formation in the 3V1-59E, 3V3-59E, R1-97, P3-97, and N6-97.

The stacking patterns of facies in the Lidam Formation in the studied area suggest that it consists of one major transgressive depositional cycle and ended with one regressive depositional cycle, related to increasing then decreasing water depth. Some companies might include the upper regression sequence as a part of the overlying Etel Formation. An example of the typical distribution of stacking patterns of facies developed in well 3V1-59E is showing in Figure 4.21. Similar stacking patterns are seen in the other wells and are therefore not illustrated here. The lower part of the transgressive depositional cycle of the Lidam Formation starts with supratidal (sabkha deposits), passing to intertidal, and then into subtidal deposits of ooidal peloidal packstone/ grainstone facies. The transgression may be related to the latest Cenomanian eustatic rise (see below).

The upper regressive unit at the top of the Lidam Formation is probably the base of the Etel Formation. This is thought to have been deposited at the end of Cenomanian and the beginning of the early Turonian. Low diversity assemblage occur in the Etel Formation characterized by smooth ostracods, indicating a muddy lagoonal environment that was largely isolated from open marine circulation (Barbieri, 1996, El-Alami, 1996 and Gras and Thusu, 1998). This unit also includes supratidal sabkha deposits which are dominated by anhydrite intercalated with stromatolitic facies (Figures 4.21, 4.22, 4.23 and 4.24).

The Lidam Formation cycles formed during transgression have retrogradational parasequence sets which are deposited farther landward in a backstepping pattern (rate of deposition is less than the rate of accommodation) during the rise of the sea level (Figure 4.23). This sequence was followed by stillstand or a slow regression (fall in sea-level), when the rate of sedimentation was greater than the accommodation space generation resulting in the oolitic facies prograding basinward and being overlain by supratidal facies (Figure.4.24).

According to the eustatic sea-level changes of Vail et al (1977) and Haq et al (1987), a major sea-level rise occurred during the Late Cretaceous and was a global event. Bakai (1990) stated that during the late Cretaceous period, the first major marine transgression of the Mediterranean Sea also covered the entire north part of the Sirt

Basin and was coeval with a global rising of sea level. The continuation of the tectonic uplift of the Sirt Basin during Cenomanian and early Turonian time strongly affected the sedimentation rate of the Lidam and Etel transition. The reworked sandwiched sediments of sandstone facies overlying the peloidal facies at the base of the Etel Formation are interpreted as northward prograding deposits resulting from relative (and later eustatic) falling of sea level at the beginning of Turonian time. This caused subaerial exposure of the elevated area farther south of the Sirt Basin, and deposition of anhydrite and shallow, restricted lagoonal deposits during the regressive event.

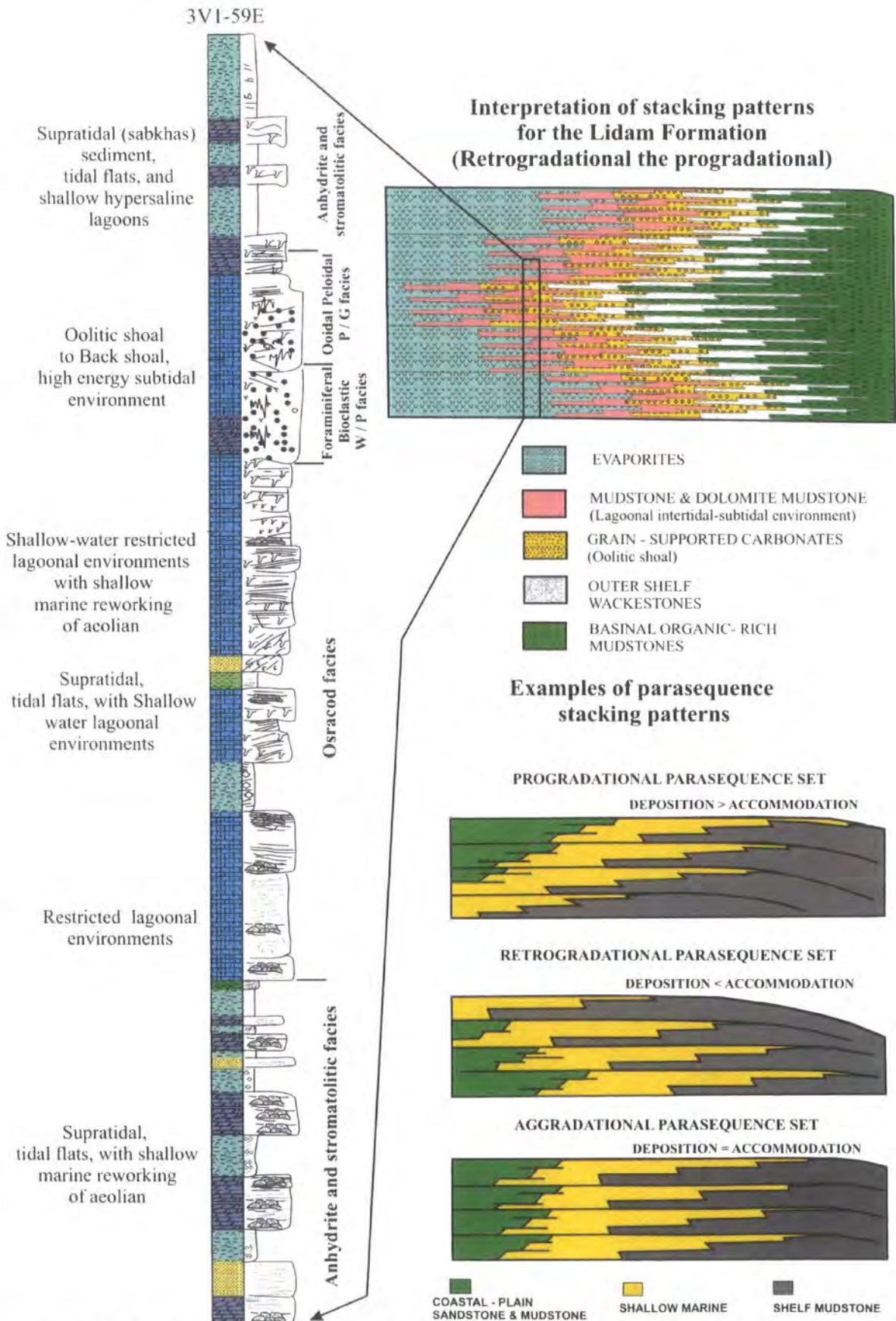


Figure 4.21. An example of the typical vertical distribution of stacking patterns of facies with retrogradational than progradational parasequence development (well: 3VI-59E).

DEPOSITIONAL SEQUENCE MODEL OF LIDAM FORMATION CARBONATE-EVAPORITE RAMP

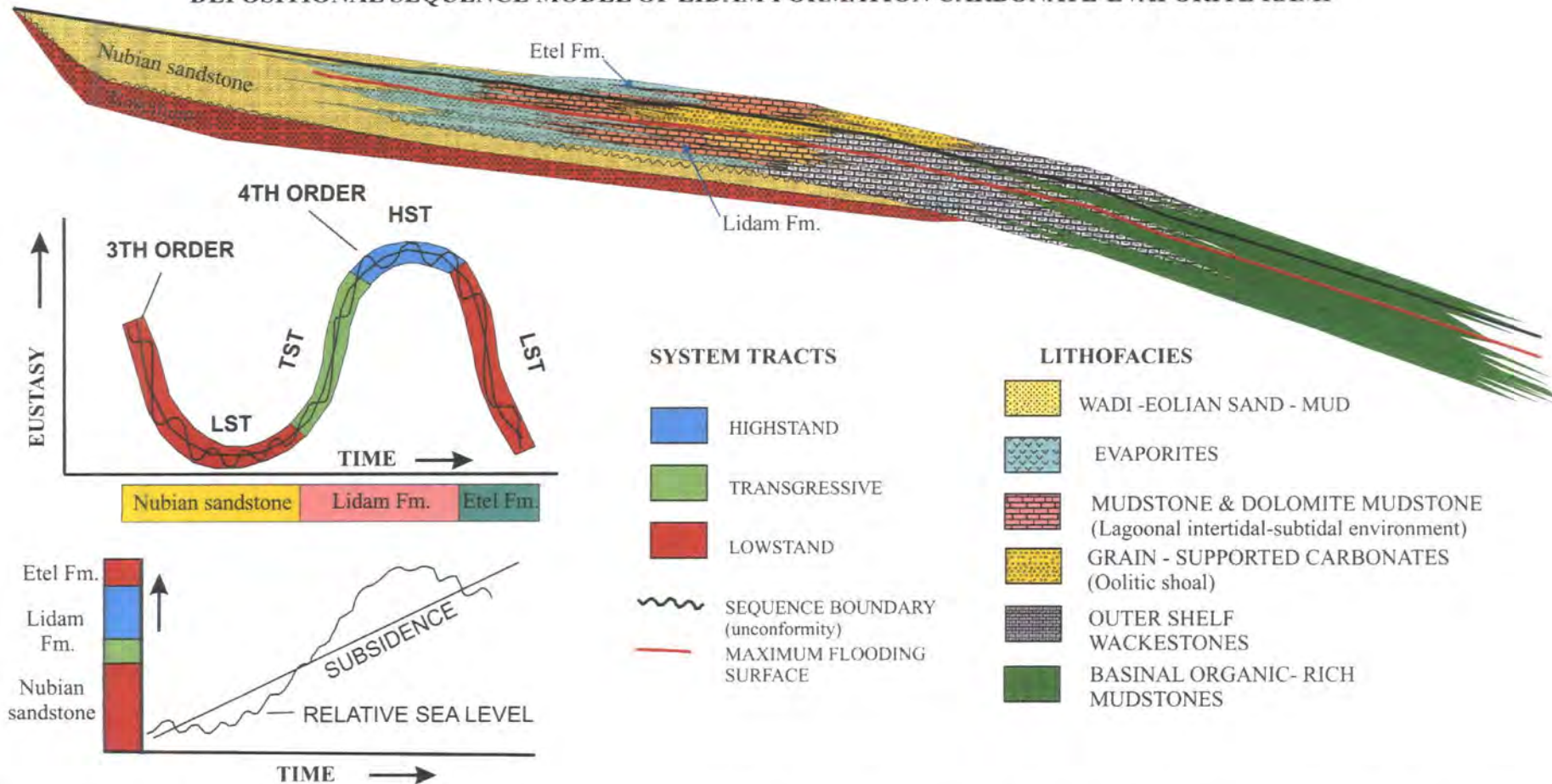


Figure 4.22. Ideal depositional model sequence and systems tract models of Lidam Formation carbonate-evaporite ramp associated with type 1 sequence boundaries of the Nubian sandstone.

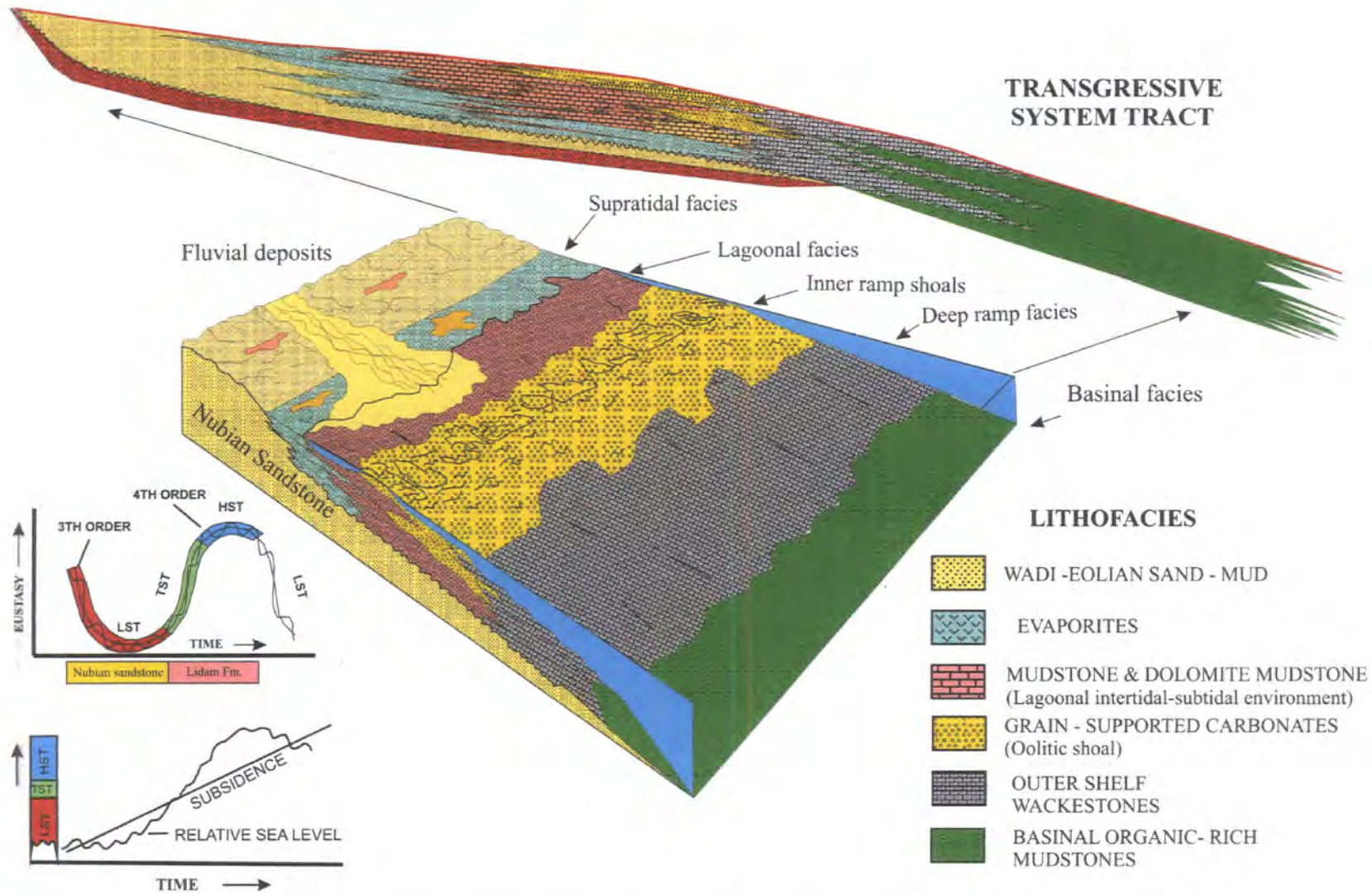


Figure 4.23. Depositional sequence model of the Lidam Formation during transgressive systems tract.

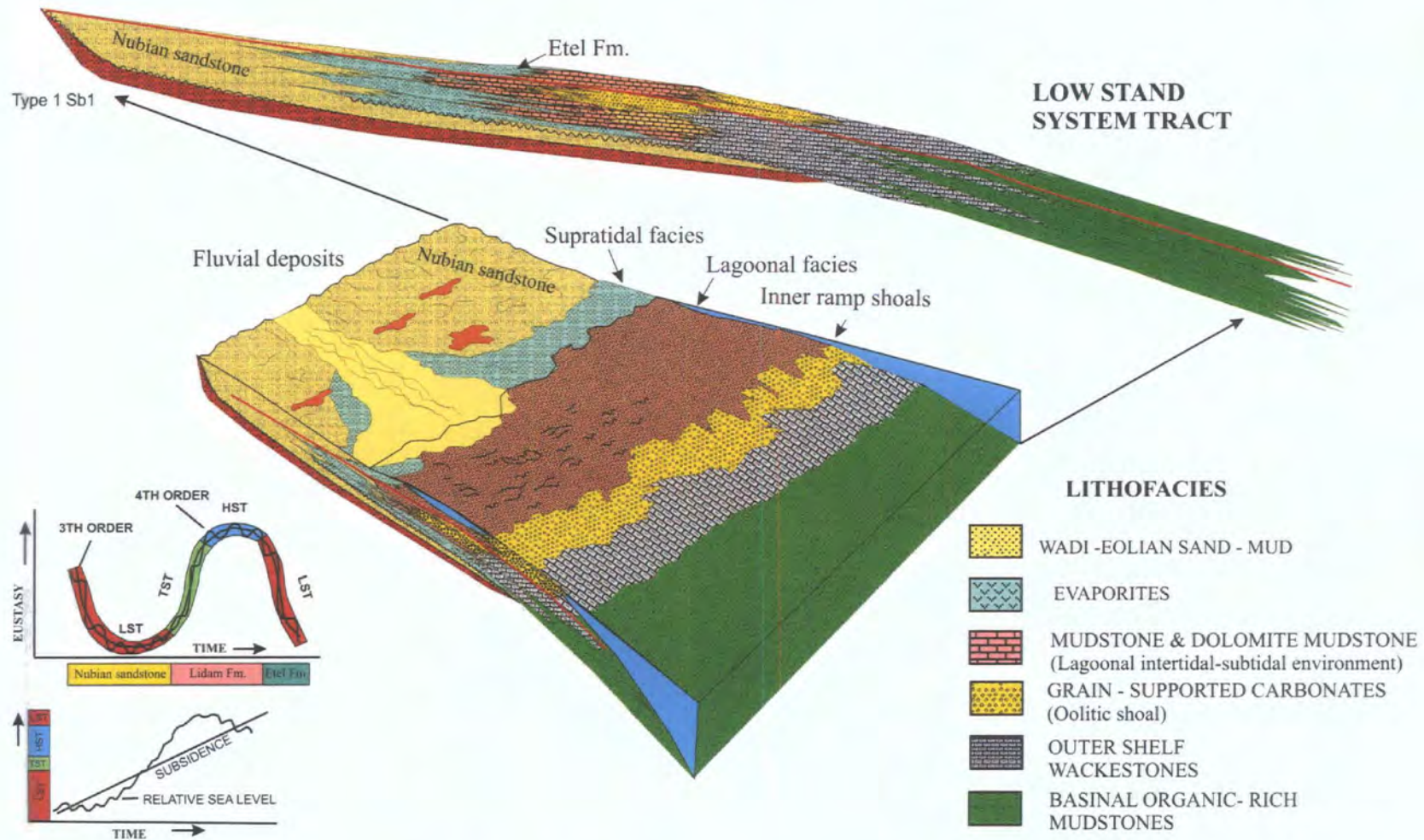


Figure 4.24. Depositional sequence model of the Lidam / Etel Formation during falling stage of the lowstand systems tract.

4.7. SEQUENCE STRATIGRAPHIC INTERPRETATION AND CONTROLS ON LARGE SCALE VARIATIONS.

Systematic variations in sequences, their component units and their stacking patterns can be related to large-scale (12-50 km) changes in accommodation space, and sediment supply. Successive facies of the Lidam Formation are stacked systematically into upward-coarsening units on a small (0.1–1.0 m) scale with upward-coarsening and fining packages on a larger scale. The small-scale shallowing-upward units are interpreted to be parasequences (section 4.4). The large scale coarsening-upward packages are interpreted to be retrogradational parasequence sets and thinner packages of progradation at the top of the Lidam Formation (section 4.5). Goldhammer et al. (1990) concluded that the metre-scale cycles showing systematic changes in cycle types, lithofacies and thickness vertically through a carbonate succession, reflect changes in accommodation that may be related to different orders of eustatic oscillation, most likely 4th or 5th order changes. However, there may also be other more localized controls, e.g. changes in clastic input or shifting facies belts, perhaps related to currents (see section 4.6).

Following the development of the Sirt Basin rift system and subsequent flooding of the main NNW-SSE troughs by the Tethys a thick sequence of carbonate successions has been deposited during Late Cretaceous time. The variation in thickness seen within wells could only relate to differential subsidence or infill of accommodation space related to irregular topography. A major transgression of the sea toward the south in the Sirt Basin resulted in initial deepening upward deposits. Transgression is consistent with a eustatic sea-level rise during the Cenomanian. During this transgression three different depositional environments occurred, including supratidal sabkha deposits and tidal flat, restricted shallow subtidal lagoonal and high energy oolitic shoal facies. These deposits are arranged into metre-scale, upward-shallowing peritidal and subtidal cycles.

Successive facies of the Lidam Formation can be further grouped into sequence sets according to the long-term changes in accommodation and vertical facies changes. The sequences are characterized by relatively thick cycle packages of transgressive stacked pattern with a high percentage of intermediate to shallow subtidal facies followed by regressive succession of supratidal sabkha intertidal deposits. The correlation of long-term accommodation changes in the Sirt Basin reveals that increased accommodation loss on platforms (Gialo Platform) coincided with increased

accommodation in basins (Hameimat Trough) due to the uplift and subsidence of Sirt Basin during the Late Cretaceous time.

4.8. COMPARISON WITH OTHER CRETACEOUS SUCCESSIONS.

Comparison between the platform successions and sequence patterns of the SE Sirt Basin and those from neighboring areas allow differentiation of local, regional and global controlling factors on platform development within the study area. The sequence-stratigraphic interpretation of the Lidam Formation in SE Sirt Basin is compared with the succession in west central Jordan and in Sinai, Egypt (Figure 4.25).

The Cenomanian-Turonian strata in northern Sinai, Egypt mainly consists of shallow marine carbonates and siliciclastics (Figure.4.25), changing southwards into a coastal and terrestrial facies, and subsequently non-deposition (Kuss and Bachmann, 1996, Philip et al., 2000 and Stampfli et al., 2001). A comparison of microfacies types and depositional environment of Lidam Formation in this study with facies models of the adjacent shelf area in Sinai (Bauer et al. 2003) reveals many similarities, but also some differences and arranged with different vertical patterns compared with the Lidam Formation. Bauer et al. (2003) divided the upper Cenomanian to Turonian inner shelf of Sinai into a deep-water facies belt, a subtidal belt and a siliciclastic shoreface, while the subtidal is subdivided into high-energy, open shallow and restricted (lagoonal) environments.

The upper Albian to upper Cenomanian in western central Jordan consists of marine calcareous deposits of the Naur Formation (equivalent to the Lidam Formation). The Jordanian deposits have a diachronous base (related to NW to SE transgression), overlie terrestrial clastic deposits (equivalent to the Nubian or Sarir Sandstone in Libya) and reflect an extensive transgression to the south and southeast of Jordan in upper Albian lower Cenomanian times. Shallow subtidal to peritidal deposits predominate within the Nuar Formation and small-scale cyclic stacking patterns again indicate that relative sea-level fluctuations influenced deposition on the early to early late Cenomanian platform (Schulze, 2003). Major transgression in the late Albian to earliest Turonian resulted in deposits mainly of shallow-marine environments (peritidal to subtidal, locally with high- energy areas (shoal, patch reefs) (Schulze, 2003). The types of deposit, their generally transgressive nature and ages are directly equivalent to those inferred for the Lidam Formation. Generally, the sedimentary successions in the Sirt Basin (Libya), Sinai and west central Jordan exhibit similar shelf development during Cenomanian –Turonian times.

This widespread development of carbonate platforms along the pericratonic Arabo- African platform, extending from Morocco to Oman (including Libya) have been linked along the south margin of the Tethys Ocean (Philips et al 2000). The carbonate-dominated succession in Sinai includes intercalated claystone and shale representing a shallow-marine subtidal to supratidal platform developed during Cenomanian-Turonian times as proposed by Schulze, et al (2002). Furthermore, the maximum flooding surfaces of the investigated succession allow comparison with those in Sinai and the Arabian plate (Bauer et al 2003).

The main controls of the depositional environment were probably the tectonic deformation events in large parts of North Africa and Arabia, the palaeogeography of the carbonate dominated ramp during the Cretaceous period, as well as eustatic changes.

The overall facies of the Lidam Formation are also similar to the Jurassic Smackover Formation sequence of the United States Gulf Coast as described by Ahr (1973) and Read (1982). They form a shallowing-upward sequence said to be an excellent example of the continental ramp margin. The Ordovician Hansen Creek Formation (Dunham, 1977) which is very similar to the Lidam Formation in this area of the Sirt Basin and its facies subdivisions mainly correspond to the environments described in this study.

4.9. CHAPTER SUMMARY

The shallow water carbonate facies of the Lidam Formation are described from the subsurface (five wells) in SE Sirt Basin, Libya. This chapter includes identification of thickness variation trends of the main microfacies. The Lidam Formation includes a great variety of facies and components varying from fine to coarse grained peloids and bioclasts, and different skeletal grains of mollusca fragments, echinoid fragments, miliolids, rotaliids and dascycladacean green algae. The differences in the depositional textures reflect deposition under different environments. Interpretation of the stratigraphic development of the Lidam Formation shows that the stacking patterns of the overall facies are deepening upward trends. The stacking patterns consist of one major transgressive-upward depositional cycle and ended with one regressive depositional cycle. The transgressive depositional cycle of the Lidam Formation starts with supratidal (sabkhas deposits), passing into intertidal, and then subtidal deposits of ooidal peloidal packstone/ grainstone facies.

The temporal and spatial variations in facies cycles were controlled by decrease or increase in the water depths, sea level changes, and rate of subsidence (uplift). Regional and globally Comparison are made with other Cretaceous successions between the Lidam Formation and those from neighboring areas in west central Jordan and Sinai, Egypt. In terms of sequence stratigraphic patterns and large scale temporal and spatial variations during the Cenomanian time, these show similar stacking patterns of sedimentation and thickness variation of the microfacies. The main controls of the deposition environment were probably the tectonic deformation events in large parts North Africa and Arabia, palaeogeography of the carbonate dominated ramp during the Cretaceous period, as well as eustatic changes.

CHAPTER FIVE

*DIAGENESIS AND RESERVIOR
QUALITY OF THE LIDAM
FORMATION.*

CHAPTER FIVE: DIAGENESIS AND RESERVIOR QUALITY OF THE LIDAM FORMATION.

5.1 INTRODUCTION.

5.2. INTRODUCTION TO CARBONATE DIAGENESIS.

5.2.1 MARINE DIAGENESIS.

1. Marine Phreatic Zone.

5.2.2. METEORIC DIAGENESIS.

- a. Phreatic Zone.
- b. Vadose Zone.
- c. Mixed Zone

5.2.3. BURIAL DIAGENESIS.

1. Burial Cementation.

5.3 DIAGENESIS OF THE LIDAM FORMATION

5.3.1 INTRODUCTION.

5.3.2 METHODOLOGY.

5.3.3 EARLY MARINE DIAGENESIS.

- a). Micritization.
- b) Isopachous rim cement.

5.3.4. METEORIC AND EARLY BURIAL DIAGENESIS.

- A) Meniscus Cement.
- B). Dissolution.
- C. Neomorphism.
- D) Cementation (drusy and syntaxial overgrowth).
- E) Early dolomitization (fine dolomite).
- F). Anhydrite replacement.

5.3.5. LATE BURIAL DIAGENESIS.

- 1). Compaction (concave – convex contacts dissolution seams and stylolites).
- 2). Fracturing.
- 3). Cementation (equant calcite cement).
- 4). Late dolomitization (clear coarse dolomite cement).
- 5). Replacement by Pyrite.

5.4. CATHODOLUMINESCENCE (CL) ANALYSIS AND INTERPERTATION.

5.4.1. Introduction.

5.4.2. Cathodoluminescence (CL) Analysis of the Lidam Formation.

5.5. STABLE ISOTOP ANALYSIS AND INTERPRETATION.

5.5.1 Introduction.

5.5.2. Isotopes Analysis of the Lidam Formation.

- a. Carbonate Skeletons and non-Skeletons.
- b. Micrite matrix.
- c. Carbonate Cement.

5.6 DISCUSSION OF RELATIVE TIMING AND PROCESSES OF DIAGENESIS.

5.7. RESREVOIR QUALITY OF THE LIDAM FORMATION.

5.7.1. Porosity and Permeability Variation and Relationship with Facies.

5.7.2. Hydrocarbons Emplacement.

5.8. COMPARISON OF DIAGENESIS AND RESERVIOR QUALITY WITH OTHER CRETACEOUS FORMATIONS.

5.9. CHAPTER SUMMARY.

5. DIAGENESIS AND RESERVIOR QUALITY OF THE LIDAM FORMATION

5.1 INTRODUCTION

This chapter deals with phenomena that occurred following the deposition of the sediments (i.e. diagenesis) of the Lidam Formation in the SE part of the Sirt Basin. The initial part of the chapter summarizes previous work on diagenesis (Section 5.2). Petrographic thin-section study, in addition to Scanning Electron Microscopy (SEM), Cathodoluminescence (CL) microscopy and oxygen-carbon isotopes analysis was undertaken to identify and interpret diagenetic features and these are discussed in sections 5.3, 5.4 and 5.5 respectively. This chapter also includes the reservoir characterization of the Lidam Formation and discusses the common pore types and variation of porosity and permeability related to facies variation. The relative timing of diagenetic events and processes of diagenesis are inferred.

5.2. INTRODUCTION TO CARBONATE DIAGENESIS

The diagenesis of carbonates involves many different processes and takes place in near-surface marine and meteoric environments, and down into the deep burial environment (Figure 5.1). Carbonate diagenesis involves the carbonate minerals, aragonite, calcite and dolomite, although other minerals such as quartz, feldspar, marine clays, iron oxides, sulphates and evaporites may also be involved. Diagenesis is an important control on occlusion and generation of porosity in sediments. Six major diagenetic processes can be distinguished: cementation, microbial micritization, neomorphism, dissolution, compaction and dolomitization.

The information on diagenetic processes and definitions is taken directly from Tucker (2001) "*Micritization* is the processes whereby the margins of carbonate grains are replaced by micrite at or just below the sediment/ water interface. The process involves microbes attacking the outside of the grains by boring small holes in them, and breaking them into fine grained micrite. *Cementation* is the major diagenetic process producing a solid limestone from loose sediment. The mineralogy of the cements depends on water chemistry particularly its CO₂ and Mg/Ca ratio and carbonate supply. *Neomorphism* is

used to describe replacement and re-crystallization processes where there may have been a change of mineralogy. Many limestones have suffered *dissolution* as a result of the passage of pore fluids undersaturated with respect to the carbonate phase present. This is a major process in near surface, meteoric diagenetic environments, and may lead to the formation of karst. The secondary porosity created by carbonate dissolution is important in some hydrocarbon reservoirs. *Compaction* takes place during burial, resulting in a closer packing of grains, mechanical breakage to eventual compaction through dissolution along grain contacts. Chemical compaction may lead formation to stylolites and dissolution seams, when burial exceeds many hundreds of meters of overburden. *Dolomitization* is a major alteration process for many limestone and the dolomite, $\text{Ca Mg} (\text{CO}_3)_2$, may be precipitated in near surface and burial environments.”

Three major diagenetic environments are distinguished, marine, near-surface meteoric and burial.

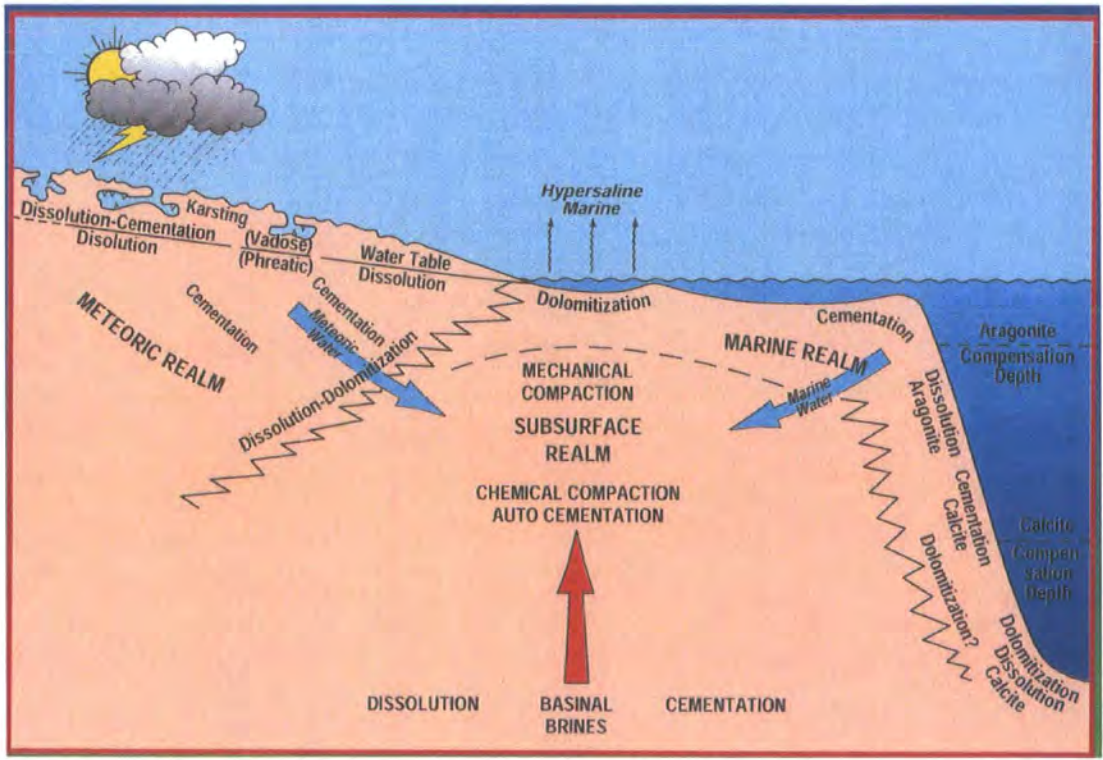


Figure 5.1. Different diagenetic environments from near surface marine and meteoric environment, down into the deep burial environment (from Moore, 2002).

5.2.1 MARINE DIAGENESIS

a. Marine Phreatic Zone:

Most of the carbonates are deposited in and begin their diagenetic history in the marine phreatic environment. This zone may be divided into two end members of a continuous spectrum: a zone of relatively little water circulation in which micritization and minor intragranular cementation occur and a zone of good water circulation near the sediment/water interface in which extensive intergranular and cavity-filling cementation occur. Marine cements are commonly isopachous fringes of aragonite fib or magnesium calcite blades (Longman, 1980).

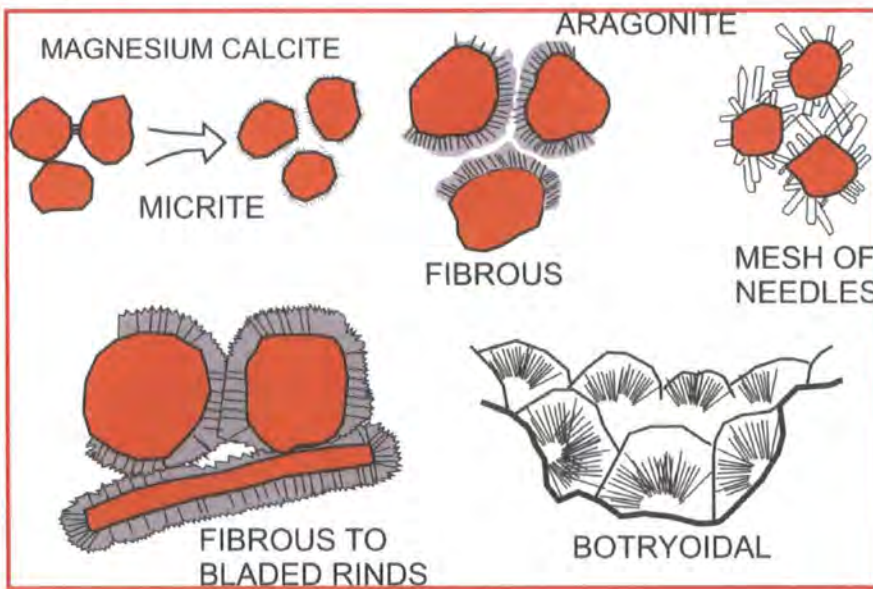


Figure 5.2 .Different types of marine carbonate cements.(After James, 1984)

In this marine environment diagenesis takes place on and just below the sea- floor in both shallow and deep water, and in the intertidal – supratidal zone (Tucker, 2001) (Figure 5.1). Aragonite typically occurs as fringes from 10 to 200 mm thick of acicular crystals, orientated normal to the grain surface. Micrite envelopes play an important role during diagenesis by maintaining the shape of an aragonite bioclastic grains after its dissolution. In many cases the aragonite cement are isopachous, i.e. of equal thickness, indicating marine phreatic (below the water table) precipitation where pores were constantly water-filled (Tucker, 2001). Cementation and microbial micritization mostly involves in shallow sub-tidal marine areas. In the stagnant, marine phreatic diagenetic

environment, cementation is restricted to intraskeletal cavities, such as occur within gastropod and foraminifera chambers (Longman, 1980).

Marine cements form in a broad spectrum of environments, extending from the deep sea to beaches (Figure.5.2). Deep sea cements, commonly from mammilated or isopachous layers of magnesium calcite and aragonite, and produce hard grounds where there is good bottom current movement. The flanks of carbonate platforms and the margins of submarine channels and canyons are also such sites. Other deep-sea cementation may also occur in areas of negligible sedimentation and may be associated with volcanics or with elevated salinities in enclosed basins (Longman, 1980).

5.2.2. METEORIC DIAGENESIS:

The meteoric diagenetic environment is the zone where rainfall-derived groundwater is in contact with sediment or rock (Figure 5.1). The zones within the meteoric environment are the phreatic, vadose and mixing zone (Tucker, 2001)

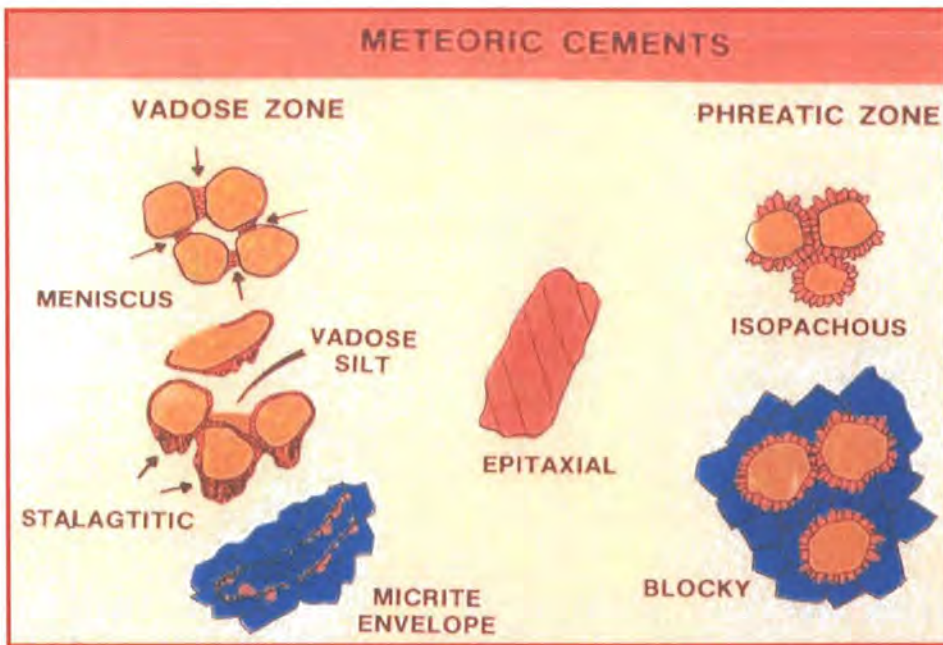


Figure 5.3. Different meteoric cements morphologies.(after: Noel P. James 1984)

a) Phreatic Zone:

The term Phreatic is used in geology to refer to matters relating to underground water below the water table (Figure 5.1). The word originates from the Greek phrear, phreat-

meaning "well" or "spring". "Phreatic surface" is a synonym for "water table." Where all the rock pore spaces are filled with water, if the water is fresh, this is fresh water phreatic zone. Below the water table, calcite cements commonly form rims of bladed to drusy crystals that completely encircle the grains (Tucker 2001) (Figure 5.3).

b) Vadose Zone:

This is the most important diagenetic zone where rapid cementation and dissolution takes place. Cementation in near shore zones is as variable as the ground water of these areas (Figure 5.3). In the vadose zone, pores periodically contain water, air or both, and an upper zone of infiltration is distinguished from a lower zone of percolation. Calcite precipitated in the zone of aeration above the water table, i.e., vadose zone, are blocky and fibrous-needle calcites (Tucker, 2001). The three most important processes in the vadose zone are: (1) gravitation drainage; (2) desiccation by evaporation and (3) evapo-transpiration (James and choquette, 1990).

c) Mixing Zone:

This zone is narrow zone that marks a diffuse boundary between the fresh water (meteoric) phreatic and marine phreatic diagenetic zones, and moves backward and forward through the sediment in response of rainfall. Calcium carbonate and dolomitization is typically the most important diagenetic process in the mixing zone (Bathurst, 1971). Cements include calcite and possibly dolomite. During deposition fresh water may interact with marine sediments in the supratidal zone and sometimes in the intertidal zone (Moore, 1989). In shallow subsurface where the marine and meteoric water interface, there is a mixing zone (Back et al. 1984). Cements precipitated from near surface meteoric waters are normally iron-free calcite (non-ferroan) with roughly equant crystal shapes (Adams, 1998) the vadose and phreatic cements in the carbonate rocks are composed of low-Mg calcite (Morse and Mackenzie, 1990) (Figure.5.3).

5.2.3. BURIAL DIAGENESIS:

Burial processes, particularly cementation, compaction and pressure dissolution operate over a considerable range of depth, pressure and temperature and in pore-fluids of varied salinity, chemistry, and origin. Burial diagenesis is generally taken to begin below the depth where sediments are affected by near-surface processes of marine and meteoric environments (Tucker 2001) (Figure 5.1). The most common result of burial diagenesis is

the destruction of porosity, through the processes of cementation, compaction and pressure solution. Two categories of compactions: mechanical and chemical. Mechanical compaction may begin soon after deposition and leads to a closer packing of grains (Tucker, 1991). Chemical compaction requires several hundred meters of burial resulting in increased solubility at grain contact and along sediment interface and resulted fitted fabric, stylolites and pressure dissolution seams (Tucker, 1991). Pre-burial cements may be similarly affected, resulting in a change of the porosity and permeability patterns in the rock. Stylolites and other pressure solution features are commonly formed during burial or tectonic stress of mudstones and wackestones. The formation of such features is important because vertical permeability patterns are created and pore fluids are displaced (Bathurst, 1971).

Dolomite is less influential at higher temperature and solubility of calcite decreases with rising temperature and precipitated easily with depth. There are many other depths - temperature- related mineral - chemical processes, involving the clay mineral, gypsum - anhydrite and organic matter. With increasing burial, there is a progressive decrease in porosity and the rates of porosity loss are generally lower in carbonate and higher in lime mud. Burial diagenesis has been discussed at length in the literature and recent reviews include Bathurst (1980a, 1986), Wanless (1983), Scholle & Halley (1985), Choquette & James (1987) and Halley (1987).

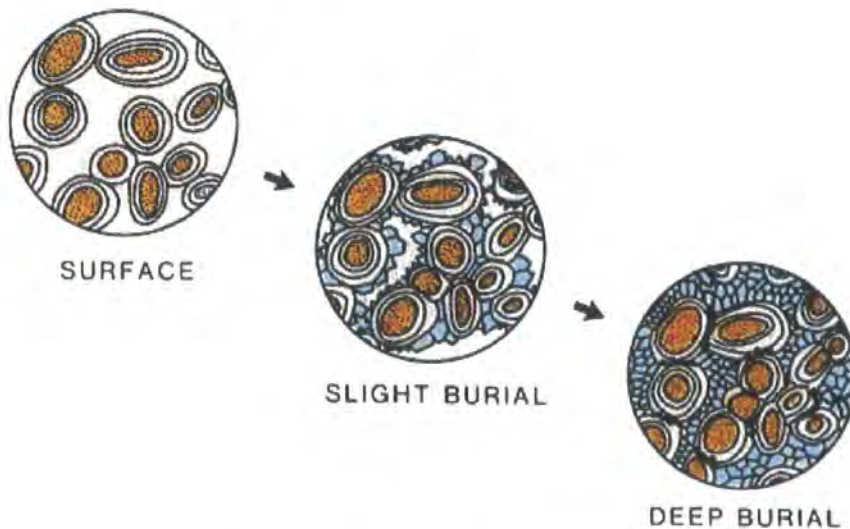


Figure 5.4. Cementation stages of carbonate rocks during burial diagenesis (Bathurst, 1971)

1. Burial Cementation: Cements precipitated in the burial environment are mostly some form of clear, coarse calcite spar and begins at depth below the sediment surface of tens to hundreds of meters that is, below the zone affected by surface processes (Tucker, 2001). There are three mosaic types:

- 1- Poikilotopic calcite, which consist of large crystals including several grains; they may reach several millimetres or more in diameter. They have probably resulted from a very low nucleation rate of calcite crystals and slow growth (Figure 5.5).
- 2- Equant mosaics of calcite spar, this texture may be produced by neomorphism of pre-existing cement, although some relics would be expected, they can also grow as a cement type within the pore space in burial environment.
- 3- Syntaxial calcite spar, which is common around echinoderm fragments, and commonly show zoning. Burial syntaxial overgrowths are precipitated in near-surface marine, meteoric or mixing zone environment.

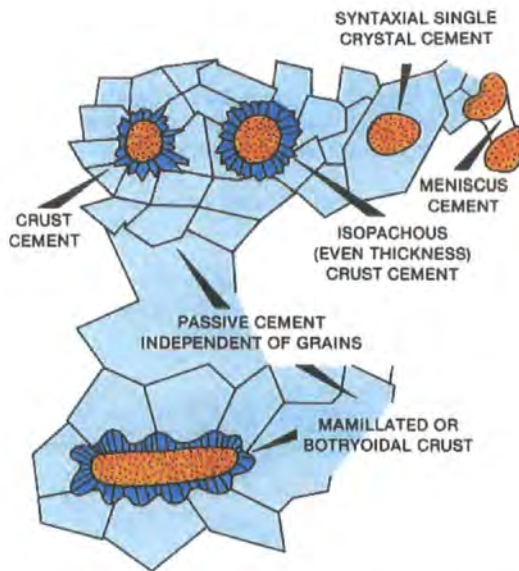


Figure 5.5. different types of cementation stages during burial diagenesis (Bathurst, 1971)

5.3 DIAGENESIS OF THE LIDAM FORMATION

5.3.1 INTRODUCTION

The diagenetic sequence of events which affected the Lidam carbonates is shown in Figure 5.51. This plot shows the relative timing of events based mainly on the textural and fabric relationships seen in the examined samples. Because of the great variation and complexity of the environments of deposition and variation in diagenesis the timing of diagenetic features is not always easy to judge.

There are three major diagenetic environments which have affected the Lidam Formation:

1- EARLY MARINE DIAGENESIS:

- a) Micritization.
- b) Isopachous fringing cement.

2- METEORIC AND EARLY BURIAL DIAGENESIS:.

- A) Meniscus Cement
- B) Dissolution.
- C) Neomorphism.
- D) Cementation (drusy and syntaxial overgrowth).
- E) Early dolomitization (fine dolomite).
- F) Anhydrite replacement.

3- LATE BURIAL DIAGENESIS:

- 1) Compaction. (Concave-convex contacts, dissolution seams and stylolites).
- 2) Fracturing.
- 3) Cementation (equant blocky calcite cement).
- 4) Clear dolomite cement.
- 5) Replacement of Pyrite.
- 6) Hydrocarbons.

5.3.2 METHODOLOGY

The diagenetic features and processes that have affected the Lidam Formation have been recognized and interpreted using the following methods:

- Petrographic analysis of 70 thin sections from all studied wells to investigate diagenetic features and the relative timing of events.

- Gold coated samples were examined using the Scanning Electron Microscope (SEM) of six samples to investigate the morphology of the grains and cements in pore spaces (see Tables in chapter 1).
- Nine polished thin sections were chosen from different wells for more detailed (CL) Cathodoluminescence microscopy to investigate pore fluids chemistry paragenesis and particularly if fluid compositions varied during cementation.
- Sixteen (16) samples were chosen for stable isotopic ($\delta^{18}\text{O}$ & $\delta^{13}\text{C}$) analysis from different wells to help in the interpretation of diagenetic environments (particularly for coarse cements).

5.3.3 EARLY MARINE DIAGENESIS.

During the deposition of the Lidam Formation, two distinct diagenetic processes are recognized that are most likely due to marine phreatic diagenesis and are present in most of the cored intervals of the Lidam Formation. These are:

a) Micritization:

i. Description:

Micritization is the most important diagenetic process that took place during the deposition of the Lidam sediments. Most of the peloids and bioclasts in the ostracod packstone, bioclastic packstone/ grainstone, mollusc, and peloidal ooidal packstone / grainstone facies are strongly affected by micritization process in which the margins of the carbonate grains were replaced by micrite. These facies are concentrated in the upper part of the Lidam Formation. Most of the skeletal grains are affected by near complete micritization making it difficult to distinguish the original grains. During later diagenesis these have dissolved and only the micrite envelope remains to outline the original allochems, e.g. mollusc (Figure.5.6).

Micritization also has been observed in the studied thin sections of the Lidam Formation in the lower part of the cored interval in well R1-97 between depths of 11048 to 11065 ft and in well 3V3-59E between depths of 10225 to 10229 ft. Later following micritization calcite spar has filled intergranular and mouldic pore spaces after mollusc shells (Figure 5.7).

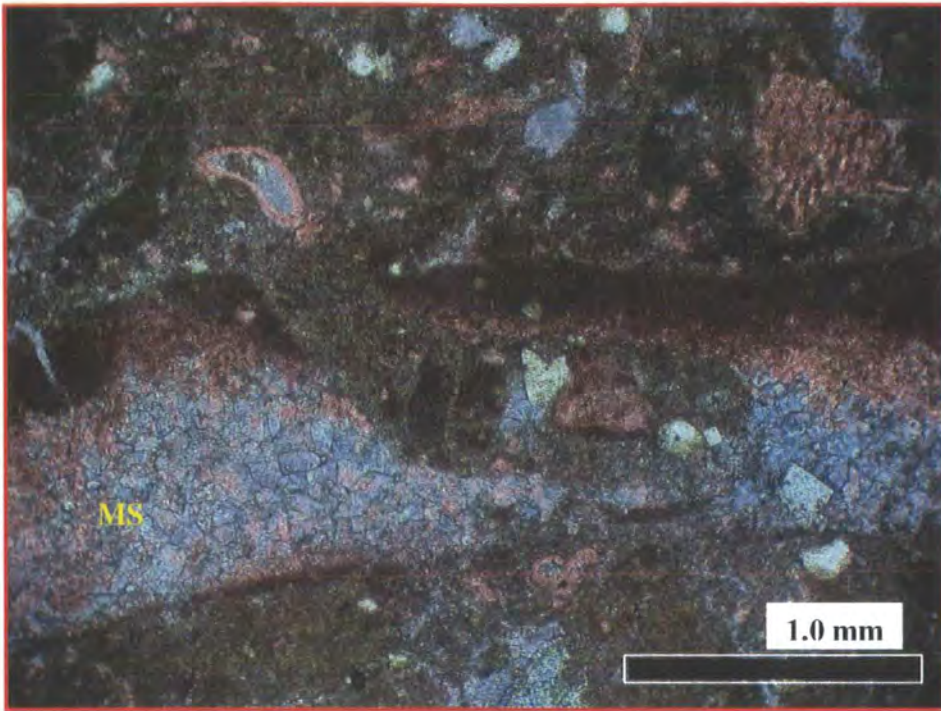


Figure 5.6. Photomicrograph showing mollusc shell (MS) affected by micritization, 10226 ft, 3V3-59E, PPL.

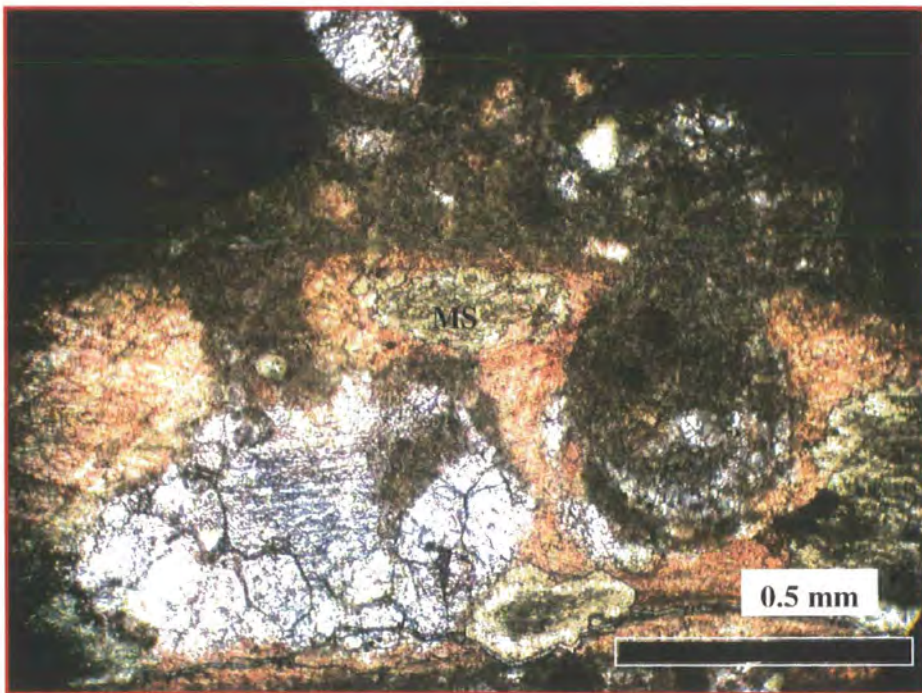


Figure 5.7. Photomicrograph shows mollusc (MS) affected by micritization prior to later diagenesis of original shell, 11025.5 ft, R1-97, PPL.

ii. Interpretation:

Most of the peloids and bioclasts are totally affected by continuous micritization process whereby the margins of carbonates grains were replaced by micrite. This process is most common in the low energy bioclastic and mollusc facies, and also moderate energy peloidal grainstone sediments, which were probably stabilized after deposition. Micritization is the process whereby the margins of carbonate grains are replaced by micrite at / or just below the sediment / water interface. Micritization of the grains by biological activity resulted in the formation of micrite envelope similar to those described by Bathurst (1966, 1975). The process involves microbes attacking the outside of the grains through boring and breaking the surface down into carbonate mud or micrite. Where micritization has led to complete circumgranular alteration, the micrite rind of the grain is called a micrite envelope (Tucker, 2001).

As in this study, El Bakai (1992) noted that micritization is common in the upper limestone facies and less common in the lower Lidam Formation and the middle dolomitized argillaceous limestone. It is likely that similar conditions existed during early diagenesis of the Lidam Formation. This early diagenetic process occurs in the stagnant marine phreatic zone, near or at the sediment/ water interface (Longman, 1980), frequently in water depths of less than 10m (Larsen and Chilingar, 1979).

b) Isopachous rim cement.

i Description:

This type of cement is observed in the peloidal ooidal packstone / grainstone facies in the middle and upper part of the Lidam Formation. The cement is usually found as a thin fringe (oriented normal to grain surface) of radial fibrous cement growing and surrounding peloids and skeletal grains (Figure 5.8 and 5.9). The isopachous rim cement is observed in the bioclastic facies and is well developed around the mollusc shell fragment and pore spaces filled by ferroan calcite cement. This type of cement is appears as a rim of crystals of equal thickness on all grains (about 0.1mm in width). Such cements are said to be "isopachous". It may originally have been aragonite, details of the texture having been lost during inversion to calcite, or it may have been high magnesium calcite marine cement in which the crystals were elongate prisms rather than needles (Figure 5.10). The isopachous have not completely infilled the pore space and are postdated by micritization later equant cements

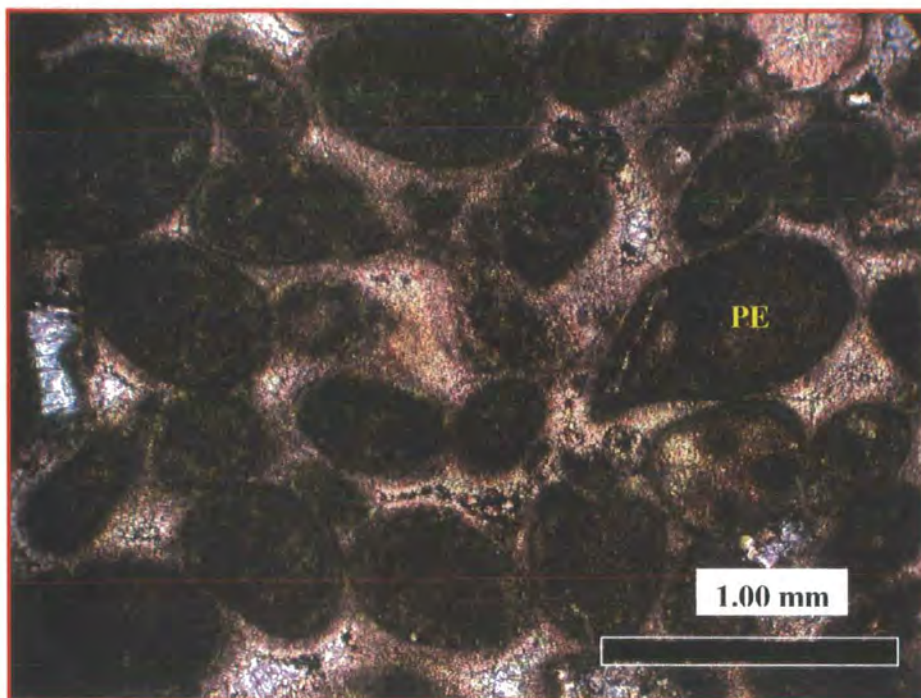


Figure 5.8. Photomicrograph showing peloidal ooidal packstone facies (PE) with dark aragonite isopachous cement coating around the peloids which is later affected by micritization. Porosity has been completely occluded by a later ferroan calcite cement, 10209 ft, 3V3-59E, PPI.

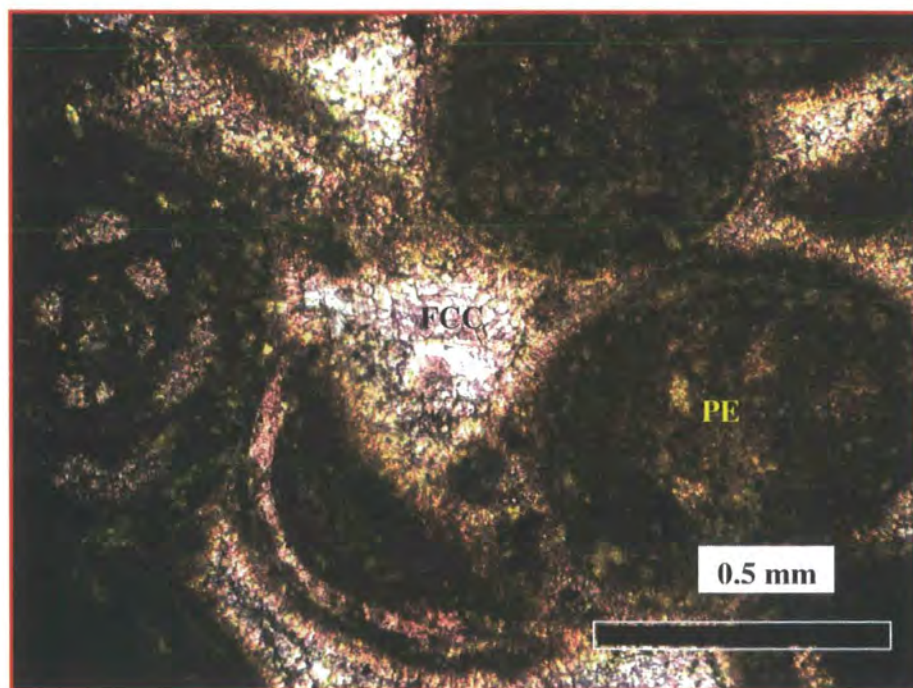


Figure 5.9. Photomicrograph showing peloidal ooidal packstone facies (PE) with well developed isopachous rim cement around the peloids and pore spaces filled by ferroan calcite cement (FCC), 11209 feet, 3V3-59, PPI.



Figure 5.10. Photomicrograph showing bioclastic packstone facies with well developed isopachous rim cement (IRC) around a mollusc shell fragment (M) and pore spaces filled by later ferroan calcite cement (FCC), 11230 feet, 3V3-59, PPI.

ii. Interpretation:

This isopachous rim cement is characteristic of deposition from marine waters or from connate waters fairly deep in the subsurface. In the Lidam Formation these cements are mostly present in the higher-energy grainstone units and most likely result from active flushing of marine waters through pores. Tucker (2001) stated that early marine rim cements are aragonite and /or high Mg calcite in form and in many cases the cement fringes are isopachous, i.e. of equal thickness. Early cementation in the marine phreatic environment resulted in isopachous rims of fibrous aragonite and bladed Mg-calcite cement and freshwater flushing is indicated by the replacement of former aragonite cement rims by finely crystalline equant calcite (Pol, 1985). The micritic crystals may be recrystallization to microspar during subsequent diagenetic stages and the thin clear isopachous crystals fringe at one side of some skeletal walls, this isopachous cement represents early marine diagenetic cement (Longman, 1980).

5.3.4. METEORIC AND EARLY BURIAL DIAGENESIS.

During the deposition of the Lidam Formation several diagenetic features are inferred to have formed in the meteoric zone (Figure 5.50). These diagenetic features are meniscus cement, carbonate dissolution, fine blocky cement rimming grains, neomorphism, (particularly of aragonite and micritic calcite), calcite cementation (drusy calcite cement, syntaxial overgrowths on echinoderms), and evaporite formation (chicken wire and nodules structure).

A) Meniscus Cement.

i. Description:

These types of cement are most common in the middle part of the Lidam Formation particularly in the peloidal ooidal facies in most of the studied wells. It is precipitated and occurred as a very fine crystalline calcite (micrite). This cement occurs at the grain to grain contacts between the peloidal grains (Figure 5.11). Cryptocrystalline cement will be used here following the advice of Friedman (1985).

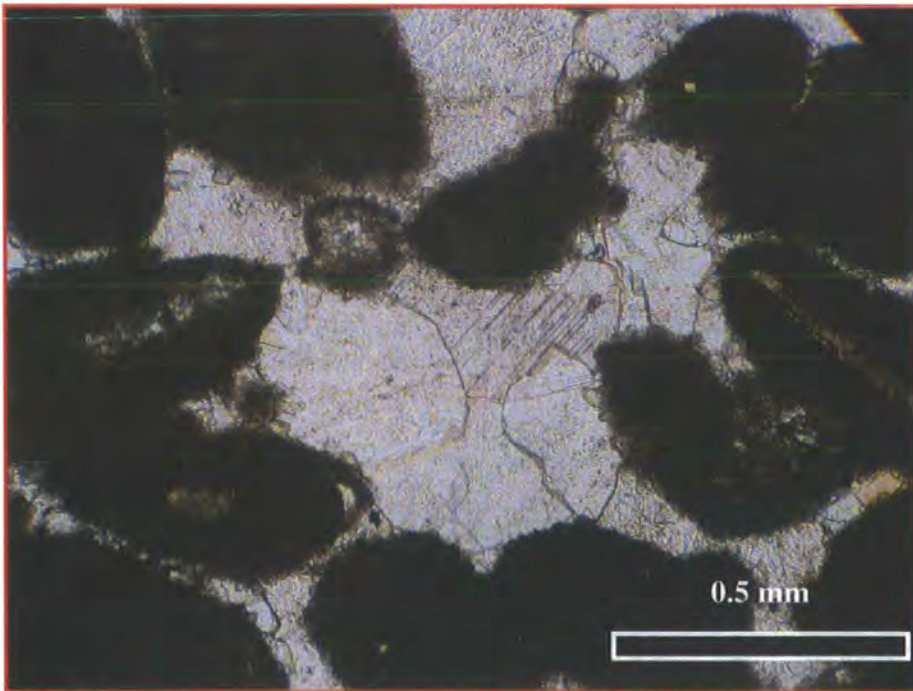


Figure 5.11. Photomicrograph showing meniscus cement in grain to grain contact, 10507 feet. 3V1-59E

ii. Interpretation:

This is the most important diagenetic zone where rapid cementation and dissolution takes place and occur shortly after deposition. Depending on depositional environment, the early lithification occurs as carbonate precipitation or particle infiltration that links framework grains by forming meniscus bridges, these cements or infiltrating material are assumed to be related to vadose environment (Dunham, 1971). The meniscus cement is early stage cements that precipitated in at the air-water interface of water bubbles, which have pulled away from the surface of grains (Mayers, 1987). Longman, (1980) pointed out that the meniscus cements are precipitated in the freshwater vadose environment.

B) Dissolution.

i. Description:

Most of the microfacies in the studied wells have been affected by dissolution, but especially those in the upper part of the Lidam Formation. Dissolution of aragonite bioclasts is common particularly in the peloidal ooidal packstone / grainstone, bioclastic packstone, mollusc packstone and ostracod wackestone / packstone facies. Dissolution is inferred from molds (sometimes demarked by micrite envelopes) retaining the shapes of earlier skeletal bioclasts, e.g. bivalve shells, ooids and foraminifera (Figures 5.12 and 5.13). However, some of the porosity created by dissolution has subsequently been partially or completely occluded by late stage calcite and dolomite cement, with examples of this shown photomicrographs and SEM images in Figure 5.14.

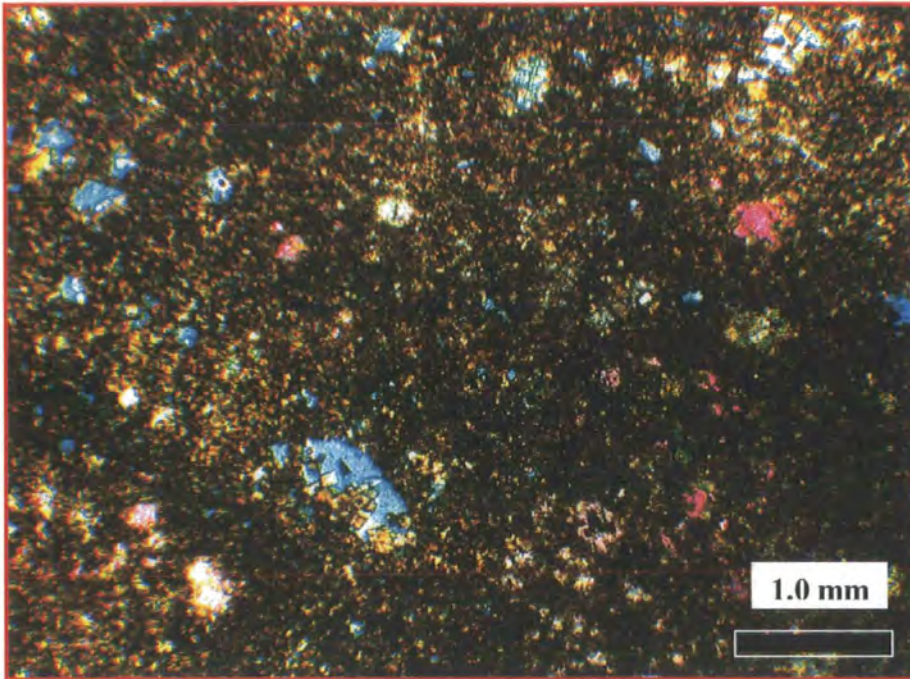


Figure 5.12. Photomicrograph showing shape of foraminifera and bioclasts which have been totally affected by dissolution. 11627.5 ft, P3-97

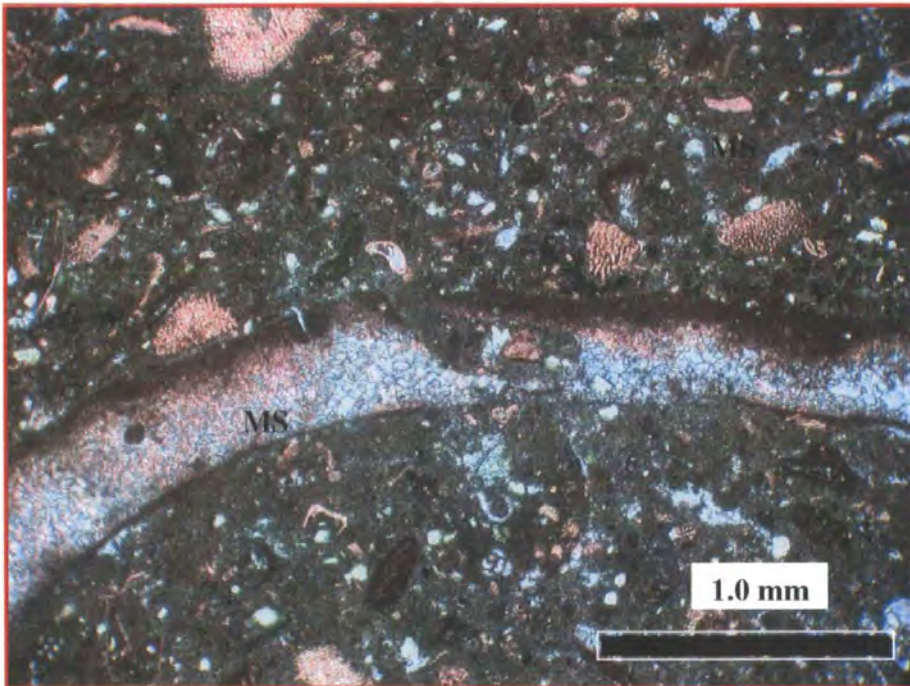


Figure 5.13. Photomicrograph showing mollusc shell (MS) that has been dissolved and a micrite envelope outline the original shell shape. The shell has been completely filled by ferroan calcite cement. 11226 ft, 3V3-59E



Figure 5.14. SEM image showing pore space of the dissolved bioclasts later filled by the growth of calcite (C) crystals. 10484.5 ft, 3V1-59E.

ii. Interpretation:

Many of limestone have suffered dissolution as a result of the passage of pore –fluids under saturated with respect to the carbonate phase present. This is the major process in near surface, meteoric diagenetic environments, and may lead to the formation of karst, but also it can take place on the sea-floor and during deep burial. Longman (1980) pointed out that the leaching probably occurred in the shallow subsurface in meteoric environment but whether it formed in the vadose or freshwater phreatic zone could not be determined. Tucker (2001) also mentioned that the secondary porosity created by carbonate dissolution is important in some hydrocarbon reservoirs. Small vuggy to extensive cavern system on the scale of tens of metres may form as a result of surfaces and near surface karstic dissolution of limestones, dissolution also takes place during deep burial in the formation of hydrothermal karsts. The dissolution of aragonite and precipitation of microspar are likely closely related to each other, and the formation of microspar can occur as an early step in limestone diagenesis and may form in a shallow burial environment without fresh water influence (Munnecke, 1997).

C) Neomorphism.

i. Description:

Neomorphism is the term used for processes of insitu replacement of one mineral by another of similar composition. It used to refer to aragonite and calcite transformations where replacement has taken place along a fluid front. Aggrading neomorphism of micrite to a fine calcite spar was observed in several thin sections and occurred in the bioclastic facies in the middle part of well 3V3-59E. Very fine, fine and coarse mosaic spar after micrite has developed mainly in the middle part of the Lidam Formation where some bioclasts are surrounded by micrite envelopes and their original structure has aggraded to incipient neomorphic spar. Most of the neomorphism occurs as microspar-(coarse neomorphic calcite) pseudospar formation from micrite. Very fine micritization has particles less than 16 μ m (Folk, 1965). Fine neomorphic crystals are larger than micrite, are now microspar and contain micritic patches. This type of neomorphism is widely developed in the Lidam Formation, commonly it took place on the margins of the large shell fragments, which were originally aragonite.

ii. Interpretation:

Recrystallization of some portions of micritic matrix into microcrystalline calcite has been observed throughout the studied section of the Lidam Formation at different depths. Tucker, (2001) pointed that the neomorphism may have taken place within an original inhomogeneous sediment, such as that resulted from bioturbation. The transformation of aragonite and high -Mg calcite grains and mud is one of the most important processes in carbonate diagenesis because it controls the ultimate petrophysical properties of limestone and their geochemical composition (Al Asam and Veizer, 1986). Depending on water chemistry and rates flow, micrite may recrystallize and neomorphose to coarse crystals in a fresh water phreatic or vadose environment (Longman, 1980; Flugel, 1982)

D) Cementation (drusy and syntaxial overgrowth).

i. Description:

The most important and common cement type is drusy calcite, which occurs in the uppermost part of the Lidam Formation, particularly in the peloidal ooidal packstone / grainstone and the bioclastic packstone facies (Figure 5.52). Syntaxial calcite cements are also seen as an overgrowth on some echinoderm fragments. Most of the primary pores,

together with secondary porosity resulting from the dissolution of aragonite skeletal material have been occluded by this calcite cement. Two types of calcite cement recognized in the studied wells are:

- i. Drusy or bladed calcite circumgranular cements in the peloidal ooidal facies. This cement fills and occludes the original intergranular and intragranular porosity. Drusy calcite cement increases in crystal size regularly toward the centre of the former void space (Figure 5.15).
- ii. Syntaxial calcite overgrowth cement around echinoderm fragments are seen in some of the echinoderm fragments and occurred in the upper most part of the limestone facies of the Lidam Formation associated with the pressure solution seams in the bioclastic and peloidal ooidal packstone facies (Figure 5.16).



Figure 5.15. Photomicrograph showing that the peloids (PE) has been completely affected by micritization and porosity occluded by drusy ferroan calcite cementation (FCC) in peloidal ooidal packstone facies, 10507 ft, 3V1-59E, PPI.

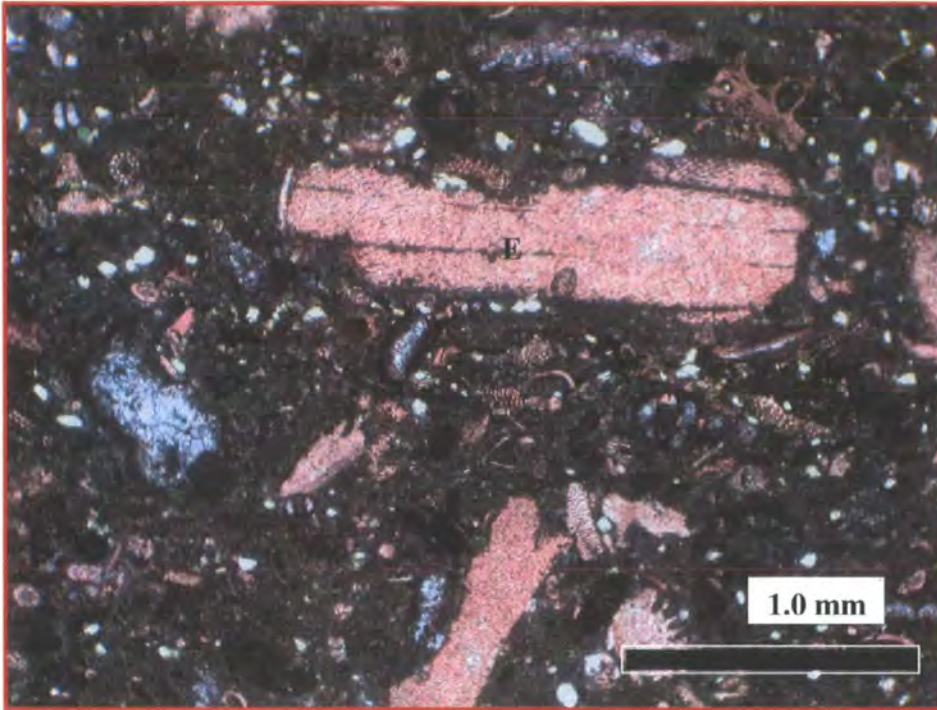


Figure 5.16. Photomicrograph showing that the Echinoderm fragments (E), cements are difficult to recognize in the dense bioclastic muddy facies 10230 ft, 3V3-59E, PPI.

ii. Interpretation:

The rims or overgrowth cements usually consist of non-ferroan clear crystals, but some contain dusty inclusions. The overgrowth calcite cement is strongly developed on echinoderm fragments and has strong affect in reducing porosity by more than 10%. The relationships of the component in the Lidam Formation indicate an early diagenetic development of cements on the echinoderm fragments.

The overgrowth rims occur in meteoric and early burial environments, but rarely in deeper subsurface diagenetic environments (El. Bakai 2001). The drusy crystals with their size increasing towards the pore centre are a distinctive characteristic of early cementation in the active saturated zone of the freshwater phreatic environment (Loucks, 1977, Longman, 1980, and Flugel, 1982). These fabrics of cement suggest that it formed from phreatic –meteoric water after subaerial exposure (Mansour, 2004).

E) Early dolomitization (fine dolomite).

i. Description:

Dolomite is common throughout the entire Lidam Formation and it occurs as a diagenetic replacement of pre-existing matrix and bioclasts in dolomite mudstone facies.

The dolomite is found in two forms: firstly, (Type 1) partially dolomitized, localized intervals are present in the upper mostpart of the Lidam Formation. Here, the dolomite is very finely to finely crystalline (> 0.1mm) rhombs of non-ferroan dolomite which selectively replace the matrix and have a dusty appearance (Figure 5.17). Where intensive dolomitization (dolomite rhombs) is seen, intercrystalline porosity is observed in SEM images (Figure 5.20). This dolomite is well recognized and scattered throughout the bioclastic, ostracod, and foraminifera packstone facies in the upper part of well R1-97.

The second type of dolomite (Type 2) is fine to medium crystalline dolomite. Here, intensive dolomitization has affected the lower part of the Lidam Formation, where it is now difficult to identify the original of bioclastic shapes. This type of dolomitization occurred in the dolomitic mudstone facies and bioclastic facies between depths of 10240 feet to 10280 feet at the base of the formation in well 3V3-59E. This type of dolomite shows well-developed rhombohedral crystals with good intercrystalline porosity and the crystals are idiotopic fabrics, also have a dusty appearance and non -ferroan (Figure. 5.19).

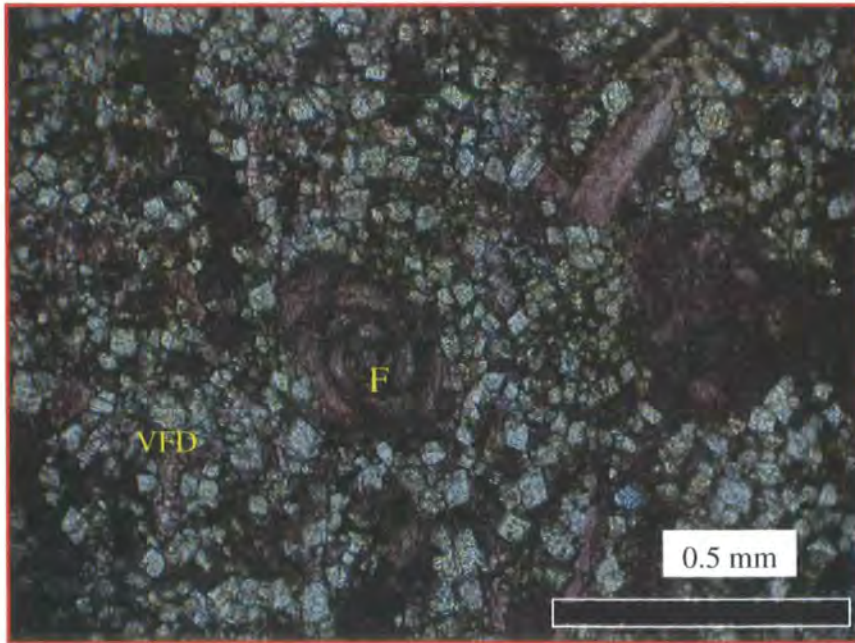


Figure 5.17. Photomicrograph shows a foraminifera (F) packstone facies containing very fine dolomite (VFD) selectively replacing the matrix, 10991 ft, R1-97, PPL.

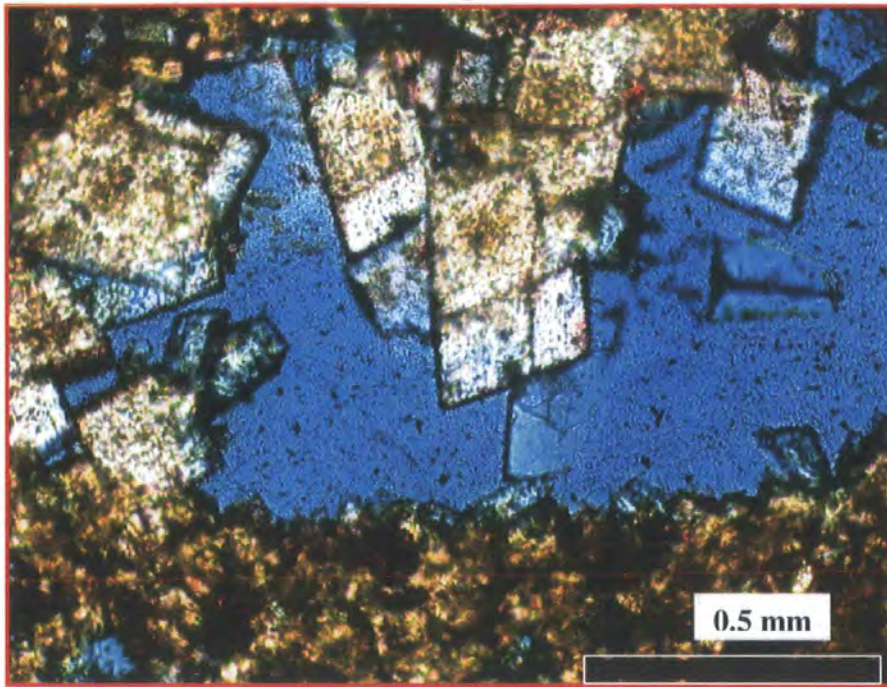


Figure 5.18. Photomicrograph showing mouldic porosity which has been infilled later with isolated dolomite rhombs. 11627ft, P3-97, PPL.

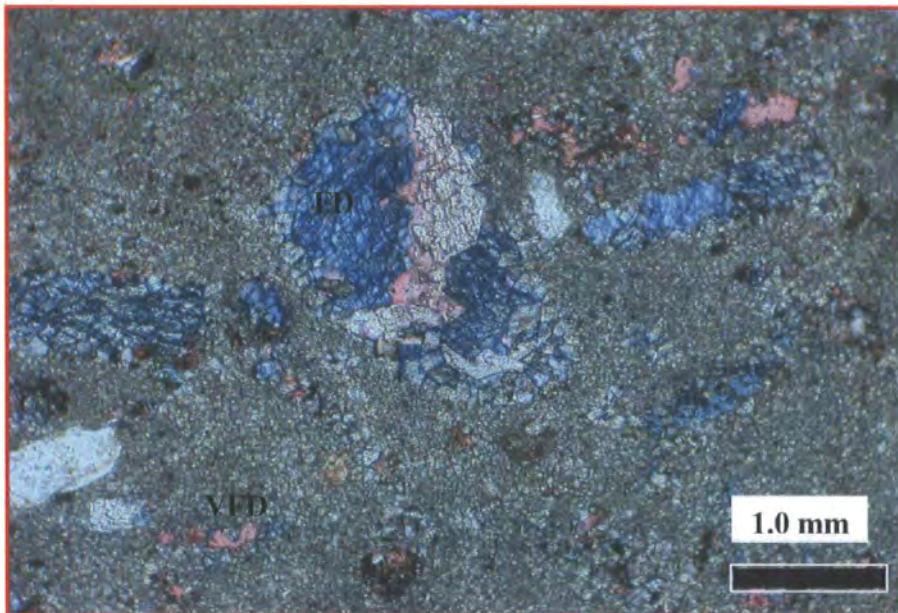


Figure 5.19. Photomicrograph showing very fine dolomite (Type 1) (VFD) mosaic texture with anhedral and irregular crystal boundaries with bioclasts molds filled by ferroan dolomite cement (FD) and relicts of micrite lime mud, 10253 ft, 3V3-59E.

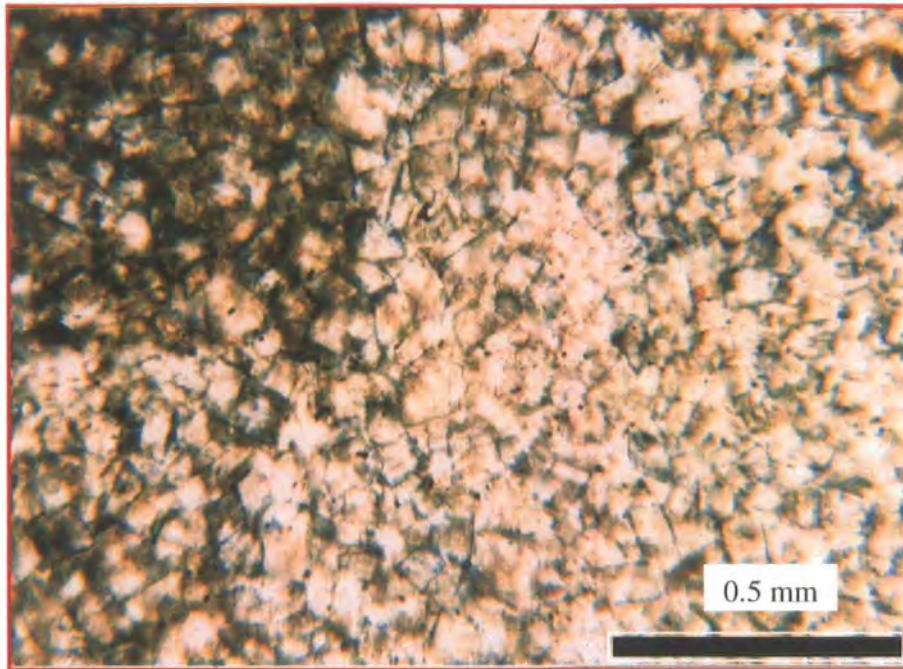


Figure 5.20. Photomicrograph showing dolomite mudstone facies with intensive dolomitization, 10260 ft, 3V3-59E.

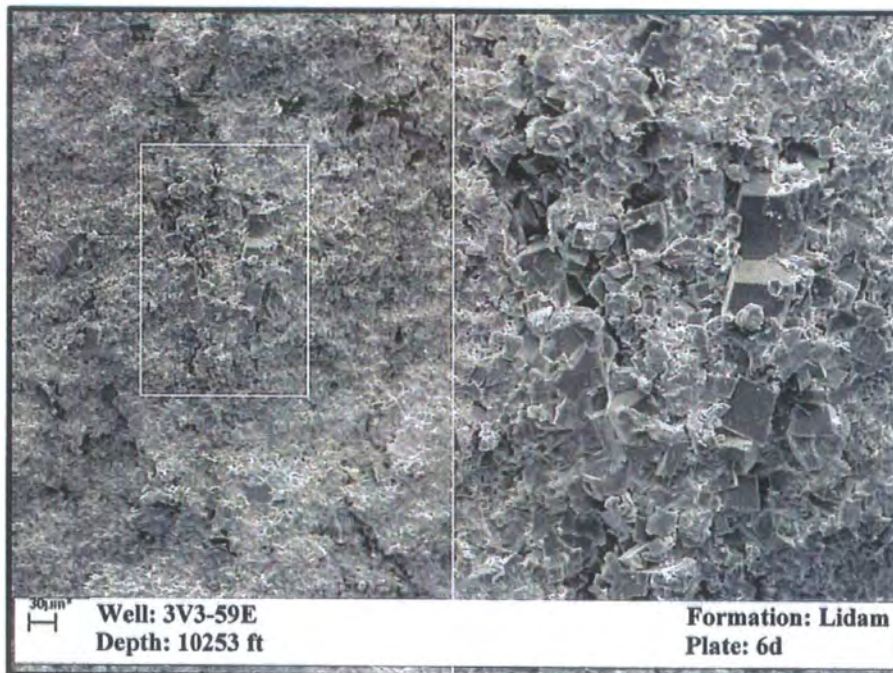


Figure 5.21. SEM image showing dolomite mudstone facies with intensive dolomitization (dolomite rhombs seen) and well developed intercrystalline porosity, 10253 ft, 3V3-59E.

ii. Interpretation:

This dolomitization which forms the dolomite-rich facies appears to have mainly affected original mud-dominated sediments characteristic of the supratidal sabkhas and adjacent subtidal marine-to-lagoonal environments from the Lidam Formation. Moore and others, (1988), suggest dolomitization preferentially affects muddy matrix. Bakai (2001) concluded that this type of dolomitization may take place in the intermediate or deep burial environment. This type of dolomite may have formed from evaporative sea water in a near-surface environment. Further evidence suggested that dolomite type 1 formed in hypersaline conditions as the dusty dolomite are usually replacive dolomite reflecting that dolomitization take place during early diagenesis and predate compaction features. The evaporite lithofacies directly overlying the dolomite lithofacies indicates an arid, strongly evaporitic environment. Dolomite units associated with evaporite units have commonly been interpreted as a resulting from reflux of hypersaline brines (Hardie, 1987).

Fresh water flushing of partially dolomitized muddy sediment would tend to dissolve the remaining undolomitized aragonite and concentrating the initially floating dolomite rhombs into a crystal – supported fabric and resulting in the porous sucrosic dolomite texture so common to many sabkha sequences (Moore, 1988). The type 1 and 2 dolomites are also similar to those of the massive sequence of the Cretaceous Edward Formation of Texas, described by Fisher and Rodda (1969). They concluded that this dolomitization may have taken place by the seepage-reflux mechanism. Because dolomitization can occur in a number of settings further work would be required to elucidate its origin in the Lidam Formation, and this was beyond the scope of this study.

F) Anhydrite replacement.

i. Description:

Anhydrite occurs throughout the anhydrite facies and stromatolitic facies in the lower and upper mostpart of the Lidam Formation in well 3V1-59E, in the lower part of wells 3V3-59E and R1-97, and the middle part of well N6-97. Two anhydrite crystal textures have been observed; lath- shaped blocky and anhydrite cement. The crystal size of lath shaped anhydrite range from <100 μm to several millimeters long as shown in SEM image (Figure 5.23). Commonly it contains fluid inclusions parallel to the crystal faces. The anhydrite occurs as cement which partially or completely fills the intergranular

porosity between the peloids and ooids particularly in peloidal ooidal packstone / grainstones (Figure 5.21). Some of the moulds and vuggy porosity are filled with the anhydrite cements overlying blocky dolomite cement (Figure 5.22).

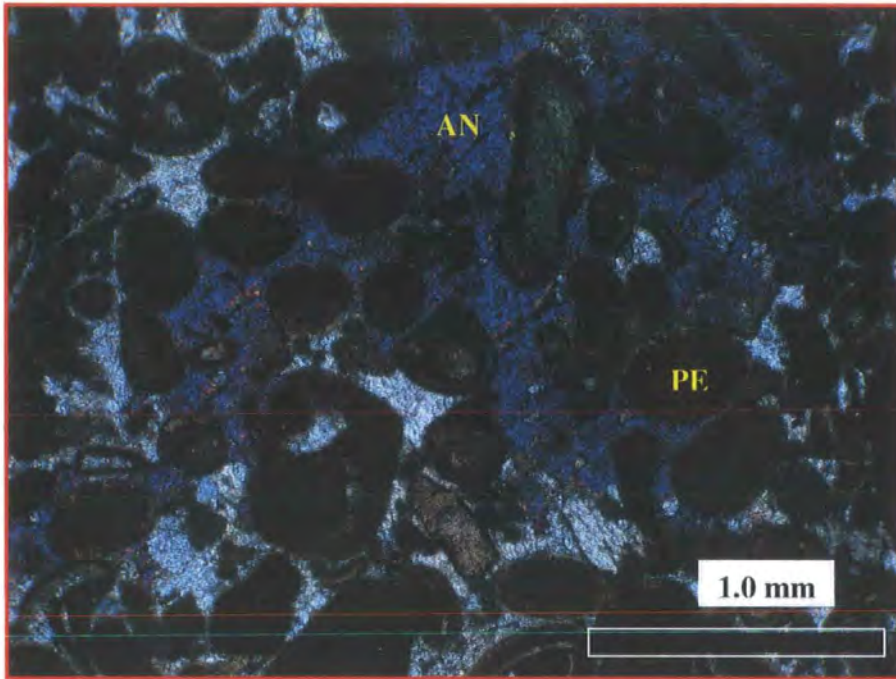


Figure 5.22. Photomicrograph showing replacement by anhydrite cement (AN) occluding intergranular porosity between peloid grains (PE), 10507 ft, 3V1-59E.

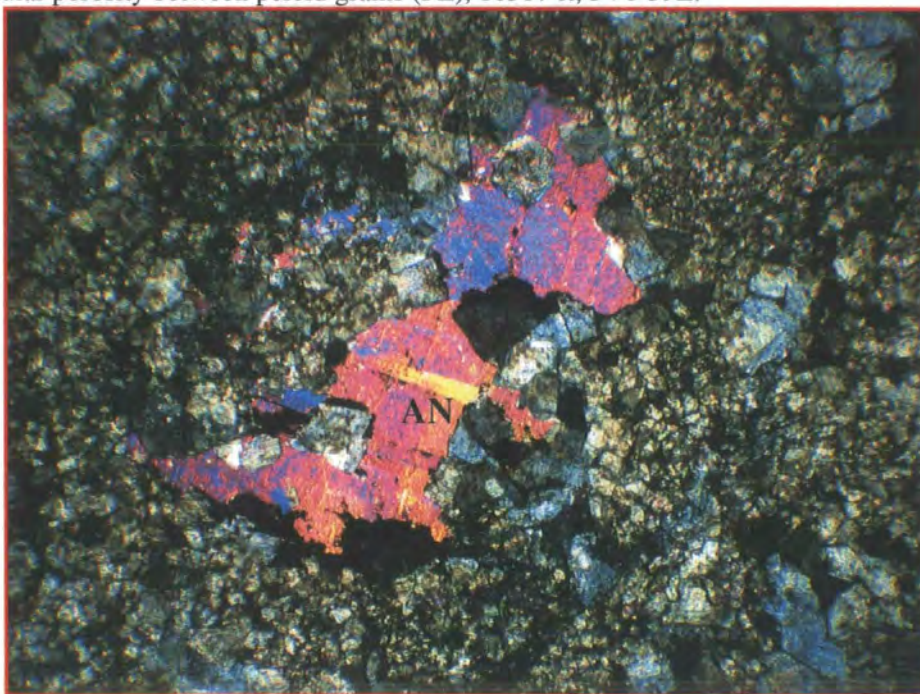


Figure 5.23. Photomicrograph showing the intergranular porosity occluded by ferroan calcite cement and anhydrite cement (AN) in the dolomite facies, 10507 ft, 3V1-59E.

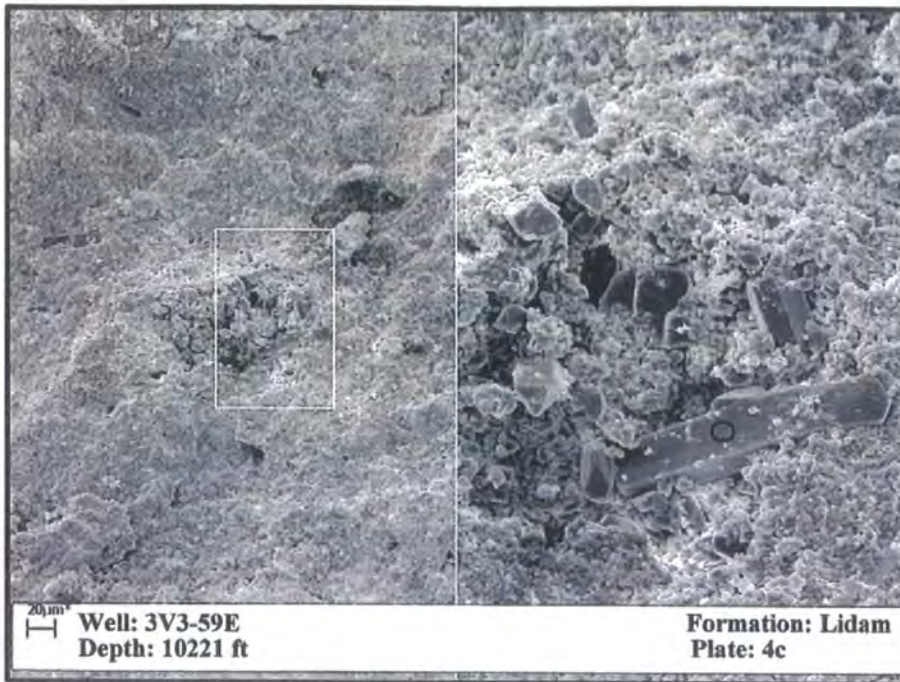


Figure 5.24. SEM photomicrograph showing the replacement of anhydrite cement partially occluding the intergranular porosity between the peloid grains, 10507 ft, 3V1-59E.

ii. Interpretation:

The geological evidence and present day show that both gypsum and anhydrite may be precipitated at the earth surface, subaqueously in shallow and deep water, and subaerially in coastal and inland sabkhas. On burial to depths greater than several hundred meters, however, all CaSO_4 is present as anhydrite, and on uplift anhydrite is normally converted to gypsum (Tucker, 1992). Anhydrite occurs as a replacement mineral and as cement in carbonates, especially those associated with evaporites. Anhydrite forms rectangular crystals with cleavages at 90° and shows bright interference colour up to mid third order (Adams, 1998). Much of anhydrite may originally precipitate as gypsum crystals within near surface sediments. It is possible that gypsum grew as displacive crystals within the sediment during early near surface diagenesis (Tucker, 1992). Murray, (1964) reported that a diagenetic cycle exists in the calcium sulfate minerals. Gypsum is deposited by precipitation or by growth of crystals in unconsolidated rocks near the surface. This primary gypsum is replaced, with burial, by anhydrite at a temperature of 42 degrees C and theoretical depths of 2,000 feet. Anhydrite (metagypsum) occurs as beds

and pore-fillings. Uplift and removal of overburden cause anhydrite to be replaced by gypsum. Variations in texture distinguish bedded, void-filling, and replacement anhydrite.

5.3.5. LATE BURIAL DIAGENESIS:

1) Compaction (concavo-convex contacts, dissolution seams and stylolites).

i. Description:

Concavo-convex contacts are common in the peloidal ooidal packstone facies throughout the studied wells. These features are very common at grain contacts and where they have concavo-convex forms with some grains truncated against others forming dense or fitted fabrics. During detailed petrographic study of the studied wells two styles of chemical compaction were recognized in the Lidam Formation. These are stylolites and pressure solution seams. The stylolites are generally irregular with amplitudes of > 1cm and sutured surfaces that cut grains, cement and matrix indiscriminately. Pressure dissolution seams have a more 'wavy, anastomosing' appearance and have concentrations of clay, iron minerals or organic matter. The insoluble residue from the limestone's dissolution, are usually concentrated along the stylolites and along dissolution seams (Figure 5.24). The pressure solution seams are more abundant than stylolites in the lower part of the Lidam Formation and occur in the ostracod and bioclastic facies (Figure, 5.25).



Figure 5.25. Photomicrograph showing stylolites and pressure solution seams with low amplitude in bioclastic foraminifera packstone. 10226 ft, 3V3-59E, PPL.

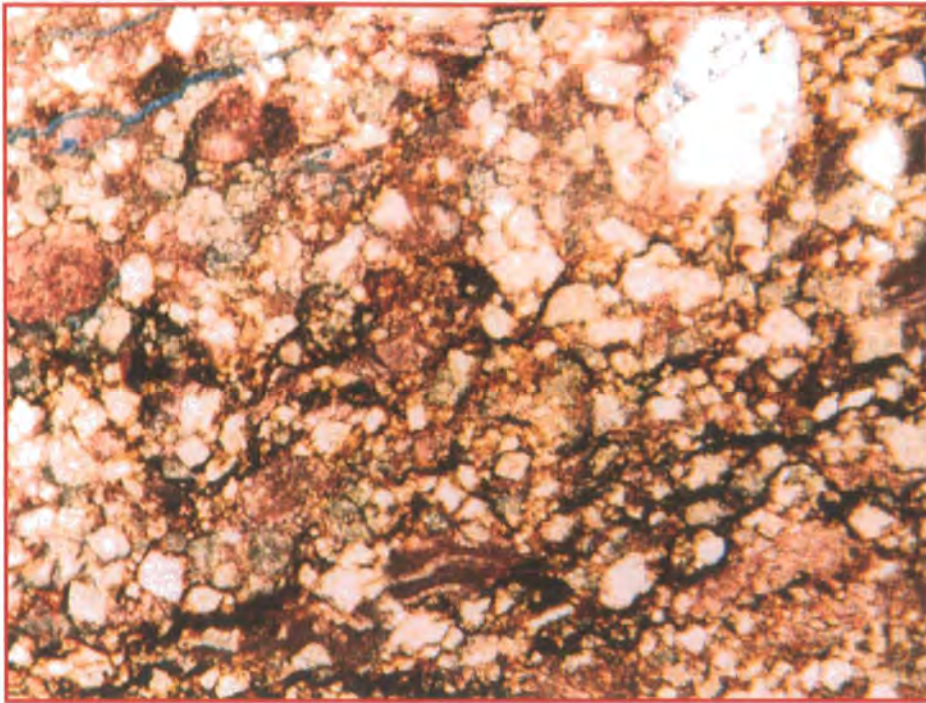


Figure 5.26. Photomicrograph showing high concentration of pressure solution seams with low amplitude in bioclastic foraminifera packstone with scattered dolomite. 10207 ft, 3V3-59E, PPL.

ii. Interpretation:

Increasing overburden pressure leads to compaction in sediments and two categories are recognized; mechanical and chemical. Mechanical compaction may begin soon after deposition, whereas chemical compaction normally requires more than several hundred meters of burial. Pressure solutions are an important process accentuating bedding plane particularly between the muddy and grainier sediments (Tucker, 2001). The high concentration of pressure solution seams with low amplitude in bioclastic foraminifera packstone with scattered dolomite indicated that the dolomitization predates compaction features. The lower part of the Lidam Formation generally had more contemporaneous clay deposition than the top, and dissolution seams rather than stylolites were better developed. Stylolitization significantly affects the carbonate reservoir quality by providing pathways for hydrocarbon migration and is one of the most common consequences of burial diagenesis in limestones (e.g. Bathurst, 1975, Tucker & Wright, 1990). Meyers, (1980) concluded that the chemical compaction processes include pressure solution and stylolites.

2) Fracturing.

i. Description:

Fractures have been observed in the middle part of the Lidam Formation particularly in the bioclastic foraminifera facies and the peloidal ooidal facies in well 3V3-59E, 3V1-59E and well N6-97. These fractures have been completely infilled by equant ferroan calcite cement, reducing the porosity as shown in Figure 5.26 and 5.27. These fractures are up to a few centimetres in length and range from less than 1mm to 5mm in width. The fractures do not greatly affect reservoir quality and most of the recorded fractures have been occluded by cementation.

ii. Interpretation:

It is not clear how much actual porosity is gained during the fracturing of the carbonate reservoir sediments, because of the difficulty in measuring this type of porosity. However, in these deposits any increase in porosity has been infilled by later cements. Fracturing can take place at practically any time during the burial history of the carbonate sequence starting with shallow burial because of common early lithification. Fractures can be associated with faulting, folding, differential compaction, salt movement and hydraulic fracturing within over pressured zones, (Moore, 1989).

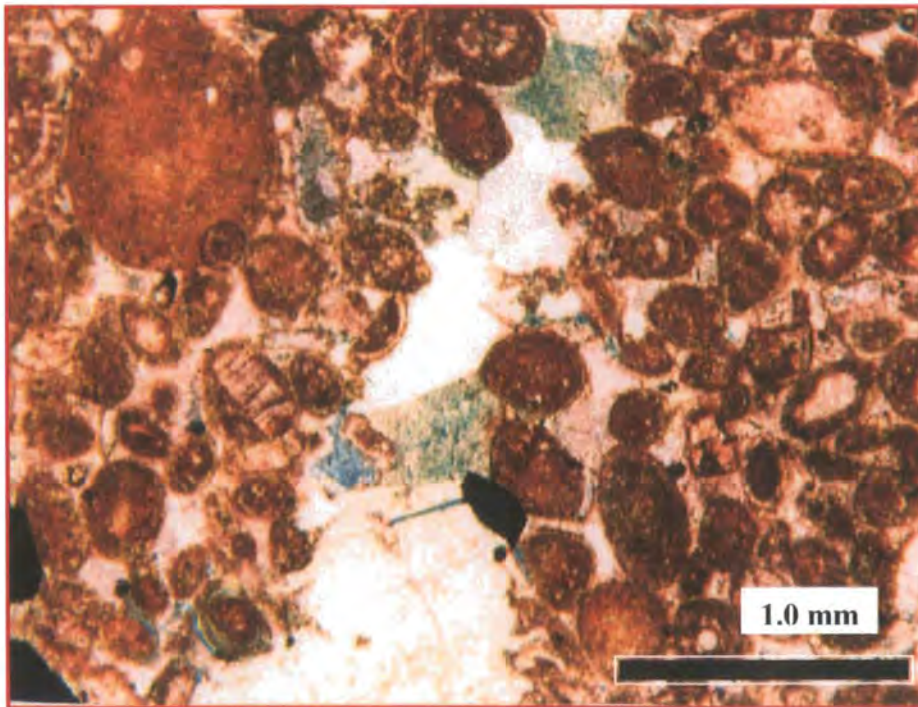


Figure 5.27. Photomicrograph showing ferroan calcite cement reducing fracture porosity in a peloidal ooidal packstone/grainstone, 10209 ft, 3V3-59E, PPL.

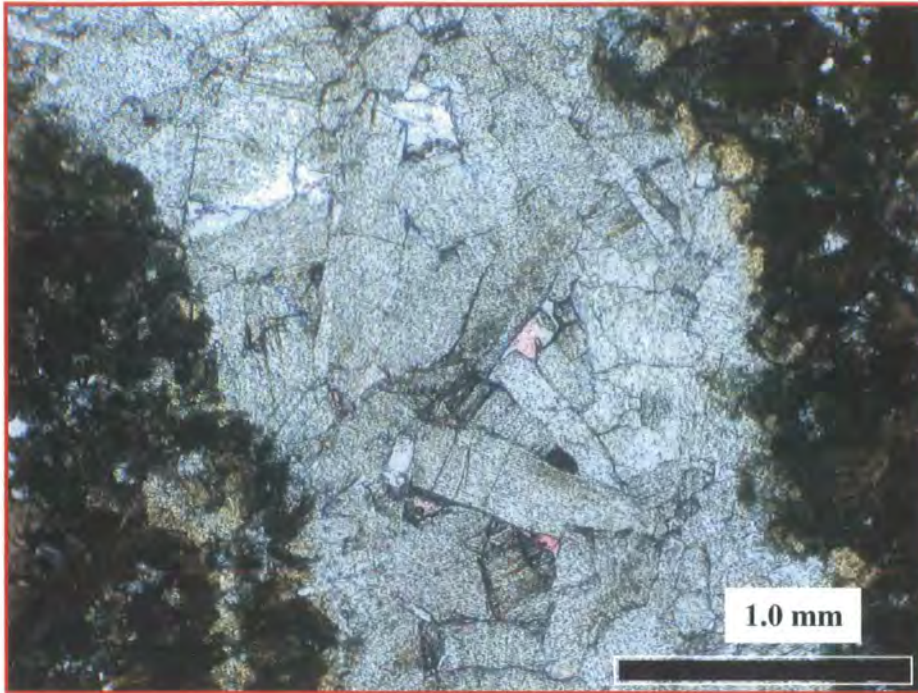


Figure 5.28. Photomicrograph showing later fracture has been completely occluded by ferroan calcite cement in the peloidal facies, 10458 ft, 3V1-59E, PPL.

3) Cementation (equant calcite cement).

i. Description:

The coarse equant calcite cements are commonly ferroan and completely occlude the pore spaces between grains in some samples (Figure.5.28). It is observed in most of the cored intervals in the studied wells. It occurs in the upper part of the well 3V3-59E, 3V1-59E, and R1-97. This cement occurs as clear large blocky or anhedral calcite cement particularly in the middle part of the Lidam Formation in the peloidal ooidal packstone / grainstone facies. These cements are filling the chambers of foraminifera and ostracods and / or replace fossil fragments of mollusc casts (Figure 5.29).

The growth of equant or blocky calcite mosaic cement showing irregular shapes between the intergranular skeletal grains. This type of cement may destroy any remaining pore space and completely filling all the original intergranular porosity (Figure, 5.28).

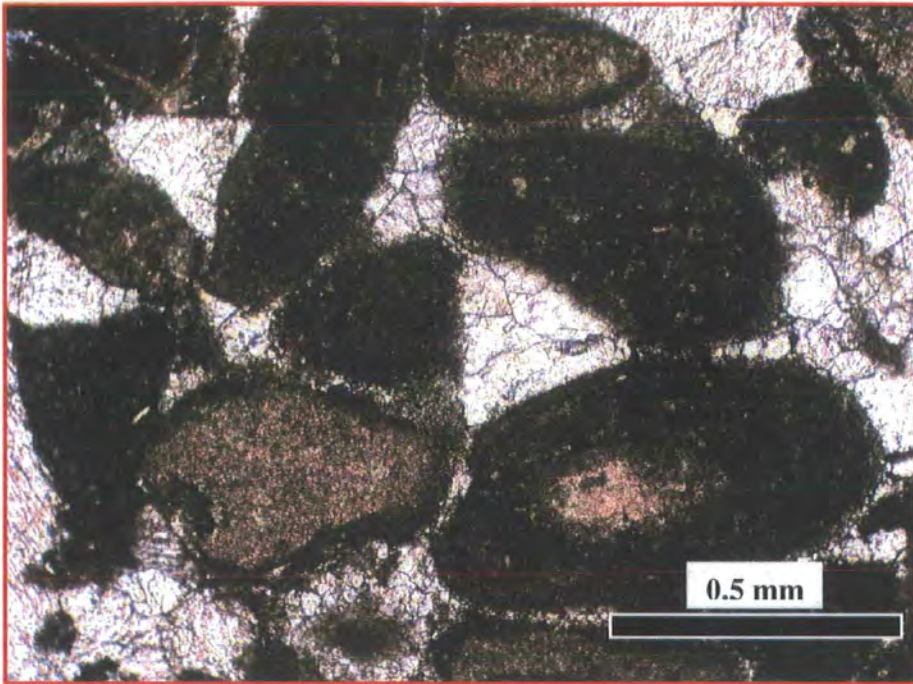


Figure 5.29. Photomicrograph showing well developed equant calcite cement occluding the most of the pore space. 10507 ft, 3V1-59E, PPL.

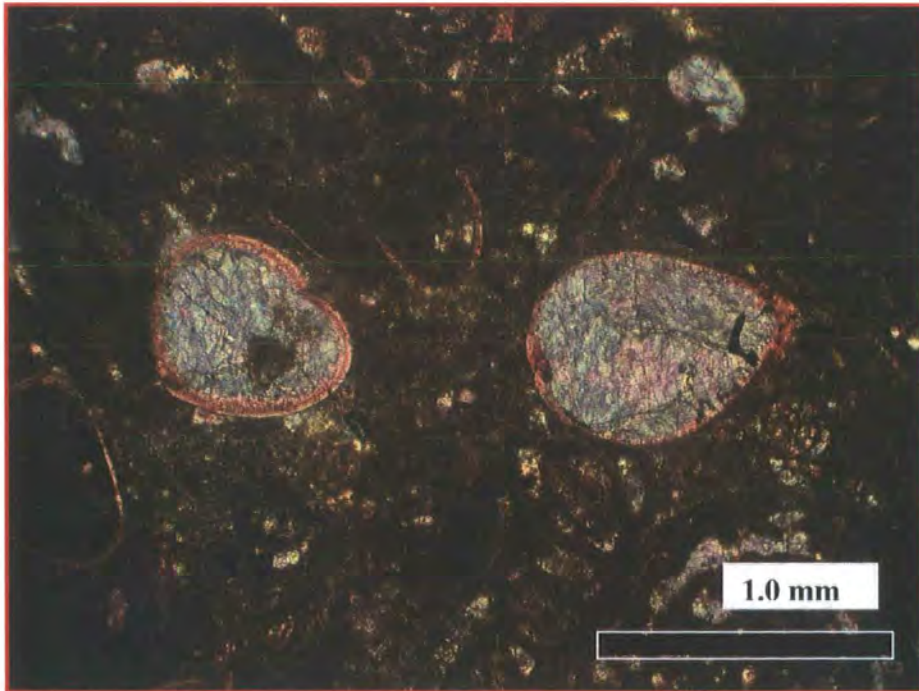


Figure 5.30. Photomicrograph shows well developed equant mosaic calcite cementation occluding intragranular porosity in ostracods. 10221 ft, 3V3-59E, PPL.

ii. Interpretation:

The equant calcite cement is common diagenetic feature found in the Lidam Formation formed during the late stage of diagenesis. This cement types post dates most earlier diagenetic features, including burial features such as fracturing. It is the most major diagenetic event in terms of porosity reduction. The coarse crystalline cement shows no coarsening toward the pore space centre similar to those described by Halley (1981) typical for late stage of cementation, or of the earlier described drusy cements. Folk (1965) also suggests that coarse crystalline composite calcite with ghosts of depositional texture form through replacement at great burial depth.

4) Late dolomitization (clear coarse dolomite cement).

i. Description:

This cement has been recognized within the middle part facies of the Lidam Formation and the upper most part of the cored section of the Lidam Formation in well 3V3-59E particularly in the bioclastic foraminifera packstone facies and mollusc facies (see section 4.3).

This clear dolomite cement (Type 3) is observed in association with the stylolites and in the open spaces in the rock adjacent to them. The cement shows slightly curved crystal faces, and is a form of dolomite known as saddle, or baroque, dolomite. This is locally present as pore filling cement in mouldic and vuggy porosity in primary pores of the packstone / grainstone facies, particularly in the bioclastic foraminifera packstone and mollusc facies. The dolomite forms fine rhombs (30-100 μ m) filling vuggy pore spaces as shown in Figures.5.30 and 5.31 and where intergrown has a coarse, interlocking, rhombic (sucrosic) fabric (Figure 5.32). The SEM image shows the filling of coarse dolomite cement in earlier vuggy or mouldic porosity (Figure 5.33). This type of dolomite is more common in the upper part of the Lidam Formation than type 1 and 2.

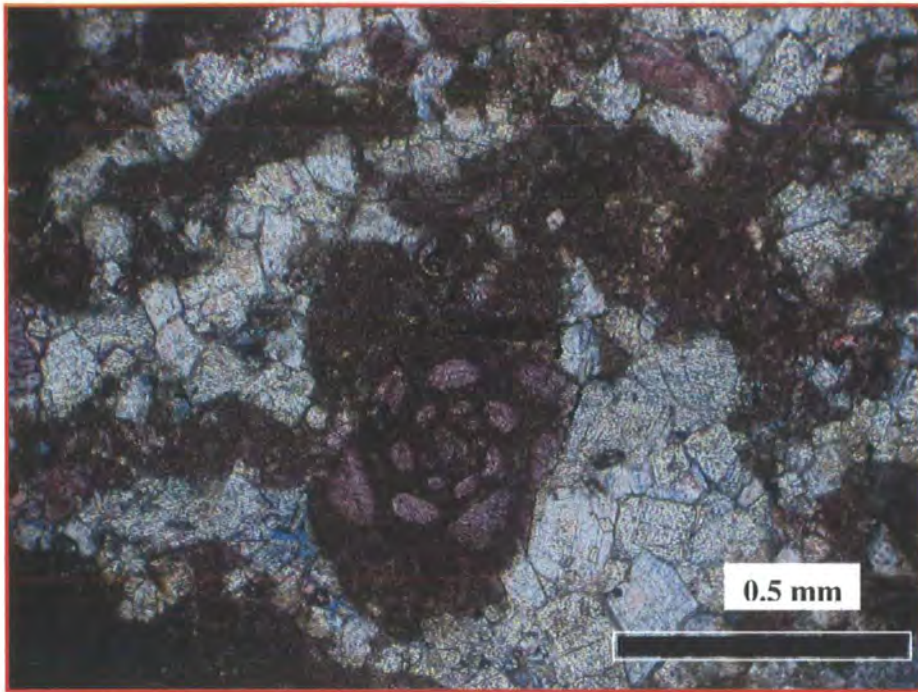


Figure 5.31. Photomicrograph showing infill of dolomite cement in vuggy or mouldic porosity. Note also oil staining and intercrystalline porosity as shown by blue resin, 10198 ft, 3V3-59E, PPL. 520

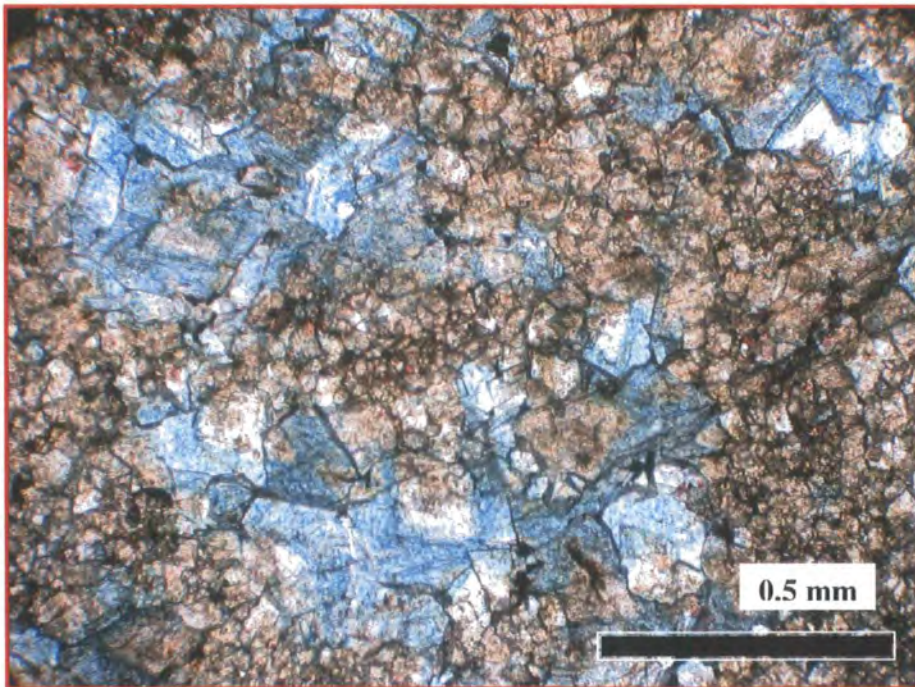


Figure 5.32. Photomicrograph shows filling of clear coarse dolomite cement in earlier vuggy or mouldic porosity, 10198 ft, 3V3-59E, PPL.

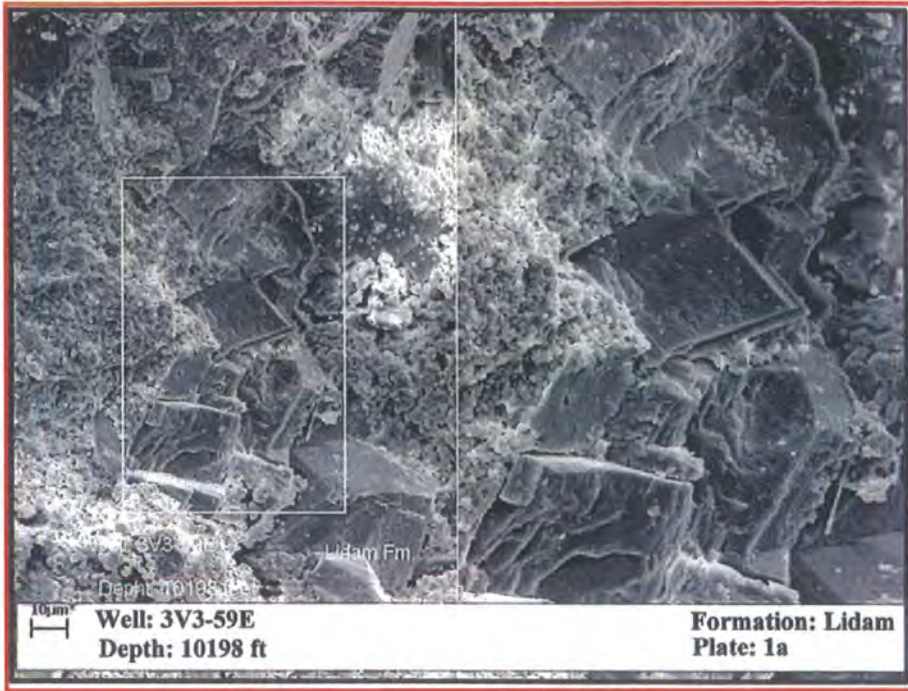


Figure 5.33. SEM image shows filling of coarse dolomite cement in earlier vuggy or mouldic porosity, 10198 ft, 3V3-59E, PPL.

ii. Interpretation:

This type of dolomite formed as a cement infilling intergranular, mould and vuggy porosity and postdates many earlier diagenetic features occurring during late burial. Tucker, (2001) pointed out that the clear dolomite rhombs and late cavity filling dolomite cements are all common form of burial dolomite in many limestones. This saddle dolomite is characteristic of high-temperature burial diagenesis (Gregg and Sibley, 1984). Folk (1965) also suggested that coarse crystalline composite dolomite with ghosts depositional texture result from replacement of limestone at burial depth. Many dolomites, especially at greater depth, have higher porosity than limestones and this makes them prime targets for hydrocarbon exploration. Warren (2000) pointed out that the burial dolomite are subsurface cements and replacement that form below the active phreatic zone (reflux and mixing zones in permeable intervals flushed by warm to hot magnesium-enriched basinal and hydrothermal waters. Machel (2004) established that flow of Mg-rich fluids, in combination with conducive geochemical conditions, is necessary for large-scale dolomitization and the majority of the reservoirs are interpreted to be reflux origin.

5) Replacement by Pyrite.

i. Description:

In the Lidam Formation pyrite is volumetrically insignificant and will not influence reservoir quality and is present usually only in trace amounts. Partial replacement of pyrite occurs in the middle and upper part of the Lidam Formation in the bioclastic packstone and ostracod facies, usually in calcispheres and foraminifera and replacing cement or matrix and along the fractured zones (Figure 5.34). Pyrite is distinguished from other opaque iron minerals by its yellowish colour in reflected light and is present as disseminated grains and crystals (Figure 5.35).

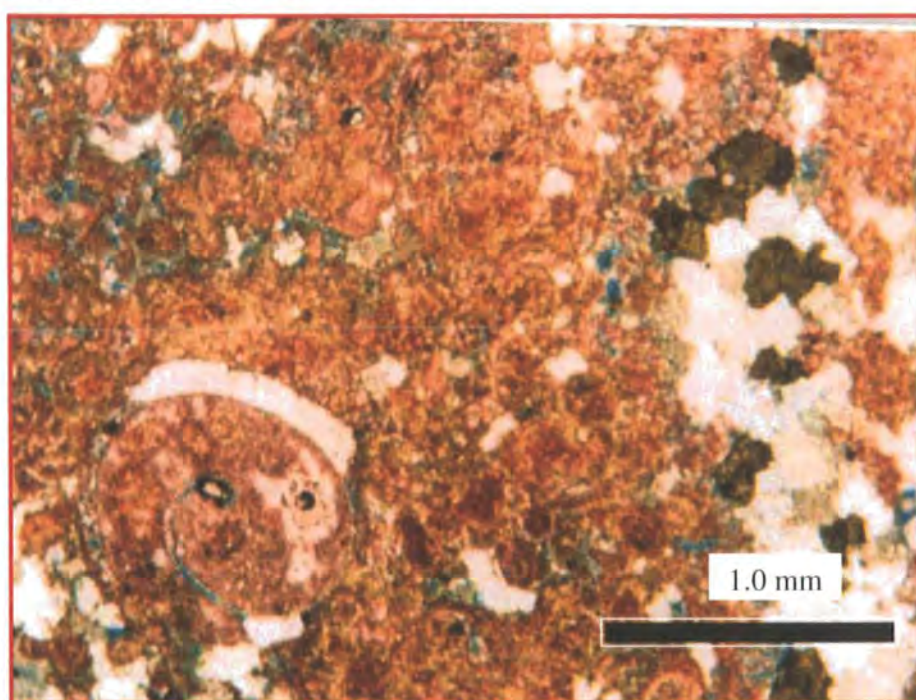


Figure 5.34. Photomicrograph showing partial replacement of pyrite in a fracture zone, 10201 ft, 3V3-59E.

ii. Interpretation:

Pyrite may replace skeletal grains and pyrite precipitation possibly occurred later in the diagenetic sequence and certainly after dolomite precipitation of which pyrite replaces. Pyrite mostly forms under reducing conditions replacing organic material or in close proximity to organic material (Tucker, 2002). Lee and Friedman, (1987) concluded that pyrite replacement often forms at very shallow burial depths as the result of the decomposition of organic matter under reducing conditions. Authigenic pyrite commonly

forms under reducing conditions replacing organic material, or in close proximity to organic material (Flügel, 2004). According to Berner, (1970) the sulphides for the precipitation of pyrite comes mainly from bacterial of dissolved sulphate in pore waters.

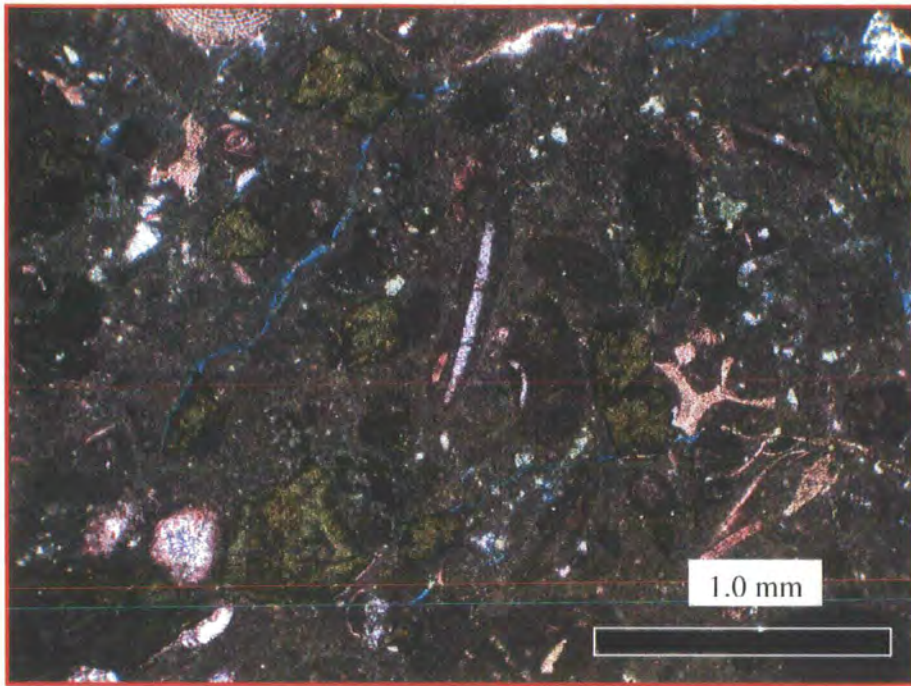


Figure.5.35. Photomicrograph showing replacement of pyrite in a bioclastic facies, 10528 ft, 3V3-59E.

5.4. CATHODOLUMINESCENCE (CL) ANALYSIS AND INTERPRETATION.

5.4.1. Introduction:

Cathodoluminescence microscopy of thin sections has become an important tool in microfacies and particularly diagenetic analysis. This is a technique where the polished surface of a sample is bombarded by a stream of electrons in a vacuum chamber. This causes many minerals to glow, and calcite and dolomite emit distinctive red, orange and yellow colors. In carbonates, this luminescence is mainly caused by Mn in the lattice. Different luminescent responses can be related to different diagenetic environments. Mn will only enter the lattice of sub-oxic conditions occur, but if the waters are reducing Fe can enter and this quenches the effects of Mn reducing the luminescence response (Machel and Burton, 1991) (Figure, 5.36). According to Miller, (1988) cement zonation due to changes in fluid chemistry can not always be seen using the transmitted light microscope. During CL analysis zones in calcite cements can be grouped into three types; non-luminescent (dead, extinguished or black), dull (brown), and luminescent (bright yellow, orange, and moderate). Non-luminescent calcite is suggested to be precipitated from oxidizing pore-water, whereas bright and dull luminescent indicates more reducing pore fluid (Meyers, 1978 and Tucker 1991). The variation between bright and dull cement luminescence indicates a change from oxidizing to more reducing condition of fluid (Meyers, 1991). Non-luminescent calcite or dolomite is normally the result of low content of an activator (Fairchild, 1983).

The major application of Cathodoluminescent (CL) microscopy for carbonate rocks are for:

- a. Observing and interpreting diagenetic phases (e.g. zonal structures within crystal reflecting changes in the chemical environment and / or in the growth speed; early diagenetic and burial cements reflecting burial depths; mineral transformations, such as the alteration of calcite to dolomite (Richter, 1984).
- b. Evaluating pore water chemistry, reflected by sector zoning in calcite crystals (Bruckschen et al. 1992), and interpretation of the diagenetic history of reservoir rocks.
- c. Reconstructing diagenetic events which identify stages of cementation and provide a "cement stratigraphy" that are used to establish cement-based stratigraphic correlations (Meyers, 1991).

- d. Recognizing fabrics (e.g. distinction of recrystallization structures, recognition of micro cracks).
- e. Studying the diagenesis of fossils.

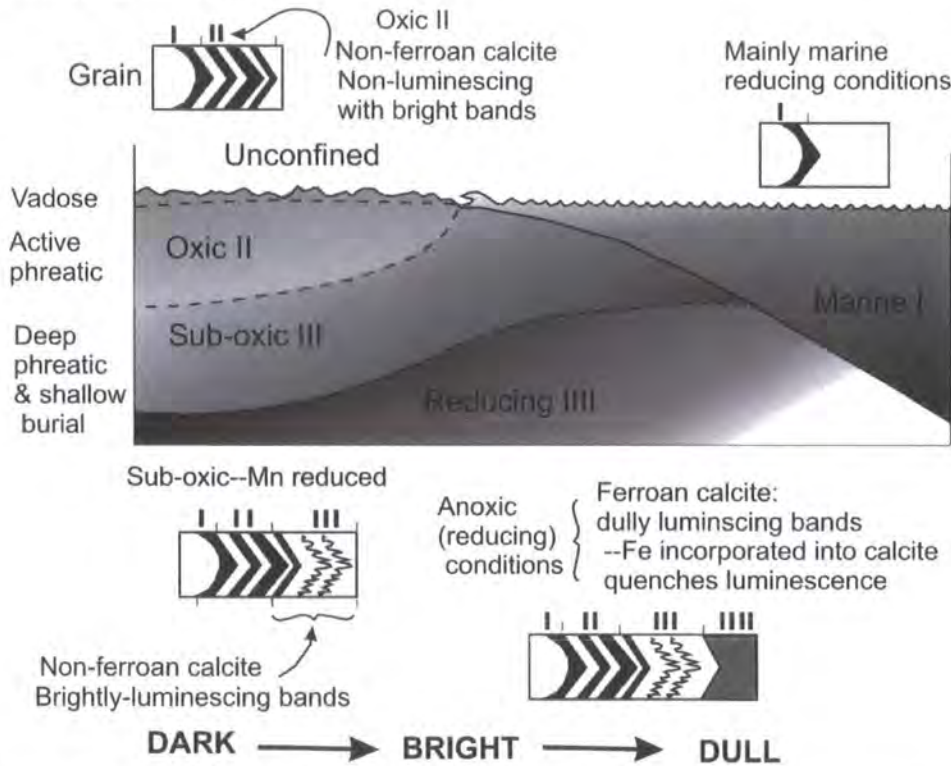


Figure 5.36. Diagram showing Cathodoluminescence properties of zoned cements formed under different diagenetic conditions.

5.4.2. Cathodoluminescence (CL) Analysis of the Lidam Formation.

Seven samples were chosen from different wells (3V1-59E, 3V3-59E, R1-97, P3-97, and N6-97) in the Lidam Formation from different depths for more detailed study by using Cathodoluminescent (CL) microscopy. Those with coarse cements were chosen to investigate the different stages of cement zonation and the affect of pore fluid chemistry on cementation. The original grains mostly peloids, but also bioclasts of the Lidam Formation show moderate to bright luminescence that formed under oxic-suboxic conditions atypical of most abiotic marine precipitates.

The results from the selected samples of the Lidam Formation reveal three different stages of cementation under Cathodoluminescent (CL). These cement stages are

non-luminescent, non luminescent with bright bands of red-orange zones and dark dull non-luminescent.

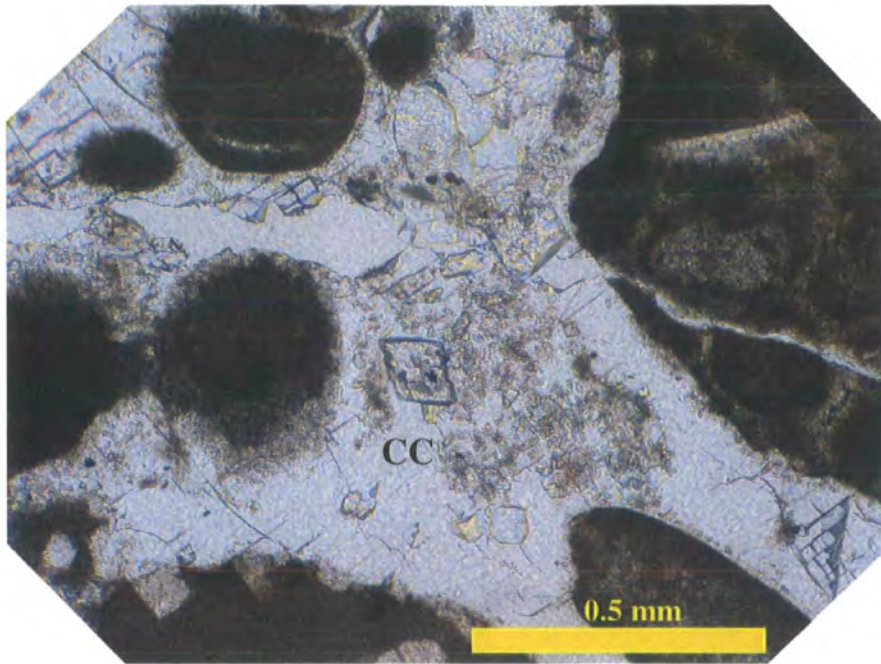
1. The first stage is a dull luminescent zone and includes microcrystalline (micrite) around peloidal grains. This first generation of relatively fine-grained cement which appears, and forms cloudy moderately dull, non-luminescent cement, most likely formed under marine conditions (Figures.5.37 and 5.39 and see above).
2. The second stage is dull to moderate luminescence with bright bands of yellow and red-orange zones. This zoning is more characteristic of calcite cement than the dolomites and is present in drusy calcite cement (Figures.5.37, 5.38, 5.39, 5.42, and 5.43). This stage of cementation probably reflects the oxidizing nature of shallow meteoric waters, with the calcite cements shows the dull to moderate luminescence with bright bands of yellow and red-orange zones reflecting fluctuation in the oxic zone of the active phreatic zone. The variation between bright and dull luminescence indicates a change from oxidizing to more reducing conditions of fluid (Meyers, 1991). Meniscus cements grain to grain contact also present and shows bright red luminescent, according to Adams, (1984). This morphology and luminescence are typical of precipitation in the vadose zone.
3. The last stage of cementation is the most abundant and occurs in most of the samples from the Lidam Formation. This stage is the coarse ferroan equant calcite cement, which has completely filled primary porosity in peloidal grainstone

Under Cathodoluminescence microscopy the coarse calcite cement shows dark dully non-luminescent cement filling any remaining porosity. This probably reflects sub-oxic and anoxic reducing conditions during deep phreatic and deep burial depths and is consistent with the interpretation of equant cements (see section 5.3).

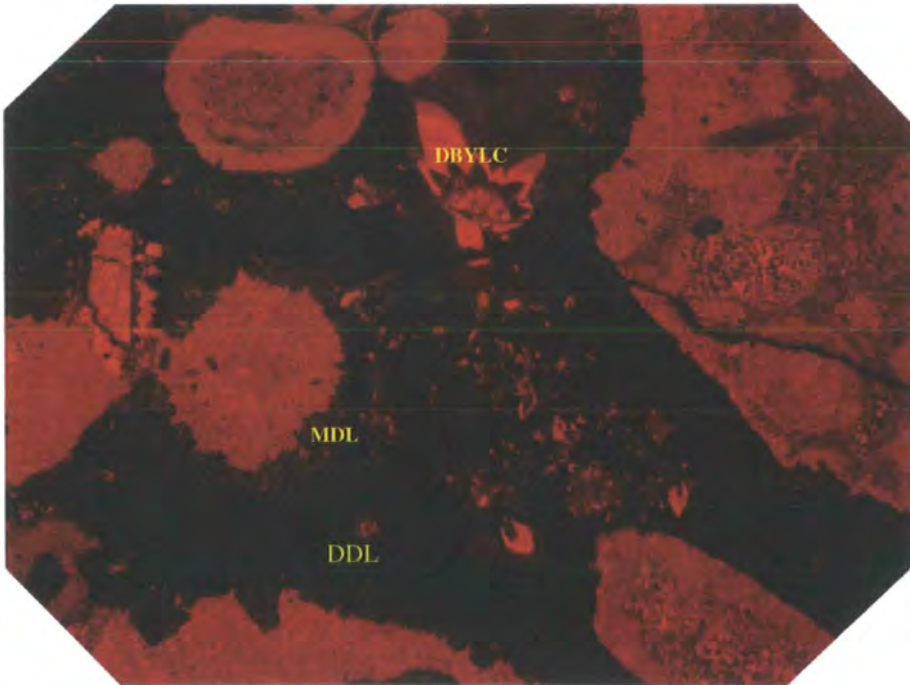
Two types of diagenetic phases are clearly recognized in the studied polished thin sections of the dolomites. These are red-orange zones luminescent and non-luminescent dolomite crystals.

1. The first type of dolomite rhombs (the “dusty” type 1 forms) shows well developed bright red-orange luminescent zonation. These are interpreted as early formed replacive dolomites (see section 5.3) and their luminescence probably reflect oxic conditions in the phreatic zone (Figure.5.40 and 5.41).

2. The Second type of dolomite (Type 3 forms) (coarse zoned dolomite cement) shows slightly curved crystal faces, and locally present as pore filling cement in mouldic and vuggy porosity in primary pores of the packstone / grainstone facies and forms fine rhombs (30-100 μ m). This dolomite is dull non-luminescent interpreted as late, possibly burial properties forms and their luminescence is consistent with sub-oxic and anoxic reducing conditions during the deep burial depths (Figures 5.40, 5.41 and 5.46).

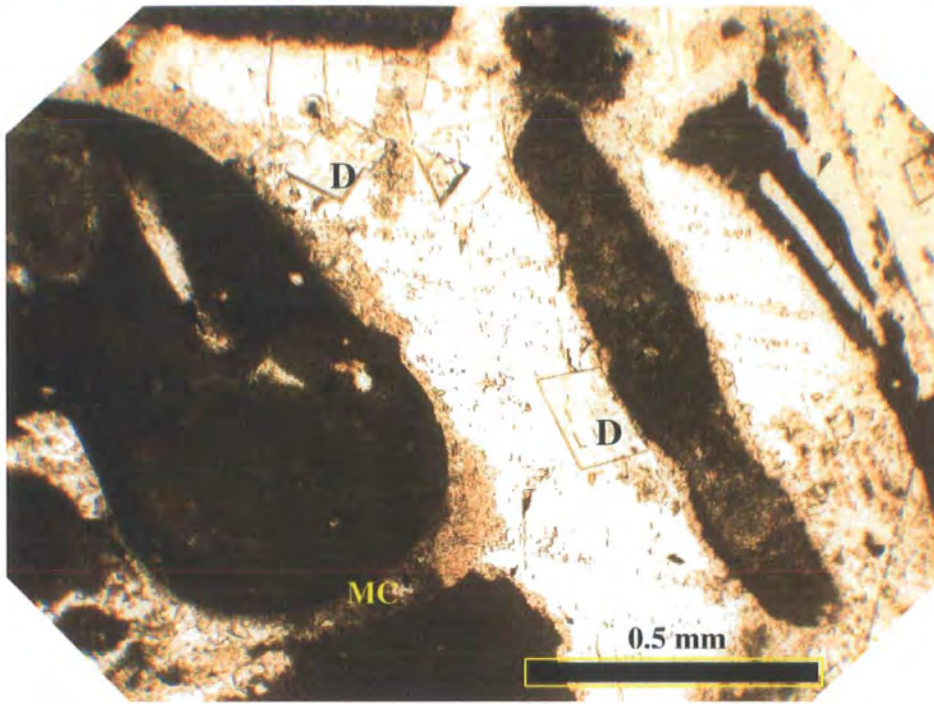


(a)

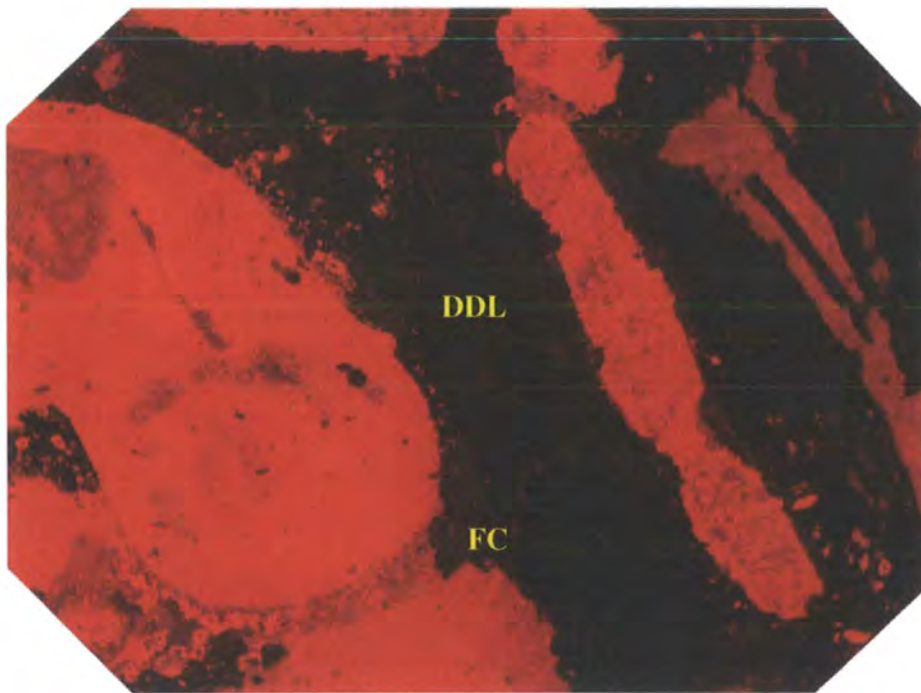


(b)

Figure 5.37. Paired photomicrographs taken under normal light (PPL) (a) and CL (b), showing grainstone with coarse calcite cement (CC). Under CL (b), three main generations of cement are visible, the first has moderate dark luminescent (MDL), the second well developed thin zonation of dark- bright yellow orange luminescent calcite crystals (DBYLC) and the third is dark non-luminescent cement (DDL) filling any remaining porosity. Lidam Formation, 10507.5 ft, 3V1-59E.

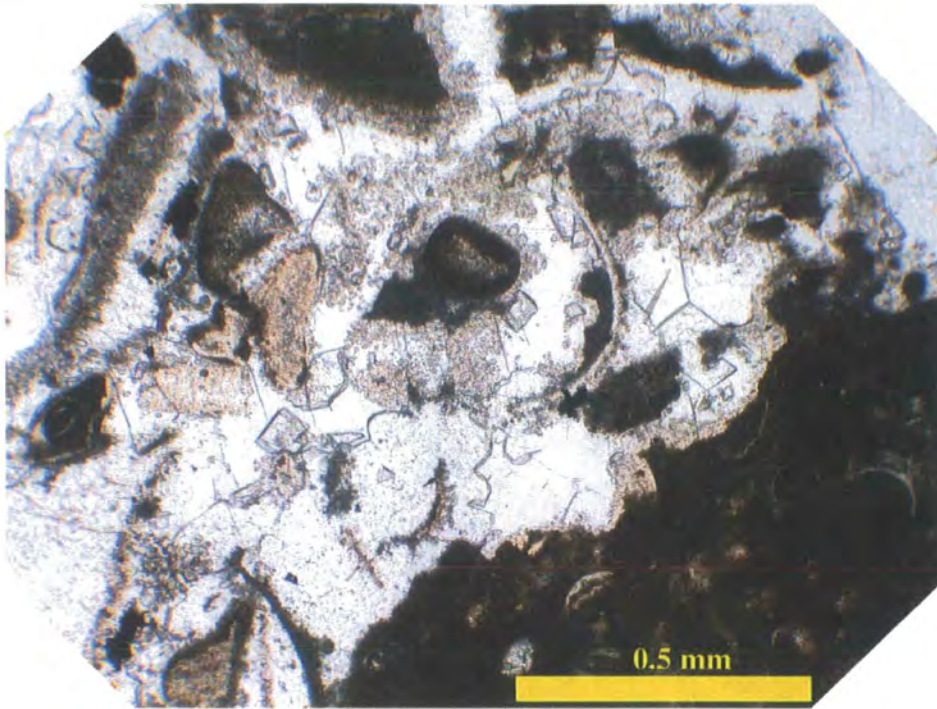


(a)

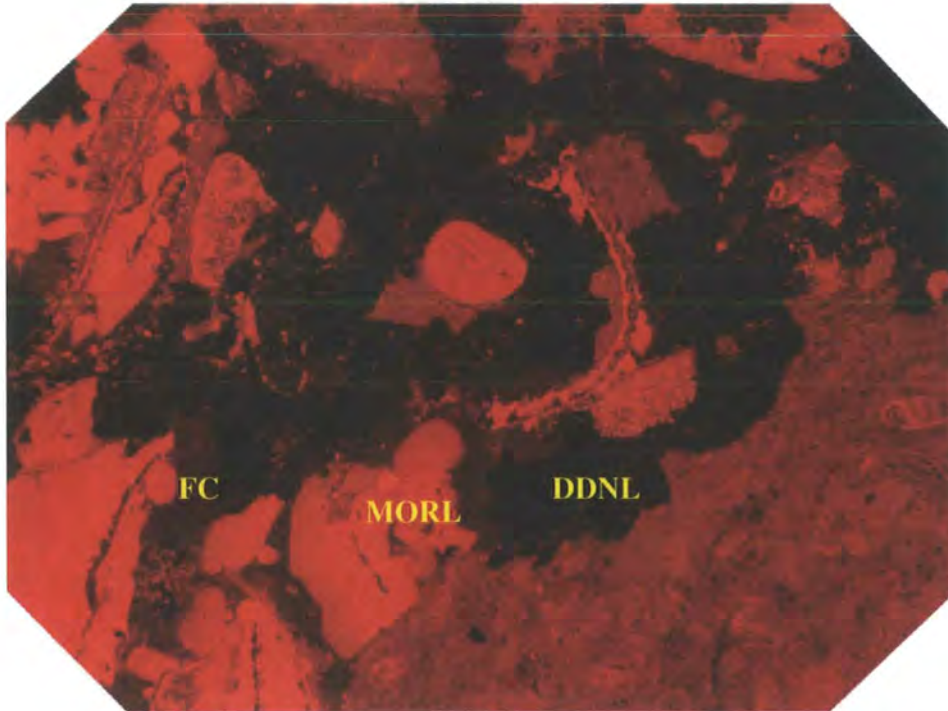


(b)

Figure 5.38. Photomicrographs under normal light (PPL) (a) and CL (b) (a) shows the grainstone texture with the cement fabric of meniscus cement (MC) grain to grain contact and coarse calcite cement filling porosity. Under CL (b), it can be seen that first generation of relatively fine-grained cement (FC) appears cloudy with moderately dull luminescence contrasts with the coarse clear cement with dark / dull luminescence (DDL) filling the pore spaces. Dolomite rhombs (D) show dull non-luminescent. Lidam Formation, 10507 feet, 3V1-59E.

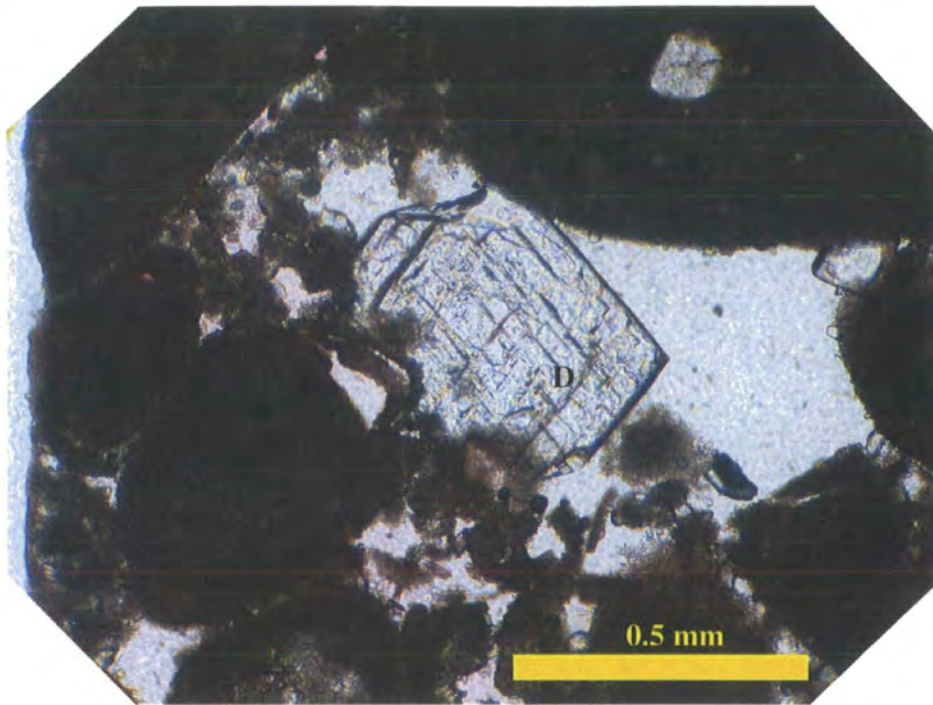


(a)

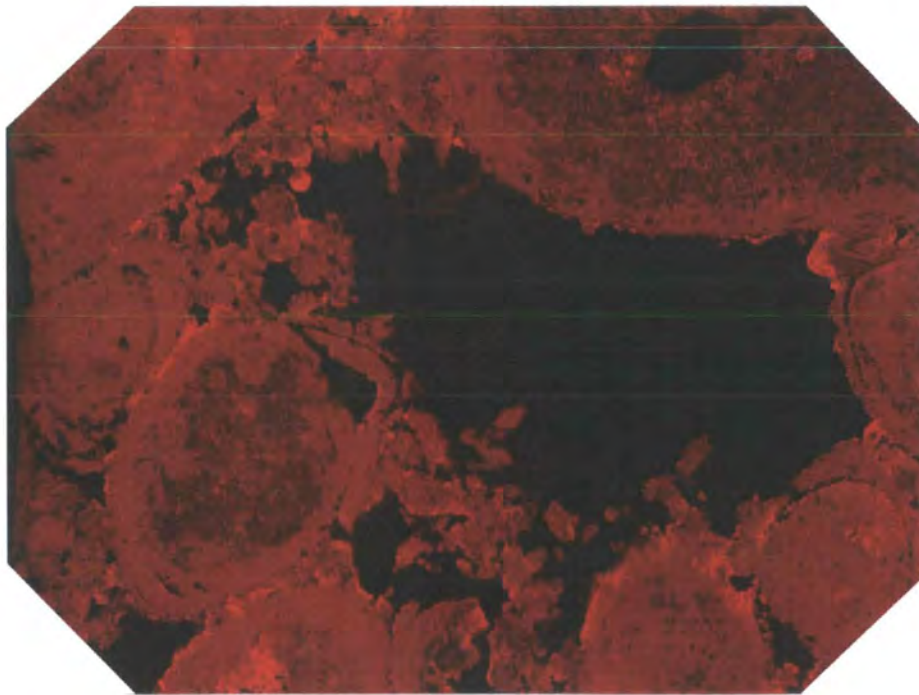


(b)

Figure 5.39. Photomicrographs had taken under normal light (PPL) (a), showing grainstone texture with coarse calcite cement. Under CL (b), it can be seen that there three different stages of cements. These cements are; 1) fine-grained cement and matrix (FC) with cloudy dull luminescent. 2) Moderately orange-red luminescing cement (MORL) and a coarse clear cement dark/dull non-luminescence (DDNL) filling the remaining pore spaces. Lidam Formation, 10507.5 ft, 3V1-59E.

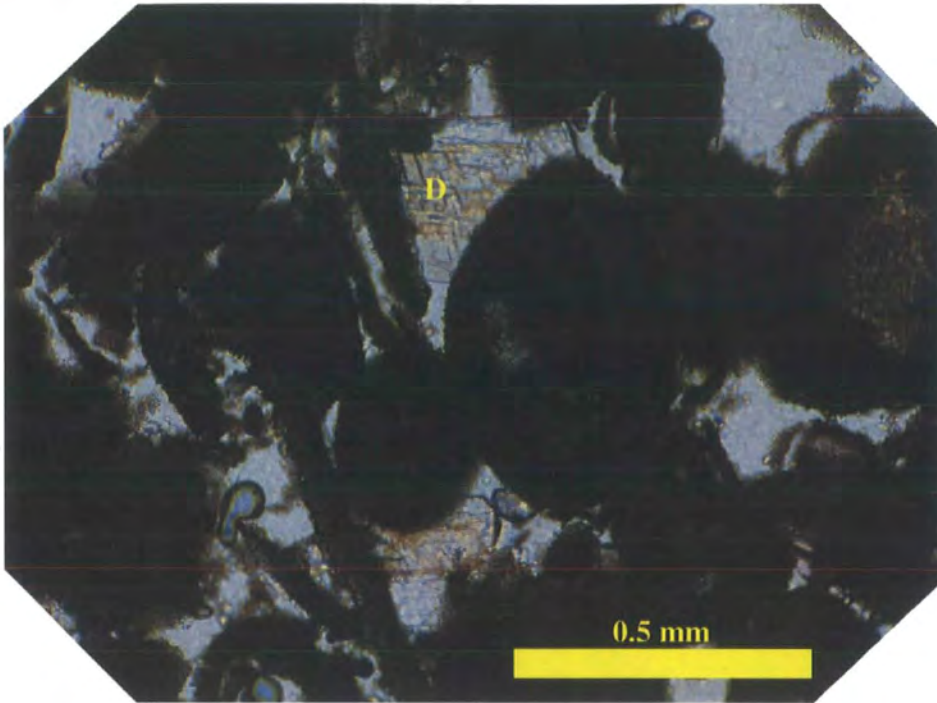


(a)

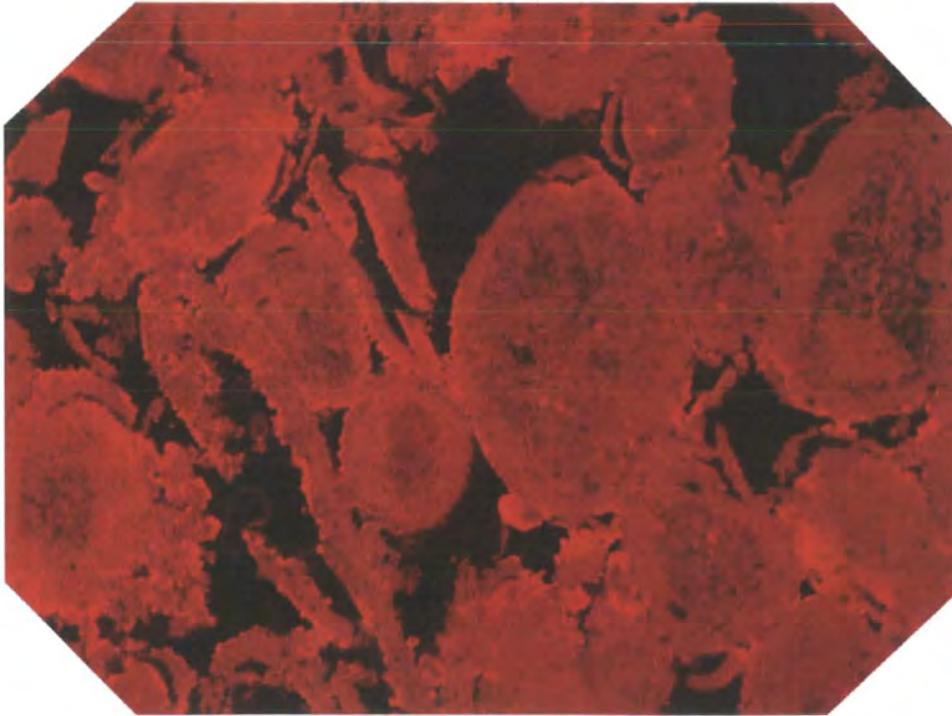


(b)

Figure 5.40. Paired photomicrographs taken under normal light (PPL) (a) and CL (b), shows grainstone with pore space partially filled by a well developed dolomite rhombs crystal (D). Under CL (b), the peloids and associated micrite first is luminesce orange red. The dolomite crystal shows dull to non-luminescence. Lidam Formation, 10211 ft, sample 7, 3V3-59E.

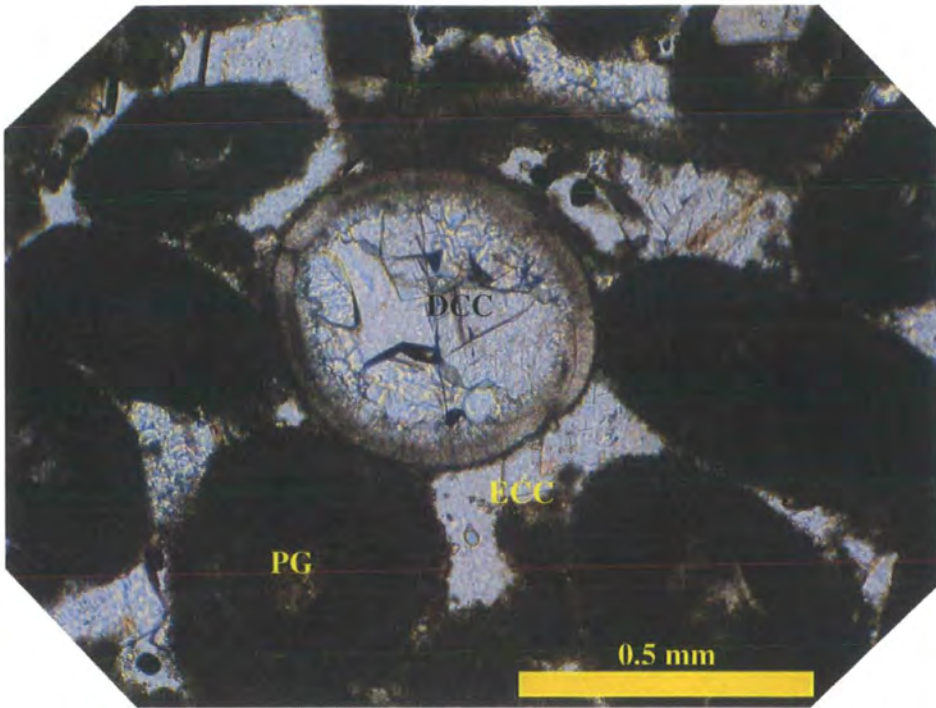


(a)



(b)

Figure 5.41. Photomicrographs taken under normal light (PPL) (a) and CL (b), similar to the previous photomicrograph showing peloidal grainstone with pore space partially filled by dolomite rhombs crystal (D). Under CL (b), peloids shows orange red luminescent with dark / dull non-luminescing filling pore spaces. Dolomite crystal shows orange red and dolomite shows dull to non-luminescence. Lidam Formation, 3V3-59E, sample 7, 10211 feet.

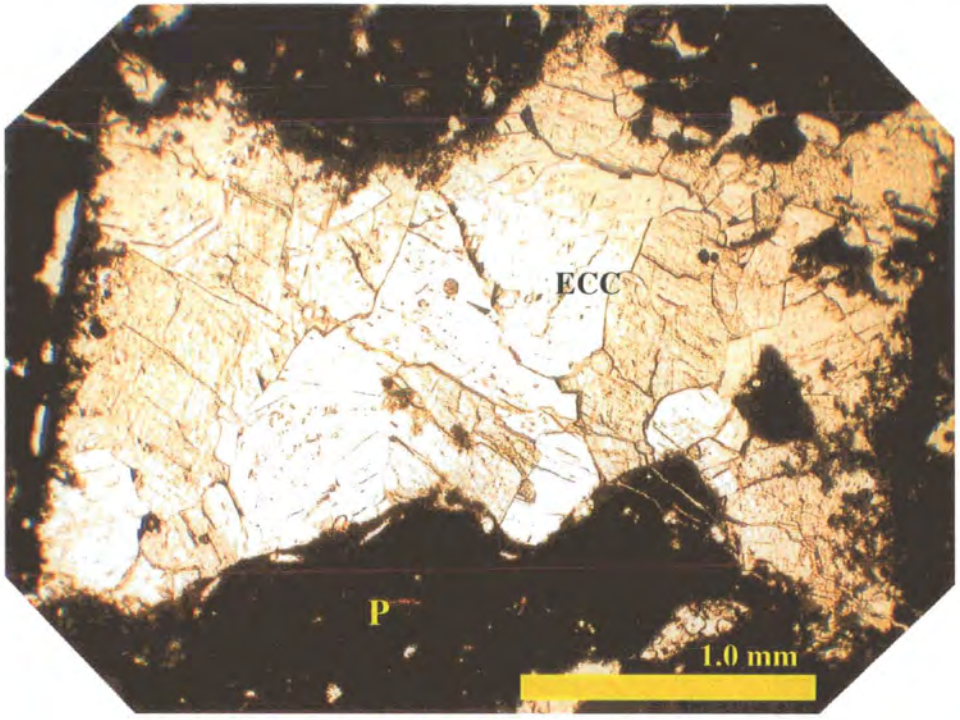


(a)



(b)

Figure 5.42. Photomicrographs taken under normal light (PPL) (a) and CL (b) showing peloidal grainstone (PG) with bioclastic fragment filled by drusy calcite cement (DCC) and later by equant calcite cement (ECC). Under CL (b), peloids shows orange -red luminescent and two generation of cement occurred. Initial bright yellow-red luminescent (BYRL) and later dark non-luminescence (DNL) coarse calcite cement. Lidam Formation. Sample 9, 10215 feet, 3V3-59E.

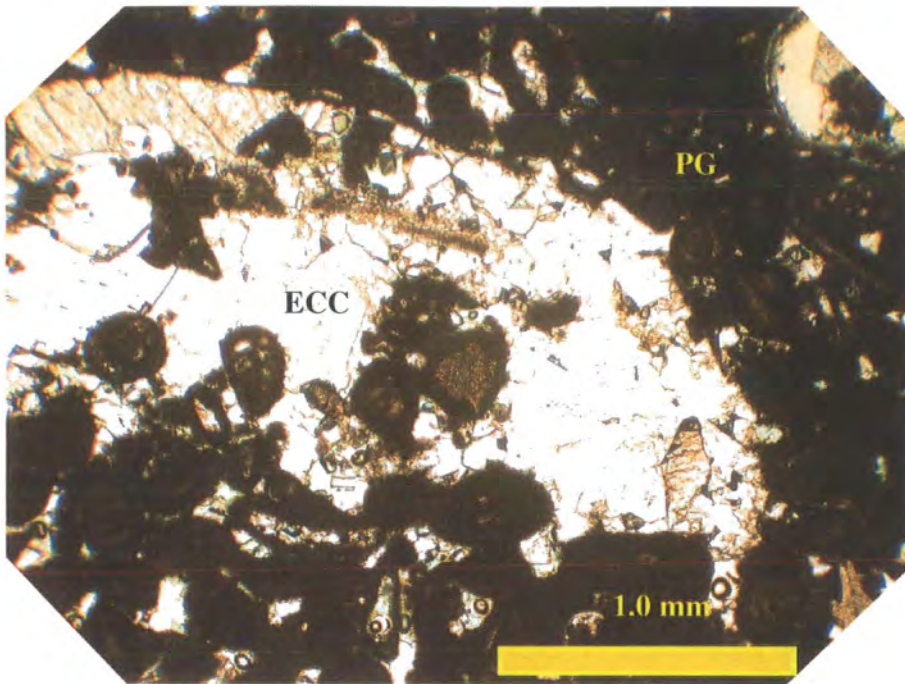


(a)

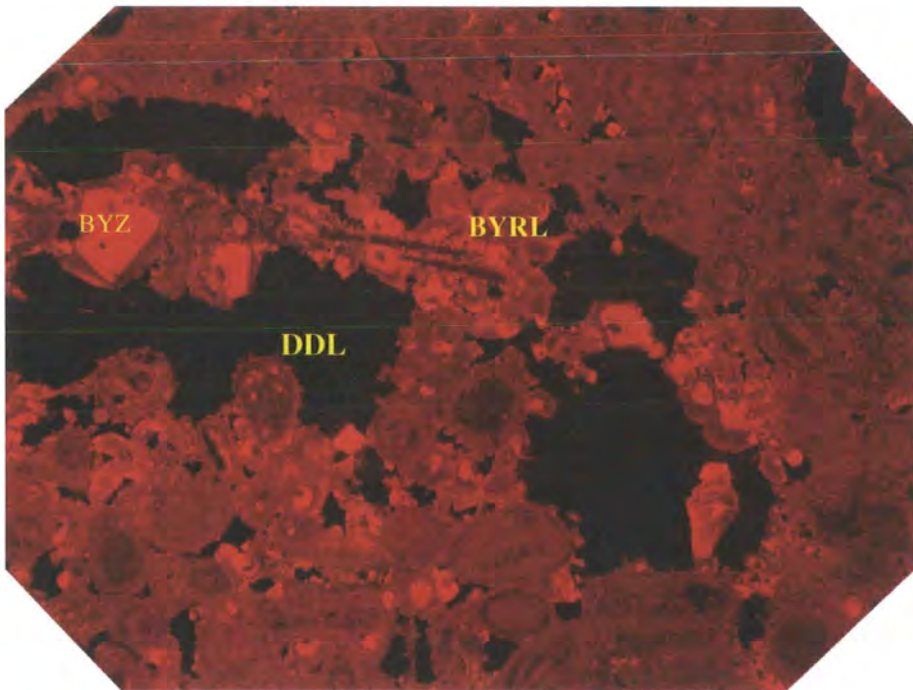


(b)

Figure 5.43. Paired photomicrographs taken under normal light (PLL) (a) and CL (b), showing equant calcite cement (ECC) filled the porosity. Under CL (b), the peloids and associated micrite (P) show orange-red luminescent and one generation of cement of drusy calcite cement, generally has dark dull non- luminescence (DDNL). Lidam Formation, sample 9, 10215 feet, 3V3-59E.

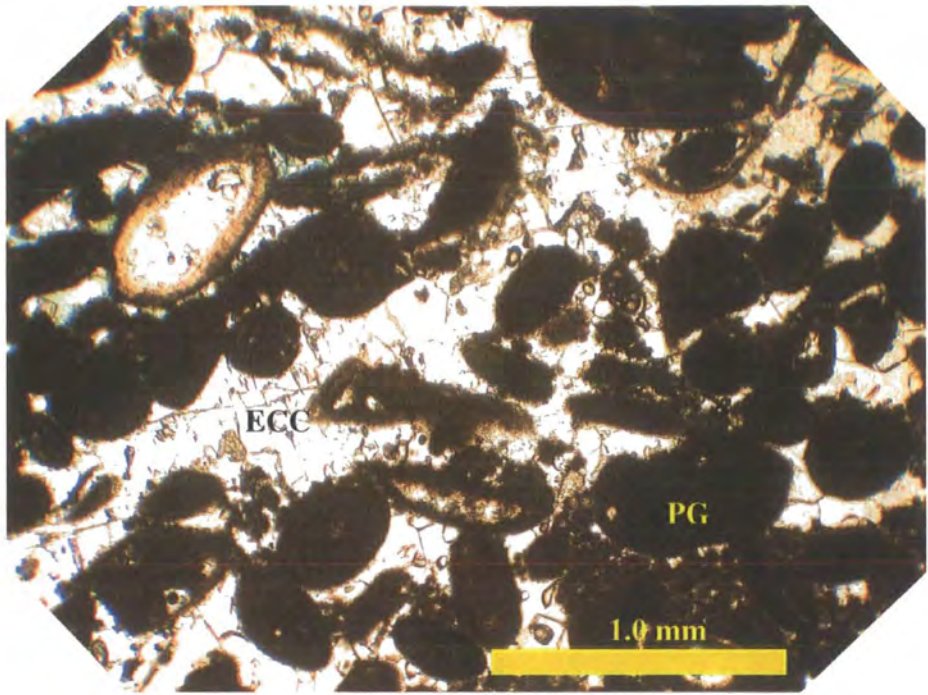


(a)

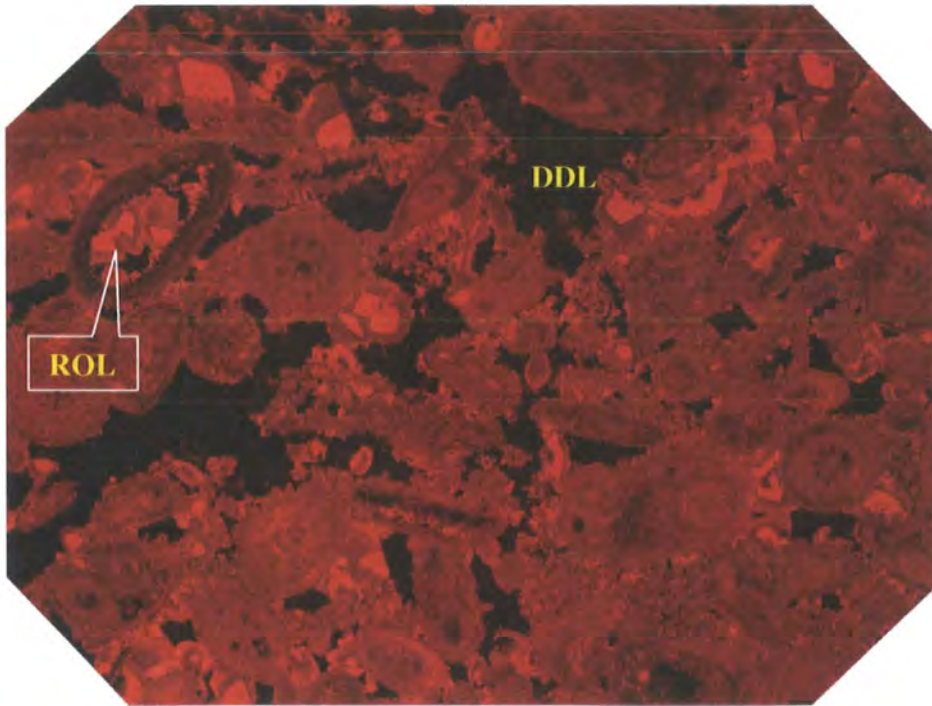


(b)

Figure 5.44. Photomicrographs under normal light (PPL) (a) showing peloidal grainstone (PG) filled by drusy and later by equant calcite cement (ECC). Under CL (b), peloids shows orange-red luminescence and three generations of cement occurred. Well developed initial bright yellow zonation (BYZ), bright yellow red luminescent (BYRL) and later dark dull non-luminescent (DDL) calcite cement filling any remaining porosity. Lidam Formation, sample 10, 11867 ft, N6-97.

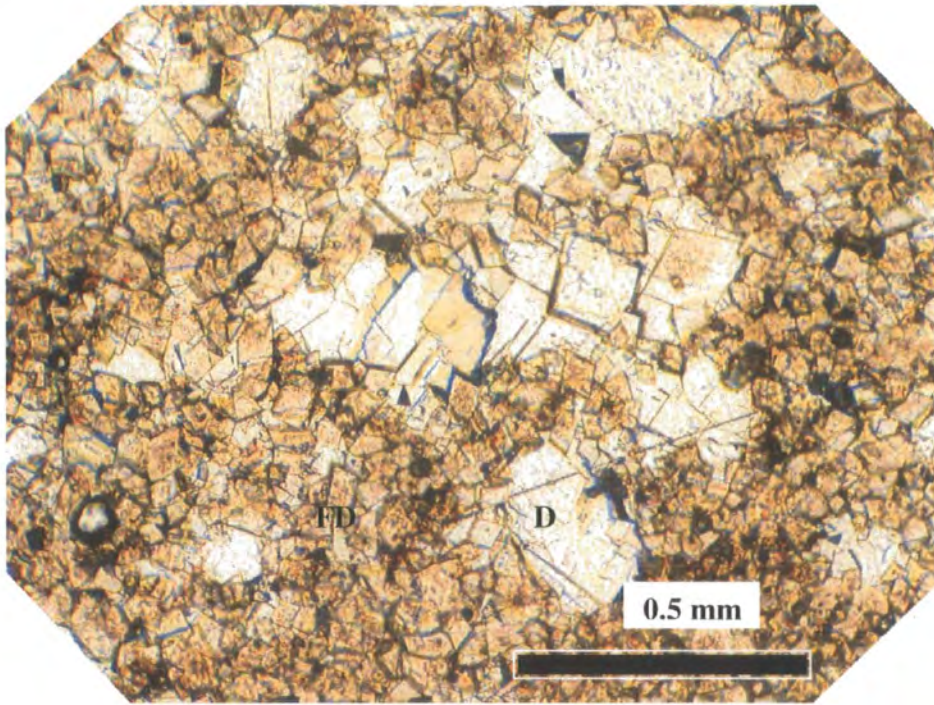


(a)

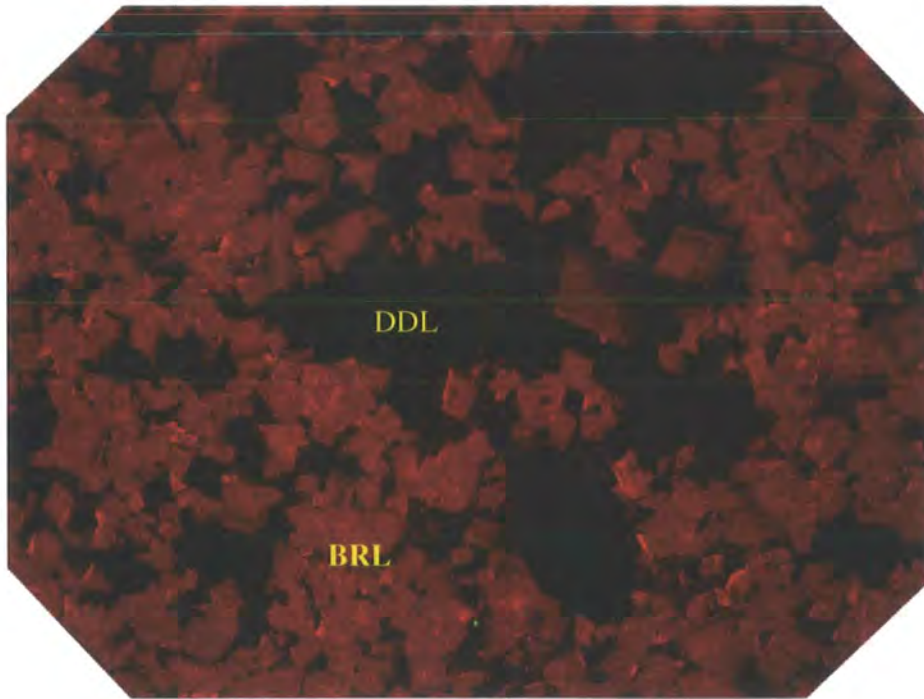


(b)

Figure 5.45. Paired photomicrographs taken under normal light (PPL) (a) showing similar peloidal grainstone (PG) pore filled with equant coarse calcite cement (ECC). Under CL (b), two generations of cement alternating are seen; dull and bright red-orange luminescing zones (ROL) and dark -dull luminescing cement (DDL) fills any remaining pore spaces. Lidam Formation, sample 10, 11867 ft, N6-97.

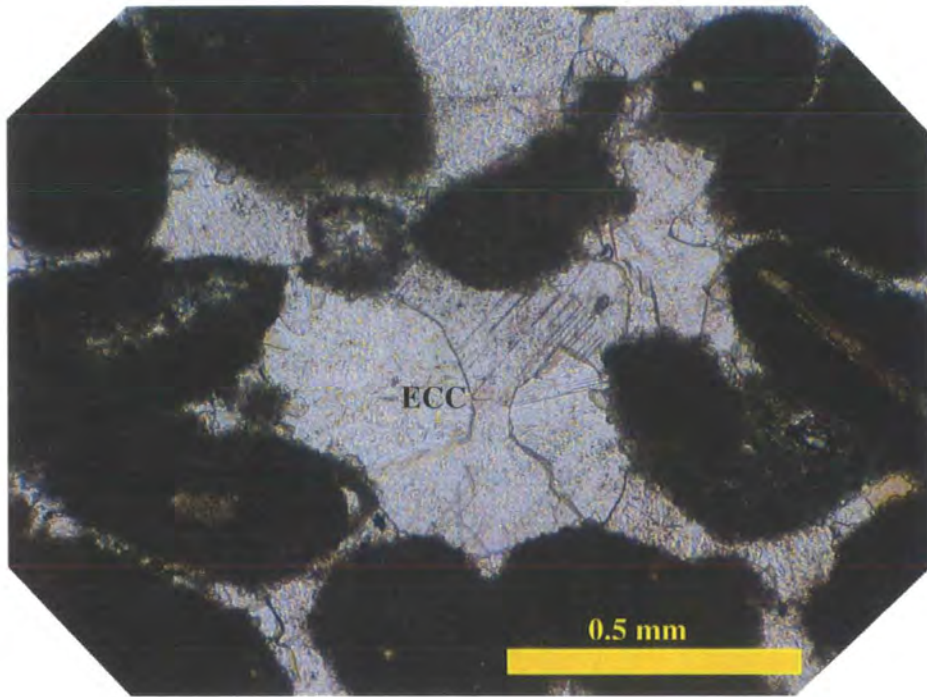


(a)

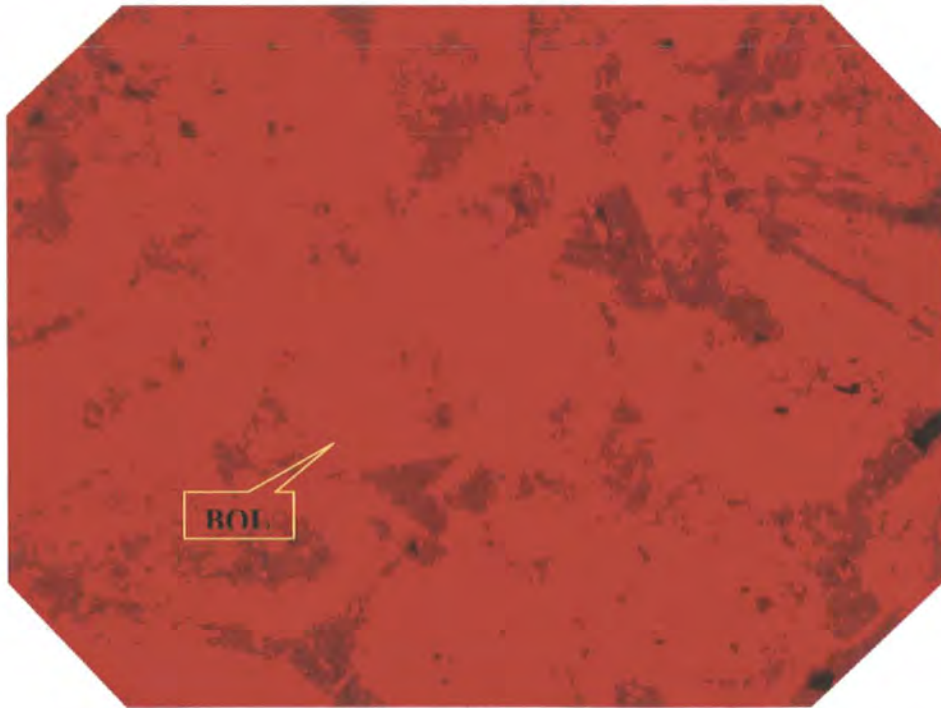


(b)

Figure 5.46. Paired photomicrographs taken under normal light (PPL) (a showing well developed cloudy fine to medium dolomite rhombs (FD) with a vuggy pores filled by later clear dolomite rhombs (D). In the CL view (b), dolomite crystals are bright to red luminescent (BRL) and some dolomite crystals show well developed zonation. The clear dolomite crystals and pore spaces show dark dull-luminescence (DDL). Lidam Formation, sample 4, 11627 ft, P3-97.



(a)



(b)

Figure 5.47. Paired photomicrographs taken under normal light (PLL) (a) showing the intergranular porosity of peloidal packstone / grainstone filled by equest mosaic of calcite cement (ECC). In CL view (b) the coarse calcite cement shows bright-orange luminescent (BOL) with well developed zonation of fine banding luminescence (dull, yellow and orange), particularly in the middle area. Lidam Formation, sample 1, 11004 ft, R1-97.

5.5. STABLE ISOTOPE ANALYSIS AND INTERPRETATION.

5.5.1 Introduction:

Analysis of oxygen and carbon stable isotopes is a geochemical technique used for the interpretation of environmental and diagenetic conditions (Anderson and Arther, 1983; Corfield, 1995). The most abundant isotopes used in nature are oxygen (^{18}O and ^{16}O) and carbon (^{13}C and ^{12}C). Variation in $^{18}\text{O}/^{16}\text{O}$ and $^{13}\text{C}/^{12}\text{C}$ ratio between samples being measured by high-precision mass spectrometry (Fairchild et al. 1988). The abundance of the ^{18}O and ^{13}C in the sample is reported as the per mil (= mg/g or %) difference in delta (δ) notation $\delta^{18}\text{O}$ and $\delta^{13}\text{C}$ between isotope ratios in the sample and those in the international Pee Dee Belemnite (PDB) standard. By definition, PDB has $\delta^{18}\text{O}$ and $\delta^{13}\text{C}$ values of 0% (Hudson, 1977). Increasingly, negative or more dependent values with respect to PDB imply a relative increase in the lighter isotopes ^{18}O and ^{13}C .

The $\delta^{18}\text{O}$ of carbonate precipitated from water depends on the ^{18}O composition and the temperature of the water. Increasingly higher (more negative) values tend to be associated with decreasing salinity and with increasingly higher temperature (Hudson, 1977). The $\delta^{13}\text{C}$ composition of precipitated carbonates primarily reflects the source of bicarbonate dissolved in the waters, which can include sea water ($\delta^{13}\text{C}$ near -10%), bacterial methanogenic fermentation ($\delta^{13}\text{C}$ +15%), oxidation of methane ($\delta^{13}\text{C}$ from -50 to -80%), or biotic reactions associated with thermal cracking and decarboxylation ($\delta^{13}\text{C}$ from -10% to -25%) (Hudson, 1977; Irwin et al .1977; Coleman, 1993; Mozley and Burns, 1993). The $\delta^{18}\text{O}$ and $\delta^{13}\text{C}$ cross-plot was prepared by Hudson, (1977), who distinguished a number of characteristic isotope fields for carbonates having different origins. His diagram has been followed, adapted, and extended by many subsequent workers (Bathurst, 1981; Choquette and James, 1987; Moore, 1989; Morse and Mackenzie, 1990, Figure 5.48)

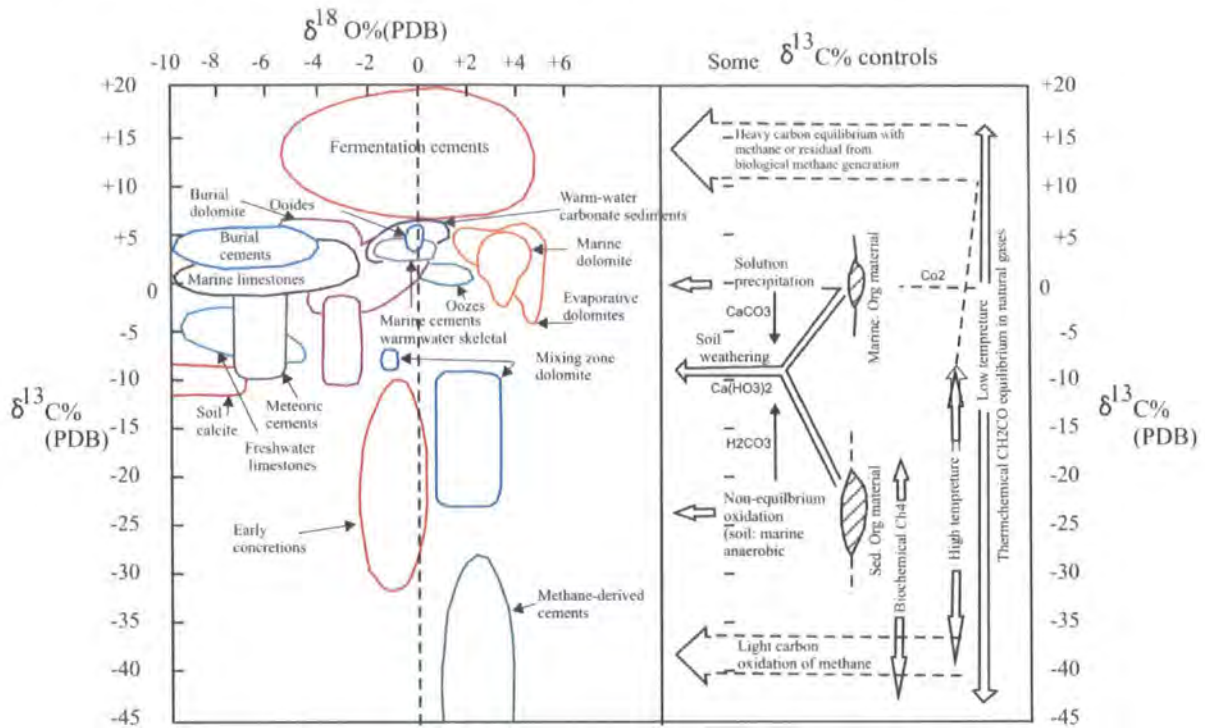


Figure 5.48. Schematic C-O cross plot showing characteristic data fields for cements formed in different diagenetic environments. (Nelson and Smith, 1996)

5.5.2. Isotopic Analysis of the Lidam Formation:

The samples for isotopic analyses were microdrilled from individual components from the Lidam Formation identified from petrographic analysis. 16 duplicate samples were collected from five wells. These include; 4 samples of shell fragments, 4 samples of micrite matrix, 4 samples of different cements (fracture-filling, coarse equant and drusy cement), and 4 samples from different carbonate sediments (stromatolite, peloid /oid, and dolomite). A summary of the isotope values for carbonate grains, matrix and cements are plotted on Table 5.1 and Figure 5.49.

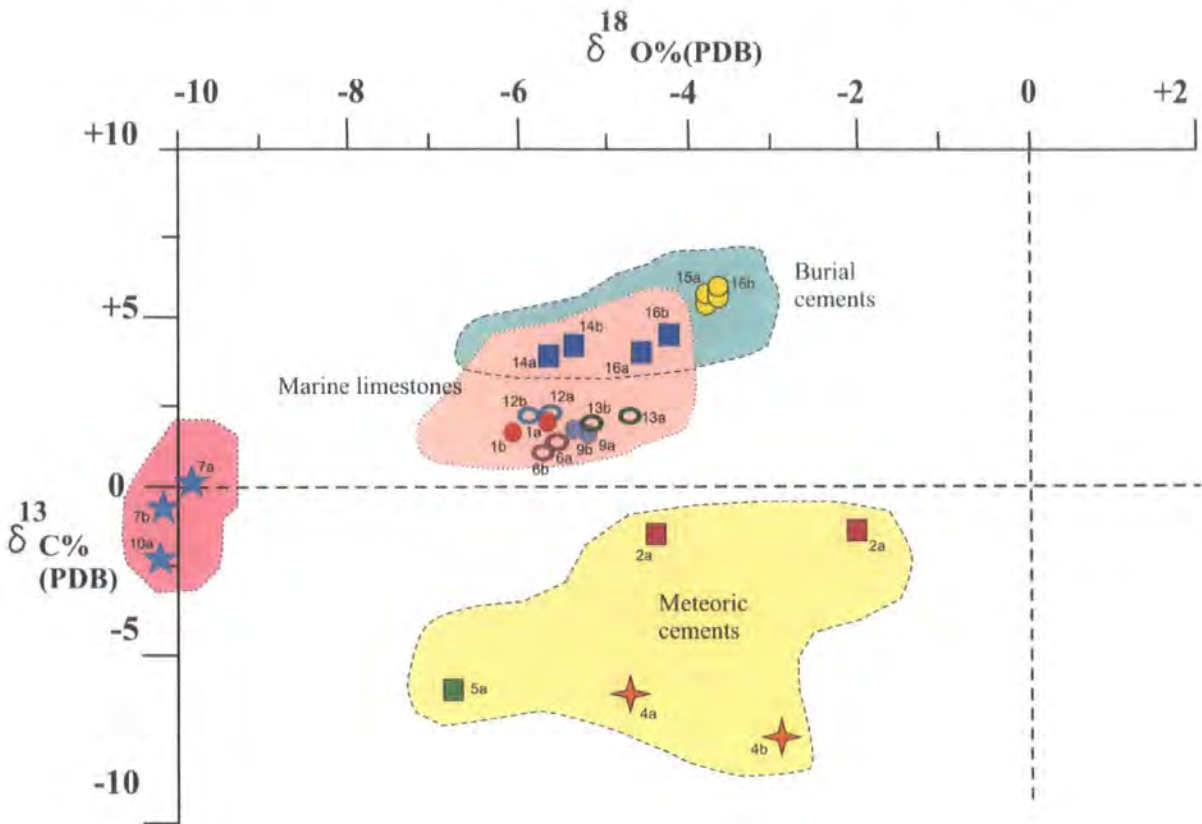
The isotope results of 16 samples from the Lidam Formation reveal that 11 samples show good isotopic values within the range trends. Three samples could not be analyzed probably because they contained anhydrite. Two samples had low yields, again probably due to moderate anhydrite content. With low yields, inaccuracies in the data are more likely (Table 5.1).

Sample No:	Well	Depth (feet)	Facies	Skeleton / Cement type	$\delta^{13}\text{C}\%$ (PDB)	$\delta^{18}\text{O}\%$ (PDB)	Notes
1	3V1-59E	10489.5	Ostracod	Dolomite cement	a. 1.83 b. 1.86	-5.83 -5.65	
2	3V1-59E	10518	Stromatolitic	Micrite (matrix lime mud)	a. -1.48 b. -1.59	-2.10 -4.53	
3	3V1-59E	10542	Stromatolitic	Stromatolite	No analysis		Probably contains anhydrite
4	3V1-59E	10545	Stromatolitic	Stromatolite (micrite)	a. - 6.65 b. -7.14	-4.56 -2.88	
5	3V1-59E	10539	Anhydrite	Micrite (matrix lime mud)	-6.74	-6.66	
6	3V3-59E	10201	Ooidal Peloidal	Shell fragment (gastropod)	a. 1.62 b. 1.41	-5.51 -5.76	
7	3V3-59E	10209	Bioclastic	Fracture cement	a. 0.01 b. - 0.74	- 9.87 -10.59	Low yield, probably contains anhydrite
8	3V3-59E	10211	Ooidal Peloidal	Shell fragment	No analysis		Probably contains anhydrite

Table 5.1 Results of oxygen and carbon isotope analyses of carbonate components from the of Lidam Formation.

Sample No:	Well	Depth (feet)	Facies	Skeleton / Cement type	$\delta^{13}\text{C}\%$ (PDB)	$\delta^{18}\text{O}\%$ (PDB)	Notes
9	3V3-59E	10212	Ooidal Peloidal	Peloid / Ooids	a. 1.67 b. 1.62	-5.23 -5.29	
10	3V3-59E	10238	Bioclastic	Fracture cement	- 2.45	-10.50	Low yield, probably contains anhydrite
11	3V3-59E	10238	Anhydrite	Fracture cement	<u>No analysis</u>		Probably contains anhydrite
12	R1-97	11025.5	Mollusca	Shell fragment	a. 2.11 b. 2.08	-5.67 -5.62	
13	R1-97	11041	Ostracod	Shell fragment	a. 2.20 b. 2.07	-4.61 -5.34	
14	N6-97	11845	Ostracod	Micrite (matrix lime mud)	a. 3.49 b. 3.51	-5.11 -5.51	
15	N6-97	11862	Ooidal Peloidal	Coarse cement (equant)	a. 5.10 b. 5.15	-3.73 -3.78	
16	P3-97	11674	Ostracod	Micrite (matrix lime mud)	a. 3.85 b. 3.90	-4.41 -4.20	

Table 5.1.cont. Results of oxygen and carbon isotope analyses of carbonate component from the Lidam Formation.



Legend:

1. Carbonate skeletons

2. Micrite matrix.

<ul style="list-style-type: none"> ○ Gastropods in peloidal ooidal p/g facies (6a,6b) ○ Mollusc fragment in mollusc facies (12a,12b) ○ Mollusc fragment in ostracod facies (13a,13b) ○ Peloids / ooids in peloidal ooidal p/g facies (9a,9b) ○ Dolomite in ostracod facies(1a,1b) 	<ul style="list-style-type: none"> ■ Micrite in stromatolitic facies (2a, 2b) ■ Micrite in anhydrite facies (5a) ★ Stromatolite in stromatolitic facies (4a, 4b).
<ul style="list-style-type: none"> ★ Fracture cement in bioclastic (9). 	<ul style="list-style-type: none"> ○ Equant calcite in peloidal ooidal p / g (15).

1. Cements.

Figure 5.49. Cross plot of the $\delta^{13}\text{C}$ and $\delta^{18}\text{O}$ isotope results from the Lidam Formation.

The range for normal marine cements in the Late Cretaceous is mostly negative shift in the $\delta^{18}\text{O}$ -values (-2.7 to -6.4‰ PDB) and positive values for $\delta^{13}\text{C}$ between (0.0 to +5.0 PDB). The isotopic results show that most of the Lidam Formation samples have $\delta^{18}\text{O}$ values between -2.10 to -10 ‰ and $\delta^{13}\text{C}$ data between -7.14 to +5.15 ‰ (Table 5.49).

a. Carbonate Skeletons and non-Skeletons.

The carbonate grains analysed were (3) mollusc fragments (including gastropods), (1) from the ostracod, mollusc, peloids/ ooid p/g facies (Table 5.1). One sample (8) from 3V3-

59E did not yield results, probably because it contained anhydrite. The isotopic results show that the two samples (12 and 13) of mollusc fragment from the ostracod and mollusc facies in well R1-97 have negative $\delta^{18}\text{O}$ ‰ values (-4.61 ‰ to -5.67 ‰) and positive $\delta^{13}\text{C}$ ‰ values (+2.08 ‰ to 2.20 ‰). Two samples (6 and 9) from the ooidal peloidal facies in well 3V3-95E have negative $\delta^{18}\text{O}$ ‰ values (-5.23 ‰ to -5.76 ‰) and positive $\delta^{13}\text{C}$ ‰ values (1.41 ‰ to 1.67 ‰) (Table 5.1). Thus, the $\delta^{18}\text{O}$ and $\delta^{13}\text{C}$ values for these components all fall within the field for marine limestones, and this is consistent with their origin (Figure 5.49).

b. Micrite matrix.

Five samples of micrite were analysed from stromatolitic, anhydrite, and ostracod facies in wells 3V1-59E, N6-97, and P3-97 (Table 5.1). Many of the micrite samples showed some aggrading neomorphism to microspar.

The isotope results reveal that two samples (14, 16) of micrite from the ostracod facies from well N6-97 and P3-97 have negative $\delta^{18}\text{O}$ ‰ values (-4.41 ‰ to -5.51 ‰) and positive $\delta^{13}\text{C}$ ‰ values (3.49 ‰ to 3.90 ‰) (Table 5.2). These values plot around the boundary between the typical field for marine limestone and burial cements (Figure 5.49). It is likely that these values reflect marine origins to burial cements and this is reflected in their isotopically positive content of $\delta^{13}\text{C}$ and negative values of $\delta^{18}\text{O}$ (Figure 5.49). This is consistent with a marine origin, perhaps with some later burial overprint (Figure 5.49).

Three samples (2, 4, and 5) of micrite from anhydrite and stromatolitic facies in well 3V1-59E have distinctively negative values of $\delta^{13}\text{C}$ ‰ from -1.48‰ to -7.14 ‰ and $\delta^{18}\text{O}$ ‰ values from -2.88 to -6.66 ‰ (Table 5.2). It is likely that these negative $\delta^{18}\text{O}$ ‰ values reflect a meteoric influence either during or after deposition, and this is consistent with the inferred sedimentary origin of these facies (see section 3.3)

c. Carbonate Cement.

Six samples for isotopic analysis were microdrilled from cements and dolomites (Table 5.1). A dolomite sample (1) from an ostracod ooidal peloidal facies in well 3V1-59E has positive values of $\delta^{13}\text{C}$ ‰ between +1.83 ‰ to +1.86 ‰ and negative $\delta^{18}\text{O}$ ‰ values between -5.65 to -5.83 ‰. This value falls within the field for marine limestones, but close to the field typical of burial dolomites. Earlier it was noted (section 5.3) that many of the dolomites have a dusty appearance, indicative of replacement. During replacement the

dolomite may retain the signature of earlier marine limestone. Alternatively the dolomites may have formed under burial conditions, given the proximity to the burial dolomite field.

An equant calcite cement from ooidal peloidal facies in well N6-97 has positive $\delta^{13}\text{C}$ values (+5.10 ‰ to + 5.15 ‰ PDB) and negative $\delta^{18}\text{O}$ (-3.73 to -3.78 ‰ PDB). The oxygen and carbon isotope values together with the cement morphology reflect that cement was precipitated under burial conditions.

Two samples (7 and 10) from fracture filling cements with equant morphology cement of the bioclastic facies in well 3V3-59E although having low yields, have $\delta^{13}\text{C}$ of 0.01 to 2.45 ‰ and $\delta^{18}\text{O}$ values of -10.50 to 10.59 ‰ (Figure 5.49). The increasing depletion in oxygen suggests that these cements were precipitated under conditions of increasing temperature under burial conditions. Increasingly $\delta^{18}\text{O}$ values (more negative) tend to be associated with decreasing salinity and with increasingly higher temperature (Hudson, 1977). Two samples of coarse (11 and 3) fracture filling cement in anhydrite facies did not yield results and probably contained anhydrite cement (Table 5.1).

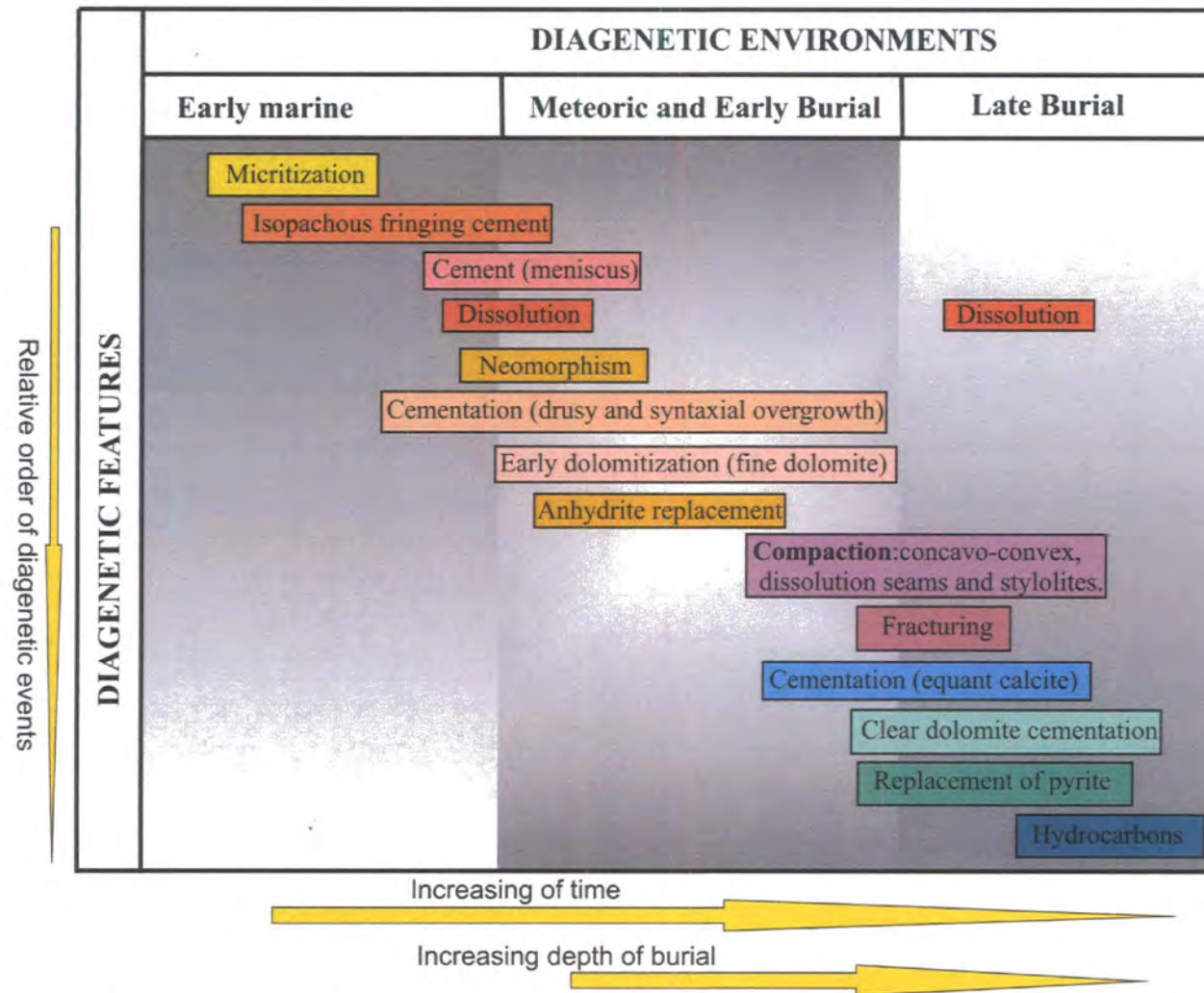


Figure 5.50. Paragenetic diagram showing the relative timing of different diagenetic events and their diagenetic environments in the Lidam Formation in SE Sirt Basin, Libya.

5.6 DISCUSSION OF RELATIVE TIMING AND PROCESSES OF DIAGENESIS.

In the previous pages, post depositional changes in the mineralogy and fabric of the Lidam Formation have been described and their diagenetic environments inferred. The inferred paragenetic sequence for the carbonate facies of the Lidam Formation in the studied wells 3V1- 59E, 3V3-59E, R1-97, P3-97, and N6-97 are shown in figure 5.50. This plot shows the diagenetic processes and their generalized relative timing. However, not all diagenetic features are seen in all facies and in some cases it was difficult to judge the relative timing of some processes, due to the great variation and complexity of the facies.

The diagenetic sequence initiated with *micritization* of the sediments which affected the original fabric of the skeletal grains. The *isopachous rim cement* is an early cement and characteristic of deposition from marine waters or from connate waters fairly deep in the subsurface. In this case, because it predates micritization a marine origin is inferred. Development of micrite envelopes around skeletal fragments must have been an early diagenetic event. *Dissolution* of the aragonite grains and bioclasts has created vuggy and moldic porosity, which are commonly partially or completely filled by drusy calcite cementation. Fine dolomitization of the matrix may have started early in the mixed phreatic environment.

Recrystallization of the lime mud matrix probably occurred either with or after the inversion of aragonite to calcite. The drusy calcite and anhydrite occur as cements, partially or completely filling intergranular, mouldic and vuggy porosity. Mechanical compaction resulted in mechanical breakage of bioclasts and chemical compaction (concavo-convex, grain contacts, dissolution seams and stylolites). These compaction processes began slightly after formation of the early stage cementation and continued as depth increased during burial.

Fracturing took place after the compaction processes, with at least some of the micro fracture developing after the stylolites. The third stage of cementation is an equant ferroan calcite filling pore spaces and precipitated along fractures.

Dolomitization took place over a long period of time and occurred as early and later cement filling any remaining porosity. Three types of diagenetic dolomite were identified in the Lidam Formation during this study on the bases of textural changes, internal structure and crystal shape (Table 5.2). These are: Type 1, Dusty (blurry) dolomite crystals, Type 2; Clear dolomite crystals and Type 3; coarse zoned dolomite crystals. Of these:

1- Dusty (Blurry) dolomite crystal (type 1): These types of dolomite are recognized within the middle part and the uppermost part of Lidam Formation, particularly in the bioclastic and mollusca facies. These dolomites are dark grey and closely packed anhedral crystals with mostly planar or irregular intercrystalline boundaries. They are fine crystalline dolomite and large spaces are filled with ferroan dolomite crystals. The crystals become dusty (blurry) from the centre outwards (Table 5.2). The limestones remained partially undolomitized during dolomitization and traces of micrite remain giving the dusty appearance. The clear rims to the dolomite are later dolomite cement. According to Gregg and Sibley (1984), mosaics with planer crystal boundaries (idiotopic) indicate growth temperature below 50°C, while those with non planer boundaries (xenotopic) results from elevated temperature greater than 50°C. Both can form as cement, or by replacement of limestone, or by neomorphic recrystallization of precursor dolomite. Moore et al, (1988), suggest dolomitization affects muddy matrix, as well as the introduction of fresh water into the environment, perhaps after dolomitization. The dusty dolomite is usually replacive dolomite reflecting dolomitization taking place during early diagenesis and these dolomites predate compaction features.

2- Clear dolomite crystal (type 2): these are mostly clear and form a dolosparitic mosaic, of very fine to fine non-ferroan dolomite crystals with a euhedral to subhedral shape. They have a character similar to the limpid dolomite crystal type defined by Folk and Land (1975). Interlocking is poorly-developed in the crystals, resulted in high intercrystalline porosity. These types of dolomite are best seen in the dolomitized mudstone and bioclastic facies at the base of the Lidam Formation (Table 5.2). These dolomites occurred during the early diagenetic stage and form concurrently with the deposition or immediately after process and reflect the conditions of environment in which they occur. These dolomites are possibly formed in areas that become shallower during sea level fluctuations (probably short lived lowering and rising of sea level). The dolomite-rich facies appears to have mainly affected original mud-dominated sediments characteristic of the supratidal sabkhas and adjacent subtidal marine-to-lagoonal environments. Bakai (2001) pointed that may have formed from evaporative sea water in a near-surface environment. Planar dolomite develops when crystals undergo faceted growth and is characteristic of dolomite crystals formed early during diagenesis and under certain conditions, at temperatures of <60°C (Warren, 2000)

3-Coarse zoned dolomite crystals (type3): This type of dolomite has been recognized within the middle part facies of the Lidam Formation and the upper most part of the cored section of the Lidam Formation in well 3V3-59E particularly in the bioclastic foraminifera packstone facies and mollusc facies. These are clear, rhomb-shaped cements. They are fine to medium (30-100 μ m) and the crystal boundaries are regular to irregular. These coarse dolomite cements infill earlier vuggy or mouldic porosity (Table 5.2). Under Cathodoluminescence and SEM crystals often display internal zonation due to varying iron and manganese content (see section 5.4). Warren, 2000 pointed that the dolomite is useful geothermometer, indicating minimum burial temperatures of 60°C to 150°C and typically related to the through flow of high-temperature hypersaline basinal brines. Land et al. (1975) documented trace element differences between cloudy centres and clear rims. The clear coarse zoned dolomite crystals probably developed at the late diagenetic stage during burial conditions. The isotopic analysis shows that the negative $\delta^{18}\text{O}$ values tend to be depleted indicating precipitation at elevated temperature (see section 5.3). This value is typical of burial dolomites.

Mosaics of anhedral to subhedral dolomite crystals apparently represent the final product of dolomitization and a pervasive coarse-grained overprint can destroy any original depositional fabrics. Typically, some of crystals in these mosaics retain cloudy cores and clear rims. The generation of dolomite mosaics indicates a lengthy diagenetic history often involving fracture and rehealing of crystals as well as overgrowths and replacements reflected in internal dissolution surfaces (Warren, 2000). Generally the type 1 and 2 dolomites are similar to those of the massive sequence of the Cretaceous Edward formation of Texas, described by Fisher and Rodda (1969). They concluded that this dolomitization may have taken place by the seepage-reflux mechanism associated with evaporites and type 3 may form under the burial conditions during the late stage of diagenesis. Only preliminary observations on dolomitization of the Lidam Formation are presented here. Further detailed work (beyond the scope of this project) would be required to learn more about their origins.

Pyrite may replace skeletal grains and minor pyrite precipitation possibly occurred late in the diagenetic sequence and certainly after dolomite precipitation of which pyrite replaces. Finally the accumulation of *hydrocarbons* is the latest stage in the diagenesis during which hydrocarbons migrated into effective porosity following generation of oil from the source rocks.

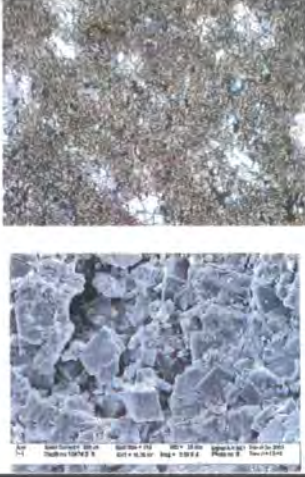
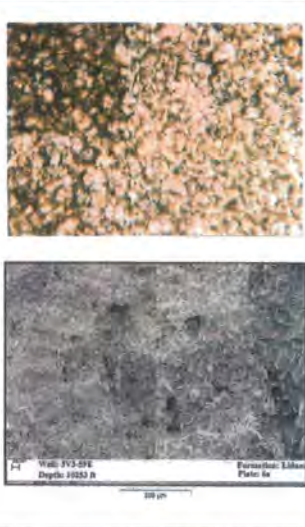
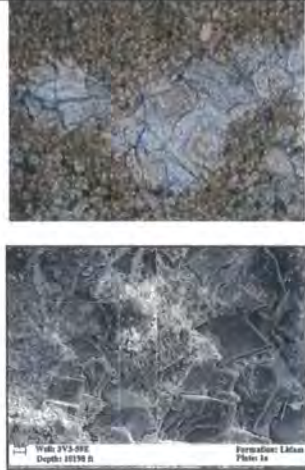
Type of dolomite	photomicrograph	Characteristics and fabrics of dolomite
<p>Dusty (Blurry) dolomite crystal (type 1)</p>		<p>These types are recognized within the middle part and the uppermost part of Lidam Formation, particularly in the bioclastic and mollusca facies. These are dark grey, subhedral and anhedral. They are fine to medium crystalline dolomite and large spaces are filled with ferroan dolomite crystals. The crystals become dusty (blurry) from the centre outward. This 'dustiness' is caused by relicts of the undolomitized lime mud.</p>
<p>Clear dolomite crystal (type 2)</p>		<p>These type of dolomite occurred in the dolomitized mudstone and bioclastic facies at the base of the Lidam Formation. These mostly light coloured and form a dolosparitic mosaic. Non-ferroan dolomite crystals are very fine to fine, euhedral and subhedral. Crystal boundaries are well-developed with good intercrystalline porosity. <i>Partially dolomitized</i>, very fine to fine crystalline of non-ferroan dolomites, localized intervals is present in the upper part of the Lidam Formation. these dolomite are scattered throughout the bioclastic and ostracod facies, selectively replace the matrix and also related to stylolites and pressure solution seams</p>
<p>Coarse zoned dolomite crystals (type3)</p>		<p>These types of dolomite occur in most of the bioclastic facies. Theses dolomites are light grey and light colored euhedral with fresh center. They are fine to medium (30-100µm) and crystal boundaries are regular and locally present as pore filling cement in intragranular, mould and vuggy. The photo and SEM image shows increasing growth tendency of the crystal inward into hollows</p>

Table.5.2. Showing different dolomite types occurred during diagenetic process of the Lidam Formation.

5.7. RESERVOIR QUALITY OF THE LIDAM FORMATION.

Porosity and permeability measurements have been obtained from analysis of the cored sections of the studied wells in the laboratories of Libyan Petroleum Institute (LPI). Primary intergranular and intragranular together with vuggy and mouldic types are the most common porosity in the Lidam Formation. The porosity is related to variations in the microfacies, depositional environments, and diagenetic processes.

5.7.1. Porosity and Permeability Variation and Relationship with Facies.

In the most of the studied wells, good intergranular porosity occurred in the uppermost part of the cored sections of the Lidam Formation compared with the lowest part. The good porosity is restricted to the ooidal peloidal packstone / grainstone facies and decreases in the bioclastic foraminifera, stromatolitic packstone, and anhydrite facies.

Well No:	Porosity (%)	Permeability (mD)
3V1-59E	6.2 - 16.0	0.01 - 1.51
3V3-59E	0.57 - 21.73	0.140 - 257.5
R1-97	0.2 - 17.98	0.07 - 28.70
N6-97	0.60 - 11.12	0.051 - 0.222
P3-97	0.970 - 25.04	0.0233 - 83.895

Table 5.3 Showing the average porosity and permeability in the studied wells.

The porosity of the Lidam Formation in the drilled wells ranges from 0.2 % to 25.0 % and includes both fabric and non-fabric selective types and permeability varies from high to low (0.01 to 257.5 mD). The lowest porosity values in the studied wells have been observed in the shallow intertidal low energy lagoonal environments; bioclastic, and ostracod packstone facies (0.24% - 10.54 %) compared with the highest porosity values in the ooidal peloidal packstone/ grainstone facies (16%). The permeability is moderate in the ooidal peloidal packstone/ grainstone compared with the bioclastic and ostracod wackestone facies (1.44md to 257.5 md). These values decrease in the supratidal and restricted lagoonal facies in the middle and lower part of the Lidam Formation

Drusy and syntaxial overgrowth calcite cementation has a great influence reducing porosity, but these early cements also help maintain remaining porosity through resisting compaction.

Generally, the diagenesis had a great influence on the rocks comprising the Lidam Formation from the time of sediments were deposited up to final lithification. Calcite cementation, late dolomitization, and compaction are the major factors controlling the reduction of the porosity in the Lidam Formation whilst the dissolution during meteoric diagenesis and fracturing has a great influence on increasing porosity and permeability and enhancing the reservoir quality of the Lidam Formation. The best reservoir quality is in the higher energy packstones/grainstones which retain some primary porosity and have also been affected by meteoric leaching resulting in additional secondary porosity development.

5.7.2. Hydrocarbon Emplacement.

The accumulation of hydrocarbons is the latest stage of diagenesis. The best reservoir intervals are observed in peloidal ooidal packstone / grainstone facies throughout the studied wells, particularly in well 3V3-59E, 3V1-59E, R1-97, and N6-97 (see section 4.3). Most of the oil accumulated between the preserved intergranular and intragranular porosity of high energy subtidal, oolitic shoal deposits. Both increasing temperature and pressure during burial triggers a series of phase changes that results in hydrocarbon maturation and the generation of oil and gas from the organic material. Porosity enhancement related to hydrocarbon maturation seems to take place just prior to the arrival of hydrocarbons in the reservoir and was seen in the dissolution of ooidal and peloidal facies(Figure 5.51).



Figure 5.51. Photomicrograph showing oil accumulation in intergranular and intragranular porosity. 10507 ft, 3VI-59E, PPL

5.8. COMPARISON OF DIAGENESIS AND RESERVIOR QUALITY WITH OTHER CRETACEOUS FORMATIONS.

Although Cenomanian carbonate deposits of the Lidam Formation are similar to the shallow marine shelf deposit of west central Jordan (see chapter 4), there are no detailed diagenetic studies of the Jordanian deposits. A literature search did not reveal diagenetic evaluations of comparable Cretaceous carbonate formations. The Jurassic Smackover Formation shows similar depositional features to parts of the Cretaceous Lidam Formation and is a prolific hydrocarbon reservoir. A brief diagenetic and reservoir comparison of the Lidam and Smackover Formations is therefore discussed below

Seven lithofacies were recognized in the Smackover Formation (Heydari and Baria, 2005). These lithofacies are (from base to top): (1) a laminated peloid wackestone (mid-ramp), (2) a bioturbated peloid packstone (mid ramp), (3) a microbial bindstone (inner ramp); (4) a laminated peloid wackestone/ packstone (inner ramp); a bioturbated peloid

packstone (lagoonal); and (6) a peloid ooid grainstone (beach). These are overlain by a mixed regime of red lime mudstone, green shale, and sandstone (lithofacies 7).

Characteristics of these lithofacies indicate deposition in a ramp environment. The stacking pattern of the Smackover consists of one shoaling-upward cycle that formed by southward progradation following rapid transgression of the Smackover. Out of the seven lithofacies of the Smackover Formation two form excellent reservoirs; these are the microbial bindstone and peloid-ooid grainstone. The two reservoirs units are separated from one another by a non-porous and impermeable horizon.

The porosity of the microbial bindstone ranges from 2 to 30%. Dominant porosity types are framework and intergranular. The dominant process which resulted in preservation of porosity was marine diagenesis including microbial binding and cementation (Ezat et al. 2005).

The upper reservoir of the Smackover consists of a cross-laminated peloid and ooid grainstone with the dominant porosity types of intergranular, moldic, vuggy and intercrystalline. The process which resulted in the reservoir formation was meteoric in nature causing dissolution of original aragonitic grains. Ezat (2005) concluded that the modification of porosity was a burial process and was directly related to the intensity of chemical compaction, which was controlled by three factors: degree of early cementation, grain type, and grain size.

The reservoir unit and development of the Smackover Formation shows similarities to that of the Lidam Formation. Early-cemented intervals have low to moderate compaction regardless of grain size or grain type. In the absence of early cementation, grain type and grain size were the dominant factors of porosity control. Coarse-grained intervals that were composed of micritic grains experienced less compaction than fine-grained, oolitic intervals. Out of an original porosity of 40%, 13 porosity units were lost by cementation, and 27 porosity units were reduced by compaction (mechanical and chemical).

5.9. CHAPTER SUMMARY

In this chapter detailed petrographic analysis was made on 70 thin, seven (7) polished thin sections were chosen for CL microscopic analysis, 16 for isotopic analysis and 6 for SEM in selected wells 3V1 and 3V3-59E. The paragenesis of events recognized in the Lidam Formation sediments are grouped into early, middle, and late stages. The early stage consists of micritization and early marine cementation (isopachous rim cement). During the middle stage, carbonate dissolution (particularly of aragonite and micritic calcite), calcite cementation (drusy calcite cements and syntaxial overgrowths), and evaporite crystals (nodules and cements) occurred during meteoric diagenesis or sub-aerial phase. The last diagenetic stage is the burial phase, and this included equant calcite cementation, late dolomitization, compaction (pressure solution and stylolites), fracturing, and hydrocarbon emplacement.

Cathodoluminescent (CL) analysis indicates three different phases of cementation. These cement stages are; non-luminescent, non-luminescent with bright bands of red-orange zones and dark dull non-luminescence. They most likely reflect changes in the oxidising conditions of the diagenetic fluids and are inferred to be related to marine, meteoric and meteoric phreatic to burial environments respectively. Two types of dolomite diagenetic phases are recognized. The red-orange luminescence zones probably reflect oxic conditions in the phreatic zone and non-luminescent dolomite crystals probably reflects sub-oxic and anoxic reducing conditions during deep phreatic and deep burial depths.

The isotopic analyses were microdrilled from the component Cretaceous Lidam Formation and were performed on sixteen (16) duplicate samples collected from five wells from different facies. Isotopic results of the Lidam Formation samples have $\delta^{18}\text{O}$ values between -2.10 to -10 ‰ and $\delta^{13}\text{C}$ data between -7.14 to +5.15 ‰. The skeletal grains samples have negative $\delta^{18}\text{O}$ values ranging from -4.61 ‰ to -5.67 ‰ PDB, and positive $\delta^{13}\text{C}$ values range from +1.41 ‰ to +2.11 ‰ PDB. These components all fall within the field for marine limestones, and this is consistent with their origin. Micrite in anhydrite and stromatolitic facies have negative $\delta^{18}\text{O}$ values ranging from -2.10 ‰ to -6.66 ‰ PDB and negative $\delta^{13}\text{C}$ values ranging from -1.48 ‰ to -6.74 ‰ PDB. These values reflect a meteoric influence either during or after deposition and marine burial cements. Cements filling fractures have negative $\delta^{18}\text{O}$ values ranging from -3.73 ‰ to -5.65 ‰ PDB and positive $\delta^{13}\text{C}$

C values range from +1.83 % to +5.15 % PDB. These cements were precipitated under conditions of increasing temperature under burial conditions

Most of the porosity types in the Lidam Formation are related to the variation of the microfacies, depositional environments, and diagenetic processes. Good porosity is restricted to the ooidal peloidal packstone / grainstone facies and decreases in the bioclastic foraminifera, stromatolitic packstone, and anhydrite facies. Best porosity was seen in units retaining some primary porosity and with additional secondary leaching.

A brief diagenetic and reservoir comparison of the Lidam with the Smackover Formation is discussed. The Jurassic Smackover Formation shows similar depositional features to parts of the Cretaceous Lidam Formation hydrocarbon reservoir. The dominant process which resulted in the preservation of porosity was marine diagenesis including microbial binding and cementation. The porosity units were reduced by cementation and compaction (mechanical and chemical).

CHAPTER SIX

CONCLUSIONS

CHAPTER SIX

6. CONCLUSIONS

Chapter 6

6. CONCLUSIONS

The Lidam Formation has been studied in five wells three are located in Gialo Platform (3V1-59E, 3V3-59E and R1-97) and two wells located in the Hameimat trough (P3-97 and N6-97), SE Sirt Basin, Libya. Core, petrographic and geochemical study help provide a better understanding of the sedimentology, diagenesis, depositional environments, reservoir development and sequence stratigraphy of the Lidam Formation.

The conclusions of the study are outlined below:

➤ **Tectonostratigraphic setting of the Lidam Formation:**

Tectonic subsidence during Late Cretaceous as a result of reversed dextral shear along the trans-tensional plate boundary of the European and African plates, resulted in the formation of a series of basins, including the Sirt Basin, Libya. Major hydrocarbon discoveries in the Sirt Basin are in the Mesozoic and Cenozoic basin fill and the Cretaceous Lidam Formation is an important carbonate reservoir interval in the southeastern part of the Sirt Basin. The Lidam Formation is considered as the first marine transgressive unit in the Sirt Basin and comprises the lower part of the Upper Cretaceous rocks overlying the Nubian (Sarir) Sandstone and is overlain by the Rakb group (Etel Formation Evaporites).

➤ **Carbonate facies of Lidam Formation:**

Based on core description and petrography, ten main facies and fourteen microfacies were recognized within the Lidam Formation during this study. These are; anhydrite (chicken wire anhydrite), dolomite (finely replacive dolomite), sandstone (lithic and bioclastic), shale, stromatolitic mudstone, ostracod, mollusc (mollusc bioturbated packstone and partially dolomitized mollusc packstone), bioclastic (foraminifera packstone / grainstone and echinoderm packstone), peloidal (peloidal grainstone and peloidal ooidal grainstone), and algal (squamariacean / coralline algae bindstone) facies.

The sediment making up the facies of the Lidam formation have been deposited as coastal and shallow-water inner carbonate platform deposits. These deposits are inferred to have formed in supratidal sabkhas, intertidal, restricted marine shelf lagoon and higher energy shallow shoal environments. The anhydrite, stromatolitic and dolomite facies

formed in supratidal and intertidal environment, whereas the bioclastic, ostracod, mollusc and peloidal facies were laid down in low to moderate energy, restricted intertidal to subtidal setting. The layers of sandstone that are sandwiched between carbonate beds are interpreted to consist of a significant proportion of eolian-derived quartz sand that were reworked together with shallow marine material. The ooidal peloidal packstone / grainstone are the most important facies for hydrocarbon accumulation in all studied wells. The overall depositional setting is interpreted as the inner part of a carbonate ramp.

➤ **Sequence stratigraphy development of the Lidam Formation:**

The whole stacking pattern of facies suggests that the Lidam Formation consists of two large scale cycles. The deposition of the first cycle began with the laminated stromatolite and anhydrite facies which overlie the Nubian Sandstone and represent initial transgressive deposits of the carbonate succession. The middle of the formation is dominated by bioturbated foraminifera wackestone / packstones formed during transgression with sabkha deposits (supratidal environment) passing up into inter tidal then subtidal environments. This large scale cycle ended with the accumulation of oolitic shoal deposits.

The second and uppermost large-scale cycle is regressive when the depositional sequence of the Lidam Formation was exposed and affected by meteoric processes. The overlying Etel Formation of Early Turonian age was deposited as a blanket of evaporites covering nearly the entire Lidam Formation during a regression of the sea level. Sequence development of the Lidam Formation was influenced by differential tectonic subsidence and uplift, perhaps palaeotopography, the arid climate, sedimentation rates together with eustatic changes in the Cenomanian and early Turonian.

➤ **Diagenetic processes and features of Lidam Formation:**

Diagenesis affecting the Lidam Formation has been recognized through petrographic, Scanning Electron Microscopy (SEM), and Cathodoluminescence (CL) microscopy as well as isotopic analysis. Three major diagenetic environments have affected the Lidam Formation. These are: early marine, meteoric & early burial as well as burial. Early marine diagenesis resulted in common micritization and development of isopachous fringing

cements around bioclasts. Meteoric & early burial diagenesis resulted in meniscus cement, neomorphism, dissolution of bioclasts (particularly of aragonite and micritic calcite), calcite cementation (drusy calcite cement and syntaxial overgrowths on echinoderms fragments), early dolomitization, and anhydrite replacement.

During the burial diagenetic phase compaction (pressure solution and stylolites) and fracturing and filling the pore spaces by equant calcite cementation and late dolomitization completely filled any remaining pore spaces and the final stage of diagenesis are replacement of pyrite and hydrocarbons emplacement.

Cathodoluminescence (CL) analyses reveal three different phases of cementation with different luminescent properties. These cement stages are dull luminescent, non luminescent with bright bands of red-orange zones and dark non-luminescent which have been related to the marine, meteoric / shallow burial and deeper burial settings described above. Isotopic analysis shows that most of the Lidam Formation samples have $\delta^{18}\text{O}$ values between -2.10 to -10‰ and $\delta^{13}\text{C}$ data between -0.74 and +5.15 ‰. Bioclasts had isotopic values consistent with marine values. Micrites from the anhydrite and stromatolitic facies showed typical meteoric values, whereas those from the ostracod facies were consistent with a marine origin, perhaps with a burial overprint. Coarse drusy and equant cements fell into the meteoric and burial fields, respectively.

➤ **Reservoir Quality of the Lidam Formation:**

The most common porosity in the Lidam Formation are intergranular, intragranular, vuggy, and mouldic types and these strongly influenced reservoir quality. Most of the good porosities are observed in the upper part of the Lidam Formation. The average porosity is fair to moderate 1.71 to 18.4 % and poor to fair permeability between 2.17 to 16.12 mD. These reach a maximum in the ooidal peloidal packstone /grainstone facies in all the studied wells, which have been deposited in the shallow shoal environment. In comparison the porosity (2.76% - 8.68 %) and permeability (0.03 to 0.1mD) are poor in the supratidal and intertidal bioclastic foraminifera wackestone / packstone and ostracod packstone in the middle and lower part of the Lidam Formation.

Primary depositional facies and subsequent secondary processes are important factors for creation of the units with reservoir quality. Dissolution and subaerial exposures and

extensive dolomitization are further critical elements for development of the porosity the upper part of the Lidam Formation. Calcite cementation and compaction during burial diagenesis has played an important role in reduction of porosity. The oolitic peloidal facies had the best reservoir quality due to good initial primary porosity, some early cementation preserving primary porosity from later compaction, and later meteoric overprint resulting in some dissolution.

RECOMMENDATIONS FOR FURTHER WORK:

Following on from this study, recommendations for further work are:

1. Further work is needed on the other wells from the Lidam Formation to help better understand the overall depositional setting (whether ramp or rimmed shelf).
2. Further work is needed on the diagenesis and origins of the dolomites and their affect on the reservoir development of the Lidam Formation.
3. Further studies are needed on the depositional environment and diagenesis of the Lidam Formation in the NE part of the Sirt Basin, to better understand regional variations and controls on development.
4. The Lidam carbonate is an important reservoir in the Sirt Basin, due to the presence of the oolitic shoal facies in the uppermost part of the formation. Further work is required to discover whether this relationship is always consistent, or whether other facies might make good reservoir targets.

REFERENCES

REFERENCES

- Abadi A. (2002).** Tectonics of the Sirt Basin, Interferences from Tectonic Subsidence Analysis, Stress Inversion and Gravity Modeling. Thesis.
- Adams, A. E and Mackenzi, W.S. (1998).** A Colour Atlas of Carbonate Sediments and Rocks under the Microscope. Manson Publishing, London.
- Adams, J, E and Rhodes, M. L (1960).** Dolomitization of Seepage Reflex, Bull. A.A.P.G. 44: 1912 -1920.
- Albert, V. C. (1989).** Carbonate Rock Depositional Models, a Microfacies Approach. Prentice-Hall.UK.
- Anketell, (1996).** Structural History of the Sirt Basin and its relationship to the Sabratah Basin and Cyrenaican Platform, Northern Libya. In : the Geology of the Sirt Basin . (Eds M. J. Salem , M. T. Busrewil, A.A. Misallati and M. A. Sola) . Elsevier, Amsterdam, III, 57-87.
- Ataby Easef (1995).** Petrography and Origin of Dolomites of Yaniktepe Formation (Upper Cretaceous) in Gurun Autochthonous, Eastern Taurus, Turkey. Mineral Res. Expl. Bull., 117. 59-67.
- Barbieri, (1996).** Micropalaeontology of the Rakb Group (Cenomanian to Early Maastrichtian) in the Hameimat Basin, northern Libya. In: M.J. Salem, A.J. Mouzoughi and O.S. Hammuda, Editors, *The Geology of Sirt Basin vol. 1*, Elsevier, Amsterdam (1996), pp. 185–194.
- Barr, F T. and Weegar (1972).** Stratigraphic Nomenclature of the Sirt Basin, Libya the Petroleum Exploration Society of Libya (Tripoli, Libya): 179pp.
- Bathurst, R. G, (1975).** Carbonate Sediments and Their Diagenesis. Development in Sedimentology. Elsevier, Amsterdam, 2nd Edition, 658pp.

- Batt, A.A. (1986).** Upper Cretaceous Biostratigraphy of the Sirt Basin, North Libya. *Revue De Paleobiologie*. 5(2), 175-191.
- Belazi, H. S. (1989).** The Geology of the Nafoora Oil Field, Sirt Basin, Libya. *Journal of Petroleum Geology*, 12, 353-366.
- Bruckschen, P., Neuser, R.D., Richter, D.K. (1992).** Cement Stratigraphy in Triassic and Jurassic Limestones of the Weserbergland (Northwestern Germany). - *Sed. Geol.*, 81, 195-214, 9 Figs., Amsterdam. K009; K039
- Back et al. (1984)., W., Hanshaw, B. B. and Van Driel, J (1984).** Role of groundwater in shaping the eastern coastline of the Yucatan Peninsula, Mexico. In: Lafleur, R. G (Ed), *Groundwater as a Geographic Agent*. P. 157-172.
- Buchbinder, B. (1985).** Occurrence and Preservation of Eocene Squamariacean and Coralline Rhodoliths: Eua, Tonga. *Paleogeology*, p 249-255.
- Carr, I. D. (2003).** A Sequence Stratigraphic Synthesis of the North African Mésozoic. *Jour. of Petrol. Geo.* Vol.26, Pp 133-152.
- Catuneanu, O., 2002.** Sequence Stratigraphy Of Clastic Systems: Concepts, Merits, And Pitfalls *Journal Of African Earth Sciences*, Volume 35, Issue 1, Pages 1-43.
- Catuneanu, Octavian (2006).** *Principles of Sequence Stratigraphy*, Elsevier pp. 375.
- Choquette, P. W and Pray, L.C, (1970).** Geological Nomenclature and Classification of Porosity in Sedimentary Carbonates. *Bull. Am. Assoc. Petrol. Geologists*, 54: 207-250.
- Choquette. P.W and Steinen. R. P. (1980).** Mississippian Non-Supratidal Dolomite, Ste Genevieve Limestone, Illinois Basin: Evidence for Mixed Water Dolomitization. *S.E.P.M Spec. Pub.* 28: 163 – 196.

- Clifford, et al. (1980).** Geology of a stratigraphic giant: Messla oil field. in giant oil and gas fields of the decade (1968-1978). (eds M. t. Halbouty). Mem. Am. Assoc. Petrol. Geol. ,30, 507-524.
- Coe, A, Dan. B, Kevin C, Steve F, John H and Chris W, (2002).** The Sedimentary Record of Sea Level Change, Cambridge University Press, 288 Pp.
- Conant, L. C. And Goudarzi, G.H. (1967).** Stratigraphic and Tectonic Framework of Libya. Bull. Am. Assoc. Petrol. Geo. 51, 719-730.
- Dickson, J. D, (1986).** Modified Staining Techniques for Carbonates in Thin Section. Nature, 205: 587p.
- Dunham, R. L (1962).** Classification of Carbonate Rocks According to Depositional Texture. In HAM, W. E. (Editor), Classification of Carbonates Rocks. Am. Assoc. Petrol. Geologists, Tulsa, Okla., Pp. 108-121.
- Duronio and Colombi, (1983).** Mesozoic Rocks of Libya. Unpublished Report, P 15
- EL - Alami, (1996).** Habitat of Oil Abu Attifel Area, Sirt Basin, Libya. In The Geology of the Sirt Basin (Eds M. J. Salem, M.T. Busrewil, A.A. Misallati and M. A. Sola) Elsevier, Amsterdam, II, 337-347.
- El- Bakai, M. T. (1987).** Petrography and Facies Analysis of Lidam Formation (Carbonate Unite) From Some Wells in Sirt Basin, Libya. Third Symposium on the Geology Of Libya, Abstracts: Page 49.
- El- Bakai, M. T. (1991).** Petrography and Diagenesis of the Lidam Formation (Carbonate Units): From Selected Wells in Sirt Basin, Libya. Petroleum Research Journal. V: 3. P.35-43.
- El- Bakai, M. T. (1992).** Environment of Deposition of the Lidam Formation in NW Sirte Basin, Libya Geology of Arab World, Cairo University .P 343-351.

- El- Bakai, M. T. (1993).** Microprobe analysis of the Glauconite Pellets of the Lidam Formation, NW Sirt Basin, Libya. PRC Journal. V.5, p 56-61.
- Ezat Heydari and Lawrence R. Baria (2005)** Reservoir characterization of the Smackover Formation at the little cedar creek field, Conecuh county, Alabama, gulfcoast Association of geological societies Transactions 1-6
- Flugel, E. (1982).** Microfacies Analysis of Limestone. Springer- Verlag, Berlin Heidelberg New York. 633p.
- Flugel, E. (2004).** Microfacies of Carbonate Rocks. Springer- Verlag, Berlin Heidelberg New York.
- Folk, R. L. (1965).** Some Aspects of Recrystallization in Ancient Limestones, In: Pray, L. C and R. C Murry (Eds.); Dolomitization and Limestone Diagenesis, Soc. Eco. Paleot. Min. Spec. Public. 13: 14-48.
- Friedman, G.M. (1959).** Identification of Carbonate Minerals by Staining Methods. Journal of Sedimentology Petrology. 34(4):643-655.
- Goldhammer, Et Al, (1990).** Depositional Cycles, Composite Sea Level Changes, Cycle Stacking Patterns and the Hierarchy of Stratigraphic Forcing- Example from Platform carbonate Of the Alpine Triassic. Geo. Soc. Am. Bull. 102, 535 – 562.
- Goudarzi, G.H. (1980).** Structure - Libya In: The Geology of Libya (Eds. M. J. Salem, M.T. Busrewil). Academic Press, London, III, 879-892.
- Gras and Thusu, (1998).** Trap architecture of the Early Cretaceous Sarir Sandstone in the eastern Sirt Basin, Libya. In: petroleum Geology of North Africa. Geol. Soc. London. Spec. Publ., 132, 317-334.
- Gregg and Sibley, J.M. Gregg and D.F. Sibley (1984),** Epigenic dolomitization and the origin of xenotopic dolomite texture, *Journal of Sedimentary Petrology* **54** (1984), pp. 908–931.

- Gregg and Silbley (1984)**, Epigenetic dolomitization and origin of xenotopic dolomite texture: *Journal of Sed. Petrology.*, 54, 908-931.
- Gumati, Y. D. and Nairn, A. E. (1991)**. Tectonic subsidence of the Sirt Basin, Libya. *J. Petrol. Geol.*, 14, 93-102.
- Gumati, Y.D, and Kanesh, W.H. (1985)**. Early Tertiary Subsurface and Sedimentary Facies, Northern Sirt Basin, Libya. *Bull. A.A.P.G.* 69(1): 39-52.
- Halley. R. B. (1980)**. Burial Cement in Suniland, Lower Cretaceous of Southern Florida (Abstract). *Bull. A.A.P.G.* 65: 934p.
- Hardie. L. A. (1987)**. Perspectives Dolomitization: A Critical View of Some Current Views. *Journal Sedimentology Petrol.*, 57, 166-183.
- Heckel, P. D. (1985)**. Recent interpretation of the Late Paleozoic Cyclothem: Proceedings of Third Annual Field Conference, Mid-content Section, Society of economic Paleontologists and Mineralogist.
- Helland-Hansen, W. Martinsen. J. (1996)**. Shoreline Trajectories and Sequences: Description of Variable Depositional-Dip Scenarios. *Journal of Sedimentary Research* 66 (4), 670-688.
- Hudson, J. D. (1977)**. Stable Isotopes and Limestone Lithification. *Journal of the Geological Society of London* 133. P 637-660.
- Jackson, C. (2006)**. Rift-initiation Development of Normal Fault Blocks: Insights from the Hammam Faraun Fault Block, Suez Rift, Egypt. *Jour. of the Geology Soc.* Jun, 2006.
- James P. N. and Kendall C. (1992)**. Introduction to Carbonate and Evaporite Facies Models. In; *Facies models, Response to Sea level Change*, Geo. Assoc. of Canada, p 265-275
- Jones. B. and Derrochers. A. (1992)**. Shallow Platform Carbonates. *Facies Models Response to Sea Level Change*, Geo. Asso. Of Canada. 277 - 301.

- Kirkham .A. (2004).** Patterned Dolomites: Microbial Origins And Clues To Vanished Evaporites In The Arab Formation, Upper Jurassic, and Arabian Gulf. Geological Society, London, Special Publications; 2004; V. 235; P. 301-308.
- Klitzch, E. (1970).** Die Struckurgeschichte Der Zelttral – Sahara:Neue Erkenntnisse Zum Bau Zur Palaeogeographie Eines Taflandes. *Geo. Rundsch.*, 59(2) 459-527.
- Klitzch, E. (1971).** The Structural Development of the Part of North Africa since Cambrian Time. In: *The Geology of Libya Tripoli University Faculty of Science, Tripoli*, 253-262.
- Koersshner, W. F. and Read, J. F. (1989).** Field and modeling studies of Cambrian carbonte cycles, Virginia Applications: *Journal of Sedimentary Petrology*, V. 59, p. 654-687.
- Kuss and Bachmann, (1996).** Cretaceous paleogeography of the Sinai Peninsula and neighbouring areas. *C. R. Acad. Sci., Ser. II, Sci. Terre Planetes* **322** (1996), pp. 915–933.
- Larsen and Chilingar, (1979).** *Diagenesis in Sediments and Sedimentary Rocks*. Elsevier, Amsterdam, 579 P.
- Lee. Y. And Friedman (1987).** Deep Burial Dolomitization in the Ordovician Ellenburger Group Carbonates. West Taxes and Southeastern New Mexico, *J. Sed. Petr.* 57(3): 544-557.
- Liszkowski, J. (1975).** Algal, its distribution and contribution to Middle Oxfordian coral reef complexes from Baltow, Central Poland. 1st international symposium on fossil algae, Erlangen, Germany
- Longman, M. W. (1980).** Carbonate Diagenetic Textures from near surface Diagenetic Environments. *Bull. A.A.P.G.* 64(4): 461- 487.
- Loucks, R.G. (1977).** Porosity Development and Distribution in Shoal Waer Carbonate Complexes- Subsurface Pesrsal Formation (Lower Cretaceous) South Texas. *Texas Uni. Bir. Eco. Geol. Rep. Inv.* 89: 97-126.

- Machel, H.G., (2004).** Concepts and Models of Dolomitization: A Critical Reappraisal In: Braithwaite, C.J.R., Rizzi, G. And Drake, G. (Eds.). The Geometry and Petrogenesis of Dolomite Hydrocarbon Reservoirs. Geological Society, London, Special Publication, 235: 7-63
- Mansour. A. (2004).** Diagenesis of Upper Cretaceous Rudists Bivalves, Abu Roash Area, Egypt: A Petrographic Study. *Geologia Croatica*, 57/1 p. 55-66.
- Massa and Delorite, (1984).** Evolution of the Sirt Basin (Libya) From Cambrian to Cretaceous. *Bull. Soc. Geo. France*, XXXI (6): 1087-1096.
- Meyers, W.J. (1991).** Calcite Cement Stratigraphy: An Overview. - In: Barker, C.E. And Kopp, O.C. (Eds.): *Luminescence Microscopy and Spectroscopy: Qualitative and Quantitative Applications.* - Soc. Econ. Paleont. Min. Short Course, 25, 133-148, 11 Figs., Dallas
- Mitchum Jr., R. M., (1977),** Seismic Stratigraphy and Global Changes of Sea Level: Part 11. Glossary of Terms Used In Seismic Stratigraphy: Section 2. Application Of Seismic Reflection Configuration To Stratigraphic Interpretation, Memoir 26 Pages 205 - 212.
- Mitchum, R. M, Vail, P. R., and Thompson, S (1977).** Seismic Stratigraphy And Global Changes Of Sea Level, Part 2: The Depositional Sequence As A Basic Stratigraphic Analysis. In: C.E Payton (Ed) *Seismic Stratigraphy- Application to Hydrocarbon Exploration.* AAPG, 26, P.53-62.
- Moore. C. H. (1989).** Carbonate Diagenesis and Porosity. *Development in Sedimentology* 46. Elsevier, Science, Publisher B.V. Amsterdam.
- Moore, C. H (2002).** Carbonate Daigenesis and porosity; Elsevier, Amstredam.
- Morrow. D (1990).** Dolomite-Part 1: The Chemistry of Dolomitization and Dolomite Precipitation. In *Diagenesis, Geosci. Can. Reprint Series*, 4, 1-13-140.

Munnecke, A and et al., (1997). Microspar development during early marine burial diagenesis: a comparison of Pliocene carbonates from the Bahamas with Silurian limestones from Gotland (Sweden). *Sedimentology*, 44, p. 977-990.

Murray, R. C. (1964). Origin and diagenesis of gypsum and anhydrite *Journal of Sedimentary Research*; v. 34; no. 3; p. 512-523

Nebelsick, J.H. and Bassi, D., (2000). Taxonomy, growth-form morphology and taphonomy: Key factors controlling the fabric of coralline algal dominated shelf carbonates. In: Insalaco, E., Skelton, P.W. and Palmer, T.J., Editors, 2000. *Carbonate platform systems: Components and interactions Geological Society Special Publications 78*, pp. 89–107.

Nummedal, D., Riley, G.W., Templet, P.L., (1993). High-Resolution Sequence Architecture: A Chronostratigraphic Model Based On Equilibrium Profile Studies. In: Posamentier, H.W., Summerhayes, C.P., Haq, B.U., Allen, G.P. (Eds.), *Sequence Stratigraphy and Facies Associations*, Vol. 18. International Association of Sedimentologist Special Publication, Pp. 55–68.

Peter Königshof, (2006). Growth Forms and Paleoenvironmental Interpretation of Stromatopoid in a Middle Devonian Reef, Southern Morocco (West Sahara).

Pettijohn, F.J. (1975). *Sedimentary Rocks*. Harper and Row, London, P. 626.

Philip et al., (2000). Late Cenomanian. In: J. Dercourt *et al.* (2000).

Piatkowski, (1975). Algal Stromatolites in the Zechsteinkalk (Upper Permian) Of Northern Poland: Distribution, Morphology, Microfacies, and Environmental Significance. 1st International Symposium on Fossil Algae, Erlangen, Germany

Pol, J.C. (1985). Early diagenetic history of Late Pennsylvanian calclithite beds, Hueco Mountains, El Paso County, Texas *Am. Assoc. Pet. Geol., and Bull.* ; Vol/Issue: 69:2; AAPG; New Orleans, LA, USA

Posamentier, H.W., Allen, G.P., (1999). *Siliciclastic Sequence Stratigraphy: Concepts and Applications*. SEPM Concepts in Sedimentology and Paleontology No. 7, 210 P

- Posamentier, H.W., Jervey, M.T., Vail, P.R., (1988).** Eustatic Controls on Clastic Deposition. I. Conceptual Framework. In: Wilgus, C.K., Hastings, B.S., Kendall, C.G.St.C., Posamentier, H.W., Ross, C.A., Van Wagoner, J.C. (Eds.), *Sea Level Changes-An Integrated Approach*, Vol. 42. SEPM Special Publication, Pp. 110– 124.
- Posamentier, H.W., Ross, C.A., Van Wagoner, J.C. (1990).** *Sea Level Changes-An Integrated Approach*, Vol. 42. SEPM Special Publication, Pp. 39–45.
- Pratt, R. B , Noel P. James and C. Cowan (1992).** Peritidal Carbonates. In; *Facies models, Response to Sea level Change*, Geo. Assoc. of Canada, p 277-301
- Qilong Fu, (2006).** Dolomitization of the Middle Devonian Winnipegosis Carbonates in South-Central Saskatchewan, Canada, *Sedimentology*, 53, 825-848.
- Richter, D.K., Zinkernagel, U. (1981).** Zur Anwendung Der Kathodolumineszenz in Der Karbonatpetrographie. - *Geol. Rundschau*, 70/3, 1276-1302, 2 Figs., 1 Tab., Stuttgart
- Robert G. Loucks. And J. Frederic Sarg (1993)** *Carbonate Sequence Stratigraphy, Recent Developments and Applications*, AAPG Memoir. 57.
- Robertson C. Handford and Robert G. Loucks., (1993).** Carbonate Depositional Sequence and System Tracts-Responses of Carbonate Platforms to Relative Sea Level Changes. AAPG Memoir, 57, 3-41 Pp.
- Rott, C. M. and H. Qing. (2005).** Sedimentology and facies description of Mississippian Alida beds, Williston Basin, southeastern Saskatchewan, vol.1, Saskatchewan, Geo. Survey. p 10.
- Sarg. J F., (2001).** The Sequence Stratigraphy, Sedimentology and Economic Important Of Evaporite-Carbonate Transitions: A Review. *Sedimentology Geology*, 140, 1-2, 9-42.
- Schreiber. , B.C & El Tabakh, M (2000).** Deposition and Early Alteration of Evaporites. *Sedimentology* 47, 215-238.

Schroder, S (2003). A Depositional Model for the Terminal Neoproterozoic- Early Cambrian Ara Group Evaporites in South Oman. *Sedimentology*, 50, 879-898.

Stampfli et al., (2001). The Paleotectonic Atlas of the Peritethyan Domain. *Eur. Geophys. Soc.* (2001) (CD-ROM realized by <e-public>—Electronic Publishing & Consulting, Berlin).

Thomas, S, Ahlbrandt. (2001). the Sirt Basin Province of Libya- Sirt- Zeltan Total Petroleum System. US Geological Survey Bulletin, 2202-F.

Tucker, M. E. (2001). Sedimentary Petrology, an Introduction to the Origin of Sedimentary Rocks. Third Edition,

Vail, P.R. ET, Al (1977). Seismic-Stratigraphy and Global Changes of Sea Level from Coastal Onlap in: C.E. Payton, Editors, and Seismic Stratigraphy. Applications to Hydrocarbon Exploration, Memoir-American Association of Petroleum Geologists, Tulsa. Vol. 26 Pp. 213–248.

Van Houten, (1980). Latest Jurassic- Early Cretaceous Regressive Facies, Northeast Africa Craton. AAPG Bull., 64, 857-867.

Van Wagoner, et, al. 1990. Siliciclastic Sequence Stratigraphy in Well Logs, Cores, and Outcrops: Concepts for High-Resolution Correlation of Time and Facies. AAPG Methods Explor. Ser., 7.

Van Wagoner, P.R., Sarg, J.F., Loutit, Hardenbol, T.S., J., (1988). An Overview of Sequence Stratigraphy and Key Definitions. In: Wilgus, C.K., Hastings, B.S., Kendall, C.G.St.C.

Wenneker et, al., (1996). The Geology and Hydrocarbons of the Sirt Basin: A Synopsis. The Geology of the Sirt Basin.-I, Elsevier, Amsterdam, Netherland, 3-56.

Wilson, J. L. (1975). Carbonate Facies in Geologic History. Springer- Verlag, Berlin.

THESIS APPENDIX

THESIS APPENDIX

A1) LITHOLOGICAL & SYMBOL CODES FOR LOGS

Lithology:



Limestone



Argillaceous limestone



Dolomitic limestone



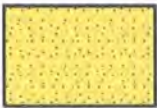
Dolomite



Anhydrite

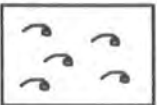


Mudstone

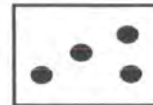


Sandstone

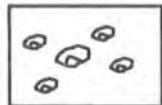
Carbonate grains:



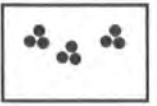
Shell Fragments



Peloid



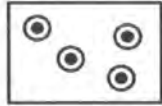
Ostracoda



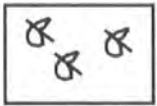
Small Foraminifera



Mollusca



Ooids



Undifferentiated bioclasts



Pellet



Echinoderm

Sedimentary structures:



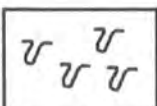
Wispy pressure solution seams



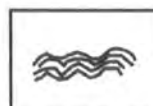
Nodular



Nodular anhydrite



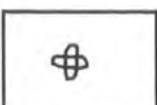
Burrows



Stromatolites



Lamination



Bioturbation



Stylolite



Fractures

A2) STAINING:

Because of the similarity in optical properties of calcite and dolomite, about half of the thin sections have been etched and stained using two stains dissolved in weak hydrochloric acid, according to the method described by Adam et al (1984) adapted from Dickson (1965).

The two stains used are Alizarin Red S, to help distinguish calcite from dolomite, and potassium ferricyanide which distinguishes carbonate minerals containing Fe²⁺ (ferroan minerals) from those with little or no iron (non-ferroan minerals). The table below shows the results of etching and staining of carbonate minerals.

Mineral	Effect of etching	Stain colour with Alizarin Red S	Stain colour with potassium ferricyanide	Combined result
Calcite (non-ferroan)	Considerable (relief reduced)	Pink to red-brown	None	Pink to red-brown
Calcite (ferroan)	Considerable (relief reduced)	Pink to red-brown	Pale to deep blue depending on iron content	Mauve to blue
Dolomite (non-ferroan)	Negligible (relief maintained)	None	None	Unstained
Dolomite (ferroan)	Negligible (relief maintained)	None	Very pale blue	Very pale blue (appears turquoise or greenish in thin section)

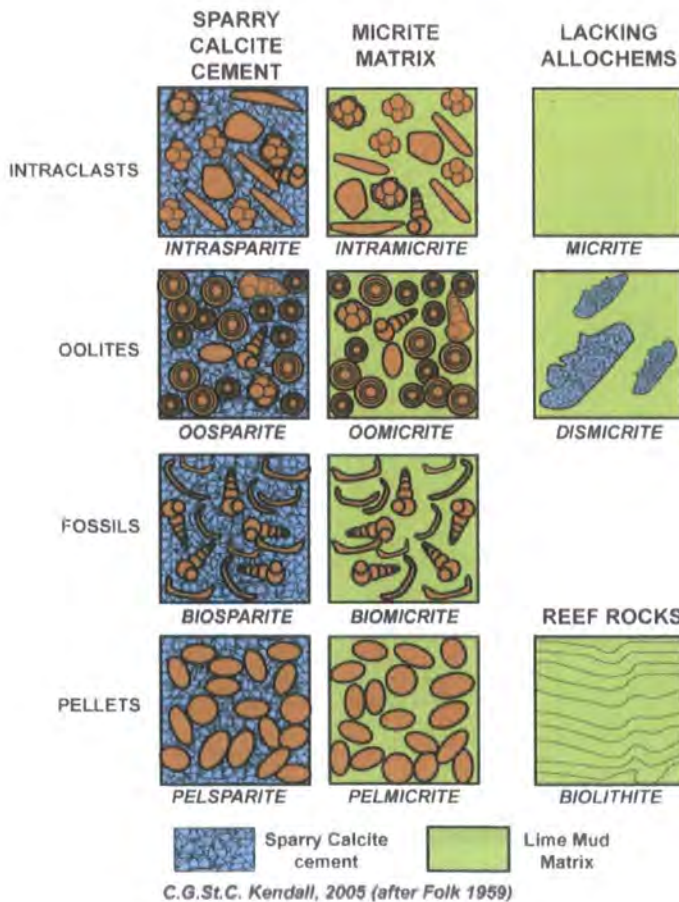
A3) CLASSIFICATION OF CARBONATES:

Two of the most widely used classifications are those of Folk (1959, 1962) and Dunham (1962). Both classifications subdivide limestones primarily on the basis of matrix content.

1- Folk's classification. (1959):

Most limestones are classified by Folk's allochemical rocks if they contain over 10% allochems (carbonate grains). Based on the percentage of interstitial material, the rocks may be further subdivided into two groups: sparry allochemical limestones (containing a sparry calcite cement) and microcrystalline allochemical limestone (containing microcrystalline calcite mud or micrite).

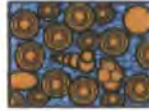
Rocks with appreciable micritic matrix are termed micrites, while matrix-free rocks that contain sparry calcite cement are termed sparites. Sparites and micrites are further subdivided by means of their most common grains.



2- Dunham’s Classification (1962):

In Dunham’s classification rocks are assigned names according to their depositional texture. These textures mainly relate to the energy of the depositional environments, although a problem with Dunham’s classification lies in the timing of introduction and origin of carbonate mud in packstones and the distinction of grain-and matrix-supported textures, as discussed by Tucker & Wright (1990).

The classification is based on depositional texture and it is often difficult, if not impossible, to determine whether carbonate mud in a packstone was introduced at the time of deposition or subsequently infiltrated a primary grainstone. The table below shows the classification of limestone according to Dunham (1962). Rock names are in capital letters.

Original components not bound together at deposition				Original components bound together at deposition. Intergrown skeletal material, lamination contrary to gravity, or cavities floored by sediment, roofed over by organic material but too large to be interstices
Contains mud (particles of clay and fine silt size)		Lacks Mud		
Mud-supported		Grain-supported		
Less than 10% Grains	More than 10% Grains			
Mudstone 	Wackestone 	Packstone 	Grainstone 	
				Boundstone 

C. G. St. C. Kendall, 2005 (after Dunham, 1962, AAPG Memoir 1)

3- Embry and Klovan classification for reef limestones (1971):

Embry and Klovan (1971) and James (1984) deal with depositional texture and modified Dunham's classification to include coarse grained carbonates. In their revised scheme, a wackestone in which the grains are greater than 2mm in size is termed a floatstone and a coarse grainstone is called a rudstone. Both terms are extremely useful in description of limestones.

Embry and Klovan's scheme also more graphically reflects the role that the organisms performed during deposition through their modification of the boundstone 'field' of Dunham. Terms such as bafflestone, bindstone, and framestone are useful in concept but are extremely difficult to apply to ancient limestones where diagenesis and sample size limit ones ability to assess an organisms function.

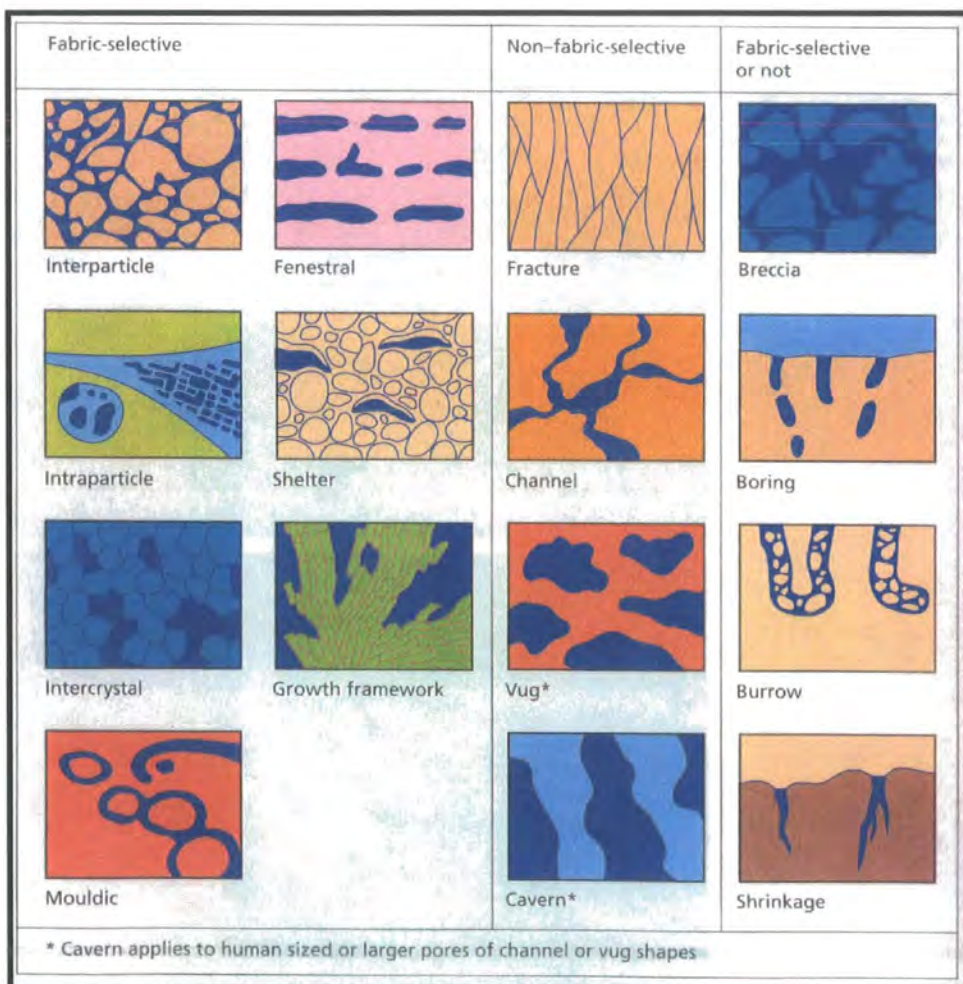
Allochthonous		Autochthonous		
Original components not bound organically at deposition		Original components bound organically at deposition		
>10% grains >2mm				
Matrix supported	Supported by >2mm component	By organisms that act as baffles	By organisms that encrust and bind	By organisms that build a rigid framework
Floatstone	Rudstone	Bafflestone	Bindstone	Framestone
				

Textural classification of reef limestones after Embry & Klovan (1971) and James (1984)

A4) CLASSIFICATION OF POROSITY:

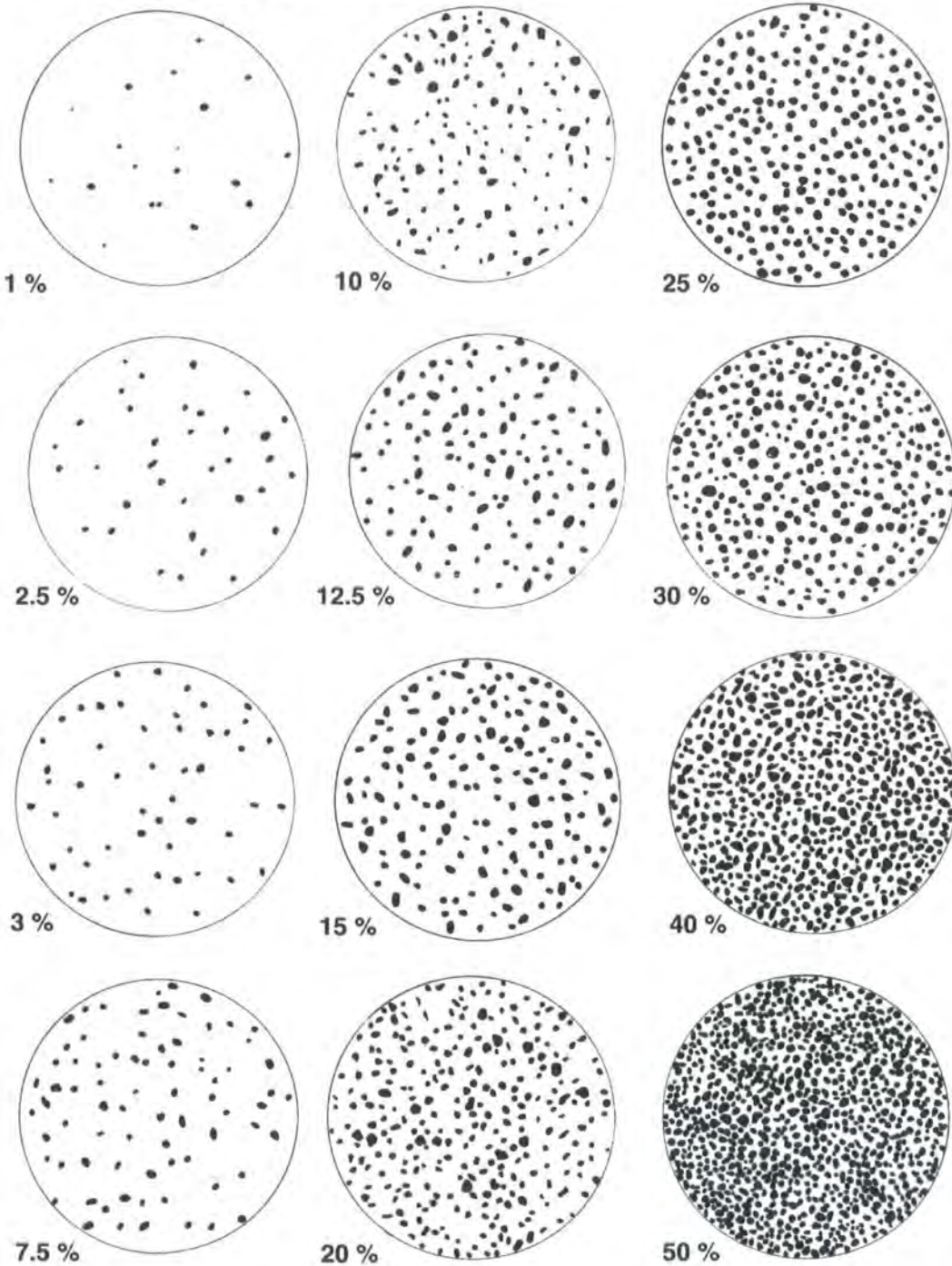
More than half the earth's hydrocarbon reserves are contained within pore systems in limestones and dolomite, and therefore an assessment of the amount and type of any porosity in carbonate sediment is an important part of any thin section description. Porosity can be described as primary, in which case it has been present in the rock since deposition or secondary when it has developed during diagenesis.

Porosity can be described as fabric-selective if its location is controlled by particular parts of the depositional or post – depositional fabric of rock. Porosity which is not fabric selective typically cuts across the fabric of the rock. This division into fabric – selective and non fabric selective porosity types is the basis of the classification of carbonate porosity proposed by Choquette & Pray (1970).



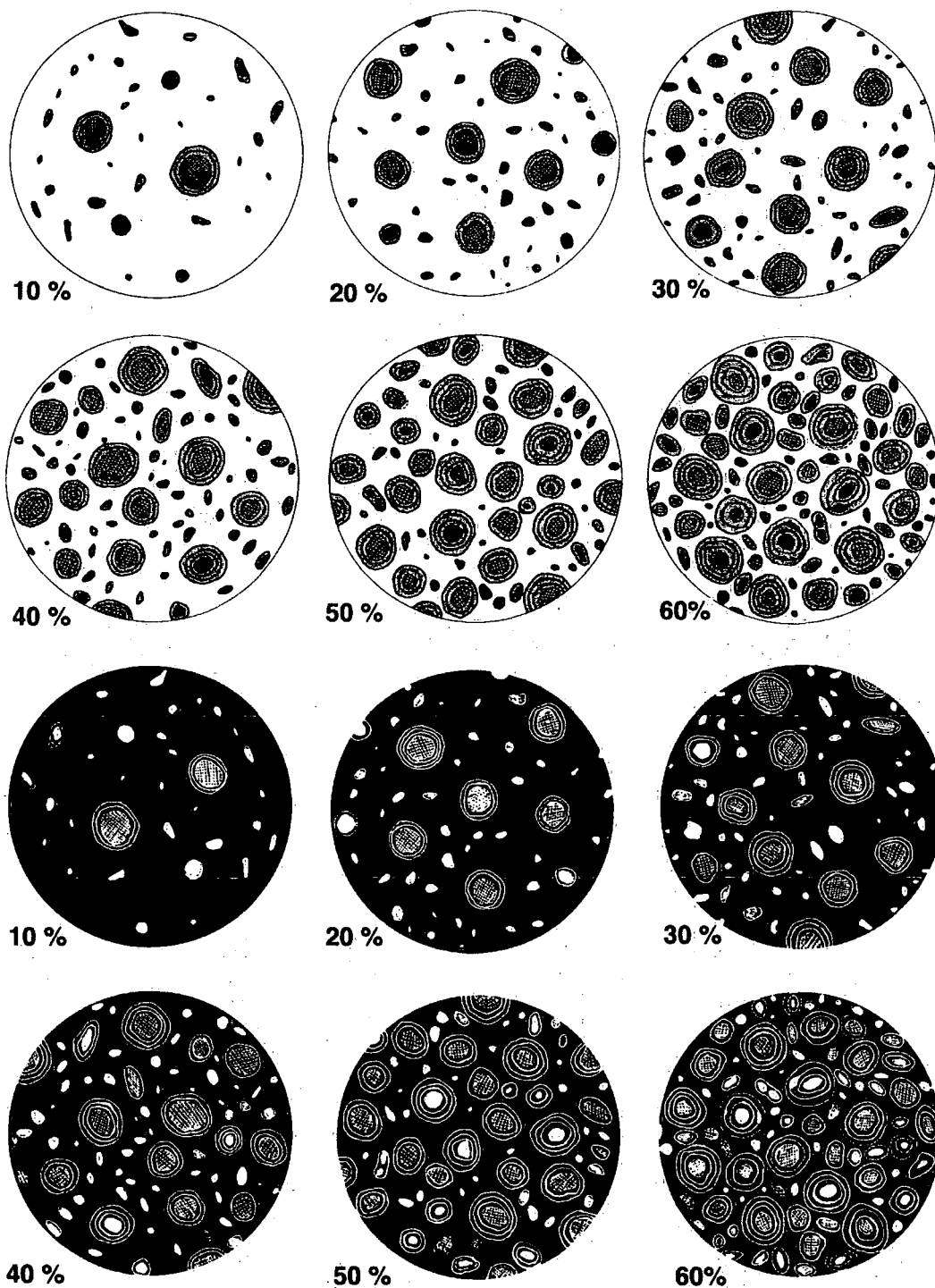
A5) CHARTS USED FOR PETROGRAPHIC DESCRIPTIONS

A The chart can be used to estimate the percentage of peloids, small micrite intraclasts, and microfossils (e.g. radiolarians)



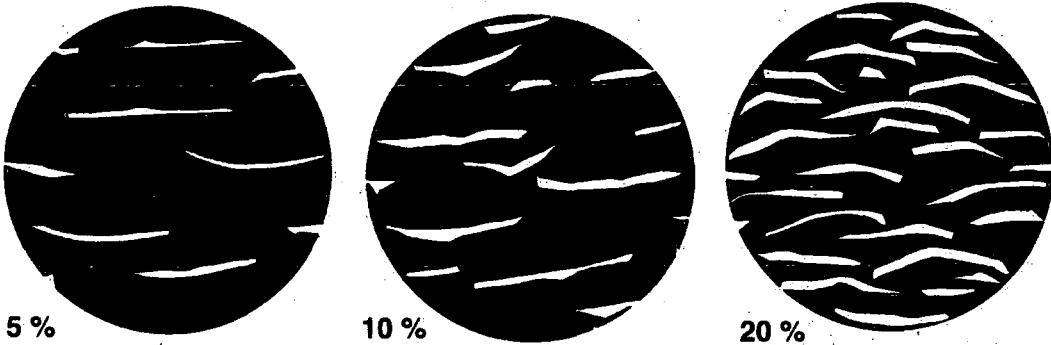
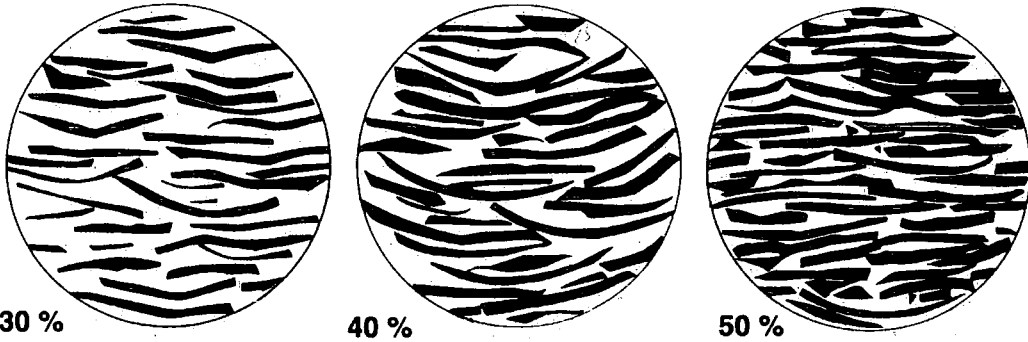
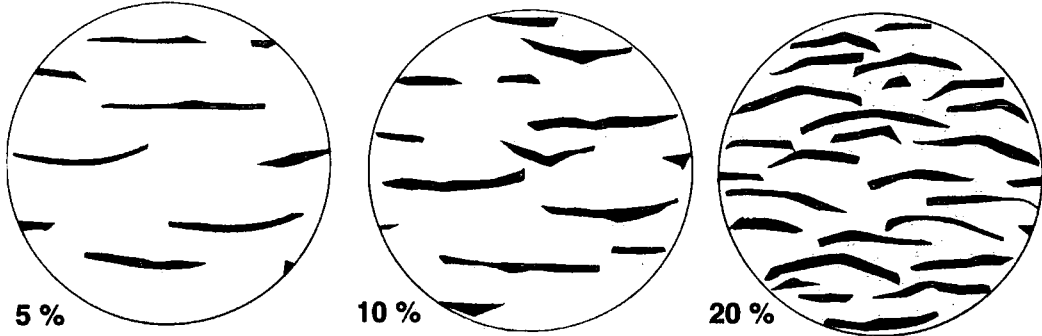
From: Baccelle, L. & Bosellini, A. (1965): Diagrammi per la stima visiva della composizione percentuale nelle rocche sedimentarie. - Annali dell'Università di Ferrara (Nuova Serie), Sezione 9, Scienze geologiche e paleontologiche, Vol.1, No. 3, 59- 62, 15 Pls.

B: This chart can be used to estimate the percentage of piddoids or oncoids associated with small grains



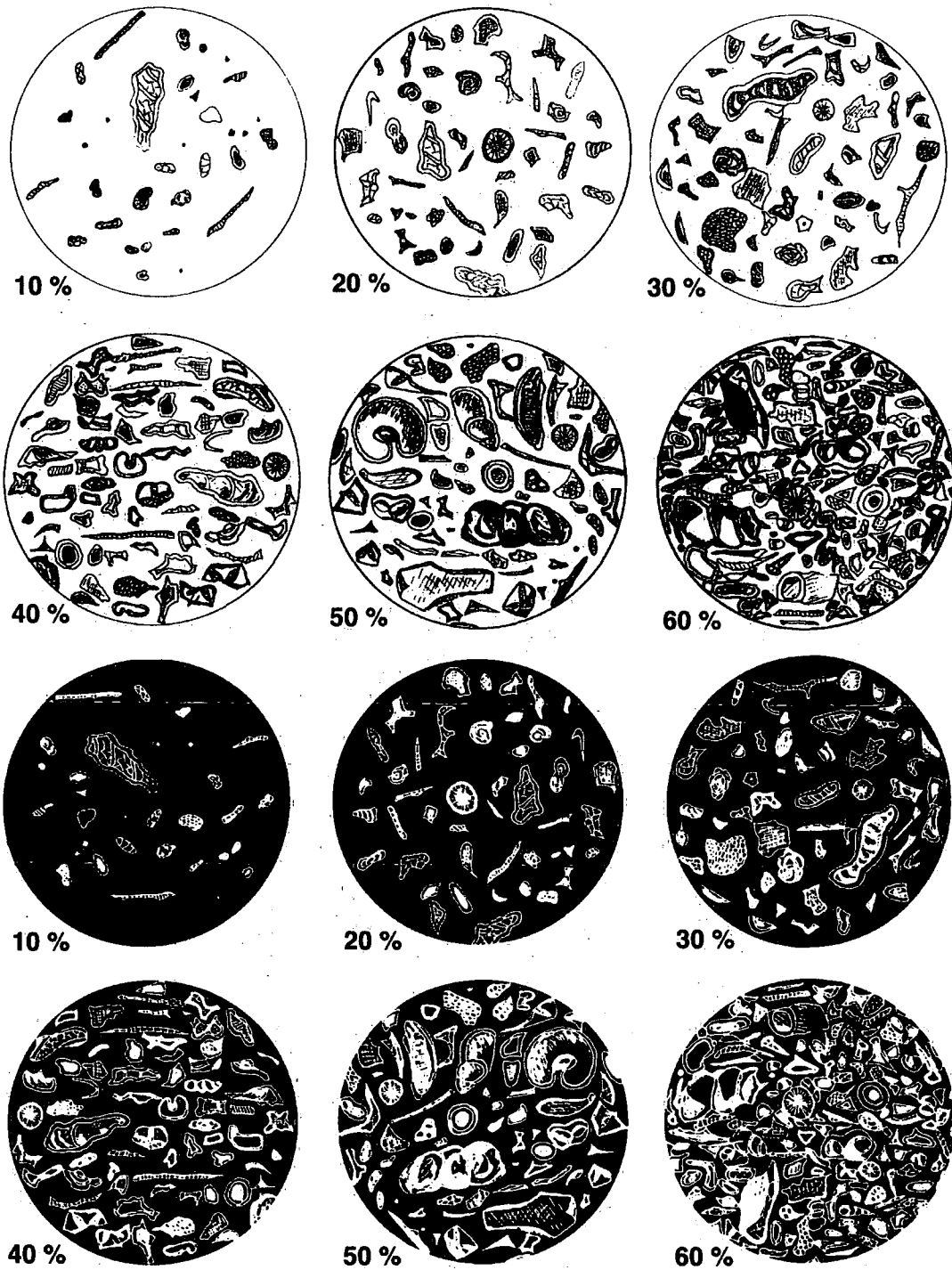
From: Baccelle, L. & Bosellini, A. (1965): Diagrammi per la stima visiva della composizione percentuale nelle rocche sedimentarie. - *Annali dell'Università di Ferrara (Nuova Serie), Sezione 9, Scienze geologiche e paleontologiche*, Vol.1, No. 3, 59- 62, 15 Pls.

C: The chart can be used to estimate the percentage of shells or platy fossils (e.g. phylloid algae)



From: Baccelle, L. & Bosellini, A. (1965): Diagrammi per la stima visiva della composizione percentuale nelle rocche sedimentarie. – *Annali dell'Università di Ferrara (Nuova Serie), Sezione 9, Scienze geologiche e paleontologiche*, Vol.1, No. 3, 59- 62, 15 Pls.

D: The chart can be used to estimate the percentage of grains in limestones composed of various skeletal grains, lithoclasts and peloids



From: Baccelle, L. & Bosellini, A. (1965): Diagrammi per la stima visiva della composizione percentuale nelle rocche sedimentarie. – *Annali dell'Università di Ferrara (Nuova Serie), Sezione 9, Scienze geologiche e paleontologiche*, Vol.1, No. 3, 59-62, 15 Pls.

